# UiO : University of Oslo

Cristiano Glessi

# Gold-NHC Complexes for Vacuum Deposition Applications: Synthesis, Characterization, and Applications in FEBID

**Thesis submitted for the degree of Philosophiae Doctor**

Department of Chemistry

Faculty of Mathematics and Natural Sciences

University of Oslo

**2021**

# ACKNOWLEDGEMENTS

III

# Preface

The work published in this thesis is part of the Marie Curie ITN ELENA (low energy ELEctron driven chemistry for the advantage of emerging Nano-fabrication methods). The aim of the ELENA project is the development of two next-generation nanofabrication techniques, Focused Electron Beam Induced Deposition (FEBID) and extreme ultra violet lithography (EUVL). The author's work is focused on the design, synthesis and testing of gold-based precursor molecules for FEBID. Gold N-heterocyclic carbene (NHC) complexes were chosen as the focus of the explorations. The main objectives of the author are:

- Synthesis of an array of gold(I) and gold(III) NHC complexes;
- Screening of the suitability of gold(I) NHC complexes as FEBID precursors;
- Testing of gold(I) NHC complexes as FEBID precursors.

Chapter 1 provides an introduction to gold NHC complexes, the FEBID process and relevant FEBID precursors and their design.

The synthetic and characterization work carried out on gold(I) NHC complexes is presented in Chapters 2-4. In these sections the synthesis, sublimation experiments, solid state investigation are presented, describing work published in **Paper I**, **III** and **IV**. The studies performed on silver carboxylates are also briefly discussed, work that is published in **Paper II**.

In Chapter 5 the FEBID testing of several gold(I) complexes is presented, expanding on the data discussed in **Paper III**. The FEBID testing was conducted in collaboration with the Hagen group at TUDelft.

Finally, the synthesis of gold(III) NHC complexes by means of *aqua regia* is discussed in chapter 6. This work has been published in collaboration with fellow Ph.D. candidate Volodymyr Levchenko in **Paper I**.

# Table of Contents

# Abstract

In this thesis, a series of gold N-heterocyclic carbene (NHC) complexes have been synthesized and characterized by spectroscopic and crystallographic means. The complexes of general formula Au(NHC)X present imidazole, triazole and imidazoline-based NHC ligands, with varied alkyl N-substituents (Me, Et, iPr, nPr) and backbone halogenation. The negatively charged ligand X was also varied (X = Cl, Br, I, $CF_3$). The complexes have been obtained in a library fashion in order to study the effect of small variation on the core structure on a) $^{13}$C NMR carbon chemical shift, b) Solid state interactions observed by single crystal X-ray diffraction studies, c) Volatility as obtained by controlled cold finger sublimation.

The volatility of the complexes was obtained by cold finger sublimation experiments and correlated to structure and packing interactions obtained by XRD. Optimization of sublimation temperature for gold(I) NHC complexes has been achieved, starting from a temperature of 100 °C down to 38 °C. *Vacuum*-TGA has been applied to a series of silver carboxylate complexes, as a pre-screening tool for low volatility Focused Electron Beam Induced Deposition (FEBID) precursors.

Seven selected complexes have been applied as FEBID precursors. A testing apparatus was custom designed for the test of the precursors at high temperatures. The study of composition and growth rate of the obtained deposits has revealed that triazole-based complexes and trifluoromethyl ligands lead to the highest gold composition and highest growth rate.

The oxidation of gold(I) NHC species by means of *aqua regia* in gold(III) NHC compounds has led to the development of a straightforward oxidation procedure. In some cases, the procedure has caused a functionalization of the NHC backbone by substitution or addition of Cl.

Electrochemical studies on selected gold NHC complexes have demonstrated the stability of gold(I) and gold(III) species in a large potential range.

The presented work aims at expanding the current knowledge on FEBID precursors and define suitable ligands for precursor design.

# LIST OF COMPOUNDS
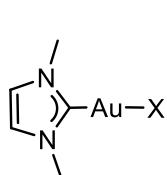
**1a** X = Cl
**2b**    Br
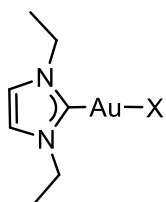
**2a** X = Cl
**2b**    Br
**2e**    $CF_3$
**2h**    NHC
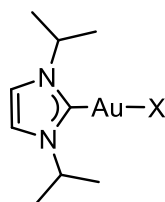
**3a** X = Cl
**3b**    Br
**3h**    NHC
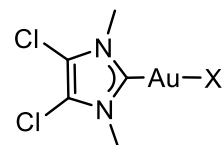
**4a** X = Cl
**4b**    Br
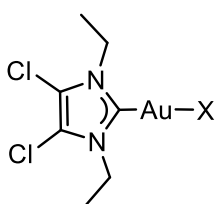
**5a** X = Cl
**5b**    Br
**5c**    I
**5d**    $CH_3$
**5e**    $CF_3$
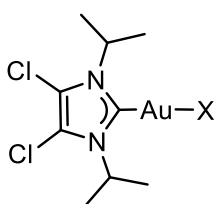
**6a** X = Cl
**6b**    Br
**6c**    I
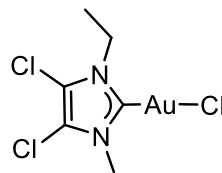
**7a**
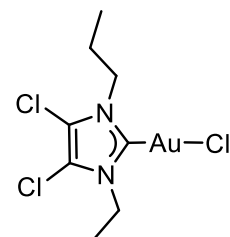
**8a**
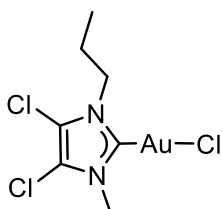
**9a**
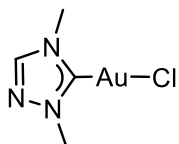
**10a**
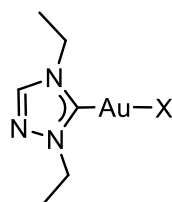
**11a** X = Cl
**11e**    $CF_3$
**11h**    NHC
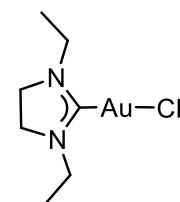
**12a**
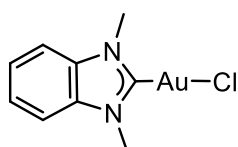
**13a**
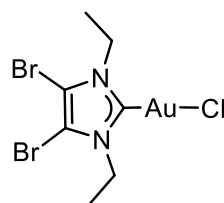
**14a**
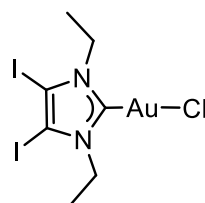
**15a**

The list of compounds is an aid for the reader and is not a complete list of discussed compounds.

# Conferences and Academic Contributions

**Low energy Electrons in Emerging nanofabrication methods, Online Event, 23-24 March 2021**
*Synthesis and pre-screening of gold(I) N-Heterocyclic Carbene FEBID precursors,* Oral presentation
Cristiano Glessi, Mats Tilset
*FEBID testing of novel gold NHC precursors*, Oral presentation
Cristiano Glessi, Aya Mahgoub, Cornelis W. Hagen, Mats Tilset

**Research stay (secondment) in TESCAN Brno s.r.o. under the supervision of Doc. Jaroslav Jiruše, Brno, Czech Republic, 2 December 2019 – 7 February 2020**
*FEBID testing of gold(I) NHC complexes on commercial instruments*, 2 months research stay

**2nd ELENA conference, Leuven, Belgium, 4-6 September 2019**
*Synthesis, characterization and investigation of gold(I) NHC complexes as FEBID precursors*, Oral presentation
Cristiano Glessi, Aya Mahgoub, Cornelis W. Hagen, Mats Tilset

**3rd ELENA Technical Training School, FEBID and related techniques, Darmstadt, Germany, 15-17 April 2019**
*Towards more volatile gold NHCs*, Oral presentation
Cristiano Glessi, Mats Tilset

**Research stay (secondment) in the group of Prof. Cornelis W. Hagen – Delft University of Technology, Delft, The Netherlands, 8 April-8August 2019**
*FEBID testing of gold(I) NHC complexes and development of testing apparatus*, 4 months research stay

**34. Organisk Kjemisk Vintermøte, OKV34, Skeikampen, Norway, 10-13 January 2019**
*Volatile gold(I) complexes for material applications,* Oral presentation
Cristiano Glessi, Volodymyr Levchenko, Mats Tilset

**21st Landsmøte i Kjemi, Lillestrom, Norway, 16-18 October 2018**
*Synthesis and characterization of gold complexes for FEBID applications,* Poster presentation
Cristiano Glessi, Jakub Jurczyk, Ivo Utke, Mats Tilset

**1st ELENA conference, Warsaw, Poland, 29 September - 1 October 2018**

*Synthesis and Characterization of gold(I) complexes suitable as FEBID precursors*, Oral presentation and Poster presentation

Cristiano Glessi, Jakub Jurczyk, Ivo Utke, Mats Tilset

**2nd ELENA Technical Training School, EUVL and other lithography methods, Brno, Czech Republic, 27-30 August 2018**

*Synthesis and Characterization of gold(I) complexes suitable as FEBID precursors*, Oral presentation

Cristiano Glessi, Jakub Jurczyk, Ivo Utke, Mats Tilset

**GOLD 2018 conference, Paris, France, 15-18 July 2018**

**7th workshop on Focused Electron Beam Induced Processing, Modena, Italy, 10-13 July 2018**

*Thermal evaluation of potential FEBID precursors*, Poster presentation

Cristiano Glessi Jakub Jurczyk, Katarzyna Madajska, Iwona Szymanska, Ivo Utke, Mats Tilset

**33. Organisk Kjemisk Vintermøte, OKV34, Skeikampen, Norway, 11-14 January 2018**

*α-Diimines with a catechol backbone: synthesis and study of coordination chemistry to palladium(II)*, Poster presentation

Cristiano Glessi, Mats Tilset, Barbara Milani

**1st ELENA Technical Training School, all aspects of ELENA, Delft, The Netherlands, 13-17 November**

*Synthesis of gold(I) and gold(III) complexes suitable as FEBID precursors*, Oral presentation

Cristiano Glessi, Mats Tilset

**Kjemi Grand Prix, Oslo, Norway, 26 October 2017**

*Gull*, Oral presentation

Cristiano Glessi

# Publications

**Paper I**

*Organometallic Chemistry in Aqua Regia: Metal and Ligand Based Oxidation of (NHC)AuCl complexes*

Volodymyr Levchenko, Cristiano Glessi, Sigurd Øien-Ødegaard, and Mats Tilset

*Dalton. Trans.* **2020**, *49*, 3473-3479.

**Paper II**

*Vacuum vs Ambient Pressure Inert Gas Thermogravimetry: A Study of Silver Carboxylates*

Jakub Jurczyk, Cristiano Glessi, Katarzyna Madajska, Luisa Berger, Jeroen Ingolf Ketele Nyrud, Iwona Szymanska, Czeslaw Kapusta, Mats Tilset, and Ivo Utke

*J. Term. Anal. Calorim.* **2021**

**Paper III**

*Gold(I) N-heterocyclic carbene precursors for focused electron beam-induced deposition*

Cristiano Glessi, Aya Mahgoub, Cornelis W. Hagen, and Mats Tilset

*Beilstein J. Nanotechnol.* **2021,** *12*, 257–269

**Paper IV**

*Halogen Rich Gold(I) NHC Complexes: Design Principles for Increased Volatility*

Cristiano Glessi, Jeroen Ingolf Ketele Nyrud, David Wragg, and Mats Tilset

**Manuscript in preparation**

# Contributions

**Paper I**

Volodymyr Levchenko: Synthesis of Au(III) NHC complexes, writing of publication.

Cristiano Glessi: Synthesis of Au(I) NHC complexes, collaboration in synthesis of Au(III) NHC complexes. Writing of publication.

Sigurd Øien-Ødegaard: X-ray diffraction analyses.

Mats Tilset: Supervision and writing of publication

**Paper II**

Jakub Jurczyk: Vacuum-TGA experiments, data analysis, result discussion, writing of publication.

Cristiano Glessi: Design and testing of vacuum-TGA experiment, writing of publication.

Katarzyna Madajska: synthesis of precursors, writing of publication

Luisa Berger: data analysis, result discussion, writing of publication

Jeroen Nyrud: TGA experiments.

Iwona Szymanska: synthesis of precursors, writing of publication

Czeslaw Kapusta: Supervision and writing of publication

Mats Tilset: Supervision and writing of publication

Ivo Utke: Supervision and writing of publication

**Paper III**

Cristiano Glessi: Synthesis and characterization of Au(I) NHC complexes, development of testing apparatus. Deposition experiments and imaging in collaboration with Aya Mahgoub. Writing of publication.

Aya Mahgoub: Deposition experiments and imaging in collaboration with Cristiano Glessi. Growth rate quantification, writing of publication.

Cornelis W. Hagen: Supervision and writing of publication.

Mats Tilset: Supervision and writing of publication.

**Paper IV**

Cristiano Glessi: Experimental work. Results discussion and writing of publication.

Jeroen Nyrud: Collaboration in synthesis of Au(I) NHC complexes.

David Wragg: X-ray diffraction analyses.

Mats Tilset: Supervision and writing of publication.

# Graphical Abstracts

## Paper I



*11 examples
3-20 hours*
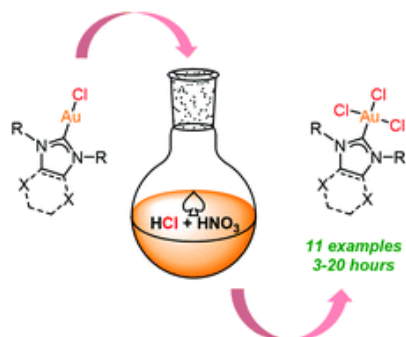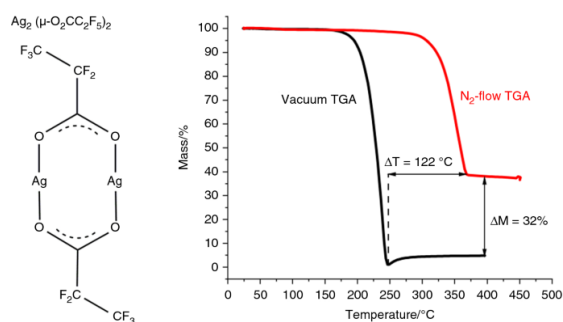
## Paper II



## Paper III



## Paper IV



| Gold(I) centre | Gold(III) centre |
|---|---|
| Bulky alkyl N-substituents (Et, iPr) | Small alkyl N-substituents (Me) |
| Halogens on the NHC backbone | Unsubstituted NHC backbone |
| Iodide ligand | Chloride or bromide ligand |
| Trifluoromehtyl ligand | Halogen ligands |
| Saturated NHC backbone | Unsaturated NHC backbone |

*Higher volatility*

Due to:
- Aurophilic interactions
- Electrostatic interactions
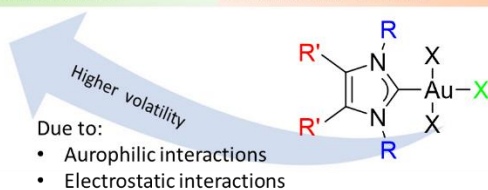
# Abbreviations

| | |
|---|---|
| A | Ampere |
| Å | Ångström ($10^{-10}$ m) |
| acac | Acetylacetonate |
| Ad | Adamantyl |
| ALD | Atomic layer deposition |
| Ar | Aryl, argon |
| br | Broad (NMR) |
| BSE | Backscattered electrons |
| Bu | Butyl |
| cif | Crystallographic information file |
| COSY | Correlation spectroscopy |
| Cp | Cyclopentadienyl |
| CV | Cyclic voltammetry |
| CVD | Chemical vapour deposition |
| Cy | Cyclohexyl |
| d | Days, doublet (NMR) |
| δ | Chemical shift (NMR) |
| DAC | N,N'-diamidocarbene |
| DCM | Dichloromethane |
| DD | Dipolar dissociation |
| DEA | Dissociative electron attachment |
| DI | Dissociative ionization |
| EBID | Electron beam induced deposition |
| EDX | Energy-dispersive X-ray spectroscopy |
| EI-MS | Electron ionization mass spectrometry |
| equiv. | Equivalent(s) |
| ESI-MS | Electrospray ionization mass spectrometry |
| Et | Ethyl |
| eV | Electronvolt |
| FEBID | Focused electron beam induced deposition |
| FEBIP | Focused electron beam induced processing |
| GIS | Gas injection system |
| h | Hour(s) |
| hfac | hexafluoroacetylacetonate |
| HBHC | H-bond supported heterocyclic carbene |
| HMBC | Heteronuclear multiple bond correlation (NMR) |
| HRMS | High resolution mass spectrometry |
| HSQC | Heteronuclear single-quantum correlation (NMR) |
| i | Iso |
| I | Imidazole |
| $J$ | Coupling constant (NMR) |
| KHMDS | Potassium bis(trimethylsilyl)amide |
| L | Neutral two electron donor ligand |
| M | Metal, molar |

| | |
|---|---|
| m | Multiplet |
| m/z | Mass-to-charge ratio (MS) |
| Me | Methyl |
| MW | Microwave |
| n | Normal |
| NAC | N-acyclic carbene |
| ND | Neutral dissociation |
| NHC | Nitrogen heterocyclic carbene |
| NMR | Nuclear magnetic resonance |
| OAc | Acetate |
| ORTEP | Oak Ridge thermal ellipsoid plot |
| Ph | Phenyl |
| ppm | Parts per million (NMR) |
| Pr | Propyl |
| q | Quartet (NMR) |
| R | An organic group |
| r. t. | Room temperature |
| s | singlet |
| SE | Secondary electrons |
| SEM | Scanning electron microscopy, scanning electron microscope |
| $SMe_2$ | dimethylsulfide |
| t | Tert, Triplet (NMR) |
| T | Temperature |
| tfac | trifluoroacetylacetonate |
| TGA | Thermogravimetric analysis |
| THT | tetrahydrothiophene |
| tpy | 2-(p-tolyl)-pyridine |
| UHV | Ultra-high vacuum |
| X | Anionic one electron donor ligand |
| XRD | X-ray diffraction analysis |

# Chapter 1.

# Introduction

## *1.1 Focused Electron Beam Induced Deposition (FEBID)*

### *1.1.1 General introduction to gold*

Gold has been since the dawn of civilization the most searched after metal, due to its colour, stability, ductility and preciousness. In the eyes of a chemist, these properties are transformed in relativistic effects, resistance to oxidation and biocompatibility. While gold complexes such as $[Au(CN)_2]^-$ and $[Au(CN)_4]^-$ were known historically in the extraction process of gold,[1] from the discovery at the beginning of the last century of organogold,[2] the precious metal has seen a booming of interest in chemistry, from catalysis,[3,4] to medicine.[5,6] Furthermore, the development of nanotechnology has seen the generation of a great array of application for gold-based nanoparticles and more in general nanomaterials, such as in medicine,[7] diagnosticts,[8] photothermal therapy,[9] sensing[10] and catalysis.[11] From jewellery, to nanomaterials, gold is a fundamental metal in making our everyday life easier and prettier.

A large array of gold nano materials can be achieved due to a wide variety of production techniques, such as Chemical vapour deposition (CVD)[12] and Atomic Layer Deposition (ALD)[13] to obtain thin films, Laser ablation[14] or chemical synthesis[15] for gold nanoparticles and Focused Particle Beam Induced Processing[16,17] for standalone gold nanostructures.

### *1.1.2 Focused Electron Beam Induced Deposition*

In order to produce three dimensional and standing nanostructures, a suitable production approach should be taken. In recent years the additive manufacturing (3D printing) of plastic, metallic and ceramic components have made its way not only to industrial production but also to the home market.[18] These 3D structures are produced with the aid of a laser that causes the deposition of the desired material. In a similar fashion, we could conceptually access nanometered sized structures. 3D free standing nanostructures can be achieved through Focused Electron Beam Induced Deposition (FEBID).[19-26]

In FEBID the electron beam of a scanning electron microscope (SEM) is focused on a substrate. The substrate is covered in physisorbed precursor molecules, generally an organometallic volatile compound, and the coverage is produced and refreshed by injection of precursor through a Gas Injection System. Under irradiation the physisorbed precursor is partially fragmented, with a loss of one or more ligands, and as a result, chemisorbed on the substrate;. The volatile byproducts desorb and are pumped away under the vacuum of the SEM chamber, while the solid deposit is grown through prolonged or repeated exposition to e-beam, allowing for obtaining the desired 3D structure (Figure 1.1).[21]
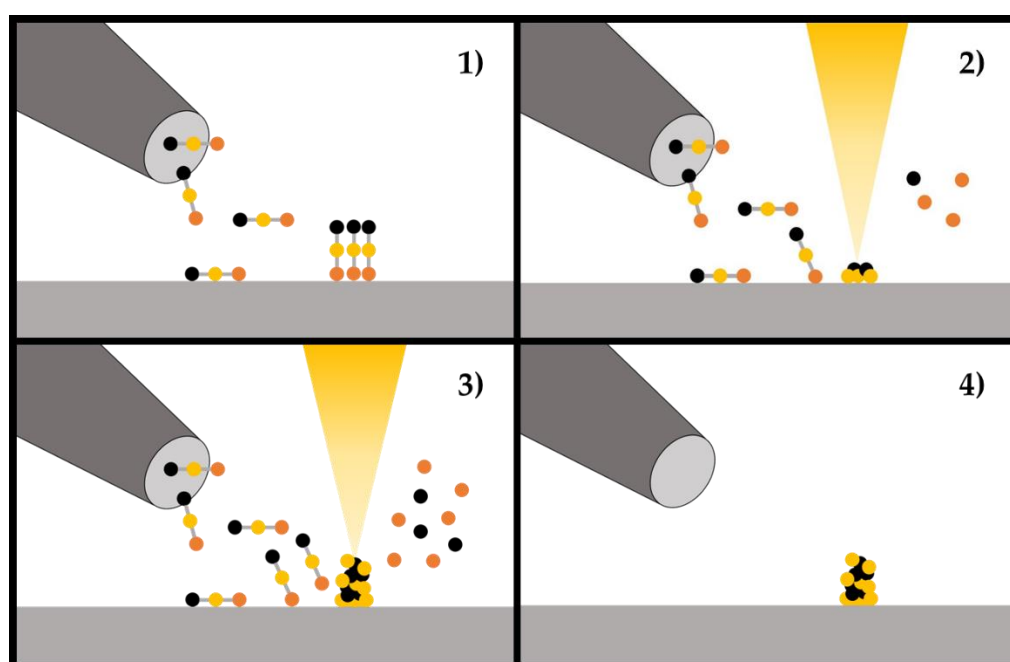


**Figure 1.1.** Schematic representation of the FEBID process. 1) Injection of precursor and physisorption, 2) exposure to the electron beam, and fragmentation 3) growth of vertical deposit, 4) stop injection of precursor and electron exposure.

FEBID is a mask-less nanofabrication technique that allows for the production of 3D vertical nanostructures. Its features are highly desirable for several applications such as lithography mask repair,[27] fabrication of nanoconnectors[28] and other nanodevices used in plasmonics,[29] optoelectronics,[30] gas and strain sensors,[31-33] AFM probe tips[34-36] and for magnetic[37,38] and biomedical[39] applications. The novelty introduced by FEBID is not only that 3D structures can be directly obtained, but they can be obtained on a sub 20 nanometer scale resolution,[40] down to 3 nm.[41] Important drawbacks are present, all linked to each of the components involved in the deposition process. Further development of each component separately and in

combination is highly needed to take FEBID from an interesting technology to a full scale industrial application.

### 1.1.3 Main components involved in FEBID: electrons and precursor molecules

In FEBID the focused electron beam used is in the energy range of 2-30 keV and the current is in the range of 10-200 pA.[20] The electrons of the primary beam are however not efficient in the decomposition of adsorbed precursor molecules due to a very small interaction cross section; the decomposition is instead mainly caused by low energy electrons in the range of 0-50 eV,[42] mainly comprised of secondary electrons (SE). Such energy is more suitable to excite and break chemical bonds, through various mechanisms, such as dissociative electron attachment (DEA), dissociative ionization (DI), dipolar dissociation (DD) and neutral dissociation (ND).[43] Backscattered electrons (BSE),[42] that are produced by elastic scattering, meaning that these electrons do not lose kinetic energy and are thus not very suitable for dissociating precursor. However, BSE can subsequently undergo inelastic scatterings and also produce reactive SE. The lateral range in the substrate of the BSE's escaping the surface is highly dependent on the energy of the primary electron beam. Due to the existence of both these electrons in FEBID it is normally observed the presence of co-deposition around the desired structure, and enhanced horizontal growth, caused by SE originated from the primary beam and by BSE (so called "halo" effect).

The other component involved in the deposition is the precursor molecule. The precursor is generally an organometallic compound that can be volatilized in the range of pressure and temperatures that are used in the FEBID process.[44] The pressures normally are the ones present in the vacuum chamber of a SEM, in the range of high vacuum ($10^{-5}$/$10^{-6}$ mbar). Several instances of EBID surface studies in high vacuum have been also reported,[45,46] and pressure plays a key role in the kinetics of the precursors and in the composition of the final structure. In fact, an ultra-high vacuum ($10^{-9}$/$10^{-10}$ mbar) can lead to more pure deposits, since co-depositing material (normally lighter than the desired one) can be more efficiently removed during deposition.[47]

Temperature is also an important factor both in the volatilization and deposition processes. Temperature and injection of the precursor molecules are controlled with a Gas Injection System (GIS).[21,48] A GIS is a reservoir containing precursor molecule that can be heated and is

equipped with a nozzle and needle in order to locally deliver precursor on the substrate. In most cases GISs have also the possibility of being opened and closed, to control the time frame of precursor delivery.[48]

In commercially available GISs the temperature range is limited up to 90 °C, and most of commercial FEBID precursor volatilize in a small temperature range around room temperature in high vacuum. Custom-built GISs with the aim of increasing the temperature window have been reported.[49-51] The necessity for higher temperatures poses several limitations, mainly in the control of the precursor flow, in the interactions between precursor and substrate and in the heating in close proximity to the electron beam pole piece. The precursor molecule should adsorb on the substrate and create a mono or multi layer coverage that is refreshed by the GIS. If the precursor needs to be heated up at high temperatures it will immediately condense when in contact with a room temperature substrate.[52] Variation of the temperature of the substrate have an influence not only on the coverage but also on the composition of the obtained deposits, with an increased purity at higher temperature.[53-55]

The two components involved in the deposition, precursor and secondary electrons, dictate the regimen of the deposition; as it happens in chemistry, an irreversible reaction with two reagents will be dependent on the limiting reagent. In FEBID similarly a precursor or electron -limited regime can be obtained.[20-22,56] Generally, the best composition in FEBID is obtained at the edge of these two regimes, when a balance of suitable electrons and adsorbed precursor is reached.[57]

Post-deposition treatment of the obtained deposits is used to further modify the composition of the structures (Figure 1.2). Exposure to heat (annealing),[58,59] high electron doses[21,60,61] or chemical oxidants[62] or reductants, often in combination,[63-68] causes a purification of the structure due to removal of co-deposited material. This method however, causes a variation of the morphology and shape of the structure[27] and a significant shrinkage.[64]
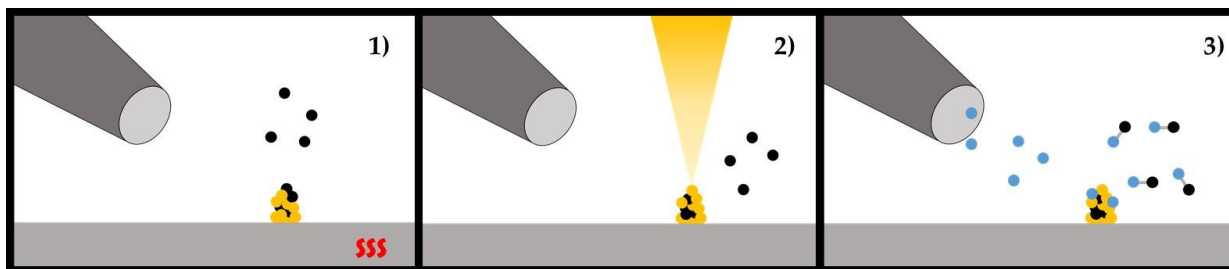
**Figure 1.2.** Post-deposition treatments of FEBID structures: 1) annealing, 2) post-deposition exposure, 3) chemical oxidation; often two of these treatments are combined.

### 1.1.4 FEBID precursors

The properties of the FEBID precursor molecule is fundamental to all aspects of the deposition process.[44,69] The target properties are well defined and can be summarized in few clear points.

The precursor molecule should:

- Be volatile in an acceptable range of pressure and temperature;
- Physisorb on the substrate;
- Be sensitive to dissociation with the electron beam;
- Decompose in a clean manner to the desired products;
- Be compatible with used materials;
- Be cheap and easy to make;
- Be easy to store and handle.

It is necessary to find a compromise between volatility, stability and reactivity to electron irradiation of the molecule.[44] This has then to be translated in a structure that can lead to deposition of the desired material.[70] Most FEBID precursors are organometallic complexes designed with the aim to obtain pure metal deposits. Normally the metal content is quite limited, and the major contaminant of the obtained deposits is carbon. Thus, it would be better to use the most limited number of carbon atoms possible in the design of the molecule: this is a hard feature to implement, as it directly affects the stability of the precursor.[70] In the early days, most FEBID precursors were taken from the already well established library of CVD precursors.[71] The necessary features for a CVD precursor in fact overlap for the most with the ones for a FEBID precursor, since both classes of compounds have to show good volatility, thermal stability and interactions with a substrate. However, while in FEBID the decomposition is carried out by electrons, in CVD the decomposition of the precursor

molecules is carried out thermally and chemically, often with the use of a reducing or oxidizing agent.[72] Thus, in CVD, regardless the composition of the precursor, high percentages of metal content can be achieved due to the fact that carbon and nitrogen are oxidized and removed as volatile species. CVD is also more suitable for a larger range of precursors since the delivery of gaseous compound can take place at temperatures higher than 100 °C. The most well-known example of CVD precursor applied for FEBID is the Pt(IV) complex MeCpPtMe[3]. While in CVD MeCpPtMe[3] leads to thin film deposits of pure platinum,[73] in FEBID metal content up to 20% is obtained,[53] with the rest of the deposit is composed of carbon.

Since few CVD precursor have led to efficient FEBID precursors, such as silver carboxylates,[49,50] the design of organometallic complexes selectively for FEBID has developed. These compounds are smaller in size, with the presence of smaller organic ligands and almost in every case of at least one inorganic ligand.

### 1.1.5 Ligand-based design of FEBID precursors

In the design of a FEBID precursor, the metal centre can be considered constant, with the notable exception of its oxidation state. Most of the properties of the precursor depend on the employed ligands.

Polyhapto ligands such as cyclopentadienyl and allyl groups have been employed in Pt, Ni and Ru precursors.[46,53,74] All these ligands have shown in the EDX analysis of the obtained deposits to heavily co-deposit, leaving a high at.% of carbon in the obtained structures. Similarly, chelating ligands such as acetylacetonates have also shown in Cu and Au complexes to leave low purity deposits, with co-deposition of C and O.[17,29,71,75-82] In the case of fluorinated acetylacetonate ligands, such as trifluoroacetonate and hexafluoroacetonate, F is mostly removed from the resulting deposits, as demonstrated by UHV surface studies on Cu, Pt and Pd complexes (Figure 1.3).[83]
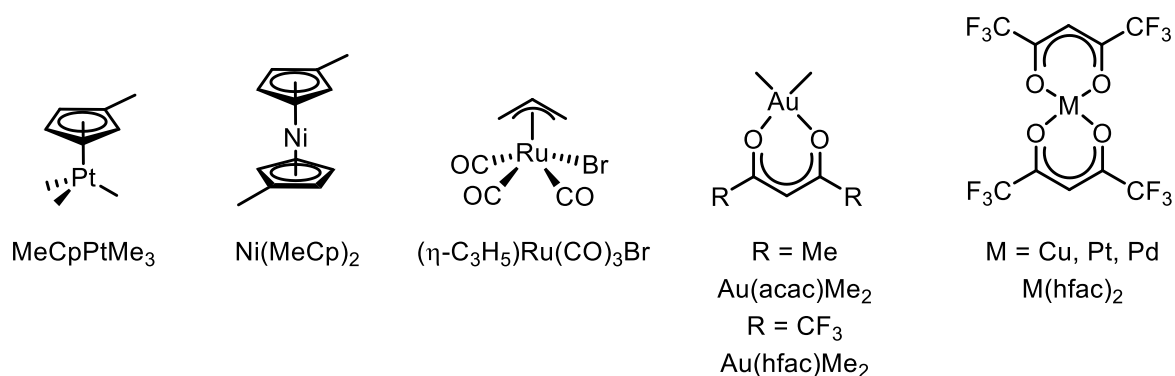
**Figure 1.3.** FEBID precursors with Polyhapto and polydentate ligands.

Monohapto alkyl ligands, like methyl and trifluoromethyl, are instead partially or totally removed during the deposition process. In $SiMe_4$ almost all the carbon present in the precursor is incorporated,[84] while for $PbEt_4$ a metal at.% of 46% is reported, consistent with an efficient removal of the alkyl ligands.[85] The methyl ligands in $MeCpPtMe_3$ are partially removed during electron irradiation, as exemplified by UHV studies.[45] The trifluoromethyl group is instead not removed during electron irradiation, as shown in Au isocyanide trifluoromethyl precursors.[86] Silver carboxylate complexes have led to deposits with a metal at.% higher than 70%, showing a high degree of removal of the carboxylate ligands (Figure 1.4).[49-52] In the copper pentafluoropropionate precursor $Cu_2(O_2CC(Me)_2Et)_2)_4$, around 80% of the ligand material is lost during electron-induced dissociation.[51] In all cases fluorine is mostly removed from the deposits, making perfluorinated alkyl groups suitable for FEBID.[83]
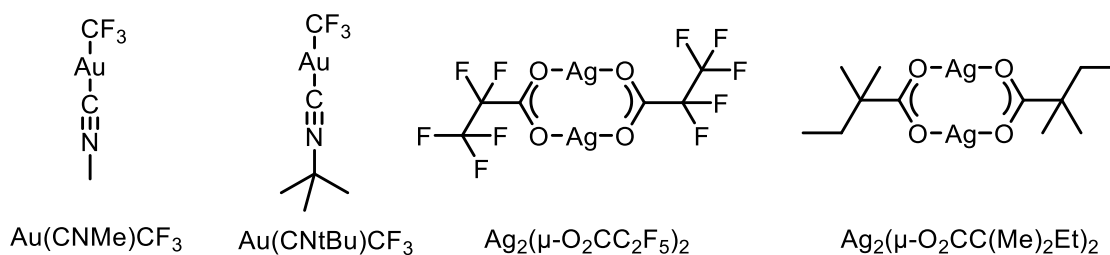


**Figure 1.4.** FEBID precursors with organic ligands.

Small inorganic ligands such as CO and $PF_3$ co-deposit only in limited amounts. The homoleptic carbonyl complexes $Fe(CO)_5$,[87] $Co_2(CO)_8$,[88] $Mo(CO)_6$,[89] $W(CO)_6$[90] and the heteroleptic complexes $Co(CO)_3NO$,[91] $(allyl)Ru(CO)_3Cl$, $(allyl)Ru(CO)_3Br$,[74] $Au(CO)Cl$,[92] $Pt(CO)_2Cl_2$,[47] $Pt(CO)_2Br_2$[47] all showed a limited amount of carbon and oxygen incorporation. The trifluorophosphine ligand led instead to phosphorus contamination in the deposits obtained from the homoleptic complex $Pt(PF_3)_4$ of around 17 at.%.[53,93,94] Similarly for the nickel

complex Ni(PF$_3$)$_4$ only 40% at.% of metal was achieved.[95] No ligands residues were obtained for the gold complex Au(PF$_3$)Cl.[96-99] The only recorded use of ammonia as a ligand is limited to cis-Pt(NH$_3$)$_2$Cl$_2$ and it has been observed that the NH$_3$ moiety is quickly removed under electron irradiation, leading to the deposition of [PtCl$_2$] and a further purification by the co-injected ammonia (Figure 1.5).[100]



Fe(CO)$_5$     Mo(CO)$_6$     W(CO)$_6$     Co(NO)(CO)$_3$

COAuCl   Pt(CO)$_2$Cl$_2$   Pt(CO)$_2$Br$_2$   Pt(PF$_3$)$_4$   Pt(NH$_3$)$_2$Cl$_2$
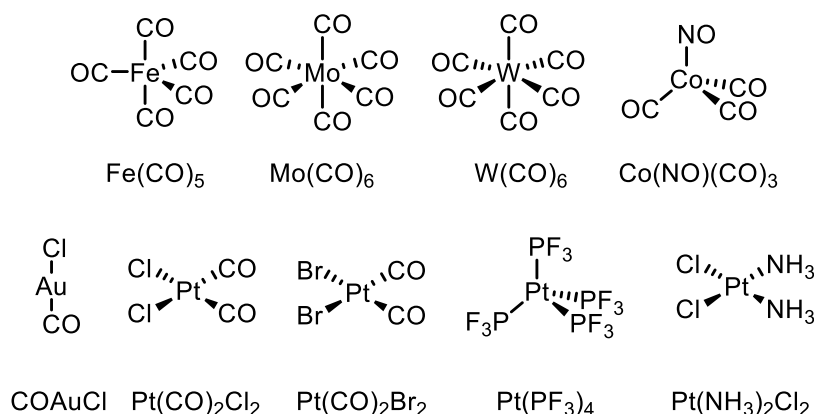
**Figure 1.5.** FEBID precursors with inorganic ligands.

Metal halides are generally not very suitable FEBID precursors. The fragmentation of the M-X bonds produces corrosive halogen products that can cause reactivity with the instrument and etching of the substrate,[101] while partial fragmentation was observed with SnCl$_x$ [102] precursors, thin films that are not stable to air were produced.[103] In contrary,WCl$_6$ and WF$_6$ led to appropriate deposits.[104] Heteroleptic complexes bearing one or more halogen ligands have shown to be suitable FEBID precursors. The effect of the variation of the halogen has been so far explored only for Pt(CO)$_2$Cl$_2$ and Pt(CO)$_2$Br$_2$,[47] and a higher purity of the deposit was obtained with the chloro-based precursor, 20.2 Pt at.% vs. 12.1% for the bromo-based compound.[47]

### 1.1.6 Gold FEBID precursors

Gold FEBID precursors have had a similar development to the other metal precursors. The first precursors were taken from the library of CVD precursors, such as dimethylgold acetylacetonate,[29,77-79] dimethylgold trifluoroacetylacetonate,[17,78,80,81] and dimethylgold hexafluoroacetylacetonate.[71] All these compounds however lead to a low to medium gold at.% in the range of 2-40% (Figure 1.6). Especially for gold, the high purity is fundamental for the production of photonic and plasmonic devices.[29,81,105,106] With the co-injection of precursor and

of an oxidant agent (e.g. water) the obtained Au% was increased for the precursor dimethylgold trifluoroacetylacetonate at 91%.[107]
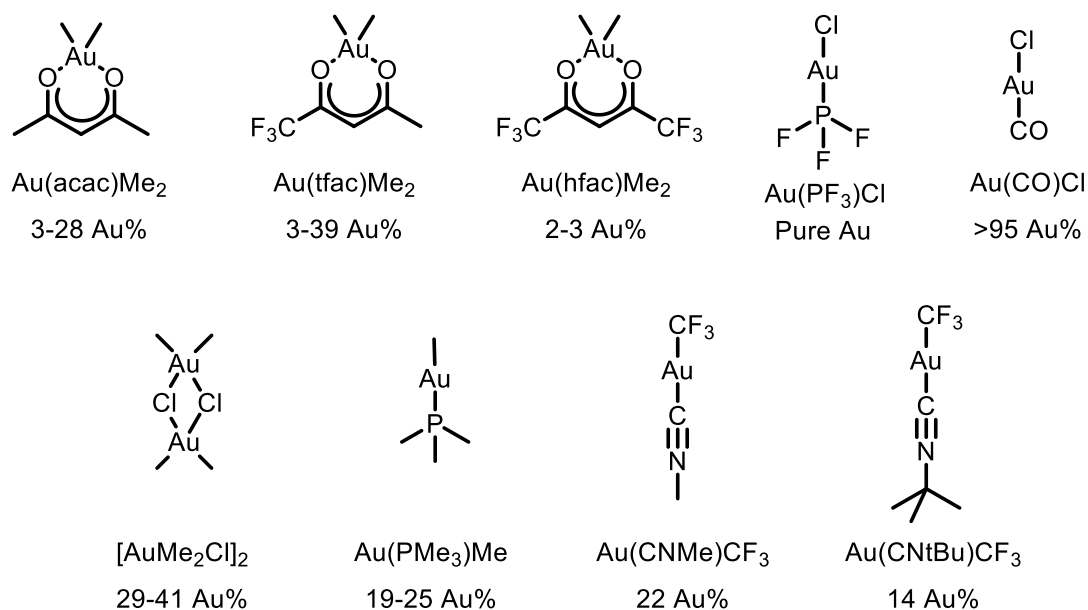


**Figure 1.6.** Previously reported FEBID precursors and indicative gold atomic % of the obtained FEBID structures.

To avoid any carbon contamination in the grown structures purely inorganic gold complexes have been studied, namely gold(I) trifluorophosphine chloride[96-99] and gold(I) carbonyl chloride.[92] While for the latter a composition of >95% was obtained, for the Au(PF$_3$)Cl precursor pure gold was obtained. Unfortunately, both compounds showed high instability and a tendency to decompose under storage or use, hence the applicability of these complexes was limited. It was then shown that more stable FEBID precursors were obtained by hybrid organic and inorganic complexes by the experiments of Van Dorp *et al*. on dimethyl gold(III)chloride[108] and methyl-trimethylphosphine gold(I).[70,108] Of the two the gold(III) precursor led to the best composition, with an at.% of 29-41% gold. Recently a series of gold(I) alkylisocyanide complexes were reported, that show to be suitable as FEBID precursors.[86] These complexes present a trifluoromethyl group as the formally negatively charged ligand, and led to at.% of gold in the range of 14 to 22%.[86] In the same study also the effect of a small substitution on the neutral ligand present on gold, in this case alkylisocyanides, was studied and it was observed how the nature of the alkyl substituent effect highly the volatility and thermal stability of the compound. When the alkyl group is a methyl the volatility and stability of the complex is more limited than when the substituent is an isopropyl group.[86]

While several gold(I) and gold(III) complexes led to suitable FEBID precursors, several other tested compounds led to negative results, such as Au(SMe$_2$)Cl and Au(PMe$_3$)Cl.[108] Both these compounds decomposed before volatilization, leading to deposition caused only by ligand fragments of the complexes. These last two compounds, together with the very unstable Au(PF$_3$)Cl and Au(CO)Cl, show a similar pattern in the coordination sphere: a chloride as the negatively charged ligand X$^-$ and a weakly coordinating inorganic neutral ligand L. This combination renders the complexes very unstable in the conditions involved in FEBID. Exemplarily, the substitution of a Cl with a methyl group on the Au(PMe$_3$)Cl complex, led to a stable and volatile FEBID precursor (Figure 1.7).[70]
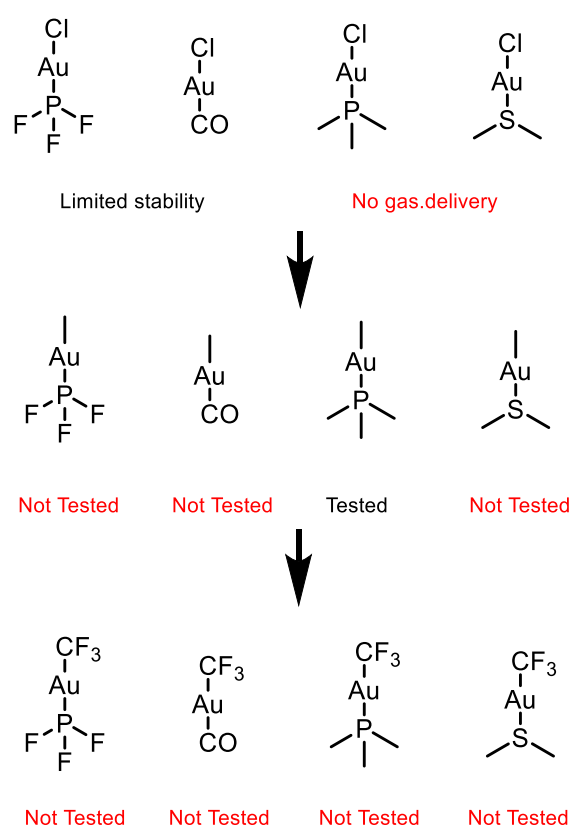


**Figure 1.7.** Ligand variation in possible gold(I) FEBID precursors.

Isocyanide-based complexes bear a strong C-Au bond between the neutral ligand and the metal centre.[86] On this class of complexes it was observed that the variation of X$^-$ with different halogens, going from Cl to Br to I, led to more volatile complexes, while having no great effect on their thermal stability. This observation is quite counterintuitive, since the introduction of a heavier halogen induces a great increase in the molecular weight of the precursor, which would expectedly lead to a decrease in volatility.[109] It was though observed that in the solid

state packing of the gold(I) species studied, aurophilicity[110] was a substantial contribution to the intramolecular packing of the molecules, dictating the packing pattern to minimize gold-gold distances. With the introduction of heavier (and thus bigger) halogens, the gold-gold distance had to be extended thus decreasing the aurophilic interaction and packing energy of the molecules. However it is not known if this observation can be extended to different classes of precursors. We can observe that in the case of the presence of a strong bond between gold and L, the nature of X$^-$ can be varied in order to tune the volatility of the compound with limited effect on the stability of the obtained complexes. The best results in volatility were obtained with the complexes bearing trifluoromethyl groups as X$^-$.[86] Also L in this case can be varied, in order to increase volatility and thermal stability. In the isocyanide ligands, the best volatility was obtained with a bulky tert-butyl substituent for the same reasons mentioned above.

## 1.2 Gold(I) NHC complexes

### 1.2.1 Nitrogen heterocyclic carbenes (NHCs)

A carbene is a neutral species containing a divalent carbon atom with two unshared valence electrons. In other terms, carbenes have both an incomplete electron octet and a coordinative unsaturation, which are both factors that contribute to their high instability. Arduengo *et al.* reported for the first time in 1991 a highly stable carbene incorporated in a nitrogen heterocycle (Scheme 1.1).[111] This first discovery gave rise to the development of NHC (N-heterocyclic carbenes) as one of the most extensively studied class of organic compounds in the last decades.[112-118] As often stated NHCs are a great example of an "academic curiosity" turned into a "powerful tool".[119]
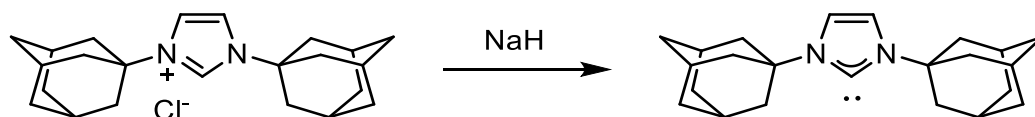


**Scheme 1.1.** Formation of the IAd stable carbene.

The high stability of NHCs can be described by different electronic and steric factors. The HOMO and LUMO of NHCs point to the presence of a singlet state of the carbene with a sp$^2$ lone pair and an empty p$_z$ orbital, a state highly favoured by the conformation forced by the NHC ring.[120] The presence of $\alpha$-Nitrogens stabilizes electronically the carbene carbon by means

of σ-electron withdrawal from the sp² lone pair and π-electron donation to the empty $p_z$ orbital (Figure 1.8) (inductive and mesomeric effects[117,120]). This push-pull interaction will not be the only one that we will see in the NHC world, and a similar interaction will be discussed upon the coordination of the carbene to a metal centre. The π-electron donation can be further enhanced by the introduction of electron donating substituents on the nitrogens. A further stabilization comes from the steric hindrance of the N-substituents, that in the case of IAd are adamantyl groups. Such hindrance prevents the dimerization of the carbenes into the olefinic product.[121]
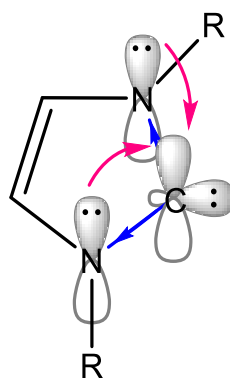


**Figure 1.8.** π-electron donation (pink) and σ-electron withdrawal (blue) on a imidazole-based carbene. On the carbene carbon we can see the empty $p_z$ orbital and the sp² lone pair.

The high development of the field of NHCs led to the synthesis and isolation as stable carbenes of a plethora of different cyclic compounds, which move away considerably from the structure of the imidazole-based adamantyl (IAd) NHC. A series of example structures are reported in Figure 1.9. Practically all the features of the NHC can be heavily modified, introducing an enormous structural variability.

In first instance, the formation of a carbene is not relegated to the C² position of the ring, but it can be obtained in other positions, thus forming what is known as an abnormal carbene.[113,122] Similarly, also the presence of two nitrogen substituents is not strictly necessary and other heteroatoms that can be used are oxygen or sulphur. Alternatively, one of the Nitrogens can be substituted with a carbon atom, giving rise to the class or cyclic alkyl amino carbenes (CAACs).[123] In all the discussed complexes though the heteroatomic ring is stabilized by aromaticity. This is also not a necessary factor for NHCs, since the saturated compound SIMes have been isolated by Arduengo *et al.*[124] Other important handles of variation are the nitrogen substituents (called also nitrogen wings), where a stable free carbene was isolated from the

highly bulky Ad substituents all the way down to simple methyl substituents.[125] Other variations can be introduced on the backbone of the ligand, with for example, the substitution of a carbon with a nitrogen (triazole-based NHCs), the substitution of the backbone protons with heteroatoms (N,N'-diamidocarbenes, DAC),[126] and the introduction of an aromatic ring (benzimidazole-based NHC). Finally, a significant link in structure and properties can be found between NHCs and other classes of persistent carbenes, that, even if structurally similar to NHCs, lack in the presence of a ring. Nitrogen acyclic carbenes (NACs)[127,128] and hydrogen bond-supported heterocyclic carbenes (HBHCs)[129,130] have recently been used as alternatives to their cyclic counterparts.
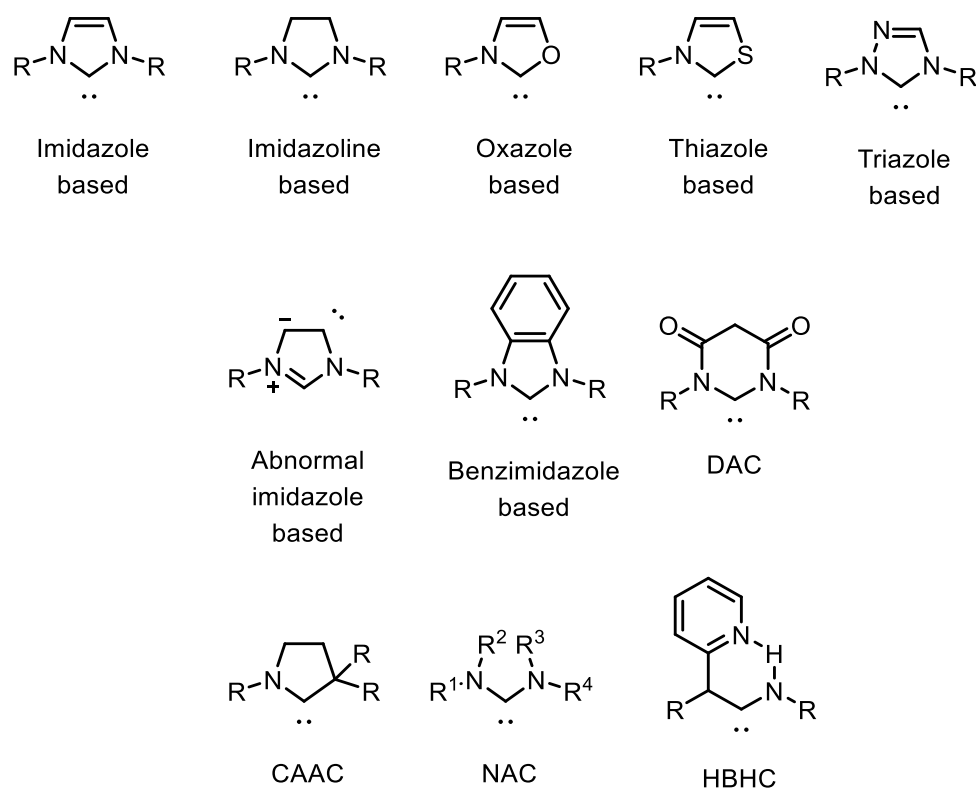


**Figure 1.9.** Selected examples of N-heterocyclic carbenes and derivatives.

NHCs have found a wide series of applications, but mainly have been used as organocatalysts[131-133] and as coordination ligands to transition metals and p-block elements.[134,135]

*1.2.2 Metal NHC complexes*

d-Metal NHC complexes pre-date the free carbene NHCs previously discussed. In fact the first NHC complexes were produced independently by Wanzlick and Öfele in 1968.[136,137] The ligand capability of the NHCs is primarily dependant on the presence of the $sp^2$ lone pair, that has a

strong σ-donor ability. Furthermore, the presence of an empty π orbital (p$_z$) allows for π-backdonation from the metal centre (Figure 1.10). This push-pull effect highly stabilizes the C-M bond in NHC complexes, making them highly stable metal-ligand complexes. Generally, NHCs have been compared to the predating phosphine ligands, that display some similarities,[138] since also for phosphines a lone pair is responsible for the σ-donation towards a σ-accepting orbital of the metal centre. The properties of these two class of compounds are however quite different, and these differences are commonly measured by steric and electronic factors, the "buried volume"[139-142] for NHC based complexes, Tolman's cone angle[143] for phosphine based complexes, and the Tolman Electronic Parameter (TEP) for electronic effects.[144]
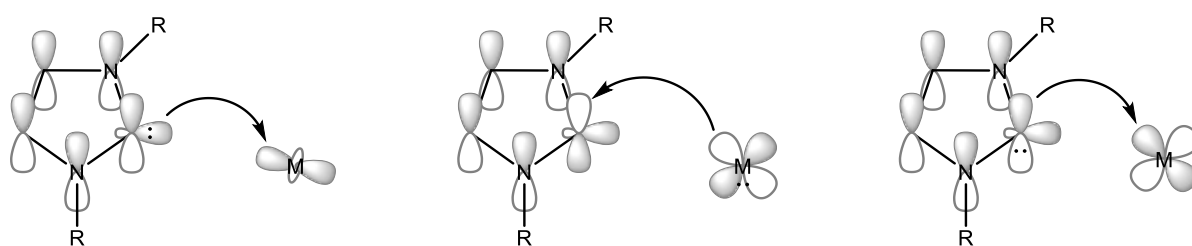


**Figure 1.10.** Main interactions involved in NHC-metal bonding: σ-donation (left), π-backdonation (centre), π-donation (right).

NHC complexes of most metals have been successfully synthesized, a testament to the high flexibility and usability of this class of ligands.[145-147] Metal NHC complexes have already found several applications, especially as homogeneous catalysts[148] and drugs.[149]

### 1.2.3 Gold(I) NHC complexes

Gold has been always considered by chemists as one of the most inert metals.[150] Its resistance to oxidation and overall low reactivity has hindered the research on possible applications of gold(I) and gold(III) species. At the start of last century the first stable gold complexes were studied, a discovery that later led to a wide spread of use of gold complexes in organometallic chemistry,[151] including carbene-based complexes.[152] One of the most well known classes of gold complexes is gold(I) NHC complexes of general formula (NHC)AuX. Gold(I) complexes are linear complexes presenting a NHC moiety as a two electron neutral two electron donor ligand (L) and an anionic one electron donor ligand (X) in *trans*, that is most commonly an halogen.[153]

Gold(I) NHC complexes can be obtained through several synthetic routes;[146,147,154-159] the precursor to the organic ligand is an azolium salt, specifically an imidazolium salt in the example in Scheme 1.2. The gold centre is introduced by the use of a gold(I) complex that presents a labile sulphur-based ligand such as tetrahydrothiophene (THT) or dimethylsulfide (DMS). To allow for the coordination of the gold centre on the NHC moiety three main synthetic pathways are reported. In first instance a strong base (such as NaH, KHMDS, KOtBu) can be used to deprotonate the salt precursor and form in situ of a NHC free carbene, that then readily reacts with the gold(I) precursor. An inert environment is needed to avoid reactivity of the in situ generated free carbene with air or moisture, and moderate to low yield are achieved with this route.[160] The formation of a free carbene can lead to the formation of unwanted dimers,[161] that is partially prevented by steric hindrance introduced by the N-substituents. Alternatively, a weak base can be used;[162-164] in this case the imidazolium salt can be first reacted with the LAuCl complex to form a $Im^+AuClX^-$ salt which is then reacted with a weak base to form the target (NHC)AuX complex.[162,163] The obtained complex presents as the anionic ligand the counterion of the imidazolium anion. In alternative silver oxide can easily coordinate on the imidazolium salt to form a (NHC)AgX species, that can be transmetalated to produce the relevant gold(I) complex.[160] Apart from the sacrificial use of silver[165] or copper,[166] no other major drawbacks are reported for this pathway. The use of silver nitrate in combination with a weak base can facilitate the isolation of the silver species for a two-step procedure.[163]
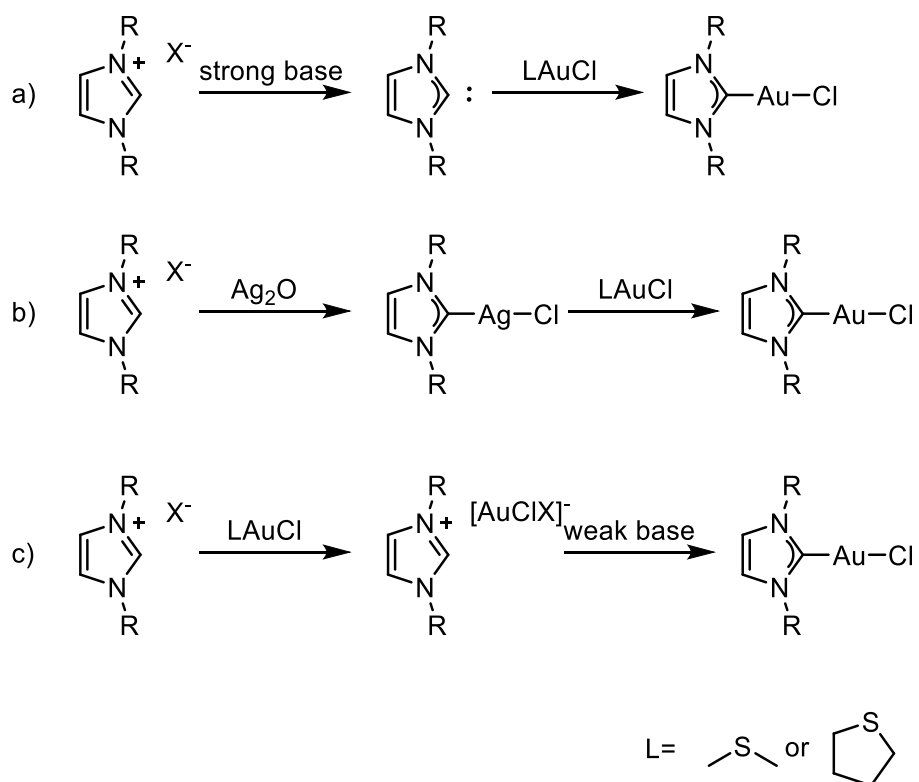
**Scheme 1.2.** Main synthetic pathways for the synthesis of gold(I) NHC complexes.

Cationic [Au(NHC)$_2$]$^+$ complexes (Scheme 1.3) can be obtained by transmetalation of the corresponding silver complexes[167-169] or by employing 1 equiv. of NHC precursor and 0.5 equiv. of the gold precursors.[170-173] Reactivity of metallic gold with imidazolium salts with weakly coordinating anions such as PF$_6^-$, BF$_4^-$, BPh$_4^-$ in presence of CuSO$_4$ also lead to the formation of [Au(NHC)$_2$]$^+$ species.[174] These complexes can also be synthesized electrochemically, by the corrosion of a gold electrolyte in a solution of the NHC ligand in its imidazolium salt form and electrolyte with low yields.[175]
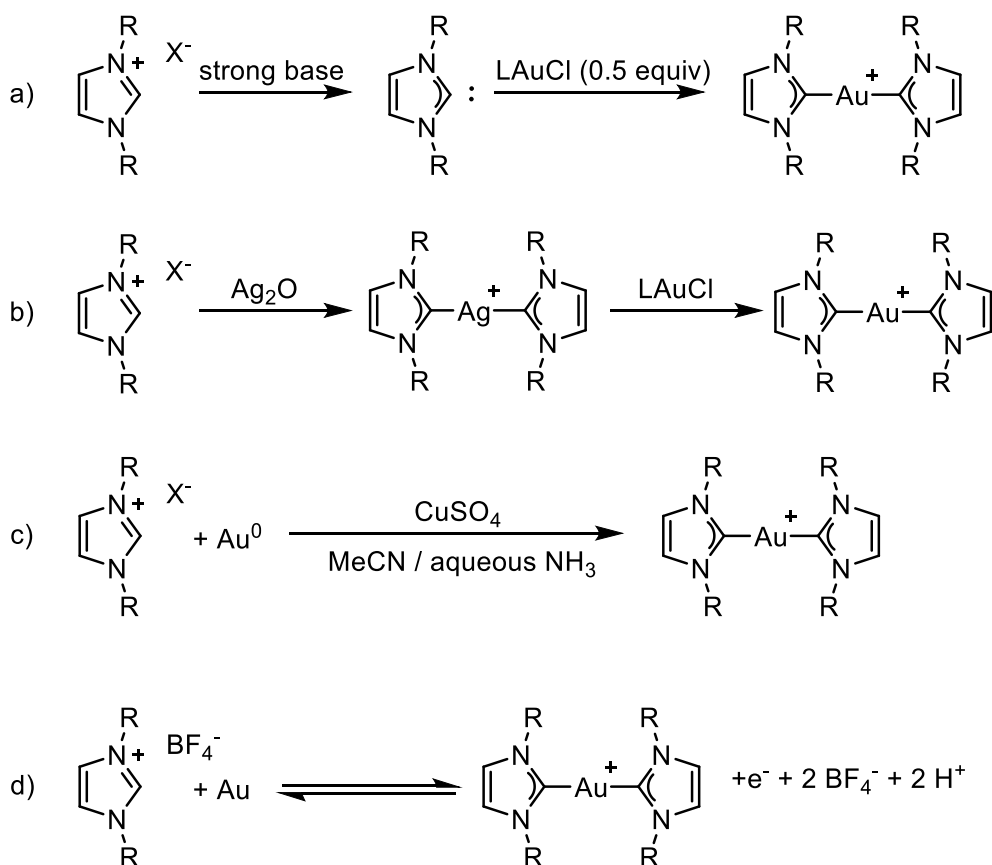
**Scheme 1.3.** Main synthetic pathways for the synthesis of bis-gold(I) NHC complexes.

### 1.2.4 Applications of gold(I) NHCs

Gold(I) NHC complexes have been already successfully applied as catalysts for a series of reactions, such as alkene activation,[176,177] C-H activation,[178,179] alkyne hydration,[180] propargylic esters rearrangement,[181] nitrile hydration,[182] hydroamination,[177] enyne cycloisomerization,[183,184] and others. Normally the used precatalyst is a (NHC)AuCl complex that is activated by means of halogen abstraction by the employment of a silver species in order to obtain the active catalyst (Scheme 1.4).[185] The produced AgCl has been demonstrate to be non-innocent in the gold catalysis,[186] and several methods have been applied to avoid the need for halogen abstraction, such as the use of (NHC)AuX complexes with weakly coordinating counterions such as $BF_4^-$ and $PF_6^-$,[187] and the use of silver-free co-catalysts.[188] Alternatively, the halogen removal from the gold centre can be achieved by N-functionalization, through the inclusion on the N-substituent a benzoyl or tosyl amide with a bridged linker.[189] The presence of a RR'NH moiety as a H-bond donor facilitates the removal of Cl⁻ from the gold centre upon coordination of a H-bond donor substrate, without the necessity of a co-catalyst.[189] Due to the large development of this field the structure of the NHC ligands catalysts have been designed

with the purpose of optimizing their electronic and steric properties. The electronics are mainly controlled by the main ring composition and by the backbone substitution,[190] while the sterics around the metallic centre are controlled by the N-substituents.[141] In fact, these substituents are normally large aromatic groups like the ones presented in Scheme 1.4, in order to introduce a substantial steric bulk around the catalytic centre both to enhance selectivity and to increase the stability, and thus lifetime, of the catalyst.[191,192]
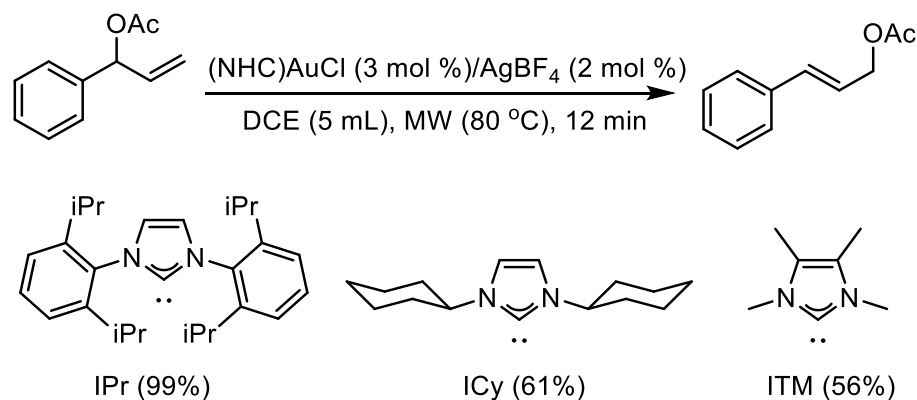


**Scheme 1.4.** Gold(I) NHC catalysed allylic rearrangement. Dependence of the yield on the steric bulk of N-substituents.

Gold(I) NHC have been proven to be also effective anticancer drugs.[193] Cationic complexes of the type $[Au(NHC)_2]^+$ have shown to lead to high antiproliferative activity against prostate and bladder cancer cells. The activity of these compounds is closely dependant on the aromaticity of the N-substituents, that in this case act as linkers.[194] Sugar-paired gold(I) NHC complexes have also shown to have anticancer properties.[195] These compounds are just a step away from the previously discussed pre-catalysts as the chloride ligand can be easily substituted with a biologically compatible sugar (Scheme 1.5). Gold(I) NHC thiosugar complexes also bearing small NHC ligands have been studied as possible analogues of the drug Auranofin.[196]
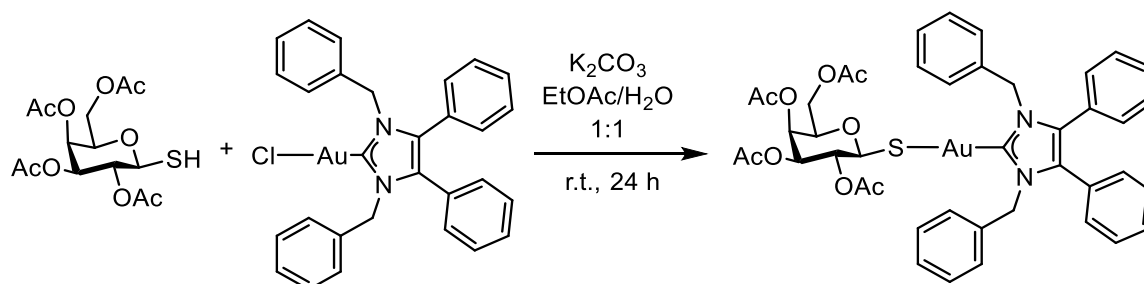


**Scheme 1.5.** Synthesis of a gold(I) NHC thiosugar complex.

Gold(I) NHC complexes have found applications in material science, as photosensytizers[197] and in very limited cases as chemical vapour deposition precursors (Figure 1.11).[198,199] Gold(I) NHC have shown to direct the growth of nanoplates[199] and enhance the stability of gold nanoparticles.[200] Silver and copper NHC-based complexes also have been applied as Atomic Layer Deposition precursors.[201,202]



(SIiPr)Au(NSi(Me$_3$)$_2$)  (SItBu)AuMe   (SItBu)Au(MeSiMe$_3$)   (SItBu)Au(C$_6$F$_5$)
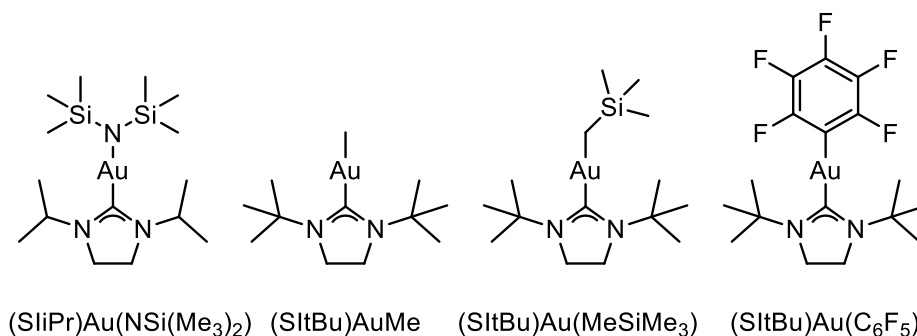
**Figure 1.11.** Gold(I) NHC complexes explored as possible CVD precursors.

### 1.2.5 Gold(III) NHC complexes

Gold(III) NHC complexes are square planar complexes that in comparison to the gold(I) NHC complexes discussed so far have two additional coordination sites on gold, which allows for different substitutions of the metal centre, allowing for example cyclometalation.[203] Gold(III) NHC complexes have proven to be suitable catalysts for dihydroalkoxylation and hydroamination reactions[204] and to be active anti-cancer agents.[205,206] Gold(III) NHC complexes are synthesized by oxidation of the relevant gold(I) NHC complex, using as an oxidizing agent PhICl$_2$,[207,208] halogens (Cl$_2$, Br$_2$, I$_2$),[208-210] CsBr$_3$[211] and N-halosuccinimides (Scheme 1.6).[212] Alternatively disproportionation of gold(I) NHC complexes using a sacrificial gold(I) compound leads to the formation of gold(III) NHC complexes.[213,214]
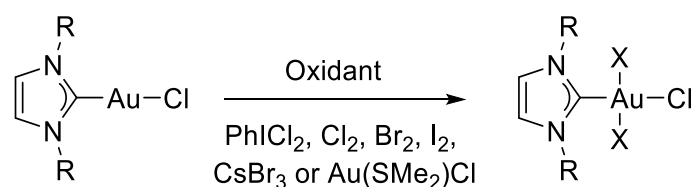


**Scheme 1.6.** Oxidation of gold(I) NHC complexes in gold(III) NHC complexes.

### 1.2.6 Rational design of a gold(I) NHC FEBID precursor

The main principles to take in consideration in the selection of a precursor structure is:

- Avoidance of chelating and polyhapto ligands
- Avoidance of metal halides, but suitability of heteroleptic halide complexes
- Large stability window, sufficient vapour pressure below 100 °C

With this in mind NHC gold(I) complexes of general formula (NHC)AuCl were chosen as the starting point of the investigations. Gold(I) NHC complexes bear a fundamental characteristic, a strong bond between a carbene carbon and the metal centre. The need for a strong bond is then reprised in the discussion of suitable structural features in a gold(I) FEBID precursor. Gold NHC complexes are well known stable species, with a straightforward synthetic pathway; most of them are bench stable and easy to store and handle. Data regarding their thermal stability and volatility at the time of the start of this work were extremely limited, but recently several reports were made on suitable gold(I) NHC complexes as CVD precursors,[198,199] indicating favourable sublimation conditions.

The first choice for a benchmark gold(I) NHC complex fell on **1a**. From the chemical formula of the compound, $C_5H_8AuClN_2$, the number of carbons for each gold centre is relatively high at 5:1, but lower than acac based precursors (7:1 in $Au(acac)Me_2$). All carbon atoms are directly bonded to a heteroatom. The worst cases of carbon contamination in FEBID is caused by purely carbon-based ligands, being it an allyl, cyclopentadienyl or alkyl group. In other cases, where heteroatoms are present, partial deposition of carbon is observed. This is true for an interesting set of complexes, such as silver carboxylates, and partially for gold acetylacetonates.

The NHC moiety can be also seen as an expansion of the isocyanide gold(I) complexes previously reported as volatile complexes by the group of McElwee-White (Figure 1.12). The reason for expanding the structure is double: on one hand it could enhance the volatility and stability of the complexes, on the other hand the increase in structural complexity leads to the introduction of different handles of modification. These handles can be used to fine-tune the desired properties of the precursor and, if modified in a library fashion, to give possible trends and a connection between structure, volatility and deposition properties.
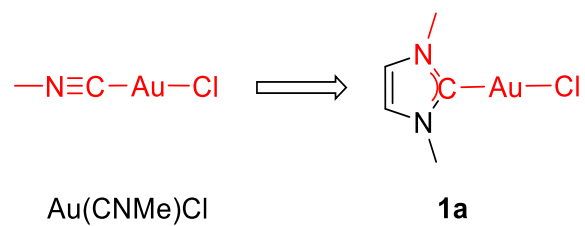
**Figure 1.12.** Structural relation between the isocyanide and the NHC based gold(I)complexes. In this example comparison between methylisocyanide gold(I) chloride and **1a**.

Thus from this early structure several modifications were implemented, both in a library fashion in order to study trends, and in an exploratory fashion, to improve (or worsen) more substantially the studied properties.

# Chapter 2.

# Synthesis and characterization of gold(I) NHC complexes

## *2.1 Introduction*

This chapter presents the synthesis and characterization of gold(I) NHC complexes. The NHC ligands explored are imidazole, triazole and imidazoline-based. The synthesis of the complexes is discussed in **Paper I, III** and **IV**. Furthermore, additional compounds not reported in the papers will be discussed.

The aim of the work presented in this chapter is the synthesis of an array of gold(I) NHC complexes to be then applied as precursors for deposition techniques, specifically FEBID (Figure 2.1). In the perspective of having a core structure that is "modified" to study the effect of substitution, different handles of modifications have been employed:

- NHC ring variation/saturation;
- NHC backbone substitution;
- N-substituents variation;
- X ligand variation;
- Variation of oxidation state of gold.
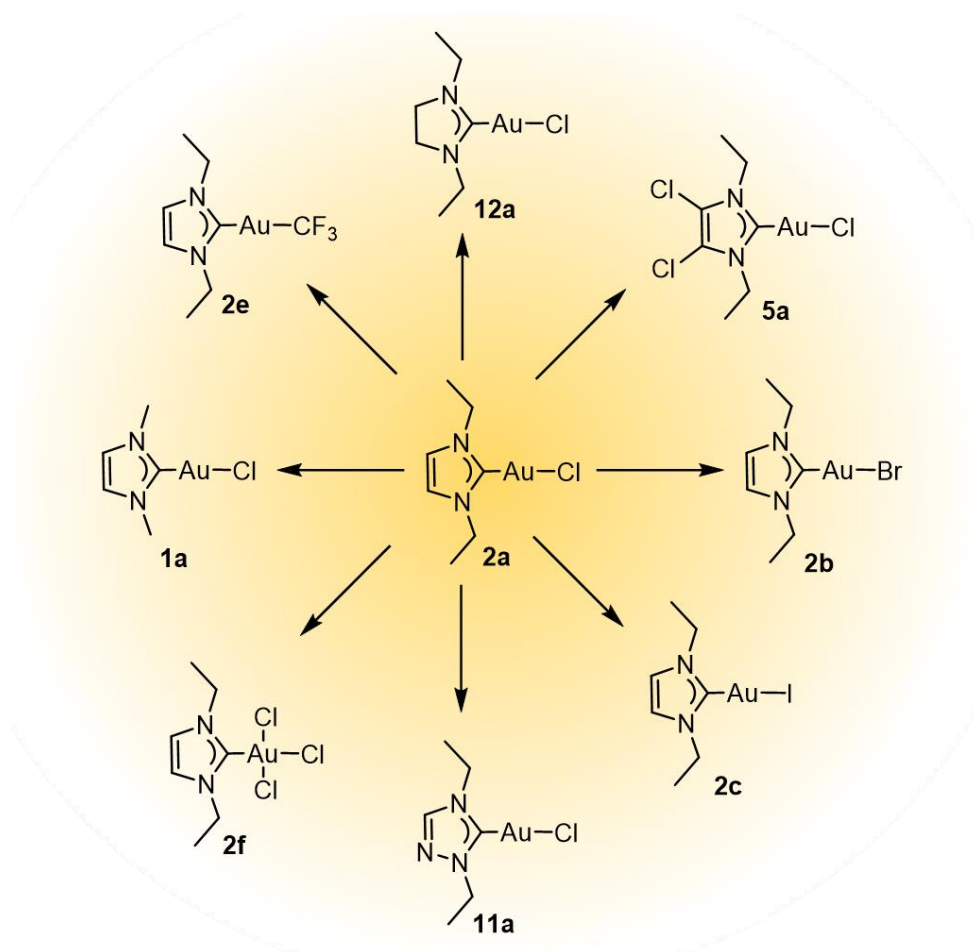
**Figure 2.1.** Target modifications on a core gold(I) NHC structure.

## 2.2 Synthesis of simple imidazole-based NHCs

Complexes **1a**-**3a** were synthesized through the Ag$_2$O route (Scheme 2.1),[156,157,215,216] with a purification through column chromatography to rule out the possible presence of any inorganic metal impurities, namely silver species and gold nanoparticles. The silver route was preferred to the more green procedures involving weak bases,[159] since **L2** was available only in its bromide salt, and such procedure would have led to the brominated complex **2b** as the major product. Instead, with the silver route, a 2:1 mixture of **2a** and **2b** was obtained due to halogen scrambling, and both products were separately isolated. These two species were distinguishable in NMR only by the variation of the carbene carbon $^{13}$C NMR chemical shift. For **1** and **3,** with respectively R = Me, iPr only the complexes **1a** and **3a** were obtained. Similarly, only the complex **13a** was obtained by employing the silver route using a benzimidazolium salt.
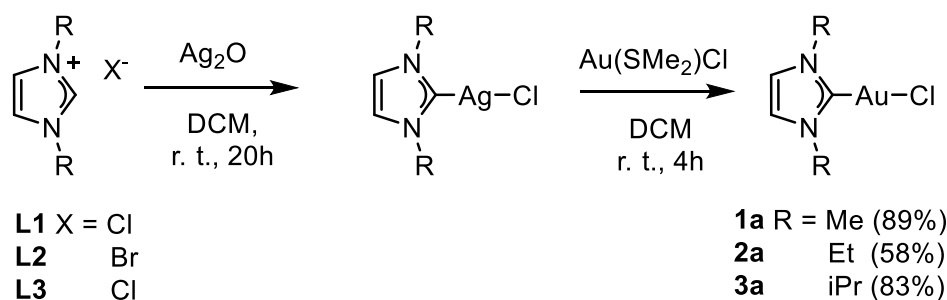
**Scheme 2.1**. Synthesis of compounds **1a**-**3a**.

With the aim of studying the effect of the modification of the halogen ligand, the synthesis of the bromo and iodo counterparts to complexes **1a-3a** was attempted. Both reactions were performed using established synthetic protocols.[217] The halogen metathesis reactions were performed by stirring the starting materials for 20-24h in dry acetone under inert atmosphere in the presence of a large excess of a Br⁻ or I⁻ salt. While the bromo complexes **1b-3b** were all obtained, for the iodo substitution reaction pure products could be isolated only for **2** and **3** (Scheme 2.2). From ESI-MS and single crystal XRD, the obtained products were identified as the dimeric compounds [Au(NHC)₂][AuI₂] **2h** and **3h** (Figure 2.2). In **2h** cases the complexes was linear with a C-Au-C angle of 175.5(2) and X-Au-X angle of 178.50(2). The XRD structures are further discussed in Chapter 3. Compound **1h** is a highly instable complex that readily decomposes and no investigation was possible. **1b** and **2h** showed limited stability, with slight discolouration over time. (NHC)AuI complexes are known to be the monomeric form in solution, and convert to the dimeric form [Au(NHC)₂][AuI₂] in solid state.[218]
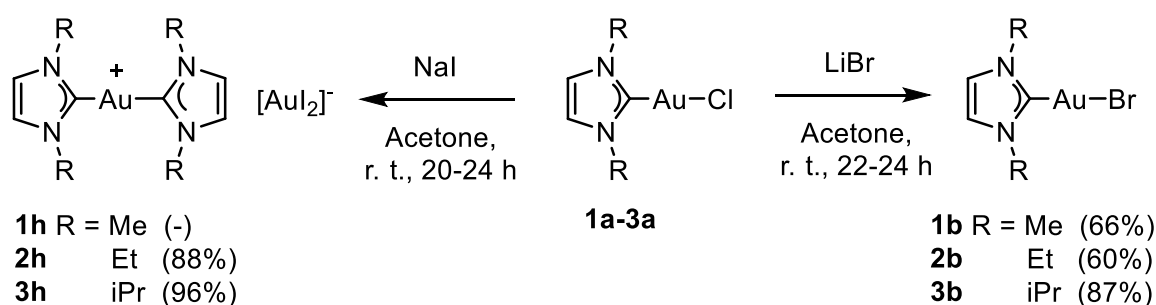


**Scheme 2.2.** Synthesis of brominated compounds **1b**-**3b** and dimers **1h**-**3h**.
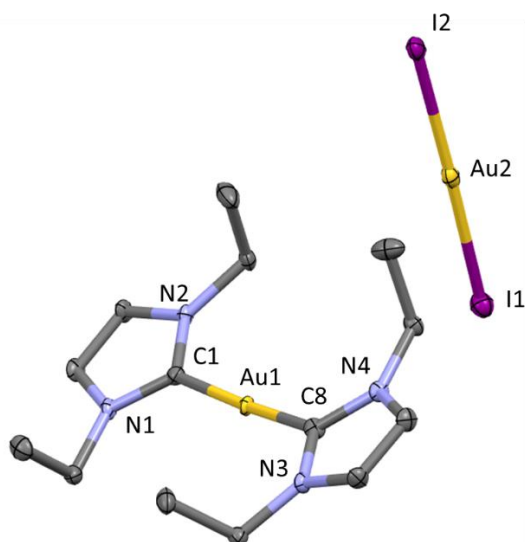
**Figure 2.2.** ORTEP plot of **2h** with 50% ellipsoids. Bond lengths (Å) and angles (deg): Au1-C1 2.019(3), Au1-C8 2.014(3), Au2-I1 2.5384(4), Au2-I2 2.5380(4); C1-Au1-C8 175.5(2), N1-C1-N2 105.4(4), N3-C8-N4 104.9(4), I1-Au2-I2 178.50(1). Hydrogens atoms were omitted for simplicity.

By comparison of the NMR data of this first array of complexes, in all cases the variation of the halogen did not involve any modification of ^{1}H NMR and ^{13}C NMR, with the exception of the carbene carbon peak. A downfield shift was observed going from Cl to Br (3.5 ppm on average) and from Br to I (7 ppm). Furthermore, it was also observed that going from R=Me to Et to iPr the carbene carbon was upfield shifted (respectively 2.0 and 1.4 ppm).

In organometallic complexes, a decrease in carbene chemical shift is linked to an increased metal Lewis acidity.[219,220] If sigma effects are independently considered, the value of chemical shift of the carbenic carbon should increase with the electronegativity of the halogen ligand in the series F > Cl > Br > I. Contrarily, the opposite order is observed ("inverse halide order"). Donation from halide lone-pair to the metal centre is often offered as a simple explanation for the inversion of trend.

## 2.3 Synthesis of backbone chlorinated NHC gold(I) complexes

In an effort to introduce a substantial variation on the structure while retaining a low content of carbon, a similar array of molecules bearing two chloro atoms on the backbone was investigated. The ligands **L4**-**L9** were obtained by two alkylation reactions on the unsubstituted 4,5-dichloroimidazole using MeI, EtI, iPrI or nPrBr as alkylating agents.[221] The first alkylation was performed in all cases with a reaction time of 3 days, and a yellow oil was

obtained (with the exception of MeI, where a yellow solid was obtained). The second step of alkylation was always performed using an alkyliodide reagent. Several reaction conditions were explored, with the use of a MW, under reflux, in a pressurized vial both neat and in solvent. The best conversions were obtained with the use of a pressurized vial, and as such the reactions were then all carried out in a Schlenk bomb and heated up to the vaporization temperature of the alkyliodide or of the solvent with a 1:1 V/V mixture of RI and MeCN (Scheme 2.3). In all cases, a white to pale yellow powder was obtained, washed with $Et_2O$ and used without further purifications.
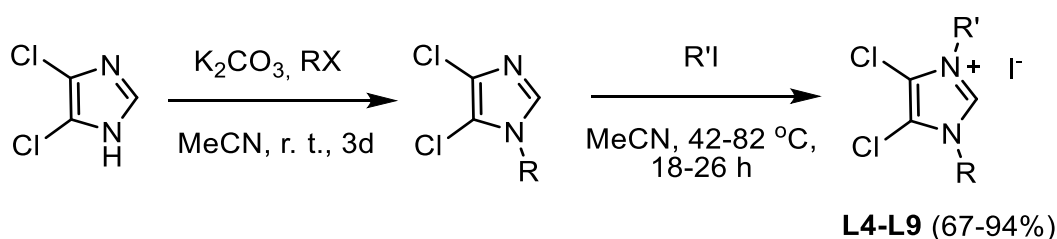


**Scheme 2.3.** Synthesis of ligands **L4**-**L9**.

The salts **L4**-**L9** were coordinated to gold(I) in the same conditions previously discussed for **L1**-**L3** (silver route).[159,216] In all cases, white powders were obtained after purification (Scheme 2.4). During column purification, a substantial amount of pink and orange impurities were removed. The orange impurities were identified as dimerization products [Au(NHC)$_2$][X], and were more prevalent in species that presented methyl groups as the N-substituents. This was mirrored in the lower yields obtained for **4a**, **7a** and **8a**, where the presence of the dimer rendered the purification of the complex more demanding (Table 2.1). Single crystals of isolated impurities of **7a** were obtained and in XRD a gold(III) complex [(NHC)AuCl$_2$Br] was observed (Figure 2.3). However, in MS, only [Au(NHC)$_2$]$^+$, [Au$_2$(NHC)$_2$Cl]$^+$ and [Au$_2$(NHC)$_2$I]$^+$ species were detected. The gold(I) centre can be oxidized in the presence of Au(SMe$_2$)Cl by disproportionation,[214] but the presence of bromo on the gold centre is unaccounted for. The pink impurity corresponded to iodine. In all cases, only (NHC)AuCl complexes were obtained.

27
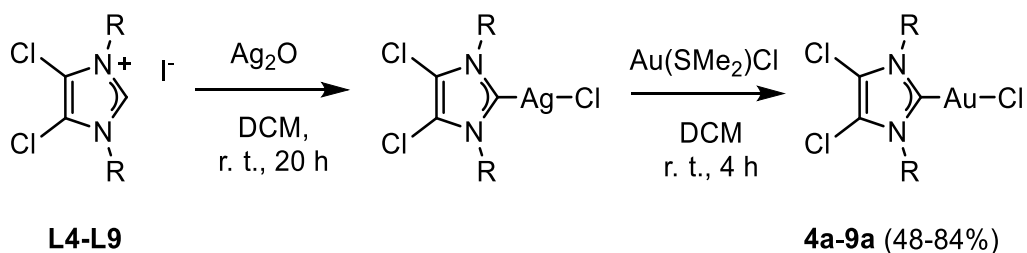
**Scheme 2.4.** Synthesis of backbone-chlorinated **4a**-**9a**.

**Table 2.1.** Yield for the synthesis of backbone chlorinated chloro complexes **4a**-**9a** with different R and R' substituents.

| Compound | R | R' | Yield (%) |
|----------|-----|-----|-----------|
| **4a** | Me | Me | 48 |
| **7a** | Me | Et | 66 |
| **9a** | Me | nPr | 77 |
| **5a** | Et | Et | 84 |
| **8a** | Et | nPr | 83 |
| **6a** | iPr | iPr | 84 |
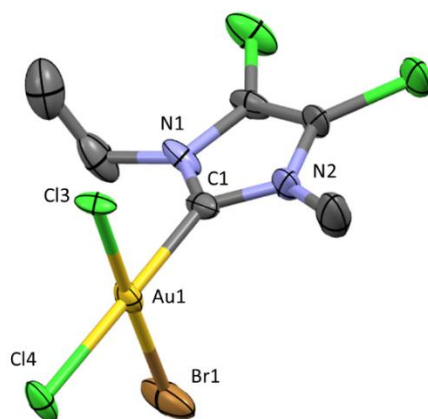


**Figure 2.3.** ORTEP plot of [(**7**)AuCl₂Br] with 50% ellipsoids. Bond lengths (Å) and angles (deg): Au1-C1 2.01(1), Au1-Cl3 2.355(2), Au1-Cl4 2.305(2), Au1-Br1 2.525(2), C1-N1 1.30(1), C1-N2 1.39(1); Cl3-Au1-Cl4 88.62(9), Cl3-Au1-C1 91.8(3), Cl3-Au1-Br1 178.07(7), Au1-C1-N1 126.8(8), Au1-C1-N2 124.5(8). Hydrogens atoms were omitted for simplicity.

Complexes **4b**, **5b**, **5c**, **6b** and **6c** were synthesized with the same procedure reported in the previous section. In this case, all of the obtained (NHC)AuBr and (NHC)AuI complexes were highly stable both to moisture, air and light, and no decomposition was observed (Scheme 2.5). The weak base protocol[159] was tried on **L5**, leading as expected to the formation of the

iodinated complex **5c**. The complexes can be easily differentiated by TLC (DCM, silica) as the $R_f$ of the compounds increases with the substitution of the halogen in the series Cl < Br < I. Compound **4c** was not obtained, similarly as what was observed for **1c**.



**4c** R = Me  (-)
**5c**     Et   (72%)
**6c**     iPr  (93%)

**4a-6a**

**4b** R = Me  (76%)
**5b**     Et   (89%)
**6b**     iPr  (89%)
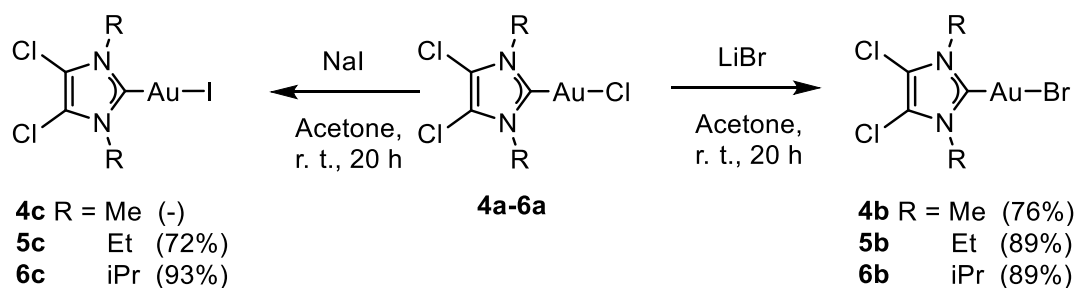
**Scheme 2.5.** Synthesis of brominated compounds **4b**-**6b** and iodinated **4c**-**6c**.

The halogen variation from Cl to Br and I leads to a downfield shift (Cl to Br 3.3 ppm, Br to I 7 ppm), while the modification of the R groups from smaller to larger gives a slight upfield shift. In the case of unsymmetrical substitution with R, R′ = Me, Et (**7a**) the carbene carbon chemical shift is exactly the intermediate value to the two symmetrically substituted compounds **4a** and **5a**. On the contrary for **9a** (R, R′ = Me, nPr), the carbene chemical shift is 1.3 ppm higher than the one observed for the symmetrical compound that presents the same molecular formula (**5a**).

Differently than for the previous series of compounds (**1-3**), in the backbone chlorinated complexes the chemical shift of the backbone carbons is almost constant in the range of 116.8 - 118 ppm, indicating that the introduction of Cl groups renders the effect of R substituents on the backbone carbon very minor. The presence of Cl on the backbone induces an irrelevant downfield shift of 0.7 ppm for the carbene carbon in comparison to the unfunctionalized compounds.

## 2.4 Synthesis of triazole-based gold(I) complexes

Triazole based NHC were explored with the primary aim of diminishing the atomic percentage carbon content in the molecular formula. The triazolium salt **L11** was obtained using a reported one-pot procedure in which both alkylations were carried out in one pot with a reaction time of 3 days.[222] The salts were then coordinated on gold(I) by the silver route (Scheme 2.6).
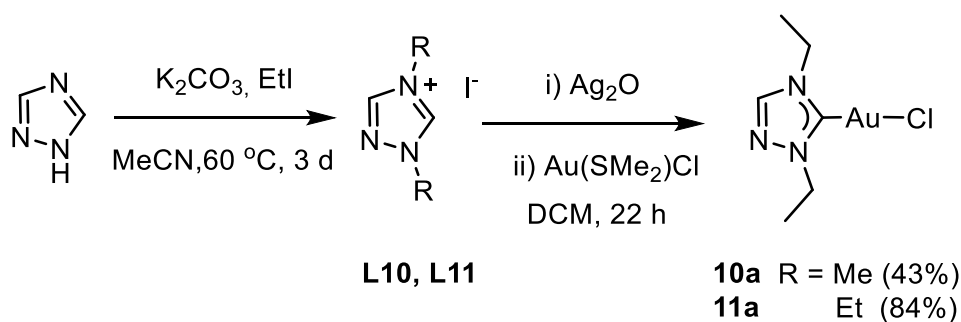
**Scheme 2.6.** Synthesis of triazole-based **10a** and **11a**.

Of these complexes only the iodo complex **11c** was investigated, as a mean of obtaining a suitable comparison for the imidazole-based iodinated compounds. Again, only the dimeric form [Au(NHC)$_2$][AuI$_2$] was obtained.

## 2.5 Synthesis of Imidazoline-based gold(I) complex

The imidazolinium chloride salt **L12** was prepared with a modification of a reported procedure.[223] Through a ring closing reaction, the coordinating carbon moiety is obtained from a triethyl orthoformate and the backbone and N substituents are yielded from a N,N′-dialkylamine. The reaction was carried out in a microwave oven and ammonium chloride was used as the source of the necessary chloride counterion. The imidazolinium chloride salt was the only ionic liquid obtained in this work, presenting itself as a bright yellow oil at ambient conditions.

While the synthesis of **12a** was already reported by the use of a tungsten carbonyl NHC precursor, no other route was studied.[156] Its coordination by means of the silver oxide route led only to a low conversion of the target product and many unidentified side products. The weak base route was also unsuccessful. The use of a strong base (KHMDS) led to the formation of the free carbene that was further reacted in situ at −78°C with Au(SMe$_2$)Cl to obtain the desired product in poor yields (Scheme 2.7). This procedure was based on a report by Griffiths *et al.* of a similar compound, although no complete purity was reported.[199]
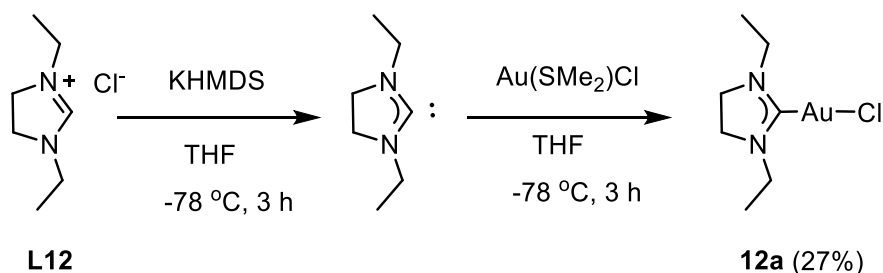
**Scheme 2.7.** Synthesis of the imidazoline-based complex **12a**.

## 2.6 Synthesis of methylated and trifluoromethylated gold(I) NHC complexes

As previously described in the introduction, carbon-gold bonds highly enhance desirable features such as volatility and thermal robustness in FEBID precursors.[86] Complex **5a** was methylated by reaction at room temperature with MeLi (Scheme 2.8). The obtained product showed in the ^{1}H NMR the presence of an additional peak at 0.18 ppm and in the ^{13}C NMR a corresponding carbon peak at -0.5 ppm, in line with previously reported methylated gold(I) NHC complexes.[219] The methylated product was never recovered in a purity sufficient for further applications as a FEBID precursor.
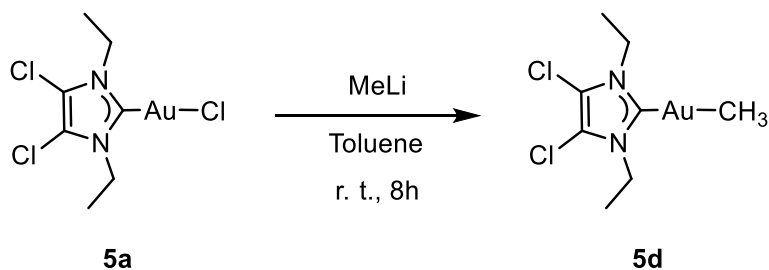


**Scheme 2.8.** Synthesis of the methylated complex **5d**.

Trifluoromethylation of a gold complex is carried out with the use of a mixture of AgF and Me₃SiCF₃, that causes the formation of AgCF₃ species that can further transfer the trifluoromethyl moiety to the gold centre.[224] AgF was observed to readily decompose upon solvent addition, with a colour variation from orange to black, however, it presents itself as a stable powder when stored under air at low temperature. The reactions were monitored in a NMR tube, and full conversion of the starting material was observed through ^{1}H NMR with at least 2 equiv. of AgF (Table 2.2). In such conditions, a reaction time of 1 day was sufficient. The formation of two major species was observed, the desired trifluoromethylated gold(I) NHC complex and a dimeric product (Scheme 2.9). The dimeric product **i** formed easily with

any starting material, while the target complexes **e** required longer reaction times and a higher amount of AgF to be formed in substantial quantities. With a reaction time of 42 h full conversion of the starting material was achieved with the use of 2 equiv. of AgF. These conditions were then applied for the full scale syntheses for compounds **2e**, **5e** and **11e**, yielding expectedly to a mixture of products and to the isolation of the target compound **e** in satisfactory yields. The synthesis of compound **5a** with 1 equiv. of AgF led to partial conversion of the starting material.

**Table 2.2.** NMR scale test and full scale yield for gold(I) NHC trifluoromethylation.

| Compound | AgF (equiv.) | Ratio **a; e; i** 1 h | Ratio **a; e; i** 18 h | Ratio **a; e; i** 42 h | Full scale yield |
|---|---|---|---|---|---|
| **2a** | 1 | 0.61; 0.04; 0.35 | 0.39; 0.14; 0.46 | 0.34; 0.17; 0.49 | 58%[a] |
| **5a** | 1 | 0.58; 0.03; 0.38 | 0.45; 0.10; 0.46 | 0.44; 0.09; 0.47 | 47% |
| **5a** | 2 | 0.51; 0.08; 0.41 | 0.18; 0.25; 0.57 | 0; 0.46; 0.54 | 66% |
| **6a** | 1 | 0.69; 0.06; 0.25 | 0.59; 0.07; 0.34 | 0.51; 0.12; 0.38 | - |
| **11a** | 1 | 0.71; 0.0; 0.29 | 0.48; 0.10; 0.42[b] | - | 64%[a] |

Ratio obtained by $^1$H NMR integration. 1equiv. of starting material, 5 equiv. of SiMe$_3$CF$_3$, in 0.6 mL of CD$_3$CN, kept under Ar in the dark. [a]2 Equiv. of AgF used in the full scale synthesis. [b]15 h.

The dimeric product has been identified in literature in similar reaction as [Au(NHC)$_2$][Au(CF$_3$)$_2$].[224] However, when performing the large scale synthesis for compound **5e**, a sufficient amount of the secondary product could be isolated and we concluded that the compound was [Au(NHC)$_2$][Au(CF$_3$)$_4$] (**5i**). While in positive MS the most intense signals were consistent for the [Au(NHC)$_2$]$^+$ ion at 581.010 m/z and above, negative MS showed as the most intense peak the ion [Au(CF$_3$)$_4$]$^-$ [225] at 472.984 m/z and no sign of the expected [Au(CF$_3$)$_2$]$^-$. This secondary product indicated that multiple unexpected processes were taking place: firstly, a rearrangement of ligands around the gold(I) centre, possibly mediated by the presence of silver(I) salts.[226] Secondly, the oxidation of a gold(I) centre to a gold(III), with addition of four CF$_3$ ligands in order to obtain the homoleptic complex. Also this second mechanism could be caused by the presence of silver salts, and more specifically through a redox process between a putative [Au(CF$_3$)$_2$]$^-$ complex and AgCF$_3$.
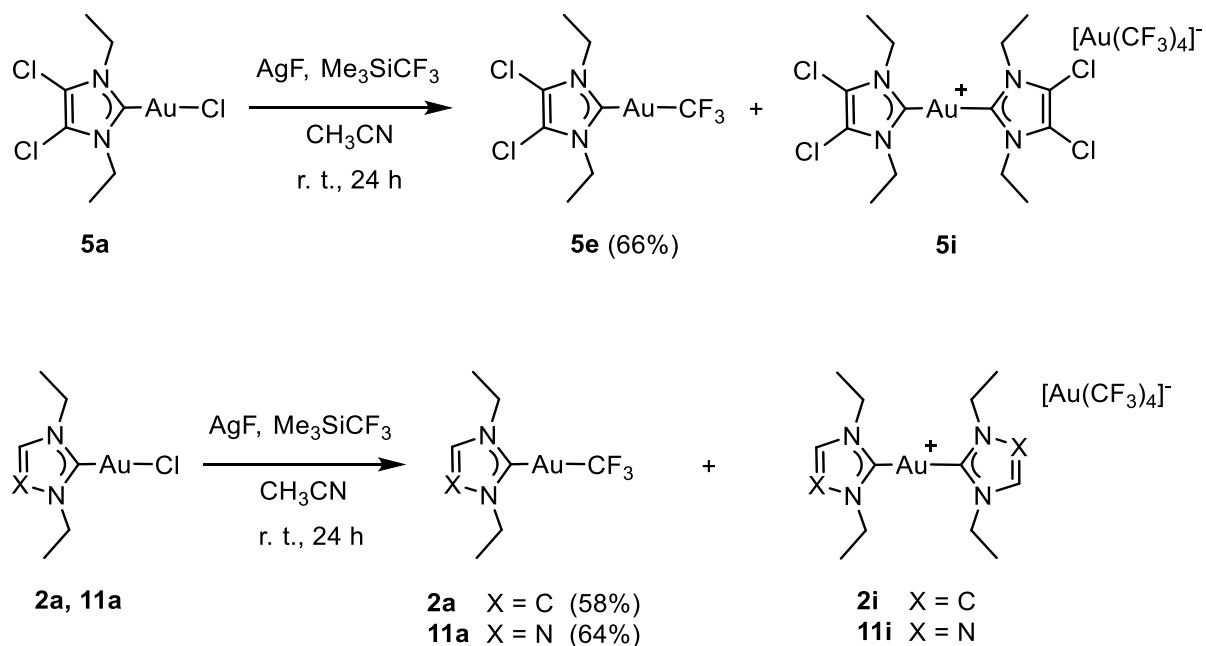
**Scheme 2.9.** Synthesis of trifluoromethylated **5e**, **2e** and **11e** and of dimers **5i**, **2i** and **11i**.

CF₃ and CH₃ groups are better sigma donors than halogens and thus decrease the Lewis acidity of the metal centre, indirectly inducing a downfield chemical shift of the carbene carbon.[219] Of the discussed groups CH₃ is indubitably the best sigma donor, and thus causes the highest carbene chemical shift at 198.2 ppm, 27.4 ppm higher than the chloro counterpart **5a**. The CF₃ has a downfield shift of 13.7 ppm in comparison to the chlorine counterpart **5a**, and it positions itself as intermediate between X = I and X = CH₃ (Figure 2.4). However, this is a simplification, since other factors such as hybridization and anisotropic effects, contribute to chemical shifts. The charge effect assumed above will be the sum of the contributions from sigma effects and π effects.
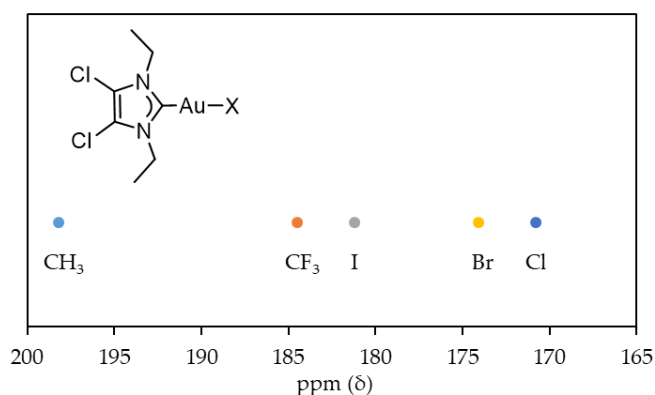


**Figure 2.4.** ¹³C NMR (101-151 Hz, CD₂Cl₂) chemical shift of carbene carbons for complexes of **5**.

## 2.7 Other complexes synthesized in the group

In the research group of Professor Mats Tilset, other (NHC)AuCl complexes have been investigated by MSc student Jeroen Ingolf Ketele Nyrud. Under the supervision of Prof. Mats Tilset and the author, Nyrud expanded on the series of backbone halogenated complexes, performing synthesis and characterization of compounds **14a** and **15a**, that are the backbone-brominated and iodinated equiv. of **2a**. Shorter reaction times were necessary to prevent full decomposition of the (NHC)AgX complex (Scheme 2.10). This is the only instance in which it was necessary to modify the conditions of the reaction.
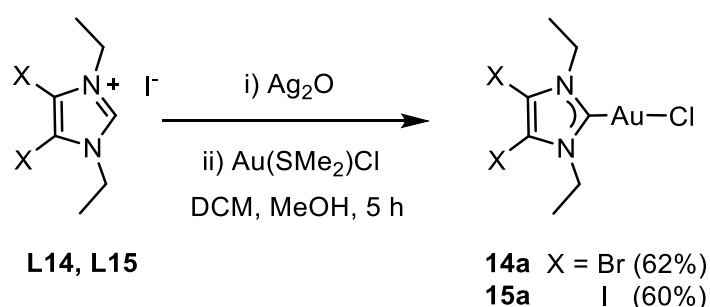


**Scheme 2.10.** Synthesis of **14a** and **15a**.

The carbene carbon chemical shift in $^{13}$C NMR is almost untouched when going from X = H to Cl (0.7 ppm) and is increased with the introduction of heavier halogens (H to Br 2.8 ppm; H to I 5.2 ppm). The chemical shift of the backbone carbons is instead very influenced by the substitution, following the series H (120.5 ppm) > Cl (117.0 ppm) > Br (107.3 ppm) > I (85.9 ppm).

## 2.8 Conclusions

A substantial library of gold(I) NHC complexes has been synthesized. All of the synthesized compounds show to have enough stability to be further tested as FEBID precursors, with the exception of **1b** and **2h**, which show sensitivity to light and are not stable in normal conditions. Structural variation was successfully implemented on a core structure in order to further study the effects of the substitutions. The $^{13}$C NMR chemical shift of the main ring carbons is highly diagnostic of the electronic effect of the studied substitutions (Table 2.3).

**Table 2.3.** ^{13}C NMR (101-151 Hz, $CD_2Cl_2$) chemical shift of carbene carbons and backbone carbons for (NHC)Au(I)X complexes.

| Compound | Carbene δ (ppm) | Au-X δ (ppm) | Backbone carbon δ (ppm) | Backbone carbon/nitrogen δ (ppm) |
|---|---|---|---|---|
| **1a** | 172.1 | - | 122.3 | 122.3 |
| **1b** | 175.6 | - | 122.3 | 122.3 |
| **2a** | 170.1 | - | 120.5 | 120.5 |
| **2b** | 173.7 | - | 120.4 | 120.4 |
| **2h** | 180.7 | 180.7 | 120.3 | 120.3 |
| **2e** | 183.9 | 164.4 | 120.6 | 120.6 |
| **3a** | 168.9 | - | 117.4 | 117.4 |
| **3b** | 172.2 | - | 117.2 | 117.2 |
| **3h** | 179.3 | 179.3 | 117.2 | 117.2 |
| **4a** | 172.4 | - | 117.9 | 117.9 |
| **4b** | 175.7 | - | 118.0 | 118.0 |
| **5a** | 170.8 | - | 117.0 | 117.0 |
| **5b** | 174.1 | - | 116.9 | 116.9 |
| **5c** | 181.2 | - | 117.1 | 117.1 |
| **5d** | 198.2 | -0.5 | 116.2 | 116.2 |
| **5e** | 184.5 | 162.8 | 117.4 | 117.4 |
| **6a** | 170.0 | - | 117.0 | 117.0 |
| **6b** | 173.4 | - | 116.8 | 116.8 |
| **6c** | 180.3 | - | 116.8 | 116.8 |
| **7a** | 171.6 | - | 118.0 | 116.9 |
| **8a** | 171.09 | - | 117.2 | 116.8 |
| **9a** | 172.1 | - | 117.9 | 117.3 |
| **10a** | 174.9 | - | 143.2 | - |
| **11a** | 173.2 | - | 142.2 | - |
| **11h** | 183.1 | - | 141.8 | - |
| **11e** | 186.3 | 163.0 | 142.3 | - |
| **12a** | 191.8 | - | 48.2 | 48.2 |
| **13a** | 179.6 | - | 134.3 | 134.3 |
| **14a** | 172.9 | - | 107.3 | 107.3 |
| **15a** | 175.3 | - | 85.9 | 85.9 |

## 2.9 Experimental part

The results discussed in this chapter are reported in **Paper I**, **Paper III** and **Paper IV**. Supplementary information about the synthesized of compounds not reported is given here. The XRD table for [(**7**)AuCl₂Br] is reported here, while all other XRD will be further discussed in chapter 3.

**1b**
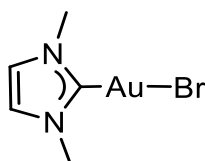


A solution of **1a** (151.3 mg, 0.46 mmol, 1 equiv.) and LiBr (393.0 mg, 4.6 mmol, 10 equiv.) in 20 mL of dried acetone was left stirring in the dark under an Ar atmosphere for 22 h. Upon removal of solvent on rotary evaporator the resulting solid was partially dissolved in DCM, filtered, and purified by column chromatography (silica, DCM). The product was obtained as a pale yellow solid (120.7 mg, 66%).

$^1$H NMR (400 MHz, CD$_2$Cl$_2$): δ 6.95 (s, 2H, =C$H$-), 3.81 (s, 6H, -C$H_3$). $^{13}$C NMR (101 MHz, CD$_2$Cl$_2$): δ 175.6 (NHC-$C$), 122.3 (=$C$H-), 38.5 (-$C$H$_3$).

MS (ESI$^+$,MeOH): $m/z$ 389.104 ([(NHC)$_2$Au]$^+$, 59.2%), 394.943 ([M($^{79}$Br)+Na]$^+$, 100%), 396.941 ([M($^{81}$Br)+Na]$^+$, 97.2%). HRMS (MeOH): $m/z$ meas. 394.9428, calcd. 394.9429 for [C$_5$H$_8$Au$^{79}$BrN$_2$Na]$^+$ (Δ= 0.1 ppm).

**3b**
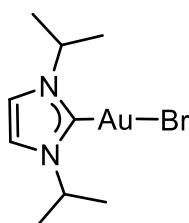


A solution of **3a** (173.1 mg, 0.45 mmol, 1 equiv.) and LiBr (338.5 mg, 4.0 mmol, 9 equiv.) in 50 mL of dried acetone was left stirring in the dark under an Ar atmosphere for 22 h. Upon removal of solvent on rotary evaporator, the resulting solid was partially dissolved in DCM and filtered. After concentration to dryness, the obtained oil was purified by column

chromatography (silica, DCM) and the product was obtained as a pale yellow solid (168.1 mg, 87%).

$^1$H NMR (400 MHz, $CD_2Cl_2$): δ 7.02 (s, 2H, =C$H$-), 5.01 (hept., $J$ = 6.8 Hz, 2H C$H$Me$_2$), 1.47 (d, $J$ = 6.8 Hz, 12H, -C$H_3$). $^{13}$C NMR (101 MHz, $CD_2Cl_2$): δ 172.2 (NHC-$C$), 117.2 (=CH-), 54.0 (-$C$HMe$_2$), 23.5 (-$C$H$_3$).

MS (ESI$^+$,MeOH): $m/z$ 451.005 ([M($^{79}$Br)+Na]$^+$, 100%), 453.003 ([M($^{81}$Br)+Na]$^+$, 97.7%), 501.229 ([(NHC)$_2$Au]$^+$, 40.2%). HRMS (MeOH): $m/z$ meas. 451.0054, calcd. 451.0055 for [C$_9$H$_{16}$Au$^{79}$BrN$_2$Na]$^+$ (Δ= 0.2 ppm).

**5d**
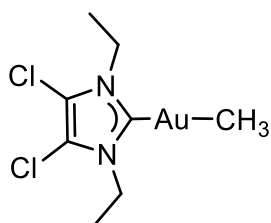


A MeLi solution (1.6M in Et$_2$O, 300 μL) was added to a solution of **5a** (45.3 mg, 0.11 mmol, 1 equiv.) in dry toluene (10 mL) under inert atmosphere. After stirring for 8 h, the resulting grey suspension was concentrated, filtered through a celite pad, and purified by column chromatography (DCM, silica). No yield is reported due to the low purity of the product.

$^1$H NMR (400 MHz, $CD_2Cl_2$): δ 4.29 (q, $J$ = 7.2 Hz, 4H C$H_2$-CH$_3$), 1.42 (t, $J$ = 7.2 Hz, 6H, -C$H_3$) 0.18 (s, 3H, -C$H_3$). $^{13}$C NMR (101 MHz, $CD_2Cl_2$): δ 198.4 (NHC-$C$), 116.3 (=CH-), 45.2 (CH$_2$-CH$_3$), 16.3 (-$C$H$_3$), -0.5 (Au-$C$H$_3$).

MS (ESI$^+$,MeOH): $m/z$ 427.001 ([M($^{35}$Cl$^{35}$Cl)+Na]$^+$, 100%), 428.998 ([M($^{37}$Cl$^{35}$Cl)+Na]$^+$ 64.9%). HRMS (MeOH): $m/z$ meas. 427.0013, calcd. 427.0014 for [C$_8$H$_{13}$Au$^{35}$Cl$_2$N$_2$Na]$^+$ (Δ= 0.1 ppm).
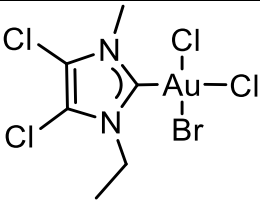
**11h**
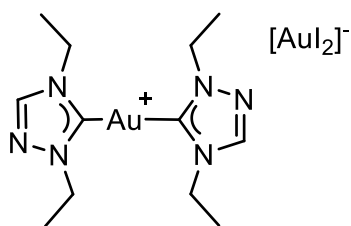


A suspension of **11a** (52.8 mg, 0.15 mmol, 1 equiv.) and NaI (212.8 mg, 1.40 mmol, 10 equiv.) in 7 mL of dried acetone was left stirring in the dark under an Ar atmosphere for 20 h. Upon removal of solvent on rotary evaporator the resulting pale solid was partially dissolved in DCM and filtered. Upon concentration of the resulting solution a pale orange solid was obtained (64.1 mg, 95%).

^{1}H NMR (400 MHz, $CD_2Cl_2$): δ 8.06 (s, 1H, =C*H*-), 4.41 (q, *J* = 7.3 Hz, 2H, -C*H*$_2$-, CH side), 4.26 (q, *J* = 7.4 Hz, 2H, -C*H*$_2$-, N side), 1.54 (t, *J* = 7.4 Hz, 3H, -C*H*$_3$, N side), 1.52 (t, *J* = 7.3 Hz, 3H, -C*H*$_3$, CH side). ^{13}C NMR (101 MHz, $CD_2Cl_2$): δ 183.1 (NHC-*C*), 141.8 (=*C*H-), 48.9 (-*C*H$_2$-, CH side), 44.4 (-*C*H$_2$-, N side), 16.4 (-*C*H$_3$), 15.5 (-*C*H$_3$).

MS (ESI[+], MeCN): *m/z* 447.156 ([(NHC)$_2$Au]$^+$ 100%). MS (ESI[-], MeCN): *m/z* 450.776 ([I$_2$Au]$^-$ 100%).

Crystal and refinement data for [(**7**)AuCl₂Br].

| | |
|---|---|
| |   [(**7**)AuCl$_2$Br] |
| **Crystal data** | |
| Identification code | cg_chec_hp_0m_a |
| Chemical formula | $C_6H_8AuBrCl_4N_2$ |
| $M_r$ | 526.82 |
| Crystal system, space group | Monoclinic, P2$_1$/n |
| Crystal color, shape | Brown needle |
| Temperature (K) | 100 |
| a, b, c (Å) | 8.6374 (6), 14.1299 (10), 10.8416 (7) |
| α, β, γ (°) | 90, 96.804 (2), 90 |
| $V$ (Å$^3$) | 1313.85 (16) |
| $Z$ | 4 |
| Radiation type | Mo Kα |
| μ (mm$^{-1}$) | 15.02 |
| Crystal size (mm) | 0.35 × 0.08 × 0.08 |
| **Data collection** | |
| Diffractometer | Bruker D8 Venture |
| Absorption correction | Multi-scan |
| T$_{min}$, T$_{max}$ | 0.357, 0.747 |
| No. of measured, independent and observed [I > 2σ(I)] reflections | 21339, 4030, 3389 |
| $R_{int}$ | 0.072 |
| (sin θ/λ)max (Å$^{-1}$) | 0.716 |
| **Refinement** | |
| $R[F^2 > 2\sigma(F^2)]$, $wR(F^2)$, S | 0.061, 0.156, 1.14 |
| No. of reflections | 4030 |
| No. of parameters | 129 |
| No. of restraints | 0 |
| H-atom treatment | H atom parameters constrained |
| | $w = 1/[\sigma^2(F_o^2) + (0.0591P)^2 + 29.1263P]$ where $P = (F_o^2 + 2F_c^2)/3$ |
| Δρ$_{max}$, Δρ$_{min}$ (e Å$^{-3}$) | 4.99, −1.91 |

# Chapter 3.

# Thermal evaluation of gold(I) NHC complexes

## 3.1 Introduction

This chapter presents the physical characterizations carried out on selected gold(I) NHC complexes, work that is briefly presented in **Paper III** and consolidated in **Paper IV**. The sublimation and melting of the complexes is presented in the first part of the chapter. In the second part of this chapter, the intermolecular packing of the complexes obtained by single crystal X-ray diffraction is discussed and correlated with the obtained sublimation data. The work was carried out in collaboration with David Wragg. Lastly, the development of *vacuum-TGA* as a suitable tool for the pre-screening of the volatility of FEBID precursors is discussed, work that is presented in **Paper II**. Primarily Jakub Jurczyk, with the contribution of the author, performed the TGA related work.

The interest in the NHC gold(I) complexes presented in Chapter 2 lies in their use as precursors for FEBID and other deposition techniques such as ALD and CVD. Information about the volatility and thermal stability is a fundamental tool for the pre-screening of these complexes for their application as precursors. Thermogravimetric Analysis (TGA) and cold finger sublimation are two commonly applied methods for obtaining the sublimation point for FEBID precursors.[86,109,227] While both very informative, TGA significantly differs in sublimation conditions from the volatilization of the precursor molecule in a Gas Injection System (GIS), mainly in pressure conditions.[228] While such differences can be circumvented,[198,229] cold finger sublimation has been preferred to TGA as a tool for identification and comparison of volatile metallorganic compounds due to the great applicability demonstrated by the group of McElwee-White.[86,109] The aim of this chapter is to confirm the volatility of gold(I) and gold(III) NHC complexes by means of cold finger sublimation, and to rationalize the sublimation points by comparing intermolecular packing in solid state.[70,86,109]

## 3.2 Cold Finger sublimation

A sublimation apparatus is used in chemistry as a purification tool. Bulk material is heated under vacuum in a tube until sublimation and is then condensed on a cold surface (Figure 3.1). The cold surface is generated by a cold finger, a glass piece inserted in the heated tube and cooled down through water flow. If a constant vacuum is maintained throughout the experiment, the incipient sublimation temperature can be registered at the formation of condensed material on the cold finger. The condensed material can then be collected and analysed to confirm identity. The employed method is presented in detail in **Paper III** and **IV**.
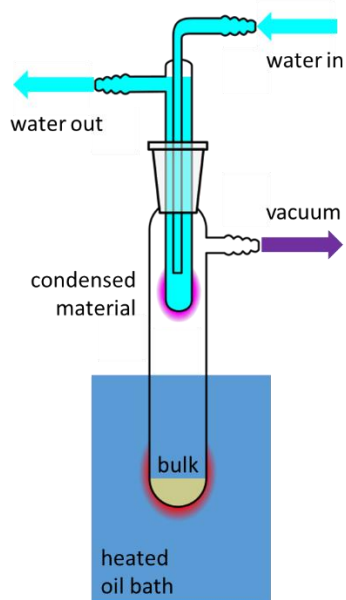


**Figure 3.1.** Schematic representation of cold finger sublimation apparatus.

### 3.2.1 Sublimation of early gold(I) NHC complexes

For the complexes **1a**-**3a**, a roughly constant sublimation temperature on the range of 82-87 °C was observed, with a sensible decrease in sublimation temperature only for the isopropyl-substituted **3a** (Table 3.1). The variation from X = Cl to X = Br led only to a 2 °C sublimation temperature decrease for **2b**. The indication of this first array of compounds is that the modification of R and X groups do not influence highly the sublimation temperature of the compounds. For all complexes, a sublimation window higher than 50 °C ($T_{m.p.}$-$T_{subl.}$) was obtained.

**Table 3.1.** Sublimation temperature, melting point and sublimation window of unsubstituted NHC gold(I) complexes.

| Compound (R; X) | Sublimation temperature[a] (°C) | Melting point[b] (°C) | Temperature window for sublimation[c] (°C) |
|---|---|---|---|
| **1a** (Me; Cl) | 86-87 | 161-162 | 75 |
| **2a** (Et; Cl) | 87 | 163-164 | 76 |
| **2b** (Et; Br) | 85 | 136-137 | 51 |
| **3a** (iPr; Cl) | 82-83 | 184-185 | 101 |

[a]Sublimation temperatures obtained by cold finger sublimations. [b]Melting point obtained by melting point apparatus; [c]Range of temperature for sublimation of the compound at a pressure of $10^{-3}$ mbar.

### 3.2.2 Sublimation of backbone-chlorinated gold(I) NHC complexes

The backbone-chlorinated gold(I) NHC complexes were sublimed in the established conditions and no decomposition or variation of bulk material during sublimations was observed. A greater sublimation temperature difference was observed for this array (Table 3.2). Compounds **4a** and **4b** showed exactly the same sublimation point at 100 °C. For compounds **5** and **6** the difference between X = Cl and X = Br was also limited, in the range of 1 °C, too small to be considered significant. For the iodo compounds **5c** and **6c**, an increase in volatility of 5-6 °C was observed in comparison to the chloro compounds.

**Table 3.2.** Sublimation temperature, melting point and sublimation window of backbone chlorinated NHC gold(I) complexes.

| Compound (R; X) | Sublimation temperature[a] (°C) | Melting point[b] (°C) | Temperature window for sublimation[c] (°C) |
|---|---|---|---|
| **4a** (Me; Cl) | 100 | 266-269[d] | 166 |
| **4b** (Me; Br) | 100 | 258-259[e] | 158 |
| **5a** (Et; Cl) | 78 | 185-186 | 107 |
| **5b** (Et; Br) | 77 | 204-205 | 127 |
| **5c** (Et; I) | 73 | 178-179 | 105 |
| **6a** (iPr; Cl) | 75 | 202-203 | 127 |
| **6b** (iPr; Br) | 74 | 225-226 | 151 |
| **6c** (iPr; I) | 69 | 219-220 | 150 |
| **7a** (Me, Et; Cl) | 90 | 205-206 | 115 |

[a]Sublimation temperatures obtained by cold finger sublimations. [b]Melting point obtained by melting point apparatus; [c]Range of temperature for sublimation of the compound at a pressure of $10^{-3}$ mbar. [d]Decomposition prior to melting at 220 °C; [e]Decomposition and melting.

The data on the halogen variation fit very well the trend obtained from a series of isocyanide gold(I) complexes.[109] This is in first instance counterintuitive: the increase of the halogen size (and thus molecular weight) should in theory decrease the volatility of a compound, but the effect is opposite. Such trend will be discussed further in the chapter by comparing sublimation temperature and molecular packing.

In all cases, the variation of the R group led to a decrease of sublimation temperature with the increase of the size of the alkyl substituent. The greatest variation was observed going from R = Me to R = Et, with a difference of 22 °C. The variation between R = Et and R = iPr was only of 3 °C. This trend was also confirmed by the bromo array **4b**, **5b**, **6b** and by the iodo complexes **5c** and **6c**. Compound **7a** ( R, R′ = Me, Et) showed an intermediate volatilization temperature between **4a** and **5a** (90 °C).

No direct correlation between sublimation temperature and melting point was found. All the backbone chlorinated compounds have a sublimation window of at least 100 °C. Such indication is highly positive, as a large sublimation window is desirable for the application of

the precursors for both FEBID and CVD/ALD. For FEBID applications, the most promising N-substitution is R = Et, as it is a compromise between volatility and carbon composition limitation. Furthermore, while the variation from X = Cl to X = I bring a relevant increase in volatility, the variation X = Cl to X = Br does not introduce any optimization.

### 3.2.3 Sublimation of other gold NHC complexes

The triazole complexes **10a** and **11a** showed a decreased sublimation temperature from their imidazole-based counterparts **1a** and **2a** of 5 and 27 °C respectively (Table 3.3). For these two complexes the variation from R = Me to R = Et induced a substantial drop of sublimation temperature of 21 °C, similar to what was observed for the backbone chlorinated complexes. The effect of the triazole ring is highly positive both from the volatility and the composition point of view, since the number of carbons per molecule is decreased by one.

**Table 3.3.** Sublimation temperature, melting point and sublimation window of NHC gold(I) and gold(III) complexes.

| Compound (R; X) | Sublimation temperature[a] (°C) | Melting point[b] (°C) | Temperature window for sublimation[c] (°C) |
|---|---|---|---|
| **10a** (Me; Cl) | 81[d] | 138-139 | 57 |
| **11a** (Et; Cl) | 60 | 131-132 | 71 |
| **12a** (Et; Cl) | 70 | 70-72 | - |
| **5e** (Et; CF$_3$) | 53 | 146-149 | 93 |
| **11e** (Et; CF$_3$) | 38 | 102-103 | 64 |
| **5f** (Et; Cl$_3$) | 101[e] | 280-282 | 180 |

[a]Sublimation temperatures obtained by cold finger sublimations. [b]Melting point obtained by melting point apparatus. [c]Range of temperature for sublimation of the compound at a pressure of 10$^{-3}$ mbar; [d]preliminary data. [e]Sublimation and decomposition.

The imidazoline-based complex **12a** was the only compound that melted during volatilization studies. Melting of bulk material was observed at 70-72 °C in concomitance with the appearance of condensed solid on the cold finger. The sublimation temperature difference between the imidazole and imidazoline-based complexes **2a** and **12a** is of 17 °C. However, due to the different phase transitions for these two compounds no further comparison is

significant. The most noteworthy variation is in the melting point, that decreased from 163 °C to 70 °C, with a substantial drop of *circa* 100 °C.

In all cases, the introduction of a trifluoromethyl ligand induced a drastic drop of sublimation temperature. For the backbone chlorinated compound **5e** the temperature drop from the chlorinated complex **5a** was of 25 °C.  For the triazole complex **11d** the variation of X = Cl to X = CF$_3$ caused a drop of 22 °C to a sublimation temperature of 38 °C. This is the most volatile compound obtained in this study. These observations are in agreement with the isocyanide gold(I) series,[86,109] indicating that for all gold(I) complexes the introduction of a trifluoromethyl ligand greatly increases volatility. Fluorination and perfluorination has been commonly employed in other systems as a mean of boosting the thermal properties of organometallic compounds.[230-233]

The gold(III) complex **5f** will be further discussed in Chapter 6. The oxidation of the gold centre from Au(I) (**5a**) to Au(III) (**5f**) changes the linear complex into a square planar one, with the addition of two chloro ligands. In this case the introduction of more halogens increased the sublimation temperature to 101 °C, rendering **5f** the least volatile complex obtained. Furthermore, the collected product was a mixture of **5f** and **5a** in a ratio of 1:0.28 (Figure 3.2), indicating that under the conditions of the sublimation experiments, **5f** decomposed in **5a** through the reductive elimination of Cl$_2$. No further investigations of volatility of gold(III) complexes were carried out.
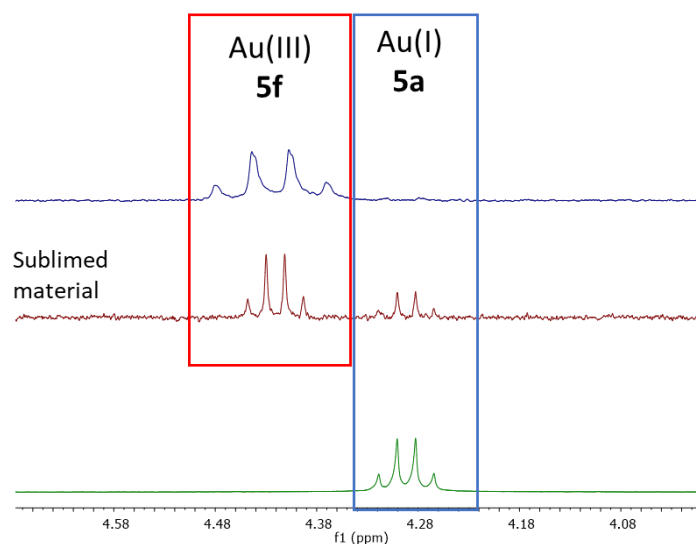
**Figure 3.2.** ^{1}H NMR spectra of **5f** (200 MHz), Sublimated of 5f at 101 °C and **5a** (400 MHz); zoom on – C$H_2$-CH$_3$ protons.

## 3.3 Molecular packing

Gold complexes show a wide variability of intermolecular packing, mainly dictated by aurophilic interactions,[234] weak interactions present at a Au-Au distance between 2.8 and 3.5 Å.[110] The sublimation temperature of organogold precursors has been linked in previous studies to the intermolecular packing of the complexes in solid state.[70,86,109] Several gold(I) FEBID precursors have been studied from this point of view, and a well-defined relation between intermolecular packing and volatilization has been established. In the discussed series of gold(I) isocyanide and phosphine complexes, that the sublimation temperature decreases together with the increase of Au-Au intermolecular distances. In such small complexes, aurophilic interactions play a great role in the overall packing energy of the molecule.[86,109] Furthermore, it has been observed that a variation in packing pattern, from monomer to oligomer to chain, has a similar effect, with decreased sublimation temperature for the shortest structures.[109]

The solid state packing of NHC gold(I) complexes is diverse, as the packing is mostly dictated by weak interactions, such as aurophilic interactions, electrostatic interactions and in some cases π-π stacking of the ligands.[235-237] The most common packing arrangement including aurophilic interactions involves the formation of dimers, where the Au-Au bond is the central interaction. In the case of formation of strong NHC-X electrostatic interaction (X-Au-Au-X

angle around 180°) it is defined as antiparallel dimer, whereas if this interaction is absent (X-Au-Au-X angle around 90°) it is defined as a perpendicular dimer (Figure 3.3). Such supramolecular organization can be extended to the formation of chains.[234]
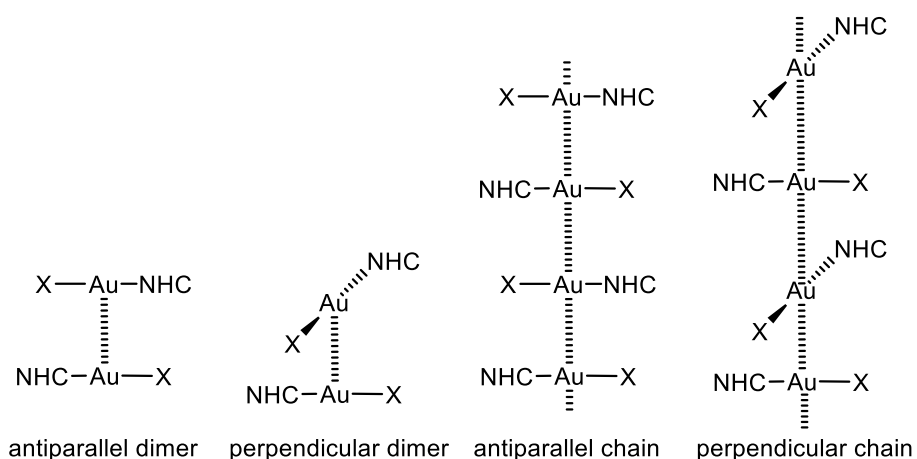


**Figure 3.3.** Possible packing modes with aurophilic interactions for gold(I) NHC complexes.

### 3.3.1 Solid state packing of 1a-3c: high variation in packing pattern

Compounds **2a** and **2b** form perpendicular dimers with a very short Au-Au distance of around 3.1-3.2 Å and no π-halogen interactions are present (Table 3.4, Figure 3.4). This conformation was previously observed for benzimidazole-based complexes[158] and imidazole-based gold(I) complexes with Cy N-substituents.[160,196] Compounds **1a** and **1b** follow the same packing pattern with perpendicular units, but forming instead chains with longer Au-Au distances at 3.3-3.5 Å. Complexes **2h** and **3h** are both identified in solid state as the dimeric form [Au(NHC)$_2$]$^+$[AuI$_2$]$^-$; while **2h** presents dimers of [Au(NHC)$_2$]$^+$ complexes with an Au-Au distance of 3.3468(3) Å, **3h** presents a chain structure of [Au(NHC)$_2$]$^+$[AuI$_2$]$^-$ units with a very long Au-Au' distance of 6.869 Å.

**Table 3.4.** Relevant distances (Å) and angles (deg) for gold(I) NHC complexes (**1-3**) as obtained by single crystal XRD

| Compound | Packing mode | Au-C (Å) | Au-X (Å) | C-Au-X (deg) | Au-Au (Å) |
|---|---|---|---|---|---|
| **1a** | Perpendicular chain | 1.972(13) | 2.281(4) | 179.0(4) | 3.525(2) |
| **1b**[a] | Perpendicular chain | 1.98(2)-2.00(2) | 2.405(2)-2.404(2) | 179.1(6)-179.3(5) | 3.351(1)-3.397(1) |
| **2a**[b] | Perpendicular dimer | 1.95(2) | 2.289(3) | 177.8(5) | 3.1804(8) |
| **2b**[a] | Perpendicular dimer | 1.988(10) – 2.000(11) | 2.4071(12) – 2.4121(11) | 175.6(3) – 176.4(3) | 3.1234(6) – 3.1352(6) |
| **2c** | [Au(NHC)$_2$]$^+$ dimers | 2.014(4)-2.019(4) | 2.5380(4) – 2.5384(4) | 175.54(17) | 3.3468(3) |
| **3a**[196] | - | 1.964(6) | 2.261(2) | 175.0(2) | - |
| **3b** | - | 1.994(3) | 2.3936(4) | 175.7(1) | - |
| **3c**[b] | [Au(NHC)$_2$]$^+$[AuI$_2$]$^-$ chain | 2.007 | 2.539 | 180.00 | 6.869 |

[a]Twinned crystal; [b]Structure obtained at room temperature.
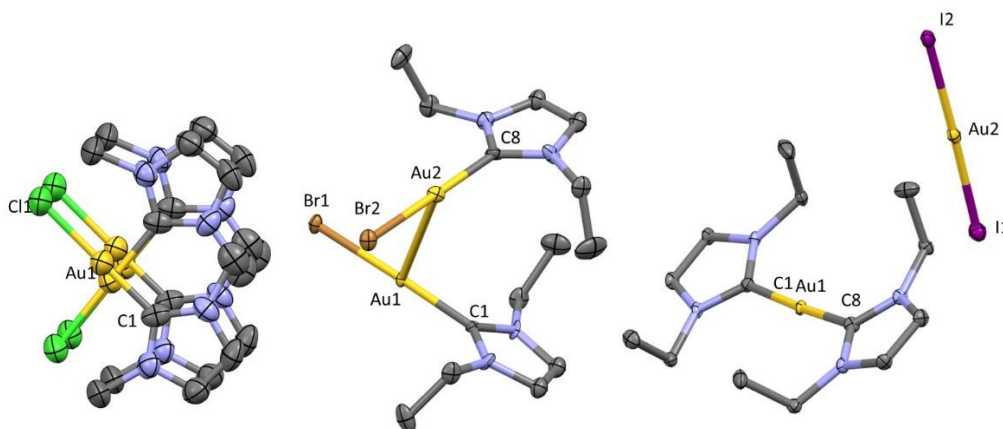


**Figure 3.4**. ORTEP plots of **1a** (left), **2b** (centre) and **2c** (right) with 50% ellipsoids. Bond lengths (Å) and angles (deg) are reported in Table 3.4. Hydrogen atoms and twinning were omitted for clarity.

### 3.3.2 Solid state packing of antiparallel complexes

Complexes **5a**, **5b**, **5e**, **7a**, **11a**, **11e**, **12a** form antiparallel dimers. Compounds **4a**, **4b**, **5c**, **6a**, **6b**, **6c**, **14a**, **15a** are again packed in an antiparallel conformation, but in this case forming a chained structure; depending on the N-substituents and on the X ligand, the chain presents

either tilted (R = Me, Et) or coplanar (R = iPr) molecules in regards to the NHC plane (Figure 3.5). For **14a**, **15a** the NHC units are all skewed in the same directions, due to the steric hindrance caused by the large halogen substituents on the NHC backbone. Short contacts are present between the backbone halogens and the X group on the gold centre.
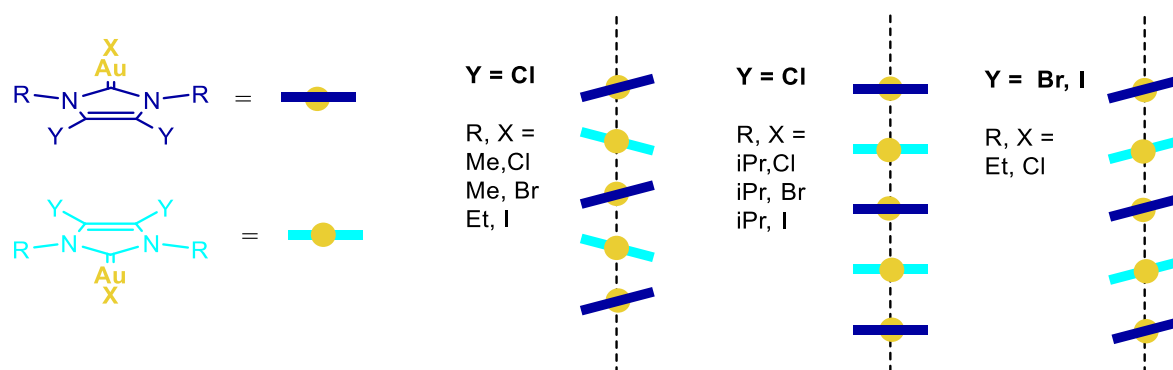


**Figure 3.5.** Graphical representation of tilted and coplanar antiparallel chains.

Considering structures of gold(I) NHC complexes bearing a chloro ligand and ethyl N-substituents (**5a**, **11a**, **12a**, **14a**, **15a**), the packing of the molecule is fairly constant, with the formation in most cases of antiparallel dimers, and in few cases chains. With the increase of the steric bulk of the backbone substituents, the Au-Au distance increases in the series Cl < Br < I (Figure 3.6). Interestingly, the shortest Au-Au distance for antiparallel dimers is observed for **11a** (3.4533(4) Å) and **11e** (3.5406(5) Å), two of the most volatile complexes studied.
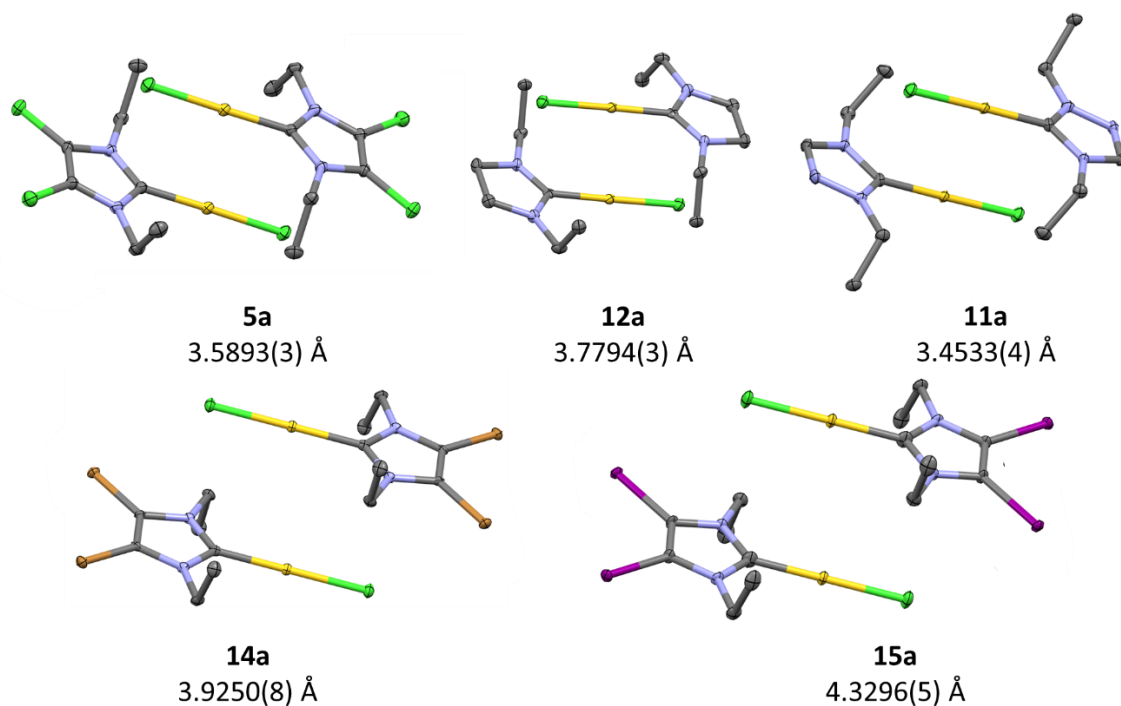
**Figure 3.6.** ORTEP plot with 50% ellipsoids of dimers of gold(I) NHC complexes presenting a chloro ligand and ethyl N-substituents. **5a**, **11a**, **12a**, **14a**, **15a**. Au-Au distances in Å. Hydrogen atoms were omitted for simplicity.

On the basis of a comparison of intermolecular distances and sublimation energies for the array of backbone chlorinated gold(I) complexes of **4**-**7** (Table 3.5), a similar trend to the reported observation on isocyanide gold(I) complexes can be seen. In all cases, the variation of the halogen ligand from Cl to Br and I leads to an increase in Au-Au distance, causing a decrease in sublimation temperature.

**Table 3.5.** Relevant distances (Å) and angles (deg) for backbone chlorinated gold(I) NHC complexes (**4-7**) as obtained by single crystal XRD.

| Cmpd. | Packing mode | Au-Au (Å) | Au-Au′ (Å) | X-Au-Au′ (deg) | NHC-X[a] (Å) | Au-X-NHC (deg) |
|---|---|---|---|---|---|---|
| **4a**[238] | Chain (tilted) | 3.818 | 3.818 | 106.90 | 3.661 | 86.29 |
| **4b** | Chain (tilted) | 3.8198(6) | 3.8198(6) | 105.339(10) | 3.692 | 86.09 |
| **5a** | Dimer | 3.5893(3) | - | 110.53(2) | 3.419 | 83.57 |
| **5b** | Dimer | 3.711(6) | - | 104.22(4) | 3.610 | 87.90 |
| **5c** | Chain (tilted) | 3.710(3) | 3.710(3) | 104.19(2) | 3.663 | 85.27 |
| **5e** | Dimer | 3.7820(3) | 4.3346(4) | 102.46(8) | 3.731 | 95.21 |
| **6a**[b] | Chain | 3.560(2) | 3.671(2) | 99.4(2) | 3.499 | 94.83 |
| **6b** | Chain | 3.8243(12) | 3.8243(12) | 110.78(4) | 3.616 | 81.25 |
| **6c** | Chain | 3.9174(7) | 3.9174(7) | 109.36(3) | 3.757 | 79.57 |
| **7a** | Dimer | 3.5582(2)-3.6148(6) | 4.3440(5) | 102.24(6)–103.71(6) | 3.389 - 3.403 | 92.03 - 90.28 |

[a]The position of the NHC is defined as a centroid calculated for the 5 atoms composing the ring.

De Proft[235] demonstrated that the main interaction leading to stabilization of antiparallel dimers of (NHC)MX complexes are the electrostatic interactions between the NHC and halogen ligands of stacked molecules. Complementarily, Pyykkö[239] demonstrated the limited importance of electrostatic interactions in complexes packing in a perpendicular dimer arrangement. The strength of the electrostatic interaction depends both on the electrostatic potential difference and on the distance between the two groups. Positive electrostatic potential has been observed on the NHC moiety, while negative electrostatic potential has been locally observed on the halogen ligand (Figure 3.7);[235] the inclusion of more electron rich groups (e.g. triazole ring) can lower the positive electrostatic potential of the NHC ring. In the same way, a less electronegative and softer halogen ligand (Cl < Br < I) leads to a X group with a smaller negative electrostatic potential. The effect of N-substituents has been proven to be

purely steric, as the increase of length of alkyl chains do not dramatically change the electron density of the NHC ring.[240]
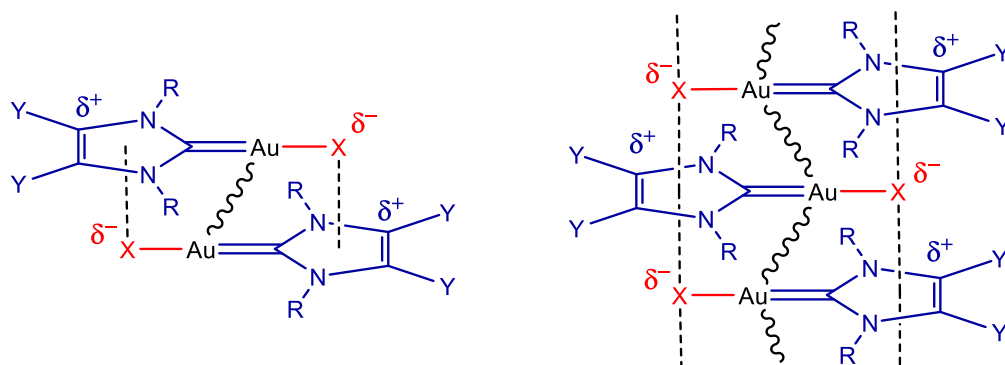


**Figure 3.7.** Antiparallel dimer and chain for gold(I) NHC complexes. Positive electrostatic potential (blue) and negative electrostatic potential (red).

## 3.4 Vacuum-TGA of silver carboxylates

Thermogravimetric analysis (TGA) is a method that has been employed extensively for the identification of thermal properties of CVD precursors such as melting, decomposition and volatilization temperature.[198,229,241,242] However, the difference in pressure conditions between sublimation of compounds in *vacuum* and TGA, which is normally performed under the protection of an inert atmosphere in atmospheric pressure, is vast. A method for obtaining the vapour pressure of volatile metallorganic CVD precursors from TGA has been developed so as to compensate for the difference in experimental conditions.[229]

Low-volatility silver carboxylates $Ag_2(\mu-O_2CC(Me)_2Et)_2$ and $Ag_2(\mu-O_2CC_2F_5)_2$ have been successfully investigated as FEBID precursors (see Chapter 1).[49,50,52] In the TGA experiments under inert gas flow the compounds were observed to decompose at a temperature of 230-321 °C, leaving silver as main remnant. However, the compounds were observed to volatilize at a temperature of 150-180 °C during FEBID experiments.[49,50,52] The behaviour observed in FEBID was instead clearly reflected in *vacuum*-TGA experiments performed in a limited vacuum of $10^{-1}/10^{-2}$ mbar: for the perfluorinated complex $Ag_2(\mu-O_2CC_2F_5)_2$ sublimation was observed starting at a temperature of 203 °C, while a concomitant decomposition and volatilization was observed for the non-fluorinated $Ag_2(\mu-O_2CC(Me)_2Et)_2$. Long isothermal sublimations at 180 °C, the temperature employed in FEBID has shown for $Ag_2(\mu-O_2CC_2F_5)_2$ the effective removal of most of the material (2% leftover mass) in a timeframe of 100 minutes. *Vacuum*-TGA has

been further tested on a larger array of silver carboxylate complexes of general formula $Ag_2(\mu\text{-}O_2CR)_2$, further confirming the observed complete sublimation for perfluorinated compounds vs. concomitant sublimation and decomposition for non-perfluorinated ones (Figure 3.8).
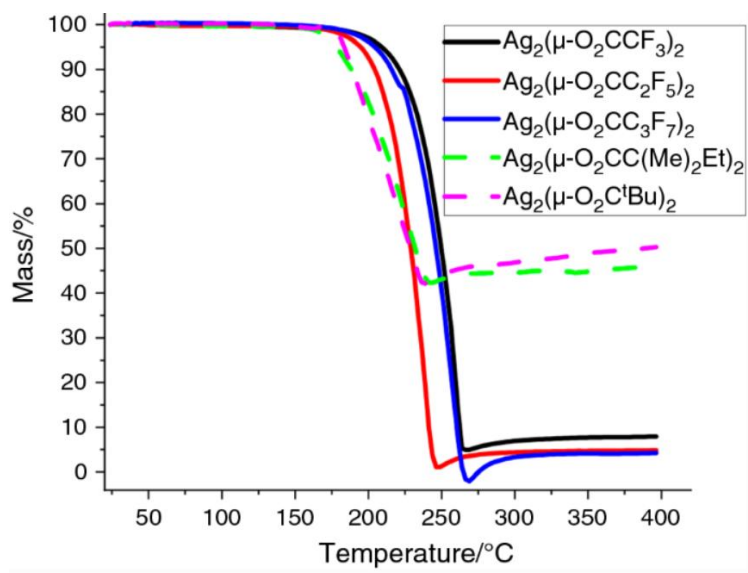


**Figure 3.8.** *Vacuum*-TGA of silver carboxylates.[228]

These observations, together with additional considerations are presented in **Paper II**. The use of *vacuum*-TGA poses itself as a suitable tool for pre-screening of FEBID precursors. However, further development of experimental conditions, such as the increase of the vacuum is highly desirable.


## 3.5 Conclusions

Cold finger sublimation is a useful tool for the comparison of sublimation temperature of organometallic complexes. Several moieties are beneficial to the increase of volatility for the studied gold(I) NHC complexes, as presented in Figure 3.9.

| Gold(I) centre | Gold(III) centre |
| Bulky alkyl N-substituents (Et, iPr) | Small alkyl N-substituents (Me) |
| Halogens on the NHC backbone | Unsubstituted NHC backbone |
| Iodide ligand | Chloride or bromide ligand |
| Trifluoromehtyl ligand | Halogen ligands |
| Saturated NHC backbone | Unsaturated NHC backbone |

Higher volatility
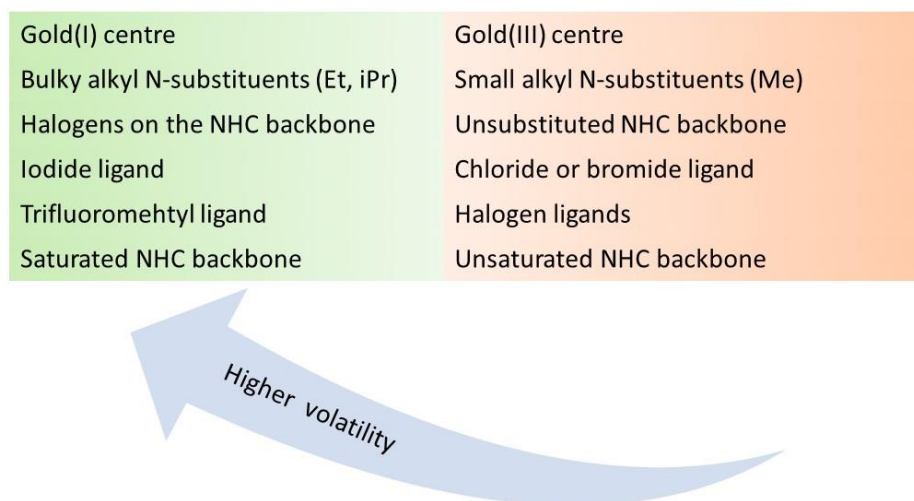
**Figure 3.9.** Dependency of the sublimation temperature on gold centre and NHC functionalization.

Through structural modifications, we were able to substantially and finely tune the volatility of the complexes in a range of sublimation temperature of 63 °C (38 to 101°C). Most of the studied complexes showed a sublimation temperature range sufficient for further application as precursors for deposition techniques, with the exception of **12a** and **5f**. Most of the complexes have shown a suitable sublimation temperature, lower than 90 °C, to be further studied as FEBID precursors, with the exceptions of **4a**, **4b** and **5f**. The complexes that delivered the best compromise between carbon content and volatility are **11e**, **11a** and **5e**, making them the most promising candidates for FEBID applications (Figure 3.10). All complexes showed a stability window (in this case limited to the sublimation window) sufficient for further studies as CVD and ALD precursors. Gold(III) NHC complexes have shown not to be suitable for deposition applications.
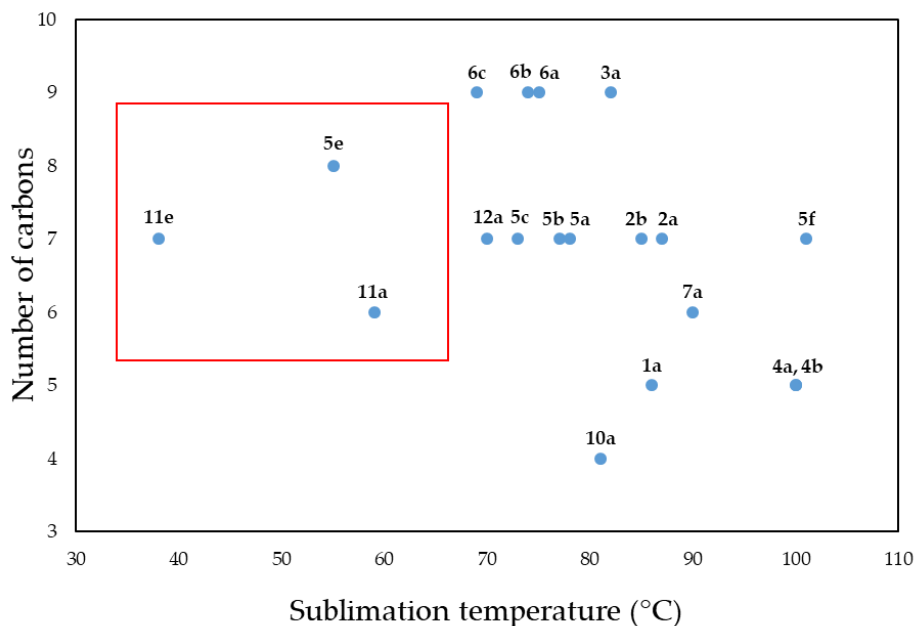
**Figure 3.10.** Plot of Sublimation temperature versus number of carbons in the molecular formula of the gold(I) and gold(III) NHC complexes.
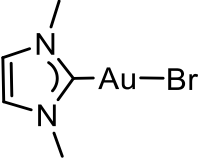
We hypothesize that these finding can be extended to other metal NHC complexes. In this direction, further development is needed.

No clear correlation between aurophilic interactions and sublimation temperature is observed. However, in (NHC)MX complexes the electrostatic interactions between dimers and chain of antiparallel oriented complexes it the most energetically important interaction. In XRD most of the complexes have been observed following this packing mode. As such, electrostatic interactions, together with steric factors, could explain the observed trends in sublimation temperatures. For future investigations, the electrostatic interactions between the L and X ligands in gold complexes are a very important parameter to consider in the *a priori* design of volatile gold(I) compounds.
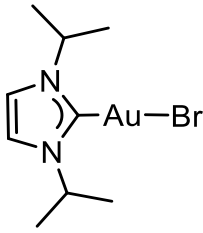
## 3.6 Experimental part

The crystal and refinement data for structures not discussed in **Paper IV** are reported here.

Crystal and refinement data for **1b**.

| | |
|---|---|
| | **1b** |
| **Crystal data** | |
| Identification code | CG_MeBr |
| Chemical formula | $C_5H_8AuBrN_2$ |
| $M_r$ | 373.01 |
| Crystal system, space group | Monoclinic, *P21/c* |
| Crystal color, shape | Colorless, needle |
| Temperature (K) | 100 |
| a, b, c (Å) | 14.8077(16), 16.0759(17), 6.6798(7) |
| α, β, γ (°) | 90, 92.191(2), 90 |
| $V$ (Å$^3$) | 1588.9(3) |
| $Z$ | 8 |
| Radiation type | Mo *Kα* |
| μ (mm$^{-1}$) | 23.46 |
| Crystal size (mm) | 0.59 · 0.09 · 0.03 |
| **Data collection** | |
| Diffractometer | Bruker D8 Venture with Photon 100 area detector |
| Absorption correction | Multi-scan |
| $T_{min}$, $T_{max}$ | 0.091, 0.495 |
| No. of measured, independent and observed [I > 2σ(I)] reflections | 4452, 4452, 3834 |
| $R_{int}$ | 6.48 |
| (sin θ/λ)max (Å$^{-1}$) | 0.717 |
| **Refinement** | |
| $R[F^2 > 2\sigma(F^2)]$, $wR(F^2)$, S | 0.073, 0.212, 1.12 |
| No. of reflections | 4452 |
| No. of parameters | 169 |
| No. of restraints | 6 |
| H-atom treatment | H atom parameters constrained |
| | w = 1/[σ$^2$(F$_o^2$) + (0.1334P)$^2$ + 48.8177P] where P = (F$_o^2$ + 2F$_c^2$)/3 |
| Δρ$_{max}$, Δρ$_{min}$ (e Å$^{-3}$) | 6.12, -6.29 |

Crystal and refinement data for **3c**.

| | |
|---|---|
| |  **3c** |
| **Crystal data** | |
| Identification code | cgr104_a |
| Chemical formula | $C_9H_{15}Au_{0.5}N_2 \cdot Au_{0.5}I$ |
| $M_r$ | 478.12 |
| Crystal system, space group | Triclinic, $P$-1 |
| Crystal color, shape | Colorless, needle |
| Temperature (K) | 293 |
| a, b, c (Å) | 7.253 (3), 8.915 (4), 10.773 (5) |
| α, β, γ (°) | 76.359 (13), 74.972 (13), 78.226 (12) |
| $V$ (Å$^3$) | 646.2 (5) |
| $Z$ | 2 |
| Radiation type | Mo $K\alpha$ |
| μ (mm$^{-1}$) | 13.74 |
| Crystal size (mm) | 0.4 × 0.2 × 0.05 |
| **Data collection** | |
| Diffractometer | Bruker D8 Venture |
| Absorption correction | Multi-scan |
| T$_{min}$, T$_{max}$ | 0.292, 0.746 |
| No. of measured, independent and observed [I > 2σ(I)] reflections | 19270, 2992, 2506 |
| $R_{int}$ | 0.053 |
| (sin θ/λ)max (Å$^{-1}$) | 0.652 |
| **Refinement** | |
| $R[F^2 > 2\sigma(F^2)]$, $wR(F^2)$, $S$ | 0.035, 0.083, 1.12 |
| No. of reflections | 2992 |
| No. of parameters | 125 |
| No. of restraints | 6 |
| H-atom treatment | H atom parameters constrained |
| | $w = 1/[\sigma^2(F_o^2) + (0.0126P)^2 + 3.1133P]$ where $P = (F_o^2 + 2F_c^2)/3$ |
| Δρ$_{max}$, Δρ$_{min}$ (e Å$^{-3}$) | 1.27, −3.03 |

# Chapter 4.

# Other investigations performed on Gold(I) NHC complexes

## *4.1 Introduction*

In this chapter, other investigations performed gold(I) NHC complexes by means of electrochemical studies and EI-MS are discussed. The data discussed in this chapter has not been published. The electrochemistry studies performed on the gold NHC complexes were carried out with the help of Kaiqi Xu, while the EI-MS were performed by Osamu Sekiguchi.

## *4.2 Cyclic voltammetry and electrosynthesis*

In recent literature greater emphasis was put on finding accessible routes to the use of gold complexes as redox catalysts.[243] Unlike its neighbour Pt, gold has a very high oxidative barrier in the process Au(I)/Au(III) at +1.4 V.[244] To overcome this high barrier, stoichiometric amounts of oxidant have been used, that led to the application of gold as a catalyst for oxidative coupling of arenes,[245] oxidative cyclisation,[246] and C-F bond formation.[247] Recently, Ye *et al.* reported the first homogeneous electrochemically facilitated redox gold catalysis, where the Au(I)/Au(III) oxidation was achieved by anode oxidation.[248] The process led to the efficient coupling of both symmetrical and unsymmetrical conjugated dienes by the use of a gold catalyst. The aim of the work presented in this section is to explore the redox behaviour of selected gold(I) NHC complexes (Figure 4.1).
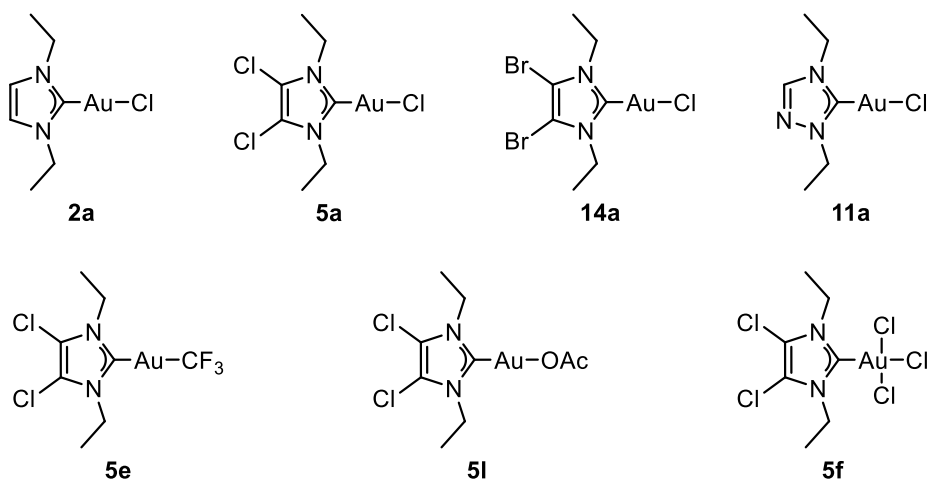
**Figure 4.1.** Gold(I) NHC complexes investigated by cyclic voltammetry.

### 4.2.1 Cyclic voltammetry of gold(I) NHC complexes

The redox behaviour of compounds **2a**, **5a**, **5d**, **14a** and **11a** was explored by means of cyclic voltammetry. Cycles in reduction (0 to -2 V) led to no reduction peaks for all compounds, indicating that no gold(0) species were formed, with the notable exception of **11a** that undergoes a reduction $Au^{I}/Au^{0}$ at -1.4 V. Previous reported gold(I) NHC complexes presented the reduction $Au^{I}/Au^{0}$ in a range of -0.91/-1.16 V.[249] The studied compounds fall outside of this range, with a high stability to negative potential, up to -2 V (Figure 4.2). In oxidation (0 to 2 V) either one or two oxidation peaks above 1.4 V were observed for all compounds, indicating oxidation of gold(I) to gold(III). While one oxidation is clearly attributed to the $Au^{I}/Au^{III}$ process, the second could be due to reactivity linked to the organic ligand. In the full potential window (2 to -2 V) for all gold complexes an additional reduction peak at around -0.3 V was observed, diagnostic of a reduction $Au^{III}/Au^{I}$.
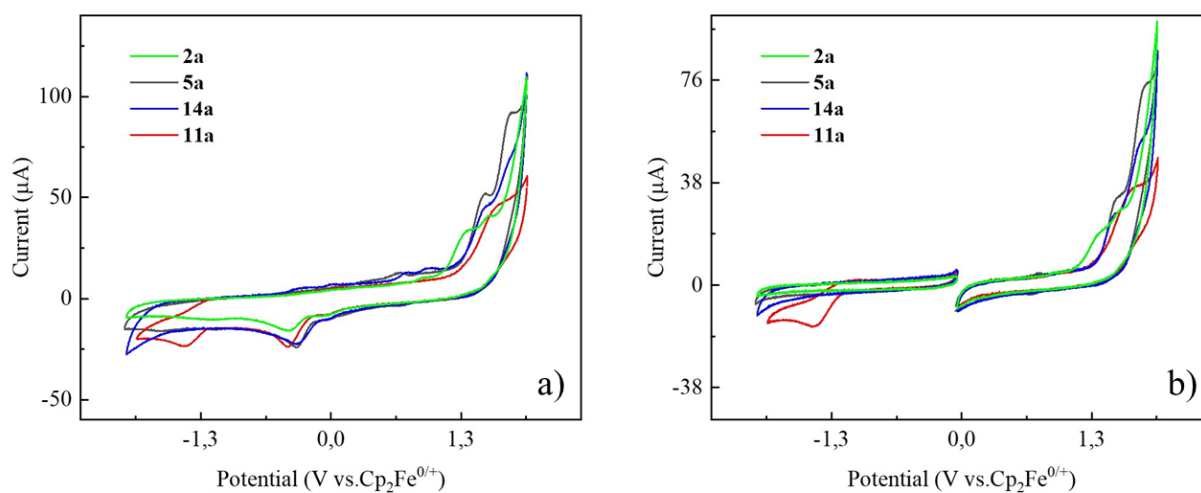
**Figure 4.2.** Left: overlaid cyclic voltammograms of gold(I) complexes with different NHC ligands (**2a**, **5a**, **14a**, **11a**); Right: selective reduction (0 to -2V) and oxidation (0 to 2V). Scan rate 0.1 V/s, 0.1 M N(nBu)$_4$PF$_6$ in acetonitrile.

Complexes **5e** and **5l** were tested in order to evaluate the effect of the presence of other anionic ligands, namely $^-$CF$_3$ and $^-$OAc. Compound **5l** was obtained by the substitution of the chloro ligand of **5a** by mixing at room temperature with silver acetate (Scheme 4.1).[219]
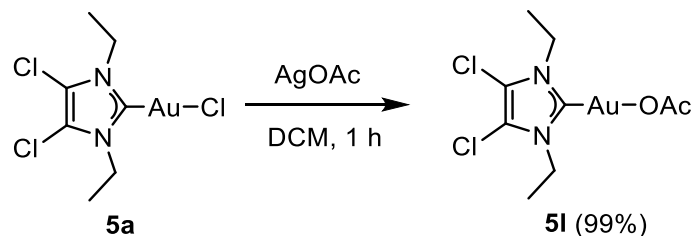


**Scheme 4.1.** Synthesis of **5l**.

For these complexes, the only observed difference from the chloro based **5a** was the lack of any reduction peak also in the full range cycles (2 to -2 V) (Figure 4.3).
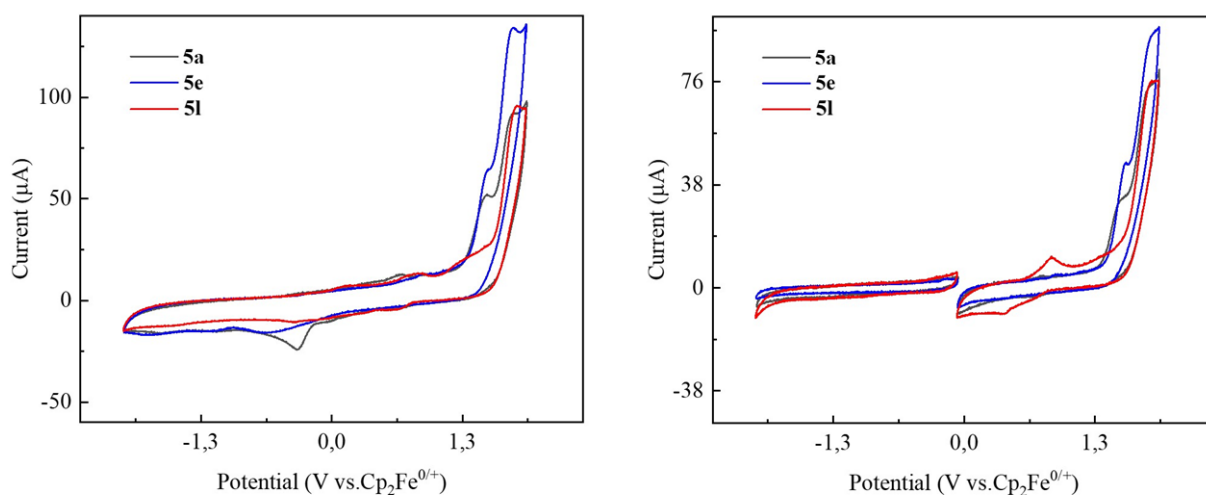
**Figure 4.3.** Left: overlaid cyclic voltammograms of gold(I) complexes with different anionic ligand (**5a** Cl, **5d** CF$_3$, **5l** OAc); Right: selective reduction (0 to -2V) and oxidation (0 to 2V). Scan rate 0.1 V/s, 0.1 M N(nBu)$_4$PF$_6$ in acetonitrile.

### 4.2.2 Gold(III) CV and electrosynthesis

In order to confirm the Au$^I$/Au$^{III}$ and Au$^{III}$/Au$^I$ processes, the Au(III) complex **5f** has been explored. As expected when scanning in reduction, only a reduction peak for Au$^{III}$/Au$^I$ was observed at –0.51 V, while in positive scanning no oxidation was observed. In the full cycle, two oxidation and one reduction peaks were present (Figure 4.4). The oxidation peak at 0.7 V was in accordance to the reported formal potential of Cl$_2$ vs. FeCp*$_2^{+/0}$ of 0.69 V,[250] thus indicating the formation of Cl$_2$ from 2Cl$^-$, generated in turn from the reduction of the Au(III) complex **5e** to **5a**. The second oxidation peak at 1.5 V corresponded exactly to the Au$^I$/Au$^{III}$ oxidation observed for **5a**.
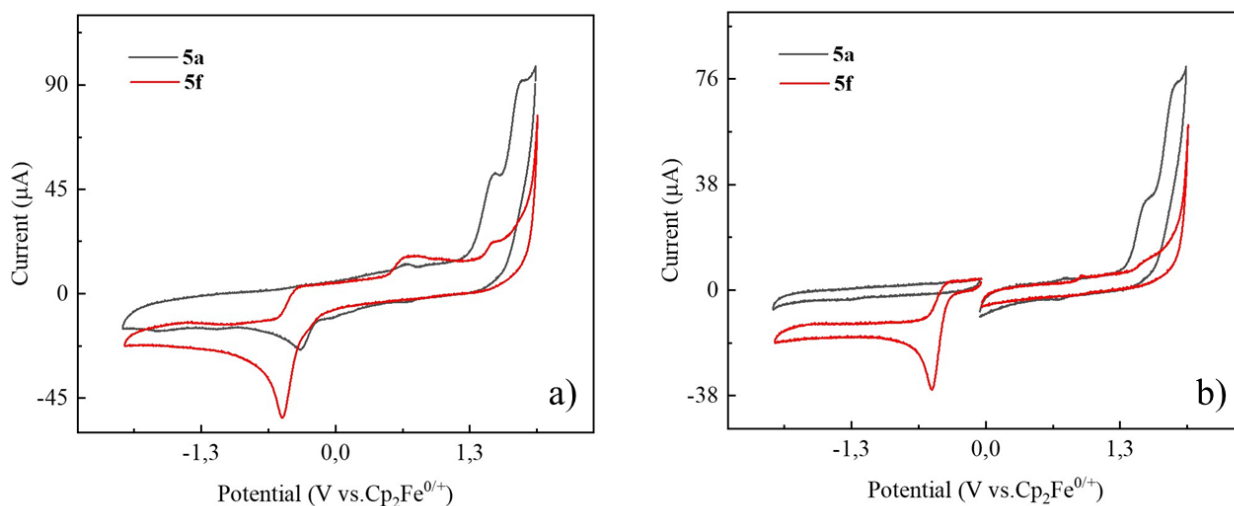
**Figure 4.4.** Left: overlaid cyclic voltammograms of gold(I) complexes with different starting oxidation state **5a** Au(I), **5f** Au(III); Right: selective reduction (0 to -2V) and oxidation (0 to 2V). Scan rate 0.1 V/s, 0.1 M N(nBu)$_4$PF$_6$ in acetonitrile.

To further confirm the assignment of the Au$^I$/Au$^{III}$ oxidation, preparative electrolysis was performed starting from **5a** at 1.6 V vs. Ag/AgNO$_3$ reference electrode. For preparative electrolysis a Pt meshed electrode with a high surface area was used; the cell was separated by a porous frit in an anodic and a catodic section. N(Me)$_4$BF$_4$ was chosen as the electrolyte, as it can be easily removed from the reaction solution by adding a large quantity of DCM and filtering of the insoluble salt. The purified solution was analyzed by $^1$H NMR and $^{13}$C NMR and peaks consistent with a [Au$^{III}$(NHC)X$_{3-z}$Y$_z$]$^{+z}$ complex were observed. The most indicative variation was the shift of the carbene carbon through the oxidation Au$^I$/Au$^{III}$ from 170.8 ppm to 141.7 ppm (Figure 4.5). The reaction mixture contained a 73:27 ratio of Au(III) and Au(I) species after 60 minutes of oxidation; the conversion was in accordance with the total current obtained by chronoamperometry for an overall 2 electron process.
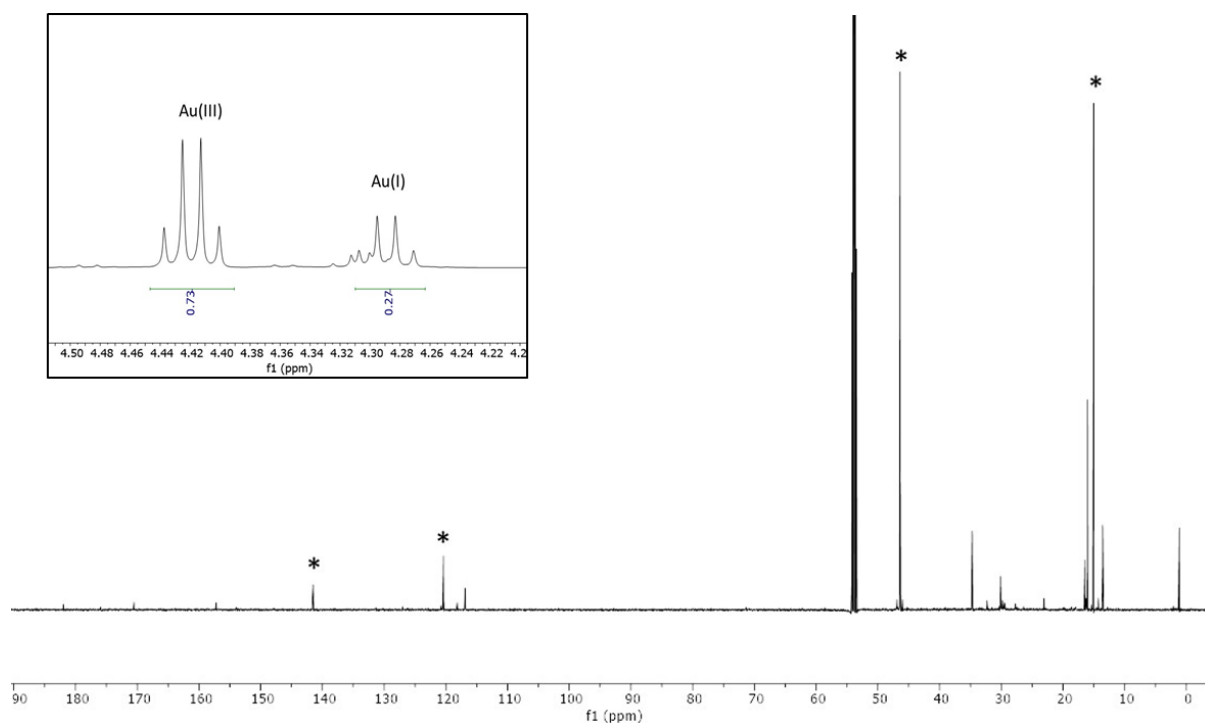
**Figure 4.5.** $^{13}$C NMR (CD$_2$Cl$_2$, 151 MHz) of the isolated mixture from electrosynthesis, peaks assigned to **5m** are marked with *; in detail, $^1$H NMR (CD$_2$Cl$_2$, 600 MHz) of the NC*H*$_2$CH$_3$ protons used for quantification.

As no chloride was present in the chosen system, an oxidation of the gold(I) centre by Cl$_2$ produced *in situ* was excluded. The most probable species formed during oxidation is [Au(**5**)(MeCN)$_2$Cl]$^{2+}$[BF$_4$]$_2{}^{2-}$ (**5m**) (Scheme 4.2).
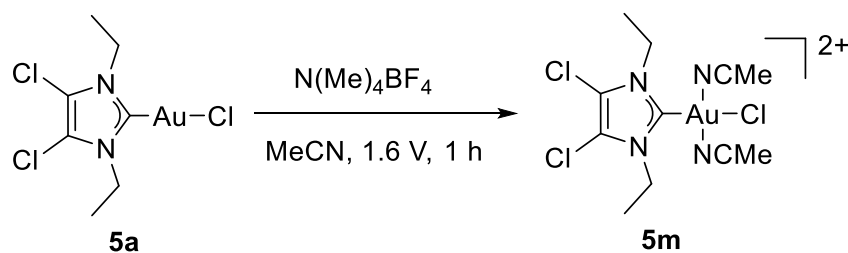


**Scheme 4.2.** Electrosynthesis of a gold(III) NHC species from **5a**.

Early catalytic experiments were performed on the homocoupling reaction of phenylacetylene using **5a** as a catalyst, with only stoichiometric formation of product. Further development of the catalytic conditions is necessary.

## 4.3 Low energy EI-MS

Electron Ionization Mass Spectrometry is used to observe electron induced fragmentations of organic and organometallic compounds. This characterization technique has some common

features with a FEBID process, since in EI-MS a gaseous compound is irradiated by an electron beam and the ions formed by the induced fragmentation are registered.

The most relevant differences lay in the state of the study matter (adsorbed in FEBID while gaseous in EI-MS) and in the nature and energy of the used electrons. While in FEBID SE electrons are used for decomposition, in EI-MS the electrons of the primary beam are responsible for the decomposition of the analyte. A further limitation is presented by the fact that in EI-MS only positive ions can be detected, which is a great restriction of the scope of observable fragments. Nevertheless, EI-MS could be a suitable tool in detecting the different decomposition pathways available for a precursor molecule, and it could be possible to link that to the obtained deposits composition.[44]

### 4.3.1 Low energy EI-MS of 5a

EI-MS of **5a** were performed at different ionization energies of 70 eV, 20 eV, 12 eV, 10 eV and 8 eV (Table 4.1). At 70 eV the most intense observable peak was the $[M]^{\bullet+}$ peak at 424 m/z, qualitatively indicating robustness of the molecule under electron beam irradiation. The other main observed peaks were for the $[M-Cl]^+$ and $[M-HCl]^+$ fragments. As such, the most favourable fragmentation involved the cleavage of the metal-halogen bond. Such fragmentation intensity is in line with the observations made in the composition of the obtained deposited structures (**Paper III**) where the at.% of Cl is very limited for **5a**. The decomposition of the molecule further progressed with the additional loss of one N-alkyl substituent ($[M-Cl-Et]^+$) or with the loss of the NHC ring integrity ($[M-Cl-C_2Cl_2+H]^+$, $[AuCNH]^+$). Other peaks relative to non gold-containing species were detected, relative to various degrees of fragmentation of the isolated NHC ring.

A clear trend for the various gold-containing species was observed with the stepwise decrease of electron beam energies. The most intense variation was observed for $[M]^{\bullet+}$, which increases its relative intensity of 16%, indicating that at lower eV the fragmentation of the molecule could be less efficient. Furthermore, also the signal for the $[M-HCl]^+$ fragment was greatly increased from 14 to 24%. The ratio between these two signals was very constant throughout these experiments, indicating that the fragment $[M-HCl]^+$ could be generated from $[M]^{\bullet+}$. The opposite trend was observed for both $[M-Cl]^+$ and $([M-Cl-Et]^+$. The ratio of the relative intensity of the two signals is also in this case roughly constant. The two other fragments, [M-Cl-

$C_2Cl_2+H]^+$ and $[AuCNH]^+$ were not present at low eV and they both disappeared between 12 and 10 eV. However, it should be noted that the signals for these species were not very intense in first instance. Fragments of the precursor not containing gold are not reported.

**Table 4.1.** Main gold containing peaks observed for the EI-MS of 5a and their intensity in percentage of the total signal.

| m/z, fragment | 70 eV | 20 eV | 12 eV | 10 eV | 8 eV |
|---|---|---|---|---|---|
| 424, $[M]^{\bullet+}$ | 34 | 36 | 41 | 47 | 50 |
| 389, $[M-Cl]^+$ | 29 | 25 | 23 | 21 | 16 |
| 388, $[M-HCl]^+$ | 14 | 16 | 20 | 20 | 24 |
| 360, $[M-Cl-Et]^+$ | 15 | 18 | 15 | 12 | 10 |
| 296, $[M-Cl-C_2Cl_2+H]^+$ | 4 | 4 | 1 | 0 | 0 |
| 224, $[AuCNH]^+$ | 4 | 1 | 0 | 0 | 0 |

While the change in eV has led to a substantial variation of the relative intensities of the fragments, no new fragmentation pathway was generated, and thus further experiments at 70 eV were taken as representative of the fragmentation also at low eV. The same comparison between high and low eV ionization energies was performed for **2a** and again no substantial difference in decomposition pathways was observed.

### 4.3.2 EI-MS of other complexes

The EI-MS analyses were carried out on compounds **1a**, **2a**, **3a**, **4a**, **5b**, **5c**, **6a**, **11a**. For all compounds a major decomposition pathway was identified in the loss of the halogen ancillary ligand, and the formation of the $[(NHC)Au]^+$ (or $[M-X]^+$ ) fragment. This observation fits well with the FEBID experiments, where the halogen at.% in the obtained deposits was always very limited (up to 3.3%).

Compound **5a** showed the presence of another intense signal corresponding to the fragment $[M-HCl]^+$. This signal was detected also for **6a**, but not for **4a**. NHC ligands with R = Et, iPr

differ from R = Me (**4a**) for the presence on the alkyl chains of β-protons, that in this case can play a fundamental role in the decomposition. Thus, the EI-MS suggests the presence of an agostic interaction between the metal centre and one or two β-protons. The proton loss can occur only from a N-substituent in compounds **4a-6a**, since no other hydrogens are present in the molecular structure. Such fragmentation is not observed for **5b** and **5c**, where X = Br, I, indicating that it is necessary to have chlorine as the ancillary ligand. This observation could indicate that a decomposition pathway is present only for complexes with X = Cl, and partially explain the difference in EDX composition of the obtained FEBID deposits of **5a** and **5b** and **5c** (see Chapter 5). Nevertheless, the Cl involved in such decomposition pathway could originate from the backbone of the molecules. To exclude this, the same experiments are performed on **1a**, **2a** and **3a**, and again the $[M-HCl]^+$ is present for **2a** and **3a**; **1a** lacks β-protons and, as observed before for the analogue **4a** a $[M-HCl]^+$ is not present. A similar trend to **5a** was observed for **11a**. The highly different composition of the deposits of the imidazole and of the triazole-based complexes is not explained by EI-MS.

## 4.4 Conclusions

Cyclic voltammetry of the selected gold(I) NHC complexes shows that imidazole-based compounds have a large range of stability both in positive and negative potential. The oxidation of gold(I) species to gold(III) and vice versa has been identified, and only in the case of the triazole-based complex **11a** reduction of gold(I) to gold(0) was observed.

In the EI-MS experiments at variable ionization energy, a different pathway of decomposition has been identified for complexes presenting a chloro ancillary ligand and β-protons on the N-substituents. This behaviour could partially explain the differences observed in Chapter 5 in the EDX composition of FEBID deposits.

## 4.5 Experimental part

Electrochemical measurements were performed on an AMETEK PARSTAT 4000 potentiostat/galvanostat at room temperature and under Argon atmosphere. Cyclic voltammetry was performed in a three electrode configuration, with a glassy carbon working electrode, a Pt wire counter electrode and an $Ag/AgNO_3$ pseudo reference electrode. All

measurements were performed using a 0.1 M solution of $N(nBu)_4PF_6$ in acetonitrile. For each experiment 10.0±3 mg of gold(I) or gold(III) complex were used. Ag reference electrode was referenced after each experiment to the ferrocene/ferrocenium couple.

**Electrosynthesis**

25.6 mg of **5a** were dissolved in 25 mL of saturated solution of $N(Me)_4BF_4$ in acetonitrile and charged in a two-compartments cell. In the first compartment the solution of gold(I) complex was charged, together with a Pt meshed working electrode and an $Ag/AgNO_3$ reference electrode. In the second compartment 25 mL of electrolyte solution and a Pt foil counter electrode were inserted. All manipulations were performed under Argon atmosphere. A 1.6 V current was applied to the working electrode compartment under stirring and Argon bubbling. After 60 minutes, the gold solution was transferred and upon addition of circa 200 mL of DCM, precipitation of the electrolyte was observed. The suspension was filtered over a type 4 filter under reduced pressure and the obtained pale yellow solution was concentrated to dryness leaving a grey solid, that was partially solubilized in $CD_2Cl_2$ and filtered prior to NMR characterization. From chronoamperometry 8.44 C were produced, corresponding to $8.7 \cdot 10^{-5}$ moles of electrons, that cause a conversion of 73% of $6.0 \cdot 10^{-5}$ moles of gold(I) complex to gold(III).

EI-MS experiments were registered on a Bruker Scion-TQ Premium GC-MS.

# Chapter 5.

# FEBID experiments on gold(I) NHC complexes and on-substrate GIS development

## *5.1 Introduction*

In this chapter the FEBID experiments performed using selected gold(I) NHC complexes as precursor molecules will be discussed.

The experiments were performed during exchange periods in 2019 and 2020 at Delft University of Technology under the supervision of Professor Cornelis W. Hagen, and at TESCAN s.r.o. Brno under the supervision of Jaroslav Jiruše. A close collaboration in the hosting institutions was active with Aya Mahoub and Dominik Marko. The FEBID experiments on compounds **1a**, **2a,** and **3a** were performed by Jakub Jurczyk under the supervision of Ivo Utke at EMPA.

Different deposition apparatuses, both homemade and commercially available have been used, but they all follow the same basic functioning. For the benefit of further discussions in this chapter we will broadly define the components and features of a Gas Injection System (GIS).

A GIS used for FEBID applications is comprised of three fundamental parts: a reservoir, where the precursor is stored, a gas supply system, and a nozzle, for the topical delivery of the precursor in the desired area (Figure 5.1.). The resulting precursor flux depends on the flow rate, the nozzle geometry, and the position relative to the substrate. One useful way of controlling the flow rate is the variation of the temperature of the reservoir to increase or decrease the vapour pressure.[48] The relation between emitted flux and reservoir temperature is exponential.[251] While in commercial apparatuses the presence of a valve between reservoir and nozzle is the norm, in experimental setups open systems are common.[252]
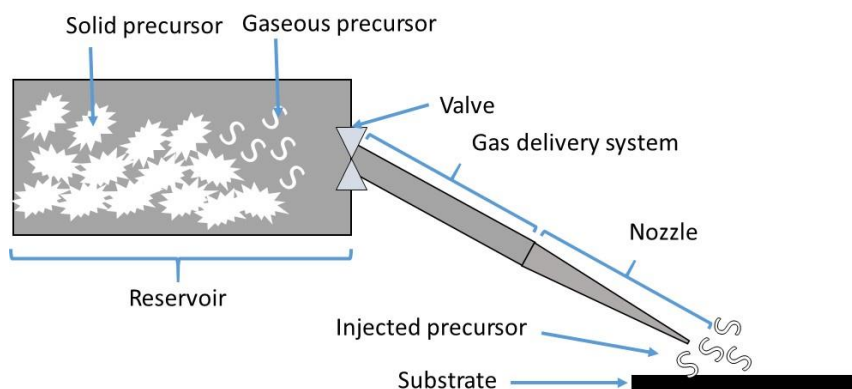
**Figure 5.1.** Generic schematic of a GIS.

For FEBID deposits, major features to be taken in consideration are shape, composition and growth rate of the obtained structures. All these features depend on several factors: on the electron beam parameters (energy, current, dwell time, draw strategy), on the properties of the precursor molecule, and on the chosen substrate (composition, temperature, tilt, surface).[48]

## 5.2 On-substrate FEBID testing

The work discussed in this section has been carried out at Delft University of Technology during an exchange period fostered by the ELENA project. The developments of the on-substrate reservoir system and the testing at low temperature are presented in **Paper III**. In this section, additional free crystal experiments and high temperature experiments will be presented. Furthermore, the discussion on some features not presented in **Paper III** will be extended in detail.

### 5.2.1 GIS and free crystal exploration

Commercially available GISs present several limitations to the test of new FEBID precursors:

- Low temperature range (up to 65 °C for FEI GIS)
- Long injection path
- Possible temperature gradient
- Possible reactivity of the precursor with materials of the GIS

During early testing with FEI GIS we ran in some of these problems, and no injection of intact precursor have been achieved, testing precursors **5a**, **4b** and **11a**.

In order to investigate the precursors, a different approach than the use of a traditional GIS had to be taken. The sublimation of free crystals of precursor on a heated silicon substrate was studied in the vacuum chamber of a SEM. A prototype for substrate heating produced by Gaudhaman Jeevanandam was used.[253] The first tested precursor was **11a**; upon heating, imaging was performed at time intervals in order to observe the volatilization of crystals without causing electron beam induced decomposition. The free crystals of this compound have been observed to volatilize at a starting temperature of 85 °C, and full sublimation was achieved at a reached temperature of 100 °C (Figure 5.2). Due to the quick heating process and to the observation of only bulk crystal sublimation, the detected incipient sublimation temperature is higher than the one observed during cold finger sublimation. This is expectable due to the different experimental conditions.
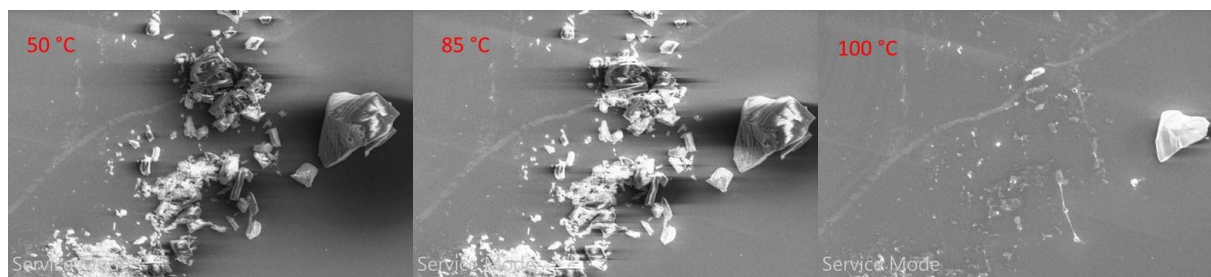


**Figure 5.2.** Disappearance of crystals of **11a** at $10^{-5}$-$10^{-6}$ mbar at different temperatures. Helios SEM.

During these first experiments, deposition in the proximity of the crystal was attempted through exposition in beam mode of a selected position. To our surprise, we observed readily the formation of deposits in the crystal proximity, together with the consumption of the crystal itself at a substrate temperature of 120 °C (Figure 5.3). This was an indication that not only the precursor was being effectively sublimed, but that a suitable amount of substrate coverage was achieved, and deposition of adsorbed material was possible at the studied temperature.
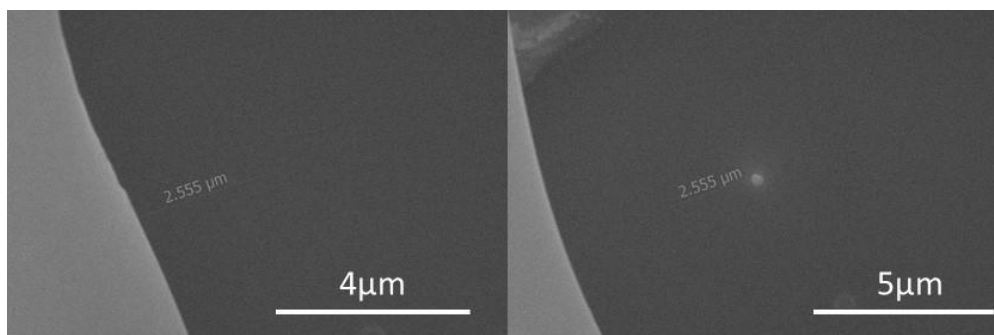
**Figure 5.3.** Deposition of a spot of **11a**, before (left) and after (right). Deposition performed at 120 °C. The large white object in the frame is a crystal of **11a**. Helios SEM.

Similar tests were carried out also on **5a** and **5c**, and in all cases it was possible to sublime the precursor crystals and to deposit structures. In all these experiments, since the temperature limitation for the substrate heater was around 200 °C, the deposition and sublimation experiments were performed at high temperatures to achieve a sufficient precursor flow in the open system.

Compound **4a** was the only tested compound where no sublimation of the crystals was observed up to a temperature of 120 °C and no deposits could be grown. As previously stated in Chapter 3, the sublimation temperature of **4a** is higher than the one of all the other precursors tested in this chapter by at least 22 °C.

### 5.2.2 On-substrate reservoir setup

In order to optimize the conditions and obtain more control over the deposition parameters, an additional piece was designed to be added to the substrate heater in order to locally mimic a Gas Injection System. This piece is an aluminium layer that is described in detail in **Paper III** (Figure 5.4). The aluminium piece was tightly fixed to the substrate heater with Kapton tape in order to prevent substantial precursor leaks and involuntary setup movements. Such behaviour was observed in an early conical design of the piece.

In this way an on-substrate GIS was designed, where reservoir, nozzle and substrate are all on the same plane and always connected. This means that such precursor tester can be utilized only for precursors that selectively sublime, as melting would cause full coverage of the substrate with liquid precursors, and that are stable and non toxic at atmospheric pressure and ambient temperature, since the setup is open during loading.
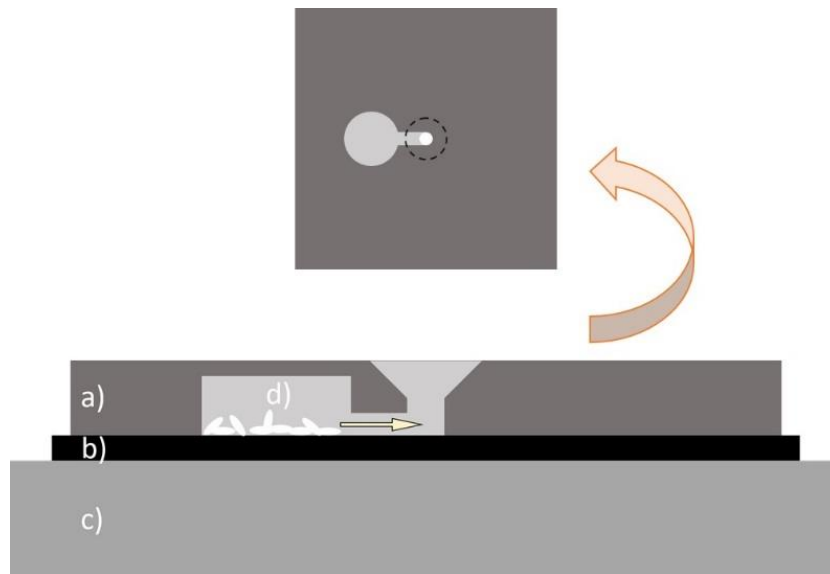
**Figure 5.4.** a) Cross section of the vapour guide on the b) substrate and c) substrate heater; d) reservoir. On top a bottom view of the vapour guide.

The temperature of the heater was controlled by an external power supply and checked by a handheld thermocouple.[253] During experiments, the current was controlled in order to obtain the desired temperature. In order to avoid interference of such devices with the imaging process, both power supply and thermocouple reading unit were grounded to the SEM (Figure 5.5).
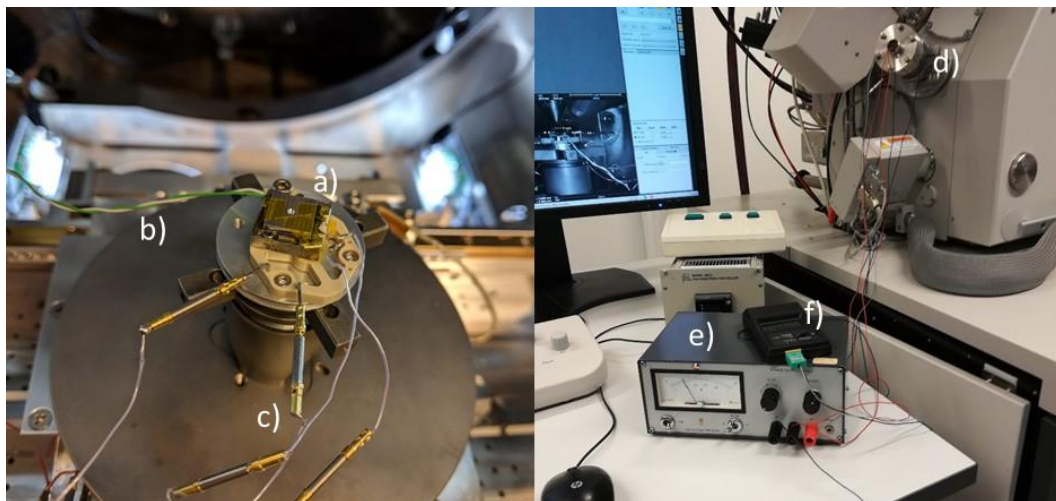


**Figure 5.5.** On-substrate reservoir setup: a) heater and sample, b) thermocouple, c) cables, d) feedtrough port, e) power supply, f) thermocouple reader.

### 5.2.3 On-substrate reservoir tests at high temperature

In initial testing high temperatures were employed in order to obtain a sufficient flow of gaseous precursor; **5a**, **5b**, **5c** and **6a** were tested at temperatures up to 160 °C, while **11a** was tested up to 120 °C in order to stay under its melting temperature.

In all cases deposits could be grown, and presence of gold in the deposit was confirmed by EDX. Due to the small dimension of the structures, the analyses can be considered only qualitative and a confirmation of presence of gold and other elements existent in the precursor, such as carbon, nitrogen, chlorine and bromine.

**11a** deposits showed to include only carbon and gold with a relatively high gold atomic percentage, up to 30%. The obtained deposits showed the presence of a halo that thickens with the increase of exposition time (Figure 5.6).
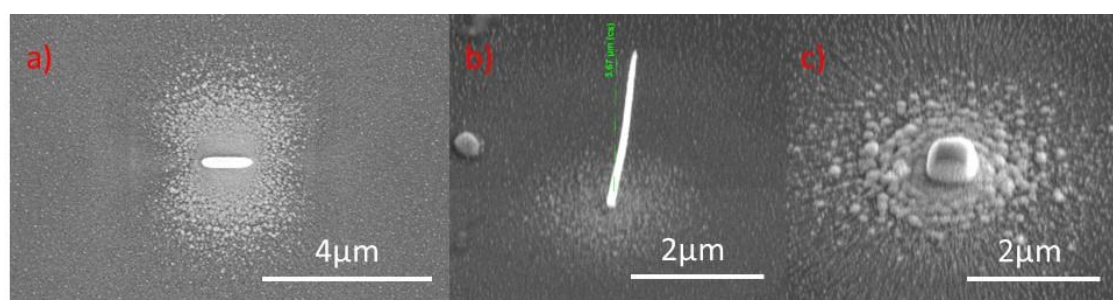


**Figure 5.6.** Selected structures obtained from **11a** at 120 °C using the on-substrate precursor tester. a) top down image of 1 μm line, pitch 4 nm, dwell 500 μs, 5kV, nominal 50 pA, 10 passes; b) 40° tilt image of pillar, 20 kV, nominal 50 pA, 2 min exposure, height 3.67 μm; c) 40° tilt image of square deposit 500x500 nm, pitch 4 nm, dwell 500 μs, 5 kV, 50 pA, 100 passes. Helios SEM.

Compounds **5a**, **5b** and **5c** led to the formation of ring structures at a nominal current of 800 pA (Figure 5.7); this high current was chosen amid an initially observed low growth for **5a** in order to expedite the growth of structures. This ring structure was also observed for high exposure time and is most probably due to a local depletion of the precursor in the centre of the structure. In FEBID, the deposited material is adsorbed precursor coming from the gas phase; as such, whenever the precursor is locally depleted, the adsorbed precursor follows the gradient and through migration reaches the depleted area. In the case of the ring structures, the deposition of material around the structure hinders the migration of adsorbed precursor to the centre of the structure, causing a local depletion. The deposited structures should be 25x25 nm wide, but in the case of 5kV a 1μm of diameter ring was deposited. This diameter

correlates well with the range of BSE caused by a 5kV focused electron beam. In all structures Au, C, N and Cl were detected; for **5b** Br was also observed.
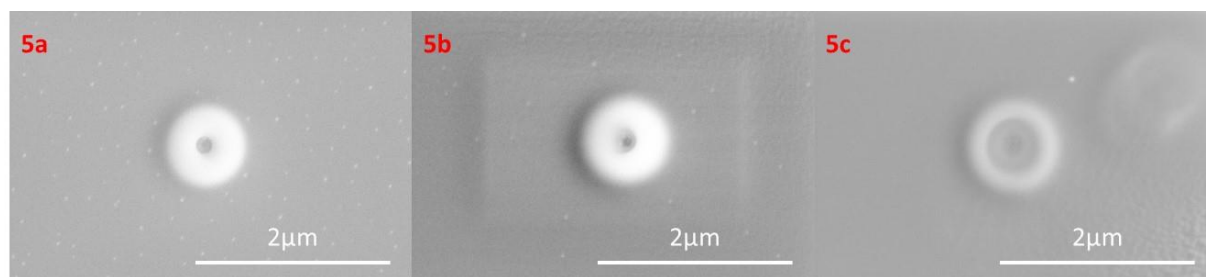


**Figure 5.7.** Selected ring structures obtained from **5a**, **5b** and **5c** at 160 °C using the on-substrate precursor tester. 25x25 nm, pitch 4 nm, dwell 500 μs, 5 kV, nominal 800 pA, 10000 passes. Helios SEM.

Compound **6a** showed to deposit in the same conditions closed structures with a great vertical growth rate. As the volatility of **6a** is the same as **5c**, this difference in behaviour could be linked to the possible presence of more precursor in the gas phase, but would be in disagreement with previous observations of sublimation temperature. Another possible explanation is that the mobility of **6a** is greater than for the precursors from **5**.

### 5.2.4 On-substrate reservoir tests at low temperature

In order to have more control over the deposition of the structures, the used temperatures were lowered considerably for all tested complexes (Table 5.1).

**Table 5.1.** Range of explored temperatures for FEBID.

| Compound | Highest tested temperature (°C) | Lowest tested temperature (°C) |
|:---:|:---:|:---:|
| **4a** | - | 120 |
| **5a** | 160 | 100 |
| **5b** | 160 | 100 |
| **5c** | 160 | 100 |
| **6a** | 140 | 100 |
| **11a** | 120 | 100 |
| **5e** | - | 100, 80 |

Two different sets of structures were grown at low temperatures for each precursor: a square 250x250 nm deposit for composition analysis and an array of 9 pillars deposited with different

dwell time for growth rate studies. In the produced structures, rings are observed only for **4a** and **5a** at a measured current of 600 pA. For compounds **5b**, **5c** and **6a** we instead observe only minor depletion in the centre of the structure. At a current of 40 pA all structures are closed and well defined, and present around double the expected thickness (Figure 5.8 - Figure 5.14). Again for **11a** the presence of an important halo was observed.
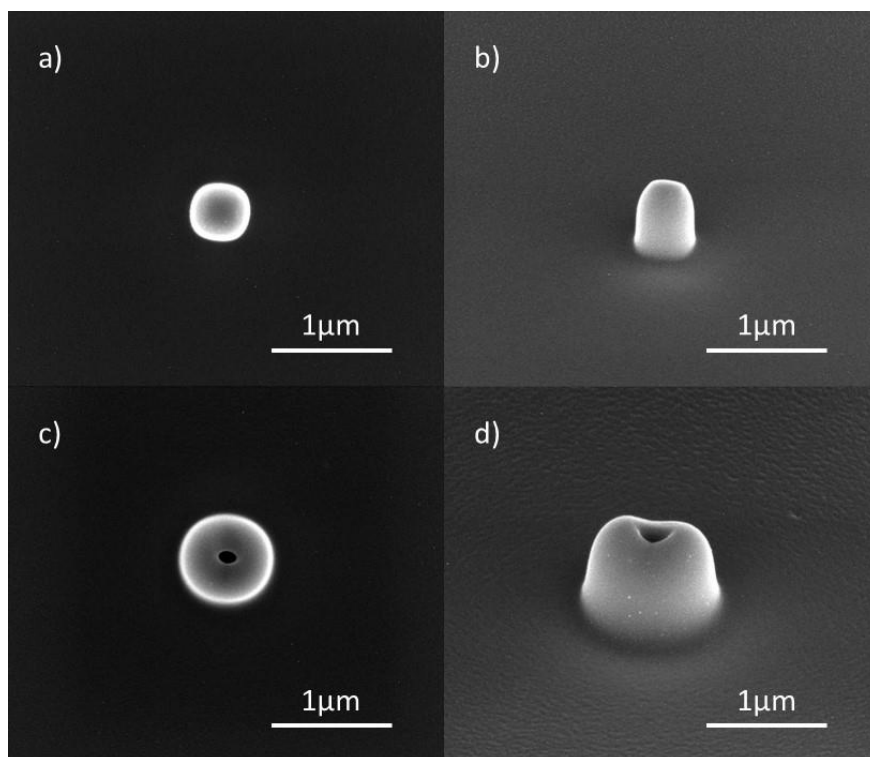


**Figure 5.8.** 250x250 nm square deposits of **4a** at 120 °C, pitch 10 nm, dwell 500 µs, 5 kV, 2000 passes. a) 40 pA, top down; b) 40 pA, 50° tilt; c) 600 pA, top down; d) 600 pA, 50° tilt.
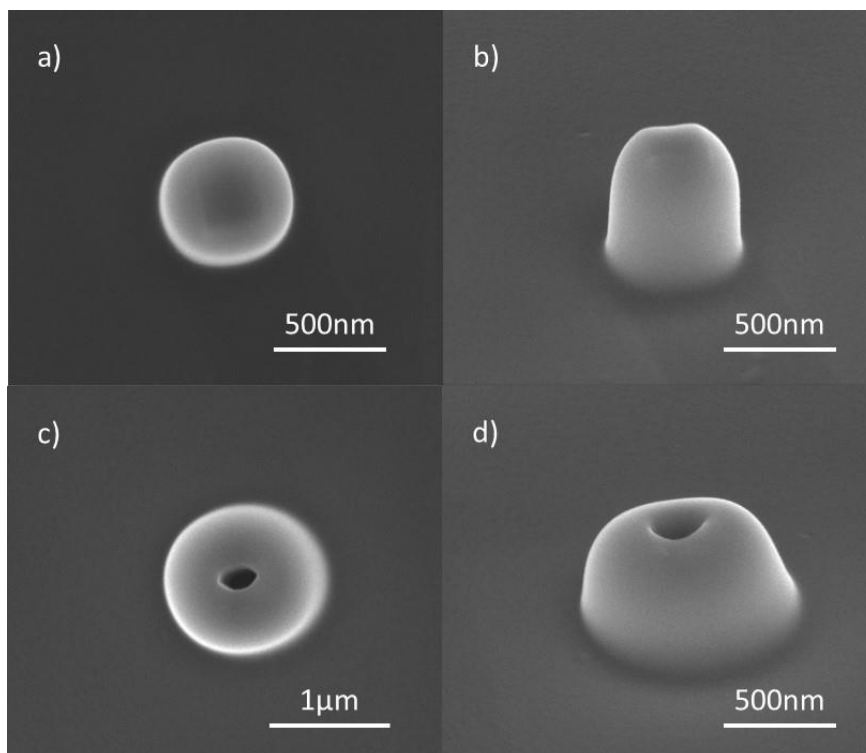
**Figure 5.9.** 250x250 nm square deposits of **5a** at 100 °C, pitch 10 nm, dwell 500 µs, 5 kV, 2000 passes. a) 40 pA, top down; b) 40 pA, 50° tilt; c) 600 pA, top down; d) 600 pA, 50° tilt.
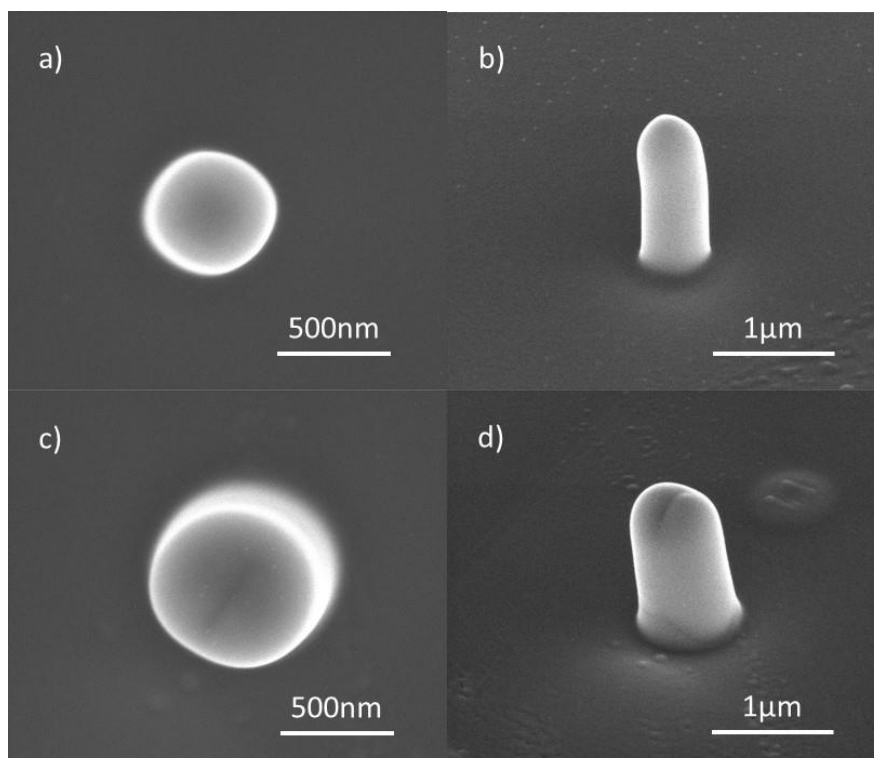


**Figure 5.10.** 250x250 nm square deposits of **6a** at 100 °C, pitch 10 nm, dwell 500 µs, 5 kV, 2000 passes. a) 40 pA, top down; b) 40 pA, 50° tilt; c) 600 pA, top down; d) 600 pA, 50° tilt.
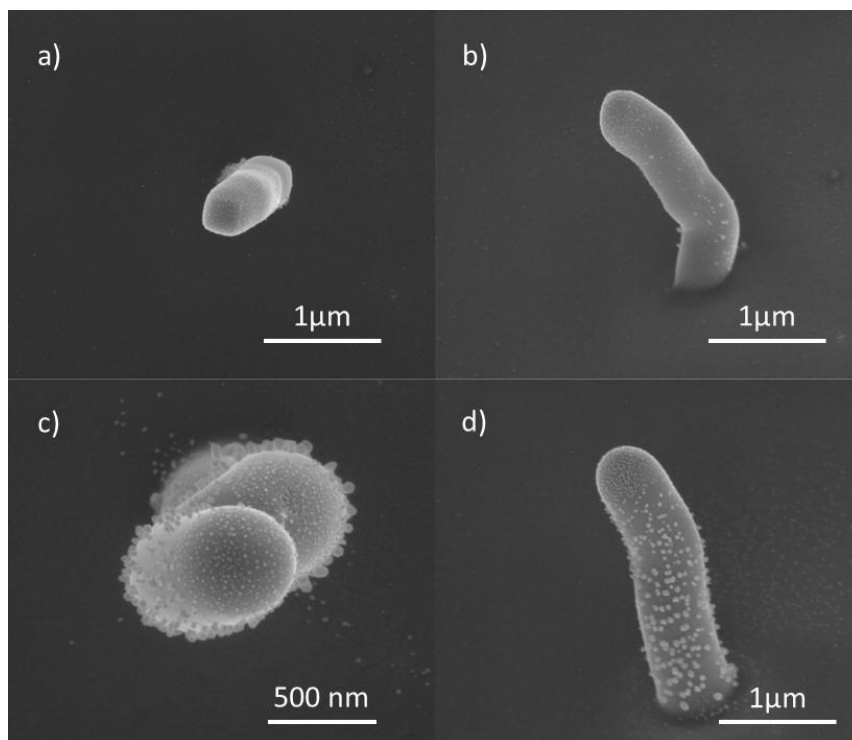
**Figure 5.11.** 250x250 nm square deposits of **5b** at 100 °C, pitch 10 nm, dwell 500 μs, 5 kV, 2000 passes. a) 40 pA, top down; b) 40 pA, 50° tilt; c) 600 pA, top down; d) 600 pA, 50° tilt. The rough deposits are due to the fact that the imaging was performed days after deposition.
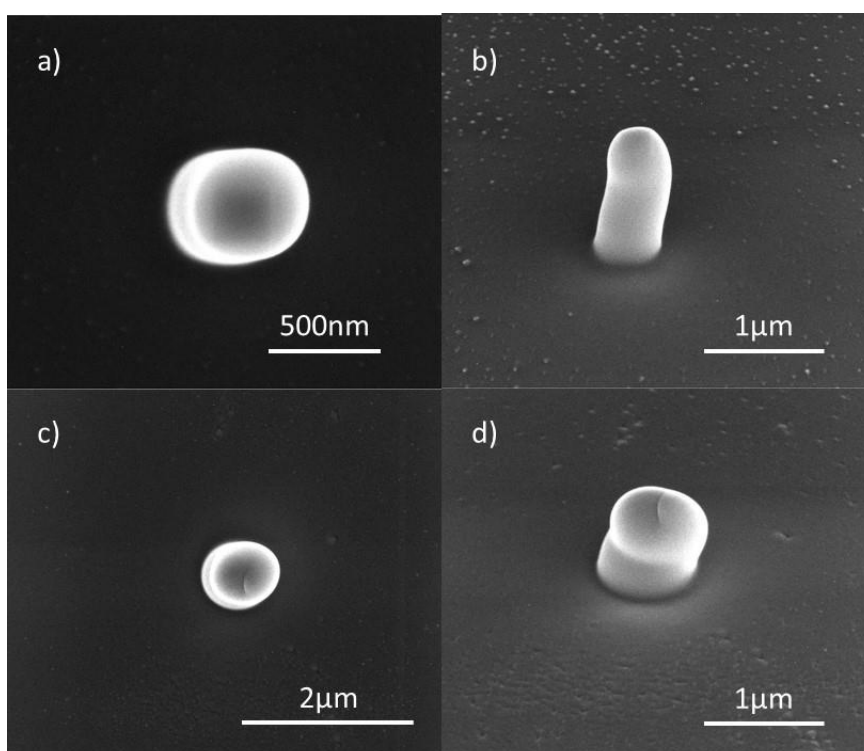


**Figure 5.12.** 250x250 nm square deposits of **5c** at 100 °C, pitch 10 nm, dwell 500 μs, 5 kV, 2000 passes. a) 40 pA, top down; b) 40 pA, 50° tilt; c) 600 pA, top down; d) 600 pA, 50° tilt.
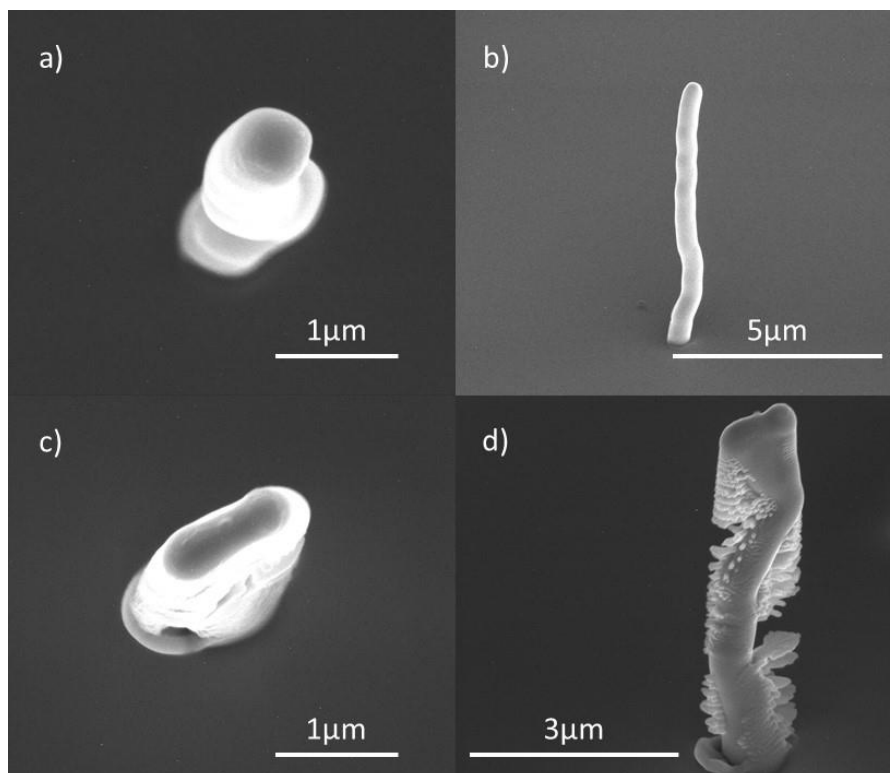
**Figure 5.13.** 250x250 nm square deposits of **5e** at 100 °C, pitch 10 nm, dwell 500 µs, 5 kV, 2000 passes. a) 40 pA, top down; b) 40 pA, 50° tilt; c) 600 pA, top down; d) 600 pA, 50° tilt.
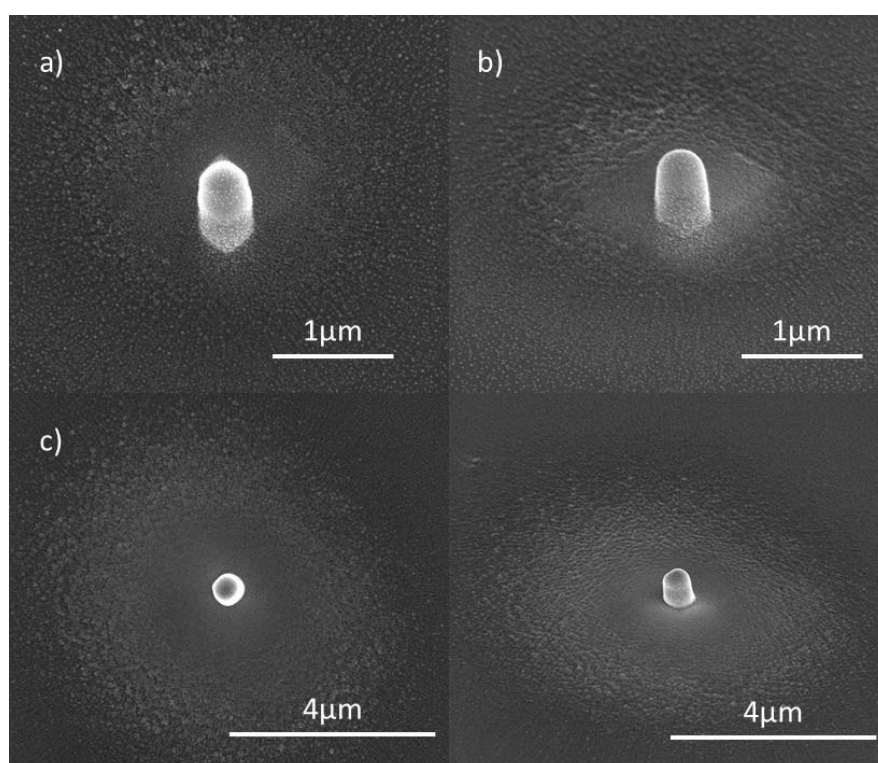


**Figure 5.14.** 250x250 nm square deposits of **11a** at 100 °C, pitch 10 nm, dwell 500 µs, 5 kV, 2000 passes. a) 40 pA, top down; b) 40 pA, 50° tilt; c) 600 pA, top down; d) 600 pA, 50° tilt.

## 5.2.5 EDX composition measurements

In order to unequivocally confirm composition for each compound at least 7 EDX spectra of at least 3 structures grown with the same parameters were registered (Figure 5.15). The only notable exception was **11a**, where the grown structures showed a slight increase of the silicon background signal when compared to the other compounds; as such, bigger structures were grown at the same deposition parameters in order to obtain a comparable Si atomic percentage (at.%) for all deposits.
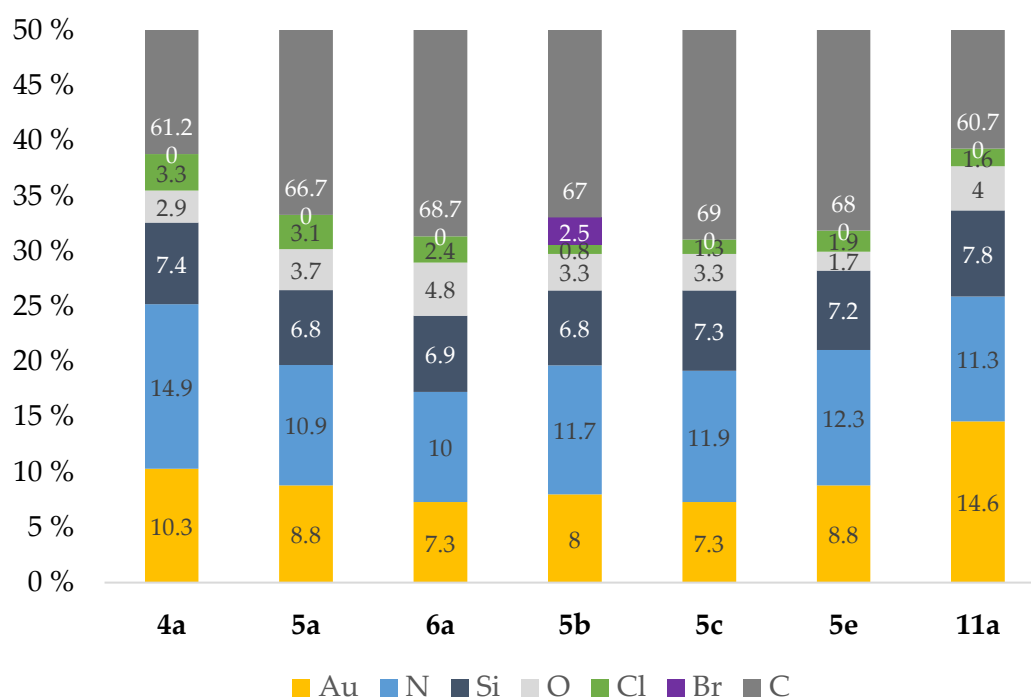


**Figure 5.15.** EDX composition in atomic percentage for the tested precursors. For **5e** 0.2% F at.% is observed.

In EDX the presence of a consistent quantity of gold in all deposits was observed, indicating that the precursor molecules were delivered to the gas phase intact in the selected experimental conditions. To consider the efficiency of the decomposition, the atomic ratio between carbon and gold in the precursor molecule and in the obtained deposit can be considered. For all compounds except **11a** the C/Au ratio is around the value observed in the precursor; slightly greater for **4a**, **5a**, **6a**, **5b** and **5c** but slightly lower for **5e**. Remarkably, **11a** shows a greatly reduced C/Au ratio, which correlates well with the loss of 2 carbons.

The highest Au at.% was observed for **11a** at 14.6%. For the imidazole-based studied precursors two arrays can be identified: substitution of the N-alkyl chains (**4a**, **5a**, **6a**) and

substitution of the anionic ligand (**5a**, **5b**, **5c**, **5e**). Based on N-alkyl chain variation, the Au at.% decreases as expected with the increase of the number of carbons of the N-substituent, from 7.3% (**6a**) to 8.8% (**5a**) and 10.3% (**4a**). Even if the composition follows appropriately the expected trend, the magnitude of the variation is lower than expected for C at.%. Based on the anionic ligand variation, the Au at.% decreases slightly in the series Cl-Br-I (8.8%, 8.0%, 7.3%); a more explicit trend is observed in the C/Au ratio that increases in the same series (7.6, 8.4, 9.5). This trend could be explained by a less favourable fragmentation of the parent molecule in dependence of the halogen ligand. As this is the first observation of the Cl-Br-I ligand series on a FEBID precursor, it is unknown if such behaviour can be extended to other systems. In a recent report by Mahgoub *et al.* A platinum precursors of general formula $Pt(CO)_2X_2$ with X = Cl, Br were tested as FEBID precursors and also in this case the composition of the deposits obtained from the precursor containing $Br^-$ ligands showed a lower metal atomic composition compared to the chloro-based complex.[47]

Throughout all deposits, co-deposition of the other elements present in the precursors was observed, namely N, Cl, Br, F. For **5c,** I was observed only in the EDX analyses performed at 8 kV, as the $L_\alpha$ at 3.937 keV is not accessible at 5 kV. In all cases, halogens are mostly removed and never exceed 3.3% at.%. In all cases, Cl co-deposits only in very limited amounts (Table 5.2). This is a good indication that perchlorination of organic ligands, as previously observed for perfluorination, is a viable method for the increase of the volatility of metallorganic complexes[254] without a major effect on the final deposit composition in FEBIP.[69]

**Table 5.2.** Comparison of X/Au ratios in precursor molecule and EDX of obtained deposits.

|  | 4a | 5a | 6a | 5b | 5c | 5e | 11a |
|---|---|---|---|---|---|---|---|
| C/Au prec. | 5 | 7 | 9 | 7 | 7 | 8 | 6 |
| C/Au dep.[a] | 5.9 | 7.6 | 9.4 | 8.4 | 9.5 | 7.7 | 4.2 |
| N/Au prec.[b] | 2 | 2 | 2 | 2 | 2 | 2 | 3 |
| N/Au dep.[a] | 1.4 | 1.2 | 1.4 | 1.5 | 1.6 | 1.4 | 0.8 |
| Cl/Au prec.[b] | 3 | 3 | 3 | 2 | 2 | 2 | 1 |
| Cl/Au dep.[a] | 0.32 | 0.35 | 0.33 | 0.1 | 0.18 | 0.22 | 0.11 |

[a]Value taken from EDX registered at 5kV and 600 pA.
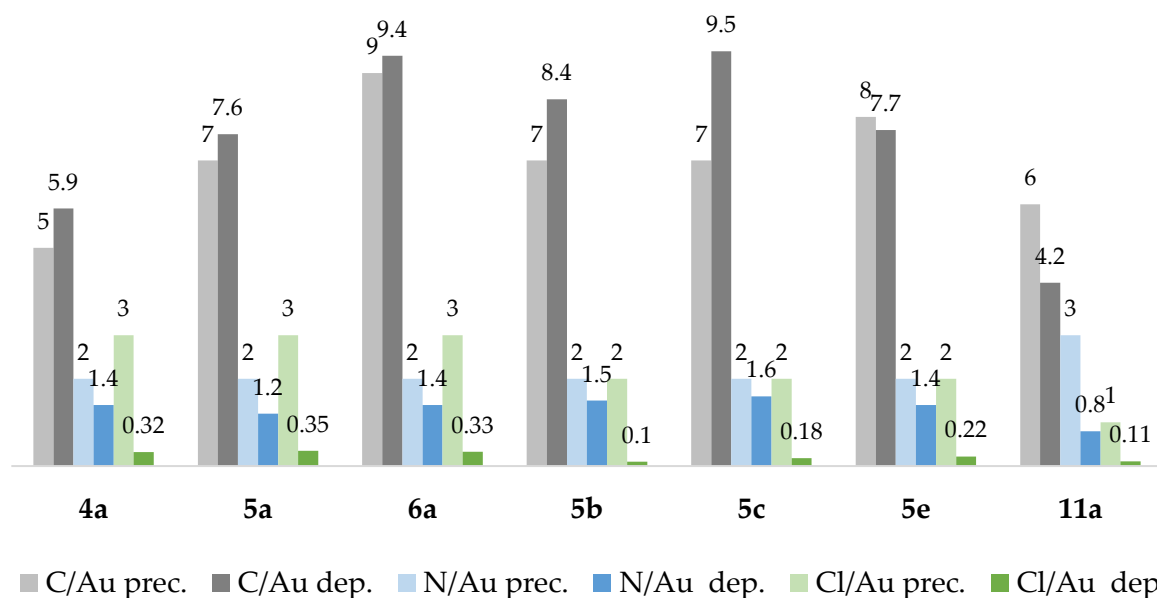


In addition to these elements, in all the obtained deposits a consistent quantity of silicon was observed (6.8-7.8%) due to the substrate signal. Oxygen was also present in moderate quantities, also originating from the native silicon oxide layer. Structures grown at 600 pA showed a constant minor increase in gold at.% of around one point percentage.

Post-deposition processing has been tried on a deposit of **11a**. After deposition, the square structure was exposed again at room temperature with a patterning (without any precursor injection) of 180x180 nm, 5 kV, 600 pA, 500 µs dwell, 10 nm pitch, 10000 passes (Figure 5.16).
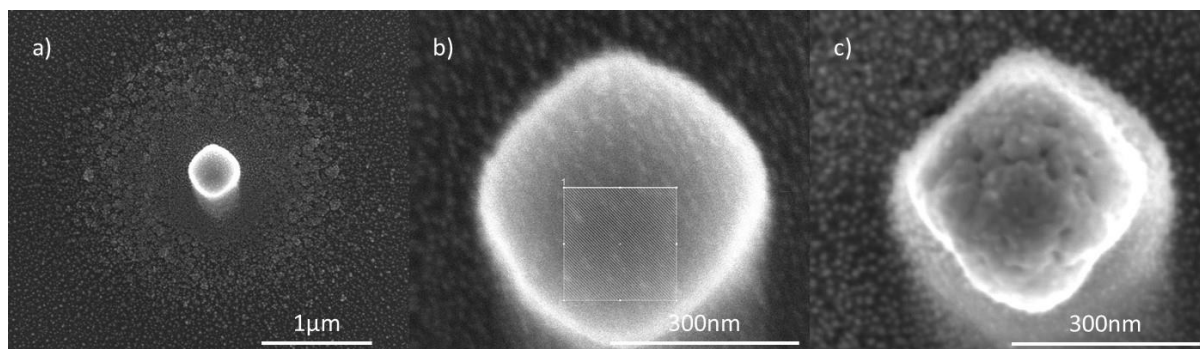
**Figure 5.16.** a) Deposit of **11a** grown at 100 °C, pitch 10nm, dwell 500μs, 5kV, 40pA, 2000 passes. b) Same deposit at room temperature with post-exposure patterning area highlighted. c) Same deposit after post-exposure processing.

After a second exposure, a great variation of the appearance of the deposit was observed, with shrinkage and presence of a granular structure. In the EDX comparison of the post-processed structure of **11a** and the average of analogue structures built with the same parameters partial removal of C and N, and total removal of Cl is registered. Furthermore, there is a steep increase in gold at.% (+24.6%) and an increase of both Si and O, in connection with the shrinkage of the structure (Table 5.3).

**Table 5.3.** Comparison of EDX spectra of deposits of **11a** and **11a** after post-exposure processing.[a]

| | **11a**[b] | **11a after exposure**[c] | **Difference in composition** |
|---|---|---|---|
| C | 52.5±0.27 | 24.1±2.36 | -28.4 |
| N | 12.7±0.16 | 4.9±0.62 | -7.8 |
| Au | 15.9±0.27 | 40.5±2.41 | +24.6 |
| Si | 10.3±0.28 | 20.0±0.82 | +9.7 |
| O | 7.0±0.15 | 8.5±0.23 | +1.5 |
| Cl | 1.6±0.08 | 0 | -1.6 |
| C/Au dep.[d] | 3.3 | 0.6 | - |



[a]In atomic percentage; [b]**11a** average of 7 EDX spectra with a respective total integration of 100.0±0.1%. The value is reported with ±standard error. [c]Average of 5 EDX spectra of post-exposure processed **11a** registered on the same structure with a respective total integration of 100.0±0.1%. The value is reported with ±standard error. EDX performed at 5 kV and 600 pA.

This effect has been already observed for MeCpPtMe$_3$,[60,63,255] for which upon post-exposure irradiation the metal content is highly increased with partial loss of carbon and a significant loss of volume.

### 5.2.6. Growth rate studies

Growth rate is a significant parameter to study in a new FEBID precursor, as it gives information on the rate of the deposition with regards to the electron dose.[21] In FEBID the most suitable precursors show a high rate of vertical growth while deposition horizontally only in the patterned area. The first indication of different growth rates for each precursor was obtained from the square 250x250 nm structures. By the comparison of the structures grown at 40 pA, the highest vertical growth was recorded for **5e**, followed by **5b**, **6a**, **5c**, **5a**, **4a** and **11a**. The horizontal growth was instead roughly constant in a range of 599-413 nm. The total deposited volume follows the same trend as the height series. Overall, the most important observation is that **5e** shows a great vertical growth rate when compared to all the other studied species (in all cases at least 3 times the height). From the comparison of the structures grown at 600 and 40 pA an increase in the diameter of all the deposits in the range of 133-368 nm is observed, while generally a shorter structure is obtained, with the exception of **5b** and **11a**, where the growth rate is increased also vertically. Nevertheless, an increase in volume growth is observed for all precursors (Table 5.4).

**Table 5.4.** Dimensions of the structures in Figure 5.8. - Figure 5.14.

| Compound | Current (pA) | Diameter (nm) | Height (nm) | Volume ($\mu m^3$) |
|---|---|---|---|---|
| **4a** | 40 | 508 | 658 | 0.133 |
| | 600 | 771 | 577 | 0.263 [a] |
| **5a** | 40 | 599 | 705 | 0.199 |
| | 600 | 941 | 629 | 0.428 [a] |
| **6a** | 40 | 547 | 1567 | 0.368 |
| | 600 | 680 | 1482 | 0.538 |
| **5b** | 40 | 413 | 2278 | 0.305 |
| | 600 | 599 | 3114 | 0.877 |
| **5c** | 40 | 478 | 1336 | 0.240 |
| | 600 | 846 | 787 | 0.443 |
| **5e** | 40 | 451 | 8171 | 1.305 |
| | 600 | 615[b] | 6923 | 2.057[c] |
| **11a** | 40 | 452 | 586 | 0.094 |
| | 600 | 613 | 772 | 0.228 |

Deposits are approximated as cylinders. [a]Volume calculated as the difference of the volume of the cylindrical deposit and the elliptic hole, assuming that the hole is empty throughout the height of the deposit. [b]Diameter calculated on the point in which the structure mostly resembles a cylinder. [c]Due to the uneven shape of the deposit the total volume is expected to be underestimated.

A series of 3x3 pillars at constant deposition parameters with the sole variation of the exposition time (in this case dwell time) was produced in order to have a dynamic overview of the growth process. Due to the different growth rates of the precursors, three different time ranges have been used: Short (S): 0.01, 0.02, 0.05, 0.1, 0.2, 0.5. 1, 2, 5 s; Long (L): 0.1, 0.2, 0.5. 1, 2, 5, 10, 20, 50 s; ExtraLong (XL): 1, 5, 10, 20, 40, 60, 80, 100, 120 s.

In all cases except **5e** the ExtraLong experiment is used in the growth rate calculations. For **5e** due to the great growth rate the Long experiment is used (Figure 5.17), and for comparison in both cases the growth is normalized to the electron dose.
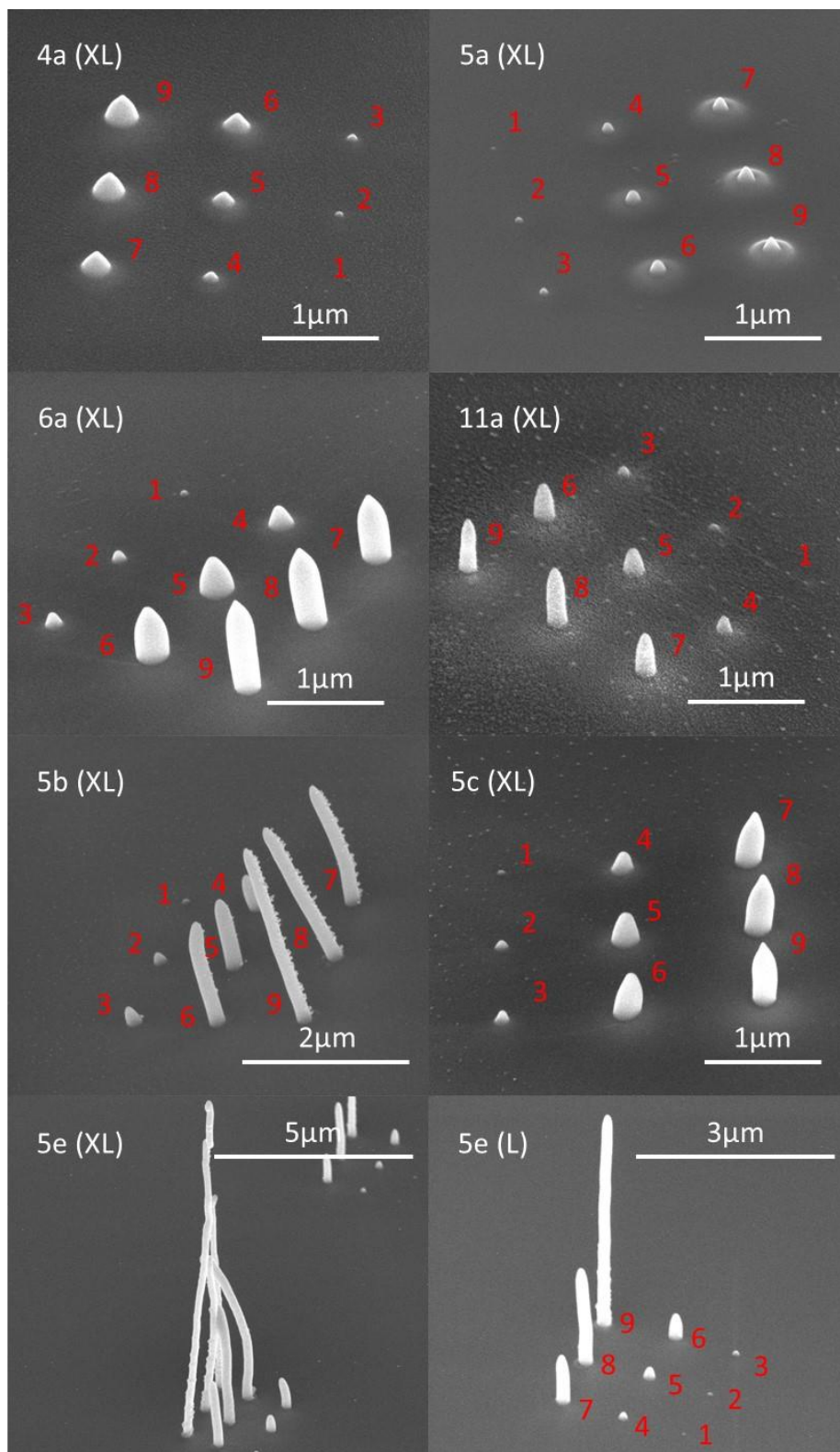
**Figure 5.17.** Pillars of the studied precursors, grown at 100 °C (**5a**, **6a**, **5b**, **5c**, **5e**) and 120 °C (**4a**), 40 pA, 5 kV. L=Long dwell, XL= ExtraLong dwell. Shortest to longest dwell 1 - 9.

Aya Mahgoub plotted the height vs. dose, diameter vs. dose and volume vs. dose obtained for the tested precursors.

Vertical growth is linear with the dose for each precursor and, as observed in the square deposits, **5e** has by far the highest vertical growth rate. From the other precursors we can distinguish also the bromo compound **5b** as a high growth rate compound, while all other precursors led to somewhat similar results (Figure 5.18).
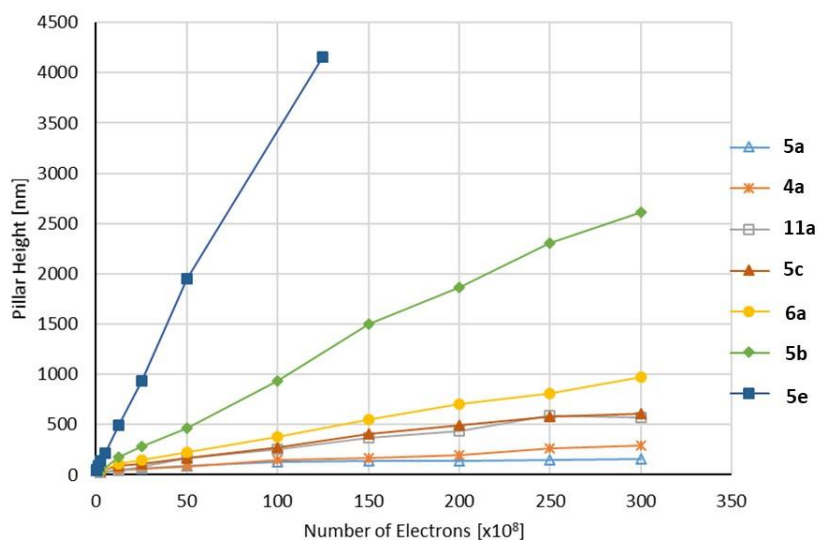


**Figure 5.18.** Vertical growth at 5 kV and 40 pA given as a function of total primary electron dose. Deposition performed at 100 °C for all compounds except **4a** (120 °C).

A completely different situation is presented for the horizontal growth: for all complexes we reach a saturation point in which the diameter does not grow with an increase dose. This plateau point is different for each precursor. For **5e** and **5b** the point in which the plateau starts is very well defined, at a diameter of 200 nm and $1 \cdot 10^9$ electrons for **5e** and 210 nm and $2.5 \cdot 10^9$ electrons for **5b** (estimates). The maximum diameter series in the explored conditions is **4a** > **6a** > **5c** > **5b** > **5e** > **11a** > **5a**. It is not clear if the plateau is completely reached in the explored conditions for **4a** (Figure 5.19).
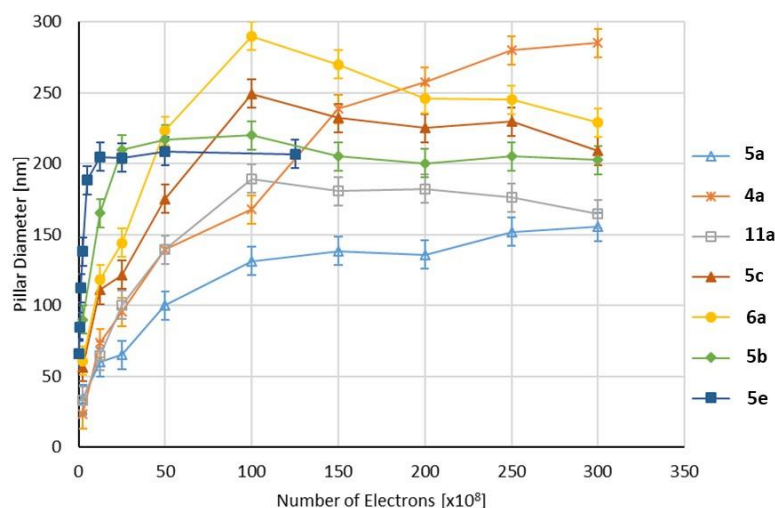
**Figure 5.19.** Horizontal growth at 5 kV and 40 pA given as a function of total primary electron dose. Deposition performed at 100 °C for all compounds except **4a** (120 °C).

The trend in total volume of the structure closely follows the vertical growth trend, and shows again the highest growth rate for **5e** at $1 \cdot 10^{-2}$ nm$^3$/e$^-$. The growth rate series goes as follows: **5e** > **5b** > **5a** > **5c** > **11a** > **4a** > **5a**. However, we have to consider that deposits for **4a** were obtained at a different temperature, as no sufficient deposition was achieved at 100 °C, hence we should consider **4a** the compound with the lowest growth rate (Figure 5.20).
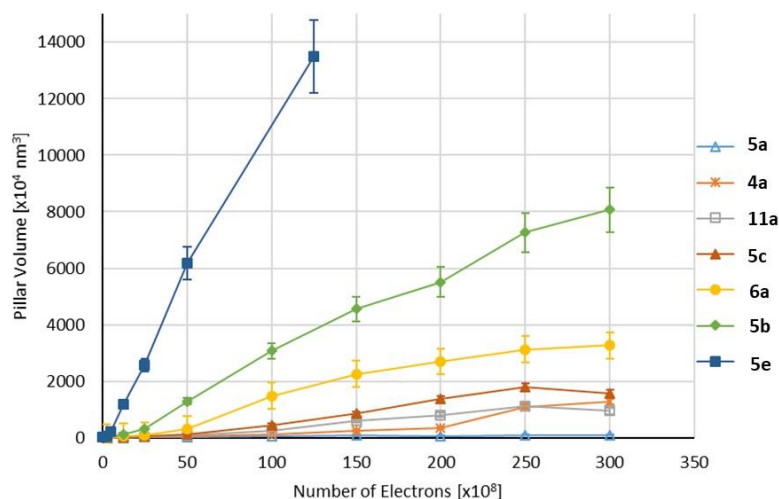


**Figure 5.20.** Volume growth at 5 kV and 40 pA given as a function of total primary electron dose. Deposition performed at 100 °C for all compounds except **4a** (120 °C).

From these observations we can conclude that the most suitable FEBID precursor for growth of well-defined vertical structures is **11a**, and that the most suitable anionic ligand in the series Cl, Br, I, CF$_3$ is CF$_3$ by far. The applicability of this observation to other type of FEBID precursors is still to be proven. Work carried out in the group of McElwee-White on isocyanide

gold(I) complexes could point in a similar direction.[86,109] The growth rate series do not follow the same trend as the sublimation temperatures; while the sublimation temperature controls mostly the replenishment rate, other factors have to be taken into account when discussing deposition rates, such as surface diffusion, and deposit composition.[21] Nevertheless, the most volatile compound is the one that showed the highest growth rate, and a substantial decrease of deposition rate can be observed with just a decrease in temperature of 20 °C. This effect is connected to the fact that the deposits grown at 80 °C were deposited after the 100 °C ones. The lowering of the temperature in the on-substrate reservoir setup has been observed to cause a great decrease of growth rate also for experiments performed on **5a**. This could be linked with the condensation/deposition of previously airborne material on the substrate with the lowering of the temperature, and thus cause a greater growth rate drop than expected (Figure 5.21).
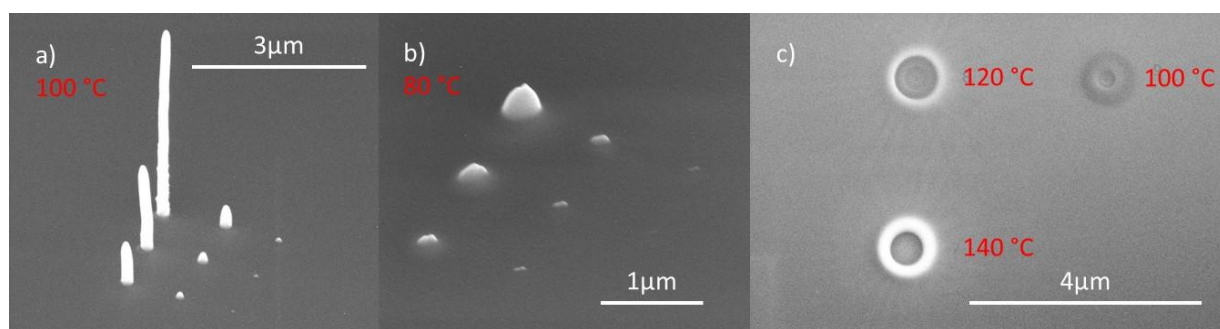


**Figure 5.21.** a) L deposit of **11a** at 5 kV, 40 pA, 100 °C; b) L deposit of **11a** at 5 kV, 40 pA, 80 °C. Nova SEM; c) square deposits of **5a** grown at different temperatures: 100x100 nm, 4 nm pitch, 500µs dwell, 5 kV, 800 pA nominal, 4000 passes. Elios SEM.

## 5.3 Other FEBID experiments

### 5.3.1 FEBID experiments performed by partners

In the early phase of our studies, the first three complexes synthesized, **1a**, **2a** and **3a** were tested as FEBID precursors by Jakub Jurczyk under the supervision of Ivo Utke at EMPA. These precursors were tested with the use of a custom made in-chamber GIS and heated substrate.[52] A suitable precursor flow has been achieved at a reservoir temperature of 120 - 150 °C for **1a**, 140 °C for **2a**, 120 - 130 °C for **3a**. All the deposits were carried out with a heated substrate at circa 130 °C to avoid condensation of the precursors.

The composition obtained for the three different precursors shows that all complexes lead to a modest gold atomic percentage (EDX) of 3 to 16 %, in line with what was observed for complexes **4a**-**6a, 11a**. In all cases, the major co-deposition was carbon, followed by nitrogen and chlorine. For **2a** and **3a,** oxygen,presence was observed in the EDX spectra of the deposits. The difference in deposition condition between the experiments carried out at Delft University of Technology and EMPA is so great that no direct comparison is possible. However, we can claim that both data sets are in line with each other, both regarding composition and structure. As such, we can state that the chlorination of the backbone for gold(I) NHC based FEBID precursors, brings no benefit to the efficient fragmentation and removal of the organic ligand, while leading to an enhancement of the volatility. Presented results are based on the data provided by Jakub Jurczyk and will be further described and analysed in his PhD Thesis.

### 5.3.2 Commercial GIS experiments

Compounds **4b**, **5a** and **11a** were unsuccessfully tested on FEI GIS. While it was possible to inject material and a pressure rise was observed for the opening of the GIS to the chamber, no gold was observed in the obtained deposits and mostly carbon and silicon was observed in the EDX of the obtained deposits. During retrieval of the crucible (reservoir), reactivity of the precursor **11a** with the metallic crucible was observed. Reactivity of FEBID precursors with the materials of the GIS is not unheard of, and was reported for the first time for iron carbonyl.[251]

Compounds **11a** and **12a** were tested during an exchange period at TESCAN Brno on ORSAY GIS systems; again, only deposition of carbon and silicon was observed, hinting at a reactivity of the precursor before injection. This reactivity could be linked to the presence of the halogen ligand Cl on both complexes. Since complex is **11e** is the most promising compound obtained, the reactivity of this complex with aluminium and steel was tested by performing a variation of the cold finger sublimation experiment. The compound was charged either on aluminium foil or on a steel plate and contained in either a metallic or alumina crucible. The precursor was heated at 50 °C under a vacuum of circa $10^{-3}$ mbar until complete sublimation. In both cases, no variation of the metal substrate was observed, hinting at a compatibility to commercial GIS of Au-CF$_3$ complexes rather than the Au-Cl and Au-Br counterparts.[86]

## 5.4 Conclusions

Ten gold(I) NHC complexes presented in Chapter 2 were tested as FEBID precursors. A custom-made on-substrate reservoir system has been designed and used for the testing of seven gold(I) NHC complexes. We aim to further develop this testing unit towards a modular single use tester for the quick screening of new FEBID precursors. In the ligand series X = Cl, Br, I, $CF_3$ the most suitable ligand was X = $CF_3$, based on both composition and growth rate of the deposits. For the NHC ligand, the most suitable was the triazole-based ligand, the only one that effectively shows a lower C/Au ratio than the parent molecule, and thus an efficient fragmentation. As such, we suggest **11e** as the most promising gold(I) NHC based FEBID precursor. Due to a limited volatility of the complexes and to unexpected reactivity with the material of commercial GIS, no successful deposition with commercial apparatuses was achieved. Through further testing, it was demonstrated that such problems should not arise for **11e**. Deposits with reasonable gold at.% were obtained (7.3 - 14.6%) without any parameter optimization. The studied precursors are in the composition range of previously reported gold FEBID precursors (see Chapter 1). Testing of **1a**-**3a** by partners led to the conclusion that chlorination of the imidazole ligand, while promoting volatility in some cases, does not lead to more pure deposits.

## 5.5 Experimental part

This experimental data section is to be considered supplementary to the Supporting Information of **Paper III**.

The discussed structures were produced in a Thermo Fisher Nova NanoLab DualBeam unless otherwise specified. Helios SEM refers to a Thermo Fisher Helios NanoLab DualBeam.

All reported EDX measurements were performed in a Nova Nanolab 600 dual beam SEM using an Oxford Instruments X-MAX 80 EDX detector.

**EDX of 4a**

EDX of structures deposited at 5 kV, 40 pA, 120 °C. EDX performed at 5 kV and 600 pA.

|     | a    | b    | c    | d    | e    | f    | g    | h    | Average |
|-----|------|------|------|------|------|------|------|------|---------|
| C   | 61.8 | 61   | 58.5 | 63.4 | 59.3 | 61.9 | 63.4 | 60.6 | 61.2    |
| N   | 15.8 | 15.9 | 13.5 | 15.7 | 12.8 | 15.6 | 14.6 | 14.9 | 14.9    |
| Au  | 10.1 | 10.4 | 12   | 9.4  | 11.5 | 9.7  | 9.7  | 9.5  | 10.3    |
| Si  | 6.2  | 6.7  | 9.2  | 5.6  | 9.9  | 6.9  | 6.1  | 8.7  | 7.4     |
| O   | 2.7  | 2.6  | 3    | 2.7  | 3.1  | 3.1  | 2.8  | 3.5  | 2.9     |
| Cl  | 3.5  | 3.4  | 3.8  | 3.2  | 3.4  | 2.8  | 3.3  | 2.9  | 3.3     |

EDX of structures deposited at 5 kV, 600 pA, 120 °C. EDX performed at 5 kV and 600 pA.

|     | a    | b    | c    | d    | Average |
|-----|------|------|------|------|---------|
| C   | 56.1 | 58   | 54.7 | 56.6 | 56.35   |
| N   | 15.4 | 18.8 | 14.8 | 17.8 | 16.7    |
| Au  | 13.1 | 9.8  | 13.6 | 10.8 | 11.825  |
| Si  | 8.8  | 7.4  | 9.8  | 8.3  | 8.575   |
| O   | 2.5  | 2.9  | 2.6  | 2.9  | 2.725   |
| Cl  | 4.2  | 3.2  | 4.5  | 3.6  | 3.875   |

**EDX of 5a**

EDX of structures deposited at 5 kV, 40 pA, 100 °C. EDX performed at 5 kV and 600 pA.

|     | a    | b    | c    | d    | e    | f    | g    | Average |
|-----|------|------|------|------|------|------|------|---------|
| C   | 69.9 | 64.2 | 72.2 | 66.2 | 63.2 | 68   | 63   | 66.7    |
| N   | 10.4 | 9.4  | 10.3 | 11.3 | 12.8 | 10.9 | 11.4 | 10.9    |
| Au  | 8.4  | 11   | 7.6  | 8.9  | 7.9  | 8.3  | 9.2  | 8.8     |
| Si  | 5.2  | 8.6  | 3.9  | 6.8  | 8.7  | 6    | 8.7  | 6.8     |
| O   | 3.1  | 3.9  | 2.8  | 3.8  | 4.5  | 3.4  | 4.6  | 3.7     |
| Cl  | 3    | 2.8  | 3.2  | 3    | 2.9  | 3.4  | 3.1  | 3.1     |

EDX of structures deposited at 5 kV, 600 pA, 100 °C. EDX performed at 5 kV and 600 pA.

|     | a    | b    | Average |
|-----|------|------|---------|
| C   | 63.7 | 59.8 | 61.8    |
| N   | 16.2 | 13.5 | 14.9    |
| Au  | 8.4  | 9.7  | 9.1     |
| Si  | 5.5  | 9.3  | 7.4     |
| O   | 2.9  | 4    | 3.5     |
| Cl  | 3.3  | 3.7  | 3.5     |

**EDX of 6a**

EDX of structures deposited at 5 kV, 40 pA, 100 °C. EDX performed at 5 kV and 600 pA.

|     | a    | b    | c   | d   | e    | f   | g   | Average |
|-----|------|------|-----|-----|------|-----|-----|---------|
| C   | 70.6 | 64.1 | 71  | 70  | 66.5 | 71  | 67  | 68.7    |
| N   | 10.2 | 10.1 | 10  | 10  | 10.1 | 9.5 | 9.9 | 10.0    |
| Au  | 7.1  | 8    | 7.7 | 7   | 6.9  | 7   | 6.9 | 7.3     |
| Si  | 5.1  | 10.3 | 4.8 | 6   | 8.9  | 5.1 | 8.3 | 6.9     |
| O   | 4.4  | 5.4  | 3.6 | 5   | 5.5  | 4.4 | 5.5 | 4.8     |
| Cl  | 2.5  | 2.1  | 2.5 | 3   | 2.2  | 2.7 | 2.2 | 2.4     |

EDX of structures deposited at 5 kV, 600 pA, 100 °C. EDX performed at 5 kV and 600 pA.

|     | a    | b    | c    | d    | Average |
|-----|------|------|------|------|---------|
| C   | 68.2 | 69   | 65.8 | 67   | 68      |
| N   | 12.9 | 13.5 | 13.1 | 13.3 | 13      |
| Au  | 8.9  | 8.7  | 7.9  | 8    | 8.4     |
| Si  | 4.2  | 3.8  | 7.2  | 5.2  | 5.1     |
| O   | 2.8  | 2.2  | 3.7  | 3.6  | 3.1     |
| Cl  | 3    | 2.8  | 2.3  | 2.8  | 2.7     |

**EDX of 5b**

EDX of structures deposited at 5 kV, 40 pA, 100 °C. EDX performed at 5 kV and 600 pA.

|     | a    | b    | c    | d    | e    | f    | g    | h    | Average |
|-----|------|------|------|------|------|------|------|------|---------|
| C   | 70.1 | 69.2 | 66.9 | 68.7 | 66.5 | 66.4 | 64.7 | 63.3 | 67.0    |
| N   | 10.6 | 10.5 | 11.7 | 11.5 | 12.9 | 12.5 | 12.6 | 11.2 | 11.7    |
| Au  | 7.4  | 7.5  | 7.5  | 7.1  | 8.1  | 8.3  | 9.1  | 9.1  | 8.0     |
| Si  | 5.5  | 6.4  | 7.4  | 6.1  | 6.5  | 6.2  | 7    | 9.4  | 6.8     |
| O   | 3.4  | 3.6  | 3.5  | 3.7  | 2.6  | 3    | 3.3  | 3.1  | 3.3     |
| Cl  | 0.6  | 0.7  | 0.6  | 0.7  | 0.7  | 0.9  | 0.9  | 0.9  | 0.8     |
| Br  | 2.4  | 2.1  | 2.3  | 2.2  | 2.8  | 2.7  | 2.5  | 3    | 2.5     |

EDX of structures deposited at 5 kV, 600 pA, 100 °C. EDX performed at 5 kV and 600 pA.

|     | a    | b    | c    | d    | Average |
|-----|------|------|------|------|---------|
| C   | 64.5 | 63.9 | 65.1 | 63   | 64.1    |
| N   | 13.9 | 15.3 | 15   | 13   | 14.3    |
| Au  | 9.8  | 7.8  | 9    | 10.7 | 9.3     |
| Si  | 5.6  | 6.5  | 5.1  | 6.4  | 5.9     |
| O   | 2.3  | 3.3  | 2.1  | 2.5  | 2.6     |
| Cl  | 1.3  | 0.7  | 1.2  | 1.4  | 1.2     |
| Br  | 2.6  | 2.5  | 2.5  | 2.9  | 2.6     |

**EDX of 5c**

EDX of structures deposited at 5 kV, 40 pA, 100 °C. EDX performed at 5 kV and 600 pA.

|     | a    | b    | c    | d    | e    | f    | g    | h    | Average |
|-----|------|------|------|------|------|------|------|------|---------|
| C   | 67.1 | 70.8 | 67.1 | 71.2 | 68.9 | 69.4 | 69.7 | 67.7 | 69.0    |
| N   | 12.1 | 11.6 | 12.1 | 11   | 11.8 | 11   | 12   | 13.6 | 11.9    |
| Au  | 6.7  | 7.5  | 6.7  | 7.5  | 7.2  | 7.4  | 7.6  | 7.5  | 7.3     |
| Si  | 9.6  | 5.9  | 9.6  | 5.8  | 7.4  | 7.4  | 6.3  | 6.7  | 7.3     |
| O   | 3.4  | 3.1  | 3.4  | 3.3  | 3.5  | 3.4  | 3.2  | 3.2  | 3.3     |
| Cl  | 1.1  | 1.2  | 1.1  | 1.3  | 1.3  | 1.4  | 1.3  | 1.3  | 1.3     |

EDX of structures deposited at 5 kV, 40 pA, 100 °C. EDX performed at 8 kV and 600 pA.

|     | a    | b    | c    | d    | e    | Average |
|-----|------|------|------|------|------|---------|
| C   | 66.2 | 65.1 | 65.8 | 65.4 | 64.7 | 65.4    |
| N   | 9.7  | 10.8 | 10   | 10.7 | 11.1 | 10.5    |
| Au  | 5.1  | 4.8  | 5.1  | 4.9  | 5.2  | 5.0     |
| Si  | 13.3 | 13.9 | 13.2 | 13.4 | 13   | 13.4    |
| O   | 2.7  | 2.7  | 2.9  | 2.9  | 2.7  | 2.8     |
| Cl  | 0.9  | 0.9  | 1    | 0.9  | 1    | 0.9     |
| I   | 2.1  | 1.9  | 2    | 1.9  | 2.2  | 2.0     |

EDX of structures deposited at 5 kV, 600 pA, 100 °C. EDX performed at 5 kV and 600 pA.

|     | a    | b    | c    | d    | Average |
|-----|------|------|------|------|---------|
| C   | 69   | 68.4 | 66   | 69.5 | 68.2    |
| N   | 11.7 | 13.3 | 12.8 | 12.9 | 12.7    |
| Au  | 10.3 | 9.6  | 10.9 | 9.3  | 10.0    |
| Si  | 5    | 5    | 6.1  | 4.7  | 5.2     |
| O   | 2.4  | 2.2  | 2.6  | 2.1  | 2.3     |
| Cl  | 1.6  | 1.4  | 1.7  | 1.5  | 1.6     |

EDX of structures deposited at 5 kV, 600 pA, 100 °C. EDX performed at 8 kV and 600 pA.

|     | a    | b    | c    | d    | Average |
|-----|------|------|------|------|---------|
| C   | 64.9 | 64.5 | 67   | 65.6 | 65.5    |
| N   | 12.2 | 12.1 | 12.3 | 13.3 | 12.5    |
| Au  | 7.9  | 7.9  | 7.4  | 7.4  | 7.7     |
| Si  | 9    | 9.6  | 7.7  | 8.3  | 8.7     |
| O   | 2.3  | 2    | 2    | 2    | 2.1     |
| Cl  | 1.2  | 1.3  | 1.3  | 1.1  | 1.2     |
| I   | 2.6  | 2.6  | 2.4  | 2.3  | 2.5     |

**EDX of 5e**

EDX of structures deposited at 5 kV, 40 pA, 100 °C. EDX performed at 5 kV and 600 pA.

|     | a    | b    | c    | d    | e    | f    | g    | h    | Average |
|-----|------|------|------|------|------|------|------|------|---------|
| C   | 69.3 | 67.7 | 67.1 | 70.2 | 67.5 | 68   | 67.7 | 66.3 | 68.0    |
| N   | 13   | 12.3 | 11.7 | 12.9 | 11.7 | 11.1 | 14   | 11.5 | 12.3    |
| Au  | 8.5  | 8.6  | 9.1  | 8.4  | 8.2  | 9.5  | 8.4  | 9.7  | 8.8     |
| Si  | 5.5  | 7.9  | 8    | 5.3  | 8.9  | 8.2  | 5.6  | 8    | 7.2     |
| O   | 1.5  | 1.7  | 1.7  | 1.5  | 2    | 1.8  | 1.5  | 2    | 1.7     |
| Cl  | 2.3  | 1.6  | 2.1  | 1.7  | 1.1  | 0.9  | 2.8  | 2.6  | 1.9     |
| F   | 0    | 0.3  | 0.3  | 0    | 0.5  | 0.4  | 0    | 0    | 0.2     |

EDX of structures deposited at 5 kV, 600 pA, 100 °C. EDX performed at 5 kV and 600 pA.

|     | a    | b    | c    | Average |
|-----|------|------|------|---------|
| C   | 63.7 | 65.6 | 64.3 | 64.5    |
| N   | 12.3 | 13.7 | 13.6 | 13.2    |
| Au  | 11.1 | 10.3 | 11.1 | 10.8    |
| Si  | 7.2  | 5.9  | 6    | 6.4     |
| O   | 2.2  | 1.9  | 2    | 2.0     |
| Cl  | 3.1  | 2.5  | 3    | 2.9     |
| F   | 0.5  | 0    | 0    | 0.2     |

EDX of structures deposited at 5 kV, 40 pA, 80 °C. EDX performed at 5 kV and 600 pA.

|     | a    | b    | c    | d    | e    | f    | Average |
|-----|------|------|------|------|------|------|---------|
| C   | 68.2 | 65   | 67.2 | 65.3 | 61.7 | 63.3 | 55.8    |
| N   | 14.1 | 11   | 14   | 15.4 | 13   | 11.2 | 11.2    |
| Au  | 7.9  | 9.6  | 7.6  | 8.4  | 10.3 | 9.1  | 7.6     |
| Si  | 4.7  | 8.8  | 6.5  | 5.3  | 8.7  | 9.4  | 6.2     |
| O   | 1.7  | 1.8  | 1.7  | 1.5  | 2.1  | 3.1  | 1.7     |
| Cl  | 3    | 3.3  | 2.6  | 4.1  | 4.2  | 0.9  | 2.6     |
| F   | 0.3  | 0.4  | 0.3  | 0    | 0    | 3    | 0.6     |

EDX of structures deposited at 5 kV, 600 pA, 80 °C. EDX performed at 5 kV and 600 pA.

|     | a    | b    | Average |
|-----|------|------|---------|
| C   | 67.2 | 67.9 | 67.6    |
| N   | 15.3 | 14.3 | 14.8    |
| Au  | 8.5  | 9    | 8.8     |
| Si  | 4.4  | 4.2  | 4.3     |
| O   | 1.6  | 2.9  | 2.3     |
| Cl  | 2.8  | 1.6  | 2.2     |
| F   | 0.3  | 0    | 0.2     |

**EDX of 11a**

EDX of structures deposited at 5 kV, 40 pA, 100 °C. EDX performed at 5 kV and 600 pA.

|      | a    | b    | c    | d    | e    | f    | g    | Average |
|------|------|------|------|------|------|------|------|---------|
| C    | 53.7 | 53.1 | 51.7 | 51.8 | 52   | 52   | 52.9 | 52.5    |
| N    | 12.9 | 12.4 | 12.4 | 12.9 | 13.1 | 11.9 | 13.2 | 12.7    |
| Au   | 15   | 15.4 | 16.8 | 15.3 | 16.1 | 17.1 | 15.9 | 15.9    |
| Si   | 8.7  | 10.7 | 10.5 | 11   | 10.2 | 10.9 | 10   | 10.3    |
| O    | 7.7  | 7    | 7.1  | 7.3  | 7.1  | 6.4  | 6.7  | 7.0     |
| Cl   | 2    | 1.4  | 1.6  | 1.6  | 1.4  | 1.7  | 1.3  | 1.6     |

EDX of structures deposited at 5 kV, 600 pA, 100 °C. EDX performed at 5 kV and 600 pA.

|      | a    | b    | c    | d    | Average |
|------|------|------|------|------|---------|
| C    | 55.8 | 54.3 | 58.2 | 55.4 | 55.9    |
| N    | 14.4 | 16.6 | 12.9 | 16   | 15.0    |
| Au   | 17.6 | 16.3 | 17.6 | 16.2 | 16.9    |
| Si   | 8.1  | 8.2  | 6.6  | 7.1  | 7.5     |
| O    | 2.8  | 3.6  | 2.9  | 3.9  | 3.3     |
| Cl   | 1.3  | 1.1  | 1.9  | 1.3  | 1.4     |

EDX of structure deposited at 5 kV, 40 pA, 100 °C then exposed at 5 kV, 600 pA. EDX performed at 5 kV and 600 pA.

|      | a    | b    | c    | d    | e    | Average |
|------|------|------|------|------|------|---------|
| C    | 21.5 | 24.5 | 29.9 | 34.4 | 20.4 | 26.1    |
| N    | 3.4  | 4    | 5.6  | 7.3  | 4.4  | 4.9     |
| Au   | 44.4 | 44.5 | 37   | 31.5 | 45   | 40.5    |
| Si   | 22.1 | 18.8 | 18.1 | 18.5 | 22.3 | 20.0    |
| O    | 8.6  | 8.2  | 9.4  | 8.3  | 7.9  | 8.5     |
| Cl   | 0    | 0    | 0    | 0    | 0    | 0.0     |

EDX of bigger structures deposited at 5 kV, 40 pA, 100 °C. EDX performed at 5 kV and 600 pA.

|      | a    | b    | c    | d    | e    | f    | g    | Average |
|------|------|------|------|------|------|------|------|---------|
| C    | 61.4 | 61   | 58.8 | 63.2 | 61.9 | 60.2 | 58.2 | 60.7    |
| N    | 11.4 | 12.5 | 11.2 | 12   | 12   | 9.9  | 10.1 | 11.3    |
| Au   | 13.1 | 14.7 | 15.7 | 13.4 | 13.8 | 15.8 | 15.8 | 14.6    |
| Si   | 8.7  | 6.9  | 8.6  | 6.3  | 7    | 7.5  | 9.6  | 7.8     |
| O    | 4.1  | 3.3  | 4    | 3.7  | 3.6  | 4.6  | 4.4  | 4.0     |
| Cl   | 1.3  | 1.6  | 1.6  | 1.4  | 1.7  | 2    | 1.8  | 1.6     |

**Additional deposits briefly discussed in the chapter**
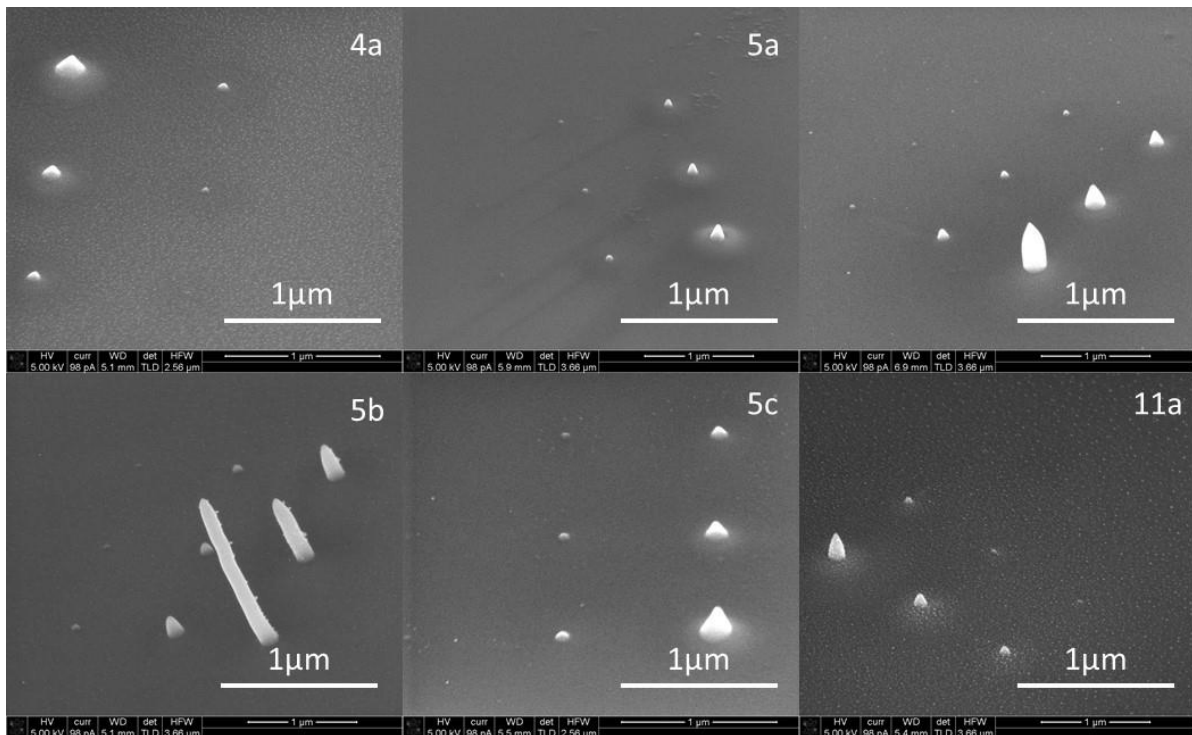


L (Long) pillar deposits at 40 pA, 5 kV, 120 °C (**4a**) 100 °C (**5a**, **6a**, **5b**, **5c**, **11a**).
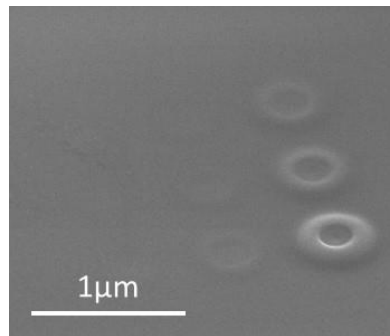


L (Long) pillar deposits at 600 pA, 5 kV, 100 °C of **5a**.
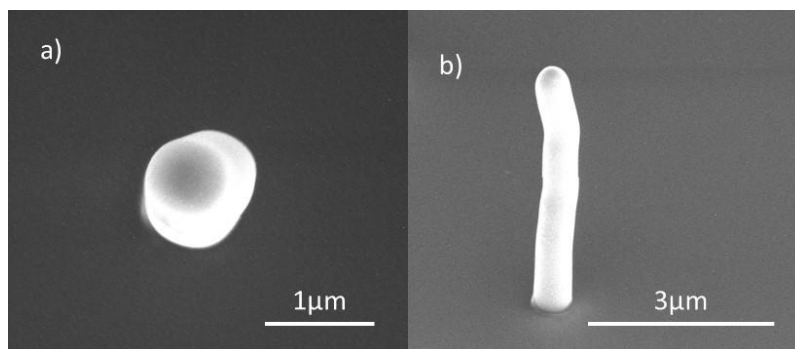


250x250 nm deposits at 40 pA, 5 kV, 80 °C of **5e** (square deposit grown before heating to 100 °C).

Example for **6a** of the overview of deposits in the hole of the vapour guide.

# Chapter 6.

# Oxidation of gold(I) NHC complexes by means of *aqua regia*

## *6.1 Introduction*

In this chapter the oxidation of gold(I) NHC complexes to gold(III) NHC complexes by the use of *aqua regia* as the oxidizing agent is discussed. The work presented in the first part of this chapter has been carried out in close collaboration with Volodomyr Levchenko and is discussed in more detail in **Paper I**. In the second part of this chapter, additional data is presented.

*Aqua regia* is a 3:1 mixture of hydrochloric and nitric acid, which in contact with each other form a complex reactive mixture of species. In such a mixture, metallic gold can be dissolved upon stirring, leading to the formation of tetrachloroauric gold.[256,257] Apart for its great historical relevance and for the removal of metallic gold in cleaning or extraction processes, *aqua regia* has seen in modern chemistry very limited applications.[258-262]

Gold(III) NHC complexes of general formula (NHC)AuCl$_3$ can be obtained by the oxidation of the relevant gold(I) compound (NHC)AuCl by the use of various oxidizing agents (Scheme 6.1), such as Cl$_2$,[197] PhICl$_2$[207,208] and Au(SMe$_2$)Cl.[214] Aqua regia, also a source of Cl, could also lead to the oxidation of the gold(I) centre.
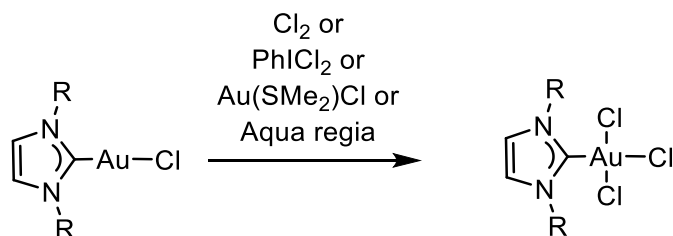


**Scheme 6.1.** Overview of the oxidation of (NHC)AuCl to (NHC)AuCl$_3$.

## 6.2 Aqua regia oxidation protocol

In the *aqua regia* oxidation protocol 8 mL of freshly made *aqua regia* were added to 50 mg of the selected (NHC)AuCl complex. The suspension was vigorously stirred in a closed vial at room temperature. Afterwards, the suspension was filtered, washed with two portions of water, and dried under a stream of air. The reaction was performed in full scale or half scale, and pale yellow to intense yellow powders were isolated.

### 6.2.1 Oxidation of 1a-3a

The first tested compounds were **1a**-**3a**. Upon overnight stirring of these complexes as suspensions in *aqua regia*, we surprisingly observed in the isolated powder the presence of a mixture of two to three products, depending on the selected starting material (Scheme 6.2). We chose the mixture produced from compound **2a** as a benchmark. In the obtained ESI-MS the presence of two main species was observed, that have been identified as gold(III) NHC complexes presenting halogenation on the backbone of the molecule. The major species isolated presented an addition of two Cl on the backbone (**2j**), with the loss of the unsaturated bond, while the minor isolated species presented the substitution of the backbone hydrogens with chlorides (**5f**). Such observations are reminiscent of previous reports of undesired chlorination of backbone methyl groups during oxidation of gold(I) NHC complexes with $Cl_2$[208] and of the substitution of backbone protons with chlorides for free carbene NHC systems.[263,264] No **2f** was observed, even through variation of the conditions. With the modification of the quantity of precursor used in relation to the volume of *aqua regia*, it was possible to obtain an optimization of selectivity towards **2j**, but no pure product could be isolated. In the same conditions **1a** and **3a** led to very different mixtures; **1a** presented again a mixture mainly comprised of the saturated product **1j**, while the backbone substituted **4f** and the desired product **1f** were observed in minor quantities. For **3a**, the main product was the desired compound **3f**, and in the obtained mixture the saturated product **3j** and the starting material **3a** were present in minor quantities. The isolated mixtures indicate that in the presence of small N-substituents, such as Me and Et, addition of chloride to the backbone of the molecule is the most favourable process. On the other hand, already with the presence of an iPr N-substituent the reactivity of the backbone is hindered and the main product is the desired NHC unfunctionalized gold(III) complex. Single crystals suitable for XRD were

obtained from the mixture of **5f** and **2j**, and the products were separately identified. Interestingly, **2j** presented an *anti* addition of chloride on the backbone of the NHC (**Paper I**). This is an indication that the mechanism for backbone addition is an electrophilic addition by a source of chlorine to the backbone of the NHC of a gold(III) complex, forming a chloronium intermediate that is further attacked by a nucleophilic source of chlorine, to form the *anti*-substituted product. In the same manner complexes **4-6f** could be generated by the repeated loss of a proton from the putative chloronium intermediate (Scheme 6.2).
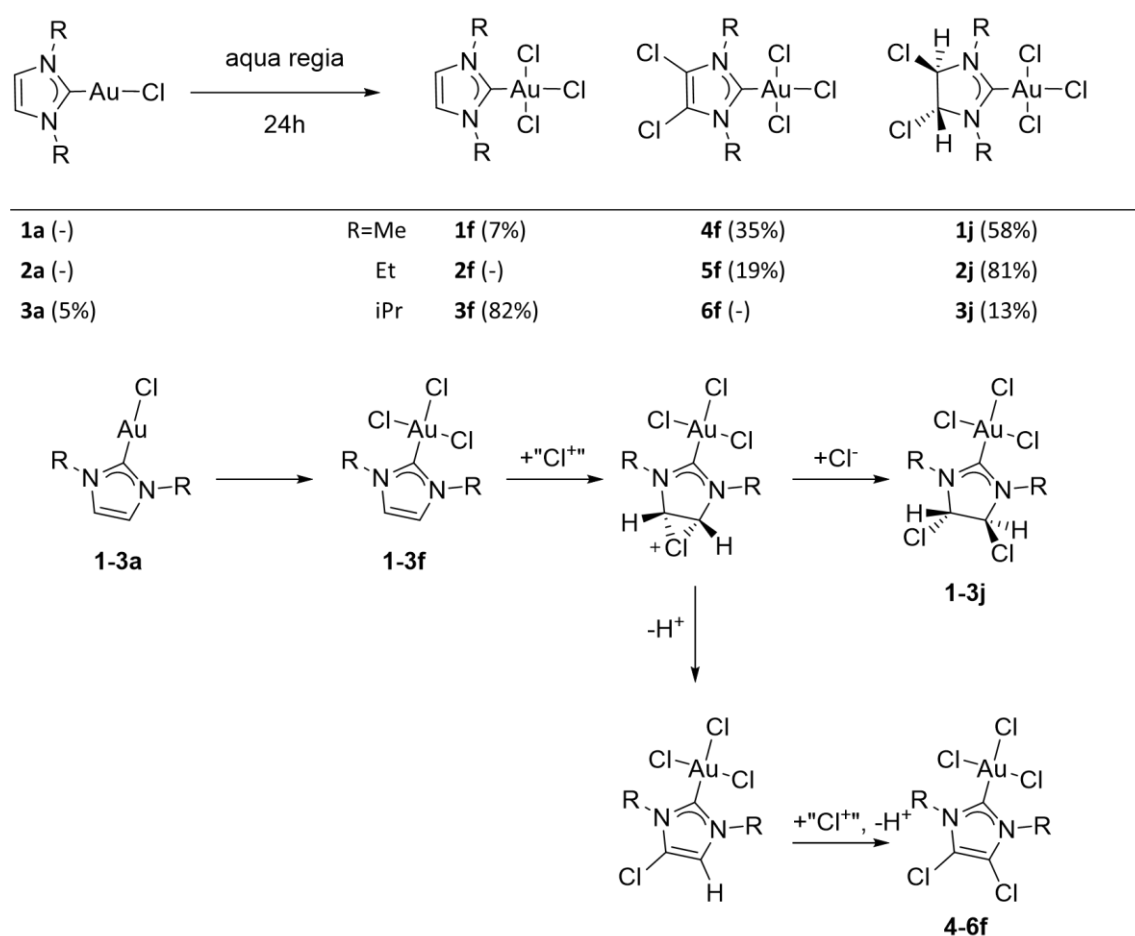


**Scheme 6.2.** Oxidation in *aqua regia* of **1a-3a** (top); suggested mechanism for the formation of **1-3j** and **4-6f** (bottom).

### 6.2.2 Oxidation of 4a-6a

For the already backbone chlorinated gold(I) complexes **4a-6a** upon stirring in *aqua regia* no reactivity of the NHC was observed and pure gold(III) complexes were isolated (**3f-6f**). An optimized reaction time of 3 hours was sufficient for R = Me, Et, while a longer reaction time was necessary for R = iPr (**5f**) (Scheme 6.3). This is a further indication of the difference between ethyl and isopropyl substituents, as seen for **2a** and **3a** in the previous section.
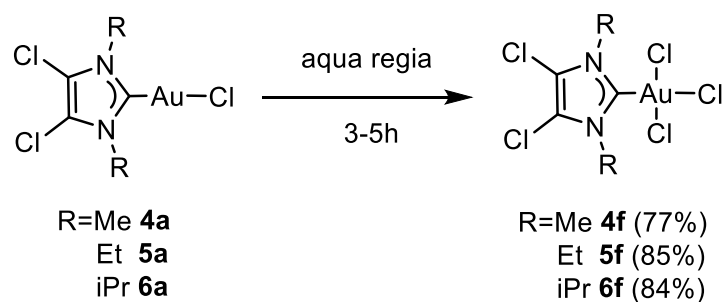
**Scheme 6.3.** Oxidation in *aqua regia* of **4a-6a**.

### 6.2.3 Oxidation of larger gold(I) NHC complexes 13a, 16a, 17a

The benzimidazole-based complex **13a** was fully oxidized to the gold(III) complex **13f** in 7 hours. The imidazole-based **16a** and **17a** were explored in order to define if the backbone functionalization was indeed controlled by the N-substituents. In both cases the unfunctionalized gold(III) complexes were obtained as the sole product (Scheme 6.4). While for the formation of **16f** only 5 hours of reaction time were sufficient, for **17f** in order to obtain full conversion 20 hours of reaction time were necessary, a feature that considerably lowered the obtained yield.
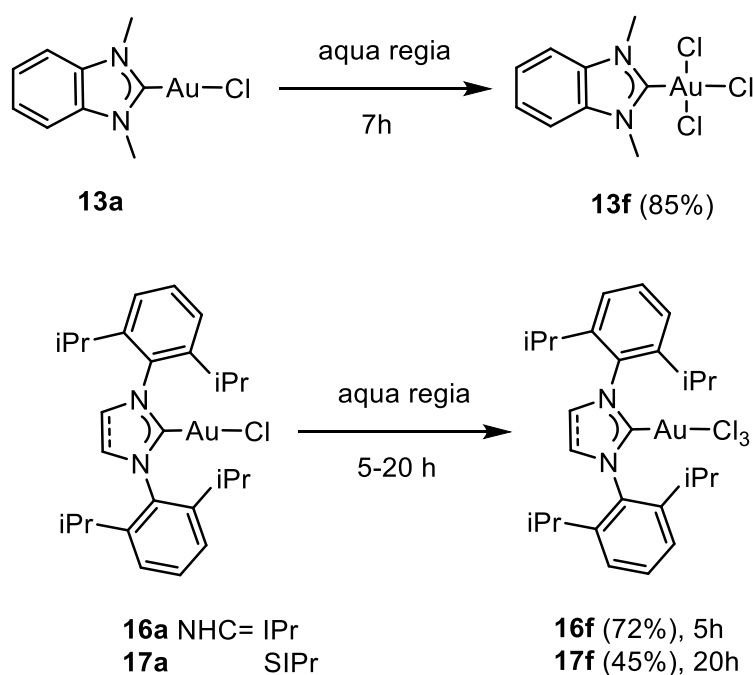


**Scheme 6.4.** Oxidation in *aqua regia* of **13a**, **16a**, **17a**.

### 6.2.4 Oxidation of 11a and 12a

The reaction of oxidation was performed on the triazole-based compound **11a**. To our surprise no chlorination of the backbone was detected and only the desired unfunctionalized Au(III) complex **11f** was obtained (Scheme 6.5). Chlorination of the backbone in *aqua regia* so far was seen exclusively in backbone unsubstituted imidazole-based rings with small N-substituents. The addition (or substitution) of Cl on the backbone of NHC gold(I) complexes is due to nucleophilic addition and not a radical mechanism. In fact, if a radical mechanism was present, for the triazole-based compound **11a** we would expect the formation of other backbone chlorinated species. The low yield was obtained due to the long reaction time employed.
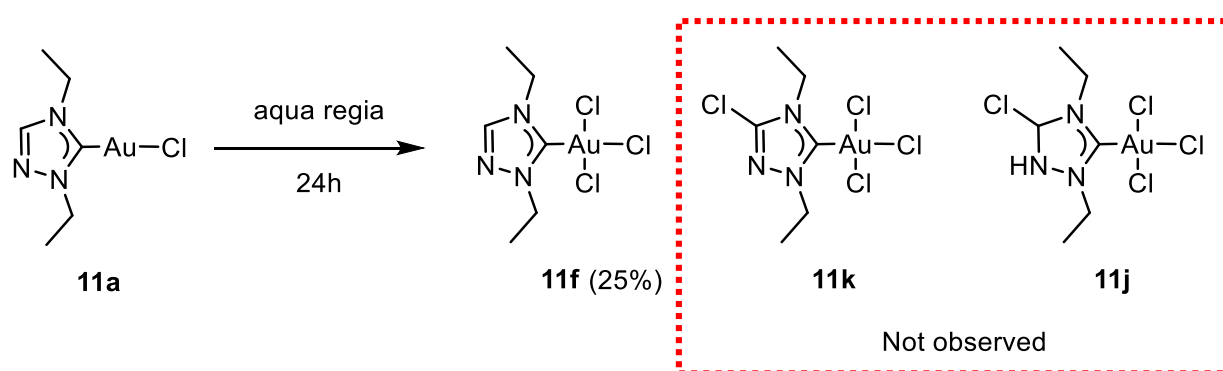


**Scheme 6.5.** Expected and observed products for the *aqua regia* oxidation of **11a**.

To confirm that no backbone reactivity happens in the absence of unsaturation, the unsaturated complex **12a** was oxidised applying the *aqua regia* protocol. Due to the sensitivity of the complex, a short reaction time (2h) was used and full conversion was achieved. As expected, no further reactivity of the NHC moiety was observed, and pure **12f** was isolated (Scheme 6.6).
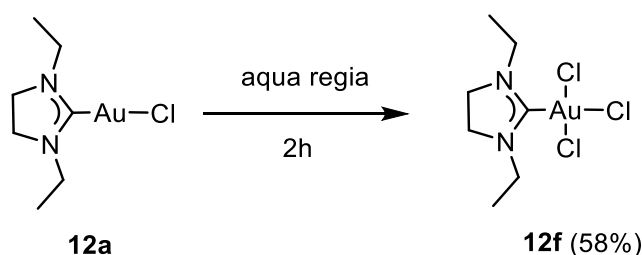


**Scheme 6.6.** Oxidation in *aqua regia* of **12a**.

### 6.2.5 Oxidation of 5e, 14a and 15a

The *aqua regia* protocol was further applied to the backbone brominated and iodinated gold(I) NHC complexes **14a** and **15a**. In *aqua regia* a great amount of chloro-containing active species

are formed, and due to the reactivity discussed for **1a**-**3a** the possibility of scrambling of the halogens present on the backbone of the already halogenated NHC rings cannot be completely ruled out. The oxidation of gold(I) NHC complexes with *aqua regia* containing other halogens by the use of HBr instead of HCl with nitric acid was attempted but no substantial product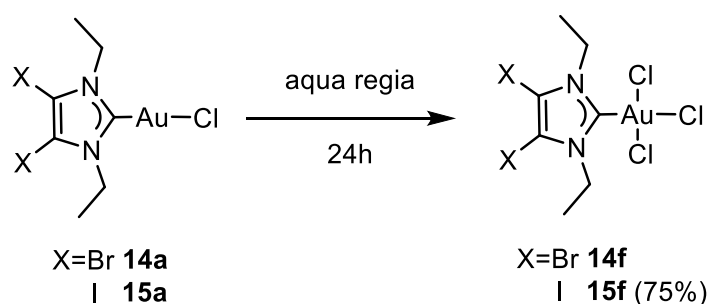s were obtained. A more accurate reference experiment was the test of the already backbone brominated or iodinated complexes **14a** and **15a** in *aqua regia*. In both cases the only observed product is the (NHC)AuCl$_3$ complex (**14f**, **15f**) (Scheme 6.7). No halogen substitution or scrambling was observed either by NMR or ESI-MS.



X=Br **14a**          X=Br **14f**
I **15a**          I **15f** (75%)

**Scheme 6.7.** Oxidation in *aqua regia* of **14a** and **15a**.

The trifluoromethylated complex **5e** was also oxidized in *aqua regia*, and only oxidation of the gold centre was observed (Scheme 6.8). No removal of the trifluoromethyl moiety was observed in both NMR and ESI-MS, suggesting that the chloride ancillary ligand in the oxidized **1a-6a**, **11a-16a** complexes was also not substituted or scrambled by *aqua regia*.



**5e**          **5g** (69%)
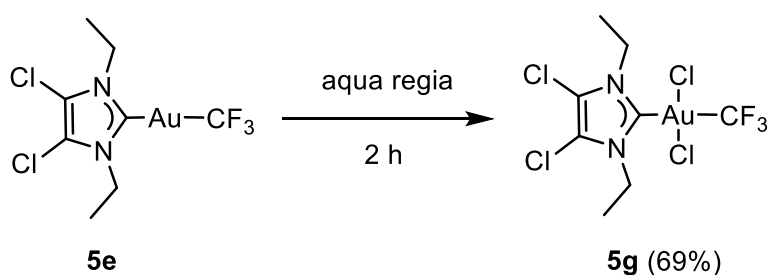
**Scheme 6.8.** Oxidation in *aqua regia* of **5e**.

### 6.2.6 Carbene chemical shift variation

The oxidation for the studied gold NHC complexes from gold(I) to gold(III) caused a substantial upfield shift of the carbene carbon in $^{13}$C NMR (Table 6.1). In the gold(I) complexes the range covered was between 168.9 - 196.4 ppm (average 176.6 ppm) while for the gold(III) counterparts was between 139.0 - 172.8 ppm (average 148.9 ppm). The average observed shift

was of 27.7 ppm. While minor shifts of the other peaks were also observed, the variation of the carbenic carbon was by far the most characteristic.

**Table 6.1.** Comparison of $^{13}C$ NMR chemical shift of carbene carbon for Au(I) and Au(III) complexes (CD$_2$Cl$_2$, 101-151 MHz)

| Compound | Au(I) (a) carbene $^{13}C$ NMR ($\delta$) | Au(III) (f) carbene $^{13}C$ NMR ($\delta$) |
|---|---|---|
| 1 | 172.1 | 141.7 |
| 2 | 170.1 | 140.3 |
| 3 | 168.9 | 139.0 |
| 4 | 172.4 | 142.6 |
| 5 | 170.8 | 141.7 |
| 5e[a] | 184.5[a] | 162.4[a] |
| 6 | 170.0 | 141.4 |
| 11 | 174.2 | 149.1 |
| 12 | 191.8 | 167.8 |
| 13 | 179.6 | 151.7 |
| 14 | 172.9 | 143.2 |
| 15 | 175.3 | 144.3 |
| 16 | 175.7[b] | 145.9 |
| 17 | 196.4[b] | 172.8 |

210    200    190    180    170    160    150    140    130

[a]**5e** is oxidized to **5g**; [b]literature values.[159]

## 6.3 Conclusions

The oxidation of gold(I) NHC complexes in *aqua regia* is a versatile protocol, that allows in most cases to obtain the relevant gold(III) NHC complexes in substantial quantities and high purity with an overall very undemanding protocol. For substrates **1a**, **2a** and **3a** in addition to the oxidation of the gold centre, reactivity of the NHC ligand by means of addition or substitution of its backbone with chlorides was observed. This reactivity has been proven to be limited only to these complexes and other side reactivity such as halogen scrambling or ligand substitution were not present in control experiments. The discussed backbone halogenation was not caused by radical reactivity and can be controlled by the variation of the substrate.

## 6.4 Experimental part

This experimental data section is to be considered supplementary to the Supporting Information of **Paper I**.

**5g**
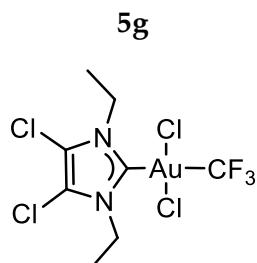


Stirring for 2 h of 24.9 mg of **5e** in 4 mL of *aqua regia* led to the isolation of a yellow powder (19.3 mg, 69%).

$^1$H NMR (600 MHz, CD$_2$Cl$_2$): δ 4.34 (q, *J* = 7.3 Hz, 4H, -C*H*$_2$-), 1.53 (t, *J* = 7.3 Hz, 6H, -C*H*$_3$).

$^{13}$C NMR (151 MHz, CD$_2$Cl$_2$): δ 162.4 (m, *J* = 30.9 Hz, NHC-*C*), 125.6 (q, J = 358.9 Hz, -*C*F$_3$), 119.4 (=*C*-Cl), 45.5 (-*C*H$_2$-), 15.4 (-*C*H$_3$).

MS (ESI$^+$,MeCN): *m/z* 550.911 ([M+Na]$^+$ 78.0%), 552.908 ([M+Na]$^+$ 100%), 554.908 ([M+Na]$^+$ 48.1%).

HRMS (MeCN): *m/z* meas. 550.9109, calcd. 550.9108 for [C$_8$H$_{10}$Au$^{35}$Cl$_4$F$_3$N$_2$Na]$^+$ (Δ = -0.2 ppm).

**11f**
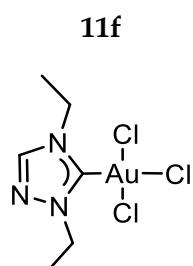


Stirring for 24 h of 50 mg of **11a** in 8 mL of *aqua regia* led to the isolation of a yellow powder (14.9 mg, 25%).

$^1$H NMR (400 MHz, CD$_2$Cl$_2$): δ 8.27 (s, 1H, =C*H*-), 4.53 (q, *J* = 7.3 Hz, 2H, -C*H*$_2$-, N side), 4.41 (q, *J* = 7.4 Hz, 2H, -C*H*$_2$-, CH side), 1.64 (t, *J* = 7.3 Hz, 3H, -C*H*$_3$, CH side), 1.61 (t, *J* = 7.4 Hz, 3H, -C*H*$_3$, N side).

$^{13}$C NMR (101 MHz, CD$_2$Cl$_2$): δ 149.1 (NHC-*C*), 144.2 (=*C*H-), 49.4 (-*C*H$_2$-, N side), 45.1 (-*C*H$_2$-, CH side), 15.7 (-*C*H$_3$), 14.8 (-*C*H$_3$).

MS (ESI$^+$,MeCN): *m/z* 449.958 ([M+Na]$^+$ 100%), 451.995 ([M+Na]$^+$ 95.9%), 453.952 ([M+Na]$^+$ 30.4%), 465.932 ([M+K]$^+$ 44.1%), 467.929 ([M+K]$^+$ 43.2%), 878.924 ([2M+Na]$^+$, 58.2%), 880.921 ([2M+Na]$^+$, 46.5%).

HRMS (MeCN): *m/z* meas. 449.9577, calcd. 449.9576 for [C$_6$H$_{11}$Au$^{35}$Cl$_3$N$_3$Na]$^+$ (Δ = -0.2 ppm).

**12f**



Stirring for 2h of 49.4 mg of **12a** in 8 mL of *aqua regia* led to the isolation of a yellow powder, (34.1 mg, 58%).

$^1$H NMR (600 MHz, CD$_2$Cl$_2$): δ 3.89 (s, 4H, -C*H*$_2$-), 3.77 (q, *J* = 7.3 Hz, 4H, -C*H*$_2$-CH$_3$), 1.33 (t, *J* = 7.2 Hz, 6H, -C*H*$_3$).

$^{13}$C NMR (151 MHz, CD$_2$Cl$_2$): δ 167.8 (NHC-*C*), 49.2 (-*C*H$_2$-), 45.3 (-*C*H$_2$-CH$_3$), 12.9 (-*C*H$_3$).

MS (ESI$^+$,MeOH): *m/z* 450.978 ([M+Na]$^+$ 100%), 452.975 [M+Na]$^+$ 94.1%), 454.972 ([M+Na]$^+$ 30.7%), 880.964 ([2M+Na]$^+$, 64.7%), 882.961 ([2M+Na]$^+$, 51.4%).

HRMS (MeOH): *m/z* meas. 450.9780, calcd. 450.9780 for [C$_7$H$_{14}$Au$^{35}$Cl$_3$N$_2$Na]$^+$ (Δ = 0.1 ppm).

**14f**
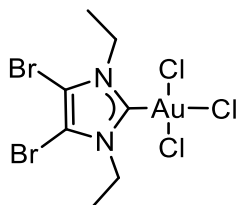


Stirring for 24 h of 51.4 mg of **14c** in 8 mL of *aqua regia* led to 55.7 mg of yellow powder; in the isolated product abundant water is present, and a small amount of starting material **14a** is still present (4%).

$^1$H NMR (600 MHz, CD$_2$Cl$_2$): δ 4.46 (q, *J* = 7.3 Hz, 4H, -C*H*$_2$-), 1.55 (t, *J* = 7.3 Hz, 6H, -C*H*$_3$).

$^{13}$C NMR (151 MHz, CD$_2$Cl$_2$): δ 143.2 (NHC-*C*), 111.0 (=*C*-Br), 47.8 (-*C*H$_2$-), 15.2 (-*C*H$_3$).

MS (ESI$^+$,MeCN): *m/z* 604.783 ([M+Na]$^+$ 30.6%), 606.781 ([M+Na]$^+$ 93.0%), 608.779 ([M+Na]$^+$ 100%), 610.776 ([M+Na]$^+$ 48.9%).

HRMS (MeCN): *m/z* meas. 604.7834, calcd. 604.7834 for [C$_7$H$_{10}$AuBr$_2$$^{35}$Cl$_3$N$_2$Na]$^+$ (Δ = 0.0 ppm).
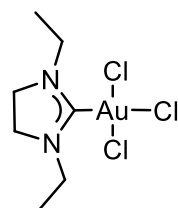
**15f**
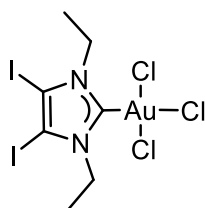


Stirring for 24 h of 48 mg of **15a** in 8 mL of *aqua regia* led to the isolation of a yellow powder (35.1 mg, 75%).

$^1$H NMR (400 MHz, CD$_2$Cl$_2$): δ 4.50 (q, *J* = 7.3 Hz, 4H, -C*H*$_2$-), 1.53 (t, *J* = 7.3 Hz, 6H, -C*H*$_3$).

$^{13}$C NMR (101 MHz, CD$_2$Cl$_2$): δ 144.3 (NHC-*C*), 90.1 (=*C*-I), 50.3 (-*C*H$_2$-), 15.5 (-*C*H$_3$).

MS (ESI$^+$,MeCN): *m/z* 700.756 ([M+Na]$^+$ 100%), 702.753 ([M+Na]$^+$ 99.5%), 704.750 ([M+Na]$^+$ 31.3%), 716.730 ( [M+K]$^+$ 28.9%), 718.727 ([M+K]$^+$ 31.3%), 1380.521 ([2M+Na]$^+$, 41.0%), 1382.518 ([2M+Na]$^+$, 31.7%).

HRMS (MeCN): *m/z* meas. 700.7555, calcd. 700.7557 for [C$_7$H$_{10}$Au$^{35}$Cl$_3$I$_2$N$_2$Na]$^+$ (Δ = 0.3 ppm).

# Chapter 7.

# Future Work

In this work it was demonstrated that gold(I) NHC complexes are suitable compounds for deposition applications, specifically FEBID. Even if we managed to prove the main hypothesis of this work, many optimizations and further studies are needed.

## *Synthesis of new FEBID precursors*

A natural continuation of the gold(I) NHC FEBID precursors would be towards a containment of the number of carbons in the structure, in order to achieve more pure deposits. A tetrazole-based gold(I) NHC complex (Figure 7.1) could lead to a great improvement of both volatility and deposit composition, however special care should be taken due to the possibility of explosions. Another direction could be towards the use of acyclic carbenes. During the exploration of the trifluoromethylation and methylation of gold(I) NHC complexes an effort was made also towards the synthesis of DMS and THT based methylated and trifluoromethylated complexes. The synthesis of these complexes could lead to two very suitable FEBID complexes, based on the observations made in this work and previously in literature.
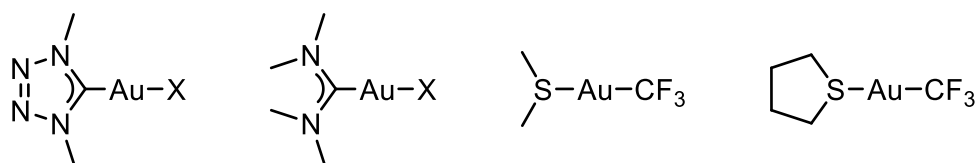


**Figure 7.1.** Proposed complexes for synthesis of FEBID precursors.

One of the key properties of NHC complexes is their compatibility with virtually all metals. In this direction, the test of other metal NHC FEBID precursors could open the road to unexplored metals in FEBID, and to study already known metals, such as silver and copper.

## *Testing of FEBID precursors*

The developed on substrate tester has been found to be very suitable for the early test of FEBID precursor. A further development of the setup in a modular fashion, where any precursor can

be pre-loaded on a closed holder, reservoir and substrate, to be then just loaded on a heated substrate could lead to the possibility of quick screening of a wider range of new precursors.

## *Sublimation point determination*

While in this work the sublimation temperature was obtained mainly by cold finger sublimation, other methods were explored. One very successful method was through the use of *vacuum*-TGA to mimic the environment of a SEM. The extension of this method to other FEBID precursors is highly desirable. Furthermore, the development of a TGA which can be used at a higher vacuum could lead to an understanding of the relation between vapour pressure, sublimation point and sufficient reservoir temperature for gas injection systems.

## *Solid state packing*

A computational background to corroborate the link between sublimation temperature and interactions involved in solid state packing is required to confirm the obtained data.

## *Synthetic use of aqua regia*

*Aqua regia* has proven to be suitable for the oxidation of a large series of gold complexes, as exemplified in **Paper I**. Volodymyr Levchenko has further explored *aqua regia* also as a manner of exchange halogens on *tpy*-based gold(III) complexes.[265] The use of *aqua regia* as a chlorinating agent could also be further explored. A drastic variation of the conditions could lead to an effective way for the production of bachkbone-halogenated NHC gold(III) complexes, specifically with the aim to obtain Br of I on the backbone by the use of HBr or HI instead of HCl in the preparation of *aqua regia* (Figure 7.2).
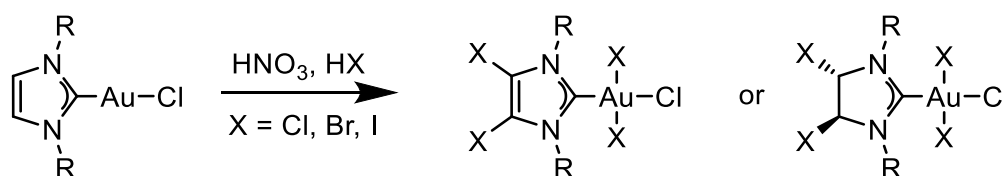


**Figure 7.2.** Proposed application of *aqua regia* as a functionalization and oxidation agent.

# References

1.  Gimeno, M. C., The Chemistry of Gold. In *Modern Supramolecular Gold Chemistry*, **2008**; pp 1-63.
2.  Mathews, J. A.; Watters, L. L., *J. Am. Chem. Soc.* **1900,** *22* (2), 108-111.
3.  Fukuda, Y.; Utimoto, K., *J. Org. Chem.* **1991,** *56* (11), 3729-3731.
4.  Hashmi, A. S. K., *Gold Bull.* **2003,** *36* (1), 3-9.
5.  Che, C.-M.; Sun, R. W.-Y., *ChemComm* **2011,** *47* (34), 9554-9560.
6.  Abdou, H. E.; Mohamed, A. A.; Fackler, J. P.; Burini, A.; Galassi, R.; López-de-Luzuriaga, J. M.; Olmos, M. E., *Coord. Chem. Rev.* **2009,** *253* (11), 1661-1669.
7.  Dykman, L. A.; Khlebtsov, N. G., *Acta Naturae* **2011,** *3* (2), 34-55.
8.  Baptista, P.; Pereira, E.; Eaton, P.; Doria, G.; Miranda, A.; Gomes, I.; Quaresma, P.; Franco, R., *Anal. Bioanal. Chem.* **2008,** *391* (3), 943-950.
9.  Ali, M. R. K.; Wu, Y.; El-Sayed, M. A., *J. Phys. Chem. C* **2019,** *123* (25), 15375-15393.
10. Priyadarshini, E.; Pradhan, N., *Sens. Actuators B Chem.* **2017,** *238*, 888-902.
11. Stratakis, M.; Garcia, H., *Chem. Rev.* **2012,** *112* (8), 4469-4506.
12. Baum, T. H.; Comita, P. B., Chemical Vapor Deposition of Gold and Silver. In *The Chemistry of Metal CVD*, **1994**; pp 303-327.
13. Griffiths, M. B. E.; Pallister, P. J.; Mandia, D. J.; Barry, S. T., *Chem. Mater.* **2016,** *28* (1), 44-46.
14. Mafuné, F.; Kohno, J.-y.; Takeda, Y.; Kondow, T.; Sawabe, H., *J. Phys. Chem. B* **2001,** *105* (22), 5114-5120.
15. Daruich De Souza, C.; Ribeiro Nogueira, B.; Rostelato, M. E. C. M., *J. Alloys Compd.* **2019,** *798*, 714-740.
16. Nagamachi, S.; Yamakage, Y.; Maruno, H.; Ueda, M.; Sugimoto, S.; Asari, M.; Ishikawa, J., *Appl. Phys. Lett.* **1993,** *62* (17), 2143-2145.
17. Belić, D.; Shawrav, M. M.; Bertagnolli, E.; Wanzenboeck, H. D., *Beilstein J. Nanotechnol.* **2017,** *8*, 2530-2543.
18. Ngo, T. D.; Kashani, A.; Imbalzano, G.; Nguyen, K. T. Q.; Hui, D., *Compos. B. Eng.* **2018,** *143*, 172-196.
19. Silvis-Cividjian, N.; Hagen, C. W., Electron-Beam–Induced Nanometer-Scale Deposition. In *Advances in Imaging and Electron Physics*, Elsevier: **2006**; Vol. 143, pp 1-235.
20. Utke, I.; Hoffmann, P.; Melngailis, J., *J. Vac. Sci. Technol. B* **2008,** *26* (4), 1197-1276.
21. Huth, M.; Porrati, F.; Schwalb, C.; Winhold, M.; Sachser, R.; Dukic, M.; Adams, J.; Fantner, G., *Beilstein J. Nanotechnol.* **2012,** *3*, 597-619.
22. van Dorp, W. F.; Hagen, C. W., *J. Appl. Phys.* **2008,** *104* (8), 081301.
23. Keller, L.; Huth, M., *Beilstein J. Nanotechnol.* **2018,** *9*, 2581-2598.
24. Winkler, R.; Fowlkes, J. D.; Rack, P. D.; Plank, H., *J. Appl. Phys.* **2019,** *125* (21), 210901.
25. Skoric, L.; Sanz-Hernández, D.; Meng, F.; Donnelly, C.; Merino-Aceituno, S.; Fernández-Pacheco, A., *Nano Lett.* **2020,** *20* (1), 184-191.
26. Fowlkes, J. D.; Winkler, R.; Lewis, B. B.; Fernández-Pacheco, A.; Skoric, L.; Sanz-Hernández, D.; Stanford, M. G.; Mutunga, E.; Rack, P. D.; Plank, H., *ACS Appl. Nano Mater.* **2018,** *1* (3), 1028-1041.
27. Noh, J. H.; Stanford, M. G.; Lewis, B. B.; Fowlkes, J. D.; Plank, H.; Rack, P. D., *Appl. Phys. A* **2014,** *117* (4), 1705-1713.
28. Fernández-Pacheco, A.; Serrano-Ramón, L.; Michalik, J. M.; Ibarra, M. R.; De Teresa, J. M.; O'Brien, L.; Petit, D.; Lee, J.; Cowburn, R. P., *Sci. Rep.* **2013,** *3* (1), 1492.
29. Höflich, K.; Yang, R. B.; Berger, A.; Leuchs, G.; Christiansen, S., *Adv. Mater.* **2011,** *23* (22-23), 2657-2661.

30. Graells, S.; Aćimović, S.; Volpe, G.; Quidant, R., *Plasmonics* **2010,** *5* (2), 135-139.
31. Liu, N.; Tang, M. L.; Hentschel, M.; Giessen, H.; Alivisatos, A. P., *Nat. Mater.* **2011,** *10*, 631.
32. Huth, M.; Porrati, F.; Dobrovolskiy, O. V., *Microelectron. Eng.* **2018,** *185-186*, 9-28.
33. Schwalb, C. H.; Grimm, C.; Baranowski, M.; Sachser, R.; Porrati, F.; Reith, H.; Das, P.; Müller, J.; Völklein, F.; Kaya, A.; Huth, M., *Sensors* **2010,** *10* (11), 9847-9856.
34. Brown, J.; Kocher, P.; Ramanujan, C. S.; Sharp, D. N.; Torimitsu, K.; Ryan, J. F., *Ultramicroscopy* **2013,** *133*, 62-66.
35. Rodriguez, B. J.; Jesse, S.; Seal, K.; Baddorf, A. P.; Kalinin, S. V.; Rack, P. D., *Appl. Phys. Lett.* **2007,** *91* (9), 093130.
36. Utke, I.; Hoffmann, P.; Berger, R.; Scandella, L., *Appl. Phys. Lett.* **2002,** *80* (25), 4792-4794.
37. De Teresa, J. M.; Fernández-Pacheco, A., *Appl. Phys. A* **2014,** *117* (4), 1645-1658.
38. Keller, L.; Al Mamoori, M. K. I.; Pieper, J.; Gspan, C.; Stockem, I.; Schröder, C.; Barth, S.; Winkler, R.; Plank, H.; Pohlit, M.; Müller, J.; Huth, M., *Sci. Rep.* **2018,** *8* (1), 6160.
39. Widyaratih, D. S.; Hagedoorn, P.-L.; Otten, L. G.; Ganjian, M.; Tümer, N.; Apachitei, I.; Hagen, C. W.; Fratila-Apachitei, L. E.; Zadpoor, A. A., *Nanotechnology* **2019,** *30* (20), 20LT01.
40. Hari, S.; Verduin, T.; Kruit, P.; Hagen, C. W., *Micro and Nano Engineering* **2019,** *4*, 1-6.
41. van Kouwen, L.; Botman, A.; Hagen, C. W., *Nano Lett.* **2009,** *9* (5), 2149-2152.
42. Wells, O. C., Scanning Electron Microscopy. In *Encyclopedia of Materials: Science and Technology*, Eds. Elsevier: Oxford, **2001**; pp 8265-8269.
43. Ingolfsson, O., Low Energy Electron-Induced Dissociation. In *Low-Energy Electrons: Fundamentals and Applications*, Jenny Standford Publishing: New York, **2019**; pp 47-120.
44. Carden, W. G.; Lu, H.; Spencer, J. A.; Fairbrother, D. H.; McElwee-White, L., *MRS Commun.* **2018,** *8* (2), 343-357.
45. Wnuk, J. D.; Gorham, J. M.; Rosenberg, S. G.; van Dorp, W. F.; Madey, T. E.; Hagen, C. W.; Fairbrother, D. H., *J. Phys. Chem. C* **2009,** *113* (6), 2487-2496.
46. Wnuk, J. D.; Rosenberg, S. G.; Gorham, J. M.; van Dorp, W. F.; Hagen, C. W.; Fairbrother, D. H., *Surf. Sci.* **2011,** *605* (3), 257-266.
47. Mahgoub, A.; Lu, H.; Thorman, R. M.; Preradovic, K.; Jurca, T.; McElwee-White, L.; Fairbrother, H.; Hagen, C. W., *Beilstein J. Nanotechnol.* **2020,** *11*, 1789-1800.
48. Utke, I.; Moshkalev, S.; Russell, P., *Nanofabrication Using Focused Ion and Electron Beam*, Oxford University Press, **2012**.
49. Berger, L.; Madajska, K.; Szymanska, I. B.; Höflich, K.; Polyakov, M. N.; Jurczyk, J.; Guerra-Nuñez, C.; Utke, I., *Beilstein J. Nanotechnol.* **2018,** *9*, 224-232.
50. Höflich, K.; Jurczyk, J. M.; Madajska, K.; Götz, M.; Berger, L.; Guerra-Nuñez, C.; Haverkamp, C.; Szymanska, I.; Utke, I., *Beilstein J. Nanotechnol.* **2018,** *9*, 842-849.
51. Berger, L.; Jurczyk, J.; Madajska, K.; Edwards, T. E. J.; Szymańska, I.; Hoffmann, P.; Utke, I., *ACS Appl. Electron. Mater.* **2020,** *2* (7), 1989-1996.
52. Höflich, K.; Jurczyk, J.; Zhang, Y.; Puydinger dos Santos, M. V.; Götz, M.; Guerra-Nuñez, C.; Best, J. P.; Kapusta, C.; Utke, I., *ACS Appl. Mater. Interfaces* **2017,** *9* (28), 24071-24077.
53. Botman, A.; Hesselberth, M.; Mulders, J. J. L., *J. Vac. Sci. Technol. B* **2008,** *26* (6), 2464-2467.
54. Botman, A.; Mulders, J. J. L.; Hagen, C. W., *Nanotechnology* **2009,** *20* (37), 372001.
55. Mulders, J. J. L.; Belova, L. M.; Riazanova, A., *Nanotechnology* **2010,** *22* (5), 055302.
56. Winkler, R.; Lewis, B. B.; Fowlkes, J. D.; Rack, P. D.; Plank, H., *ACS Appl. Nano Mater.* **2018,** *1* (3), 1014-1027.
57. Winkler, R.; Geier, B.; Plank, H., *Appl. Phys. A* **2014,** *117* (4), 1675-1688.
58. Puydinger dos Santos, M. V.; Velo, M. F.; Domingos, R. D.; Zhang, Y.; Maeder, X.; Guerra-Nuñez, C.; Best, J. P.; Béron, F.; Pirota, K. R.; Moshkalev, S.; Diniz, J. A.; Utke, I., *ACS Appl. Mater. Interfaces* **2016,** *8* (47), 32496-32503.
59. Pablo-Navarro, J.; Magén, C.; de Teresa, J. M., *ACS Appl. Nano Mater.* **2018,** *1* (1), 38-46.
60. Porrati, F.; Sachser, R.; Schwalb, C. H.; Frangakis, A. S.; Huth, M., *J. Appl. Phys.* **2011,** *109* (6), 063715.

61. Plank, H.; Kothleitner, G.; Hofer, F.; Michelitsch, S. G.; Gspan, C.; Hohenau, A.; Krenn, J., *J. Vac. Sci. Technol. B* **2011,** *29* (5), 051801.

62. Stanford, M. G.; Lewis, B. B.; Noh, J. H.; Fowlkes, J. D.; Roberts, N. A.; Plank, H.; Rack, P. D., *ACS Appl. Mater. Interfaces* **2014,** *6* (23), 21256-21263.

63. Plank, H.; Noh, J. H.; Fowlkes, J. D.; Lester, K.; Lewis, B. B.; Rack, P. D., *ACS Appl. Mater. Interfaces* **2014,** *6* (2), 1018-1024.

64. Jurczyk, J.; Brewer, C. R.; Hawkins, O. M.; Polyakov, M. N.; Kapusta, C.; McElwee-White, L.; Utke, I., *ACS Appl. Mater. Interfaces* **2019,** *11* (31), 28164-28171.

65. Geier, B.; Gspan, C.; Winkler, R.; Schmied, R.; Fowlkes, J. D.; Fitzek, H.; Rauch, S.; Rattenberger, J.; Rack, P. D.; Plank, H., *J. Phys. Chem. C* **2014,** *118* (25), 14009-14016.

66. Begun, E.; Dobrovolskiy, O. V.; Kompaniiets, M.; Sachser, R.; Gspan, C.; Plank, H.; Huth, M., *Nanotechnology* **2015,** *26* (7), 075301.

67. Elbadawi, C.; Toth, M.; Lobo, C. J., *ACS Appl. Mater. Interfaces* **2013,** *5* (19), 9372-9376.

68. Langford, R. M.; Wang, T. X.; Ozkaya, D., *Microelectron. Eng.* **2007,** *84* (5), 784-788.

69. Barth, S.; Huth, M.; Jungwirth, F., *J. Mater. Chem. C* **2020**, *8*, 15884-15919.

70. Marashdeh, A.; Tiesma, T.; van Velzen, N. J. C.; Harder, S.; Havenith, R. W. A.; De Hosson, J. T. M.; van Dorp, W. F., *Beilstein J. Nanotechnol.* **2017,** *8*, 2753-2765.

71. Folch, A.; Servat, J.; Esteve, J.; Tejada, J.; Seco, M., *J. Vac. Sci. Technol. B* **1996,** *14* (4), 2609-2614.

72. Sun, L.; Yuan, G.; Gao, L.; Yang, J.; Chhowalla, M.; Gharahcheshmeh, M. H.; Gleason, K. K.; Choi, Y. S.; Hong, B. H.; Liu, Z., *Nat. Rev. Methods Primers* **2021,** *1* (1), 5.

73. Xue, Z.; Strouse, M. J.; Shuh, D. K.; Knobler, C. B.; Kaesz, H. D.; Hicks, R. F.; Williams, R. S., *J. Am. Chem. Soc.* **1989,** *111* (24), 8779-8784.

74. Spencer, J. A.; Brannaka, J. A.; Barclay, M.; McElwee-White, L.; Fairbrother, D. H., *J. Phys. Chem. C* **2015,** *119* (27), 15349-15359.

75. Miyazoe, H.; Utke, I.; Kikuchi, H.; Kiriu, S.; Friedli, V.; Michler, J.; Terashima, K., *J. Vac. Sci. Technol. B* **2010,** *28* (4), 744-750.

76. Luisier, A.; Utke, I.; Bret, T.; Cicoira, F.; Hauert, R.; Rhee, S. W.; Doppelt, P.; Hoffmann, P., *J. Electrochem. Soc.* **2004,** *151* (9), C590.

77. Mulders, J. J. L.; Belova, L. M.; Riazanova, A., *Nanotechnology* **2011,** *22*.

78. Jenke, M. G.; Lerose, D.; Niederberger, C.; Michler, J.; Christiansen, S.; Utke, I., *Nano Lett.* **2011,** *11* (10), 4213-4217.

79. Puydinger dos Santos, M. V.; Szkudlarek, A.; Rydosz, A.; Guerra-Nuñez, C.; Béron, F.; Pirota, K. R.; Moshkalev, S.; Diniz, J. A.; Utke, I., *Beilstein J. Nanotechnol.* **2018,** *9*, 91-101.

80. Koops, H. W. P.; Kretz, J.; Rudolph, M.; Weber, M.; Dahm, G.; Lee, K. L., *Jpn. J. Appl. Phys.* **1994,** *33* (Part 1, No. 12B), 7099-7107.

81. Utke, I.; Jenke, M. G.; Röling, C.; Thiesen, P. H.; Iakovlev, V.; Sirbu, A.; Mereuta, A.; Caliman, A.; Kapon, E., *Nanoscale* **2011,** *3* (7), 2718-2722.

82. Utke, I.; Luisier, A.; Hoffmann, P.; Laub, D.; Buffat, P. A., *Appl. Phys. Lett.* **2002,** *81* (17), 3245-3247.

83. Rosenberg, S. G.; Barclay, M.; Fairbrother, D. H., *ACS Appl. Mater. Interfaces* **2014,** *6* (11), 8590-8601.

84. Perentes, A.; Hoffmann, P., *Chem. Vap. Depos.* **2007,** *13* (4), 176-184.

85. Winhold, M.; Weirich, P. M.; Schwalb, C. H.; Huth, M., *Appl. Phys. Lett.* **2014,** *105* (16), 162603.

86. Carden, W. G.; Thorman, R. M.; Unlu, I.; Abboud, K. A.; Fairbrother, D. H.; McElwee-White, L., *ACS Appl. Mater. Interfaces* **2019,** *11* (12), 11976-11987.

87. Henderson, M. A.; Ramsier, R. D.; Yates, J. T., *Surf. Sci.* **1991,** *259* (1), 173-182.

88. Córdoba, R.; Sesé, J.; De Teresa, J. M.; Ibarra, M. R., *Microelectron. Eng.* **2010,** *87* (5), 1550-1553.

89. Weber, M.; Koops, H. W. P.; Rudolph, M.; Kretz, J.; Schmidt, G., *J. Vac. Sci. Technol. B* **1995,** *13* (3), 1364-1368.

90.    Porrati, F.; Sachser, R.; Huth, M., *Nanotechnology* **2009,** *20* (19), 195301.

91.    Rosenberg, S. G.; Barclay, M.; Fairbrother, D. H., *J. Phys. Chem. C* **2013,** *117* (31), 16053-16064.

92.    Mulders, J. J. L.; Veerhoek, J. M.; Bosch, E. G. T.; Trompenaars, P. H. F., *J. Phys D: Appl. Phys.* **2012,** *45* (47), 475301.

93.    Barry, J. D.; Ervin, M.; Molstad, J.; Wickenden, A.; Brintlinger, T.; Hoffman, P.; Meingailis, J., *J. Vac. Sci. Technol. B* **2006,** *24* (6), 3165-3168.

94.    Wang, S.; Sun, Y.-M.; Wang, Q.; White, J. M., *J. Vac. Sci. Technol. B* **2004,** *22* (4), 1803-1806.

95.    Perentes, A.; Sinicco, G.; Boero, G.; Dwir, B.; Hoffmann, P., *J. Vac. Sci. Technol. B* **2007,** *25* (6), 2228-2232.

96.    Utke, I.; Hoffmann, P.; Dwir, B.; Leifer, K.; Kapon, E.; Doppelt, P., *J. Vac. Sci. Technol. B* **2000,** *18* (6), 3168-3171.

97.    Brintlinger, T.; Fuhrer, M. S.; Melngailis, J.; Utke, I.; Bret, T.; Perentes, A.; Hoffmann, P.; Abourida, M.; Doppelt, P., *J. Vac. Sci. Technol. B* **2005,** *23* (6), 3174-3177.

98.    Utke, I.; Dwir, B.; Leifer, K.; Cicoira, F.; Doppelt, P.; Hoffmann, P.; Kapon, E., *Microelectron. Eng.* **2000,** *53* (1), 261-264.

99.    Hoffmann, P.; Utke, I.; Cicoira, F.; Dwir, B.; Leifer, K.; Kapon, E.; Doppelt, P., *MRS Proceedings* **2000,** *624*, 171.

100.   Warneke, J.; Rohdenburg, M.; Zhang, Y.; Orszagh, J.; Vaz, A.; Utke, I.; De Hosson, J. T. M.; van Dorp, W. F.; Swiderek, P., *J. Phys. Chem. C* **2016,** *120* (7), 4112-4120.

101.   Shimojo, M.; Bysakh, S.; Mitsuishi, K.; Tanaka, M.; Song, M.; Furuya, K., *Appl. Surf. Scie.* **2005,** *241* (1), 56-60.

102.   Funsten, H. O.; Boring, J. W.; Johnson, R. E.; Brown, W. L., *J. Appl. Phys.* **1992,** *71* (3), 1475-1484.

103.   Christy, R. W., *J. Appl. Phys.* **1962,** *33* (5), 1884-1888.

104.   Matsui, S.; Mori, K., *J. Vac. Sci. Technol. B* **1986,** *4* (1), 299-304.

105.   Höflich, K.; Becker, M.; Leuchs, G.; Christiansen, S., *Nanotechnology* **2012,** *23* (18), 185303.

106.   Winkler, R.; Schmidt, F.-P.; Haselmann, U.; Fowlkes, J. D.; Lewis, B. B.; Kothleitner, G.; Rack, P. D.; Plank, H., *ACS Appl. Mater. Interfaces* **2017,** *9* (9), 8233-8240.

107.   Shawrav, M. M.; Taus, P.; Wanzenboeck, H. D.; Schinnerl, M.; Stöger-Pollach, M.; Schwarz, S.; Steiger-Thirsfeld, A.; Bertagnolli, E., *Sci. Rep.* **2016,** *6*, 34003.

108.   van Dorp, W. F.; Wu, X.; Mulders, J. J. L.; Harder, S.; Rudolf, P.; De Hosson, J. T. M., *Langmuir* **2014,** *30* (40), 12097-12105.

109.   Carden, W. G.; Pedziwiatr, J.; Abboud, K. A.; McElwee-White, L., *ACS Appl. Mater. Interfaces* **2017,** *9* (46), 40998-41005.

110.   Schmidbaur, H.; Schier, A., *Chem. Soc. Rev.* **2008,** *37* (9), 1931-1951.

111.   Arduengo, A. J.; Harlow, R. L.; Kline, M., *J. Am. Chem. Soc.* **1991,** *113* (1), 361-363.

112.   Tapu, D.; Dixon, D. A.; Roe, C., *Chem. Rev.* **2009,** *109* (8), 3385-3407.

113.   Schuster, O.; Yang, L.; Raubenheimer, H. G.; Albrecht, M., *Chem. Rev.* **2009,** *109* (8), 3445-3478.

114.   Hahn, F. E.; Jahnke, M. C., *Angew. Chem. Int.* **2008,** *47* (17), 3122-3172.

115.   de Frémont, P.; Marion, N.; Nolan, S. P., *Coord. Chem. Rev.* **2009,** *253* (7), 862-892.

116.   Herrmann, W. A., *Angew. Chem. Int.* **2002,** *41* (8), 1290-1309.

117.   Bourissou, D.; Guerret, O.; Gabbaï, F. P.; Bertrand, G., *Chem. Rev.* **2000,** *100* (1), 39-92.

118.   Herrmann, W. A.; Köcher, C., *Angew. Chem. Int.* **1997,** *36* (20), 2162-2187.

119.   Hopkinson, M. N.; Richter, C.; Schedler, M.; Glorius, F., *Nature* **2014,** *510* (7506), 485-496.

120.   Huynh, H. V., *Chem. Rev.* **2018,** *118* (19), 9457-9492.

121.   Alder, R. W.; Blake, M. E.; Chaker, L.; Harvey, J. N.; Paolini, F.; Schütz, J., *Angew. Chem. Int.* **2004,** *43* (44), 5896-5911.

122.   Aldeco-Perez, E.; Rosenthal, A. J.; Donnadieu, B.; Parameswaran, P.; Frenking, G.; Bertrand, G., *Science* **2009,** *326* (5952), 556-9.

123. Lavallo, V.; Canac, Y.; Präsang, C.; Donnadieu, B.; Bertrand, G., *Angew. Chem. Int.* **2005,** *44* (35), 5705-9.

124. Arduengo, A. J.; Goerlich, J. R.; Marshall, W. J., *J. Am. Chem. Soc.* **1995,** *117* (44), 11027-11028.

125. Arduengo, A. J.; Dias, H. V. R.; Harlow, R. L.; Kline, M., *J. Am. Chem. Soc.* **1992,** *114* (14), 5530-5534.

126. Moerdyk, J. P.; Schilter, D.; Bielawski, C. W., *Acc. Chem. Res.* **2016,** *49* (8), 1458-1468.

127. Bartolomé, C.; Ramiro, Z.; García-Cuadrado, D.; Pérez-Galán, P.; Raducan, M.; Bour, C.; Echavarren, A. M.; Espinet, P., *Organometallics* **2010,** *29* (4), 951-956.

128. Bartolomé, C.; García-Cuadrado, D.; Ramiro, Z.; Espinet, P., *Organometallics* **2010,** *29* (16), 3589-3592.

129. Bartolomé, C.; Ramiro, Z.; Pérez-Galán, P.; Bour, C.; Raducan, M.; Echavarren, A. M.; Espinet, P., *Inorg. Chem.* **2008,** *47* (23), 11391-11397.

130. Bartolomé, C.; García-Cuadrado, D.; Ramiro, Z.; Espinet, P., *Inorg. Chem.* **2010,** *49* (21), 9758-9764.

131. Enders, D.; Niemeier, O.; Henseler, A., *Chem. Rev.* **2007,** *107* (12), 5606-5655.

132. Barik, S.; Biju, A. T., *ChemComm* **2020,** *56* (99), 15484-15495.

133. Flanigan, D. M.; Romanov-Michailidis, F.; White, N. A.; Rovis, T., *Chem. Rev.* **2015,** *115* (17), 9307-9387.

134. Doddi, A.; Peters, M.; Tamm, M., *Chem. Rev.* **2019,** *119* (12), 6994-7112.

135. Nesterov, V.; Reiter, D.; Bag, P.; Frisch, P.; Holzner, R.; Porzelt, A.; Inoue, S., *Chem. Rev.* **2018,** *118* (19), 9678-9842.

136. Wanzlick, H.-W.; Schönherr, H.-J., *Angew. Chem. Int.* **1968,** *7* (2), 141-142.

137. Öfele, K., *J. Organomet. Chem.* **1968,** *12* (3), P42-P43.

138. Holzmann, N.; Stasch, A.; Jones, C.; Frenking, G., *Chem. Eur. J.* **2013,** *19* (20), 6467-6479.

139. Hillier, A. C.; Sommer, W. J.; Yong, B. S.; Petersen, J. L.; Cavallo, L.; Nolan, S. P., *Organometallics* **2003,** *22* (21), 4322-4326.

140. Clavier, H.; Nolan, S. P., *ChemComm* **2010,** *46* (6), 841-861.

141. Gómez-Suárez, A.; Nelson, D. J.; Nolan, S. P., *ChemComm* **2017,** *53* (18), 2650-2660.

142. Poater, A.; Cosenza, B.; Correa, A.; Giudice, S.; Ragone, F.; Scarano, V.; Cavallo, L., *Eur. J. Inorg. Chem.* **2009,** *2009* (13), 1759-1766.

143. Tolman, C. A., *Chem. Rev.* **1977,** *77* (3), 313-348.

144. Tolman, C. A., *J. Am. Chem. Soc.* **1970,** *92* (10), 2953-2956.

145. Romain, C.; Bellemin-Laponnaz, S.; Dagorne, S., *Coord. Chem. Rev.* **2020,** *422*, 213411.

146. Scattolin, T.; Nolan, S. P., *Trends Chem.* **2020,** *2* (8), 721-736.

147. Díez-González, S.; Marion, N.; Nolan, S. P., *Chem. Rev.* **2009,** *109* (8), 3612-3676.

148. Jalal, M.; Hammouti, B.; Touzani, R.; Aouniti, A.; Ozdemir, I., *Mater. Today* **2020,** *31*, S122-S129.

149. Patil, S. A.; Patil, S. A.; Patil, R.; Keri, R. S.; Budagumpi, S.; Balakrishna, G. R.; Tacke, M., *Future Med. Chem.* **2015,** *7* (10), 1305-33.

150. Hutchings, G. J.; Brust, M.; Schmidbaur, H., *Chem. Soc. Rev.* **2008,** *37* (9), 1759-1765.

151. Thayer, J. S., Organometallic Chemistry: A Historical Perspective. In *Advances in Organometallic Chemistry*, Eds. Academic Press: **1975**; Vol. 13, pp 1-45.

152. Minghetti, G.; Bonati, F., *J. Organomet. Chem.* **1973,** *54*, C62-C63.

153. Parish, R. V., *Gold Bull.* **1997,** *30* (1), 3-12.

154. Johnson, A.; Gimeno, M. C., *ChemComm* **2016,** *52* (62), 9664-9667.

155. Nahra, F.; Tzouras, N. V.; Collado, A.; Nolan, S. P., *Nat. Protoc.* **2021**.

156. Liu, S.-T.; Lee, C.-I.; Fu, C.-F.; Chen, C.-H.; Liu, Y.-H.; Elsevier, C. J.; Peng, S.-M.; Chen, J.-T., *Organometallics* **2009,** *28* (24), 6957-6962.

157. Schmidt, C.; Karge, B.; Misgeld, R.; Prokop, A.; Franke, R.; Brönstrup, M.; Ott, I., *Chem. Eur. J.* **2017,** *23* (8), 1869-1880.

158. Wang, H. M. J.; Chen, C. Y. L.; Lin, I. J. B., *Organometallics* **1999,** *18* (7), 1216-1223.

159. Collado, A.; Gomez-Suarez, A.; Martin, A. R.; Slawin, A. M. Z.; Nolan, S. P., *ChemComm* **2013,** *49* (49), 5541-5543.

160. de Frémont, P.; Scott, N. M.; Stevens, E. D.; Nolan, S. P., *Organometallics* **2005,** *24* (10), 2411-2418.

161. Liu, Y.; Lemal, D. M., *Tetrahedron Lett.* **2000,** *41* (5), 599-602.

162. Collado, A.; Gómez-Suárez, A.; Martin, A. R.; Slawin, A. M. Z.; Nolan, S. P., *ChemComm* **2013,** *49* (49), 5541-5543.

163. Visbal, R.; Laguna, A.; Gimeno, M. C., *ChemComm* **2013,** *49* (50), 5642-5644.

164. Zhu, S.; Liang, R.; Chen, L.; Wang, C.; Ren, Y.; Jiang, H., *Tetrahedron Lett.* **2012,** *53* (7), 815-818.

165. Wang, H. M. J.; Lin, I. J. B., *Organometallics* **1998,** *17* (5), 972-975.

166. Furst, M. R. L.; Cazin, C. S. J., *ChemComm* **2010,** *46* (37), 6924-6925.

167. Bertrand, B.; Stefan, L.; Pirrotta, M.; Monchaud, D.; Bodio, E.; Richard, P.; Le Gendre, P.; Warmerdam, E.; de Jager, M. H.; Groothuis, G. M. M.; Picquet, M.; Casini, A., *Inorg. Chem.* **2014,** *53* (4), 2296-2303.

168. Chen, K.; Nenzel, M. M.; Brown, T. M.; Catalano, V. J., *Inorg. Chem.* **2015,** *54* (14), 6900-6909.

169. Ghdhayeb, M. Z.; Haque, R. A.; Budagumpi, S., *J. Organomet. Chem.* **2014,** *757*, 42-50.

170. Baker, M. V.; Barnard, P. J.; Berners-Price, S. J.; Brayshaw, S. K.; Hickey, J. L.; Skelton, B. W.; White, A. H., *Dalton Trans.* **2006,** (30), 3708-3715.

171. Raubenheimer, H. G.; Lindeque, L.; Cronje, S., *J. Organomet. Chem.* **1996,** *511* (1), 177-184.

172. Penney, A. A.; Sizov, V. V.; Grachova, E. V.; Krupenya, D. V.; Gurzhiy, V. V.; Starova, G. L.; Tunik, S. P., *Inorg. Chem.* **2016,** *55* (10), 4720-4732.

173. Tubaro, C.; Baron, M.; Costante, M.; Basato, M.; Biffis, A.; Gennaro, A.; Isse, A. A.; Graiff, C.; Accorsi, G., *Dalton Trans.* **2013,** *42* (30), 10952-10963.

174. Lozada-Rodríguez, L.; Pelayo-Vázquez, J. B.; Rangel-Salas, I. I.; Alvarado-Rodríguez, J. G.; Peregrina-Lucano, A. A.; Pérez-Centeno, A.; López-Dellamary-Toral, F. A.; Cortes-Llamas, S. A., *Dalton Trans.* **2017,** *46* (12), 3809-3811.

175. Galuppo, C.; Alvarenga, J.; Queiroz, A. C.; Messias, I.; Nagao, R.; Abbehausen, C., *Electrochem. Commun.* **2020,** *110*, 106620.

176. Corberán, R.; Ramírez, J.; Poyatos, M.; Peris, E.; Fernández, E., *Tetrahedron Asymmetry* **2006,** *17* (12), 1759-1762.

177. Bender, C. F.; Widenhoefer, R. A., *Org. Lett.* **2006,** *8* (23), 5303-5305.

178. Gaillard, S.; Cazin, C. S. J.; Nolan, S. P., *Acc. Chem. Res.* **2012,** *45* (6), 778-787.

179. Boogaerts, I. I. F.; Nolan, S. P., *J. Am. Chem. Soc.* **2010,** *132* (26), 8858-8859.

180. Schneider, S. K.; Herrmann, W. A.; Herdtweck, E., *Z. Anorg. Allg. Chem.* **2003,** *629* (12-13), 2363-2370.

181. Witham, C. A.; Mauleón, P.; Shapiro, N. D.; Sherry, B. D.; Toste, F. D., *J. Am. Chem. Soc.* **2007,** *129* (18), 5838-5839.

182. Ramón, R. S.; Marion, N.; Nolan, S. P., *Chem. Eur. J.* **2009,** *15* (35), 8695-8697.

183. López, S.; Herrero-Gómez, E.; Pérez-Galán, P.; Nieto-Oberhuber, C.; Echavarren, A. M., *Angew. Chem. Int.* **2006,** *45* (36), 6029-6032.

184. Kim, S. M.; Park, J. H.; Choi, S. Y.; Chung, Y. K., *Angew. Chem. Int.* **2007,** *46* (32), 6172-6175.

185. Marion, N.; Nolan, S. P., *Chem. Soc. Rev.* **2008,** *37* (9), 1776-1782.

186. Zhdanko, A.; Maier, M. E., *ACS Catal.* **2015,** *5* (10), 5994-6004.

187. Jia, M.; Bandini, M., *ACS Catal.* **2015,** *5* (3), 1638-1652.

188. Wegener, M.; Huber, F.; Bolli, C.; Jenne, C.; Kirsch, S. F., *Chem. Eur. J.* **2015,** *21* (3), 1328-1336.

189. Seppänen, O.; Aikonen, S.; Muuronen, M.; Alamillo-Ferrer, C.; Burés, J.; Helaja, J., *ChemComm* **2020,** *56* (93), 14697-14700.

190. Gaggioli, C. A.; Bistoni, G.; Ciancaleoni, G.; Tarantelli, F.; Belpassi, L.; Belanzoni, P., *Chem. Eur. J.* **2017,** *23* (31), 7558-7569.

191.    Izquierdo, F.; Manzini, S.; Nolan, S. P., *ChemComm* **2014,** *50* (95), 14926-14937.

192.    Marion, N.; Gealageas, R.; Nolan, S. P., *Org. Lett.* **2007,** *9* (14), 2653-2656.

193.    Porchia, M.; Pellei, M.; Marinelli, M.; Tisato, F.; Del Bello, F.; Santini, C., *Eur. J. Med. Chem.* **2018,** *146*, 709-746.

194.    Zhang, C.; Maddelein, M.-L.; Wai-Yin Sun, R.; Gornitzka, H.; Cuvillier, O.; Hemmert, C., *Eur. J. Med. Chem.* **2018,** *157*, 320-332.

195.    Dada, O.; Sánchez-Sanz, G.; Tacke, M.; Zhu, X., *Tetrahedron Lett.* **2018,** *59* (30), 2904-2908.

196.    Baker, M. V.; Barnard, P. J.; Berners-Price, S. J.; Brayshaw, S. K.; Hickey, J. L.; Skelton, B. W.; White, A. H., *J. Organomet. Chem.* **2005,** *690* (24), 5625-5635.

197.    Longevial, J.-F.; Langlois, A.; Buisson, A.; Devillers, C. H.; Clément, S.; van der Lee, A.; Harvey, P. D.; Richeter, S., *Organometallics* **2016,** *35* (5), 663-672.

198.    Griffiths, M. B. E.; Dubrawski, Z. S.; Bačić, G.; Japahuge, A.; Masuda, J. D.; Zeng, T.; Barry, S. T., *Eur. J. Inorg. Chem.* **2019,** *2019* (46), 4927-4938.

199.    Griffiths, M. B. E.; Koponen, S. E.; Mandia, D. J.; McLeod, J. F.; Coyle, J. P.; Sims, J. J.; Giorgi, J. B.; Sirianni, E. R.; Yap, G. P. A.; Barry, S. T., *Chem. Mater.* **2015,** *27* (17), 6116-6124.

200.    Man, R. W. Y.; Li, C.-H.; MacLean, M. W. A.; Zenkina, O. V.; Zamora, M. T.; Saunders, L. N.; Rousina-Webb, A.; Nambo, M.; Crudden, C. M., *J. Am. Chem. Soc.* **2018,** *140* (5), 1576-1579.

201.    Boysen, N.; Hasselmann, T.; Karle, S.; Rogalla, D.; Theirich, D.; Winter, M.; Riedl, T.; Devi, A., *Angew. Chem. Int.* **2018,** *57* (49), 16224-16227.

202.    Coyle, J. P.; Dey, G.; Sirianni, E. R.; Kemell, M. L.; Yap, G. P. A.; Ritala, M.; Leskelä, M.; Elliott, S. D.; Barry, S. T., *Chem. Mater.* **2013,** *25* (7), 1132-1138.

203.    von Arx, T.; Szentkuti, A.; Zehnder, T. N.; Blacque, O.; Venkatesan, K., *J. Mater. Chem. C* **2017,** *5* (15), 3765-3769.

204.    Nair, A. G.; McBurney, R. T.; Gatus, M. R. D.; Binding, S. C.; Messerle, B. A., *Inorg. Chem.* **2017,** *56* (19), 12067-12075.

205.    Fung, S. K.; Zou, T.; Cao, B.; Lee, P.-Y.; Fung, Y. M. E.; Hu, D.; Lok, C.-N.; Che, C.-M., *Angew. Chem. Int.* **2017,** *56* (14), 3892-3896.

206.    Tong, K.-C.; Hu, D.; Wan, P.-K.; Lok, C.-N.; Che, C.-M., *Front. Chem.* **2020,** *8* (919), 587207.

207.    Orbisaglia, S.; Jacques, B.; Braunstein, P.; Hueber, D.; Pale, P.; Blanc, A.; de Frémont, P., *Organometallics* **2013,** *32* (15), 4153-4164.

208.    Gaillard, S.; Slawin, A. M. Z.; Bonura, A. T.; Stevens, E. D.; Nolan, S. P., *Organometallics* **2010,** *29* (2), 394-402.

209.    Baron, M.; Tubaro, C.; Basato, M.; Biffis, A.; Natile, M. M.; Graiff, C., *Organometallics* **2011,** *30* (17), 4607-4615.

210.    Hirtenlehner, C.; Krims, C.; Hölbling, J.; List, M.; Zabel, M.; Fleck, M.; Berger, R. J. F.; Schoefberger, W.; Monkowius, U., *Dalton Trans.* **2011,** *40* (38), 9899-9910.

211.    Kriechbaum, M.; Otte, D.; List, M.; Monkowius, U., *Dalton Trans.* **2014,** *43* (23), 8781-8791.

212.    Baron, M.; Dalla Tiezza, M.; Carlotto, A.; Tubaro, C.; Graiff, C.; Orian, L., *J. Organomet. Chem.* **2018,** *866*, 144-152.

213.    Nandy, A.; Samanta, T.; Mallick, S.; Mitra, P.; Seth, S. K.; Saha, K. D.; Al-Deyab, S. S.; Dinda, J., *New J. Chem.* **2016,** *40* (7), 6289-6298.

214.    Samanta, T.; Munda, R. N.; Roymahapatra, G.; Nandy, A.; Saha, K. D.; Al-Deyab, S. S.; Dinda, J., *J. Organomet. Chem.* **2015,** *791*, 183-191.

215.    Wang, H. M. J.; Chen, C. Y. L.; Lin, I. J. B., *Organometallics* **1999,** *18*, 1216-1223.

216.    Levchenko, V.; Glessi, C.; Øien-Ødegaard, S.; Tilset, M., *Dalton Trans.* **2020,** *49* (11), 3473-3479.

217.    de Frémont, P.; Singh, R.; Stevens, E. D.; Petersen, J. L.; Nolan, S. P., *Organometallics* **2007,** *26* (6), 1376-1385.

218.    Guo, S.; Bernhammer, J. C.; Huynh, H. V., *Dalton Trans.* **2015,** *44* (34), 15157-15165.

219.    Baker, M. V.; Barnard, P. J.; Brayshaw, S. K.; Hickey, J. L.; Skelton, B. W.; White, A. H., *Dalton Trans.* **2005,** (1), 37-43.

220.    Herrmann, W. A.; Runte, O.; Artus, G., *J. Organomet. Chem.* **1995,** *501* (1), C1-C4.

221.    Solovyev, A.; Ueng, S.-H.; Monot, J.; Fensterbank, L.; Malacria, M.; Lacôte, E.; Curran, D. P., *Org. Lett.* **2010,** *12* (13), 2998-3001.
222.    Elnajjar, F. O.; Binder, J. F.; Kosnik, S. C.; Macdonald, C. L. B., *Z. Anorg. Allg. Chem.* **2016,** *642* (22), 1251-1258.
223.    Aidouni, A.; Bendahou, S.; Demonceau, A.; Delaude, L., *J. Comb. Chem.* **2008,** *10* (6), 886-892.
224.    Blaya, M.; Bautista, D.; Gil-Rubio, J.; Vicente, J., *Organometallics* **2014,** *33* (22), 6358-6368.
225.    Pérez-Bitrián, A.; Martínez-Salvador, S.; Baya, M.; Casas, J. M.; Martín, A.; Menjón, B.; Orduna, J., *Chem. Eur. J.* **2017,** *23* (28), 6919-6929.
226.    Goetzfried, S. K.; Gallati, C. M.; Cziferszky, M.; Talmazan, R. A.; Wurst, K.; Liedl, K. R.; Podewitz, M.; Gust, R., *Inorg. Chem.* **2020,** *59* (20), 15312-15323.
227.    Tamuliene, J.; Noll, J.; Frenzel, P.; Rüffer, T.; Jakob, A.; Walfort, B.; Lang, H., *Beilstein J. Nanotechnol.* **2017,** *8*, 2615-2624.
228.    Jurczyk, J.; Glessi, C.; Madajska, K.; Berger, L.; Nyrud, J. I. K.; Szymańska, I.; Kapusta, C.; Tilset, M.; Utke, I., *J. Therm. Anal. Calorim.* **2021**.
229.    Kunte, G. V.; Shivashankar, S. A.; Umarji, A. M., *Meas. Sci. Technol.* **2008,** *19* (2), 025704.
230.    Mishra, S.; Daniele, S., *Chem. Rev.* **2015,** *115* (16), 8379-8448.
231.    Hyre, A. S.; Doerrer, L. H., *Coord. Chem. Rev.* **2020,** *404*, 213098.
232.    Gordon, D. C.; Kirss, R. U.; Brown, D. W., *Organometallics* **1992,** *11* (8), 2947-2949.
233.    Fahlman, B. D.; Barron, A. R., *Adv. Mater. Opt. Electron,* **2000,** *10* (3-5), 223-232.
234.    Schmidbaur, H.; Schier, A., *Chem. Soc. Rev.* **2012,** *41* (1), 370-412.
235.    Pinter, B.; Broeckaert, L.; Turek, J.; Růžička, A.; De Proft, F., *Chem. Eur. J.* **2014,** *20* (3), 734-744.
236.    Turek, J.; Panov, I.; Švec, P.; Růžičková, Z.; Růžička, A., *Dalton Trans.* **2014,** *43* (41), 15465-15474.
237.    Gabrielli, W. F.; Nogai, S. D.; McKenzie, J. M.; Cronje, S.; Raubenheimer, H. G., *New J. Chem.* **2009,** *33* (11), 2208-2218.
238.    Schuh, E.; Pflüger, C.; Citta, A.; Folda, A.; Rigobello, M. P.; Bindoli, A.; Casini, A.; Mohr, F., *J. Med. Chem.* **2012,** *55* (11), 5518-5528.
239.    Muñiz, J.; Wang, C.; Pyykkö, P., *Chem. Eur. J.* **2011,** *17* (1), 368-377.
240.    de Kock, S.; Dillen, J.; Esterhuysen, C., *ChemistryOpen* **2019,** *8* (4), 539-550.
241.    Jakob, A.; Schmidt, H.; Djiele, P.; Shen, Y.; Lang, H., *Microchim. Acta* **2006,** *156* (1), 77-81.
242.    Du, L.; Chu, W.; Miao, H.; Xu, C.; Ding, Y., *RSC Adv.* **2015,** *5* (88), 71637-71643.
243.    Huang, B.; Hu, M.; Toste, F. D., *Trends Chem.* **2020,** *2* (8), 707-720.
244.    Bratsch, S. G., *J. Phys. Chem. Ref. Data* **1989,** *18* (1), 1-21.
245.    Ball, L. T.; Lloyd-Jones, G. C.; Russell, C. A., *J. Am. Chem. Soc.* **2014,** *136* (1), 254-264.
246.    Zheng, Z.; Wang, Z.; Wang, Y.; Zhang, L., *Chem. Soc. Rev.* **2016,** *45* (16), 4448-4458.
247.    Miró, J.; del Pozo, C., *Chem. Rev.* **2016,** *116* (19), 11924-11966.
248.    Ye, X.; Zhao, P.; Zhang, S.; Zhang, Y.; Wang, Q.; Shan, C.; Wojtas, L.; Guo, H.; Chen, H.; Shi, X., *Angew. Chem. Int.* **2019,** *58* (48), 17226-17230.
249.    Huynh, H. V.; Guo, S.; Wu, W., *Organometallics* **2013,** *32* (16), 4591-4600.
250.    Aranzaes, J. R.; Daniel, M.-C.; Astruc, D., *Can. J. Chem.* **2006,** *84* (2), 288-299.
251.    Henderson, M. A.; Ramsier, R. D.; J. T. Yates, J., *J. Vac. Sci. Technol. A* **1991,** *9* (5), 2785-2787.
252.    Koops, H.; Weber, M.; Schossler, C.; Kaja, A., Three-dimensional additive electron beam lithography. In *Metal/Nonmetal Microsystems: Physics, Technology, and Applications,* SPIE: **1996**; Vol. 2780.
253.    Jeevanandam, G.; van der Meijden, V.; Birnie, L. D.; Kruit, P.; Hagen, C. W., *Microelectron. Eng.* **2020,** *224*, 111239.
254.    Sievers, R. E.; Sadlowski, J. E., *Science* **1978,** *201* (4352), 217-223.
255.    Lewis, B. B.; Stanford, M. G.; Fowlkes, J. D.; Lester, K.; Plank, H.; Rack, P. D., *Beilstein J. Nanotechnol.* **2015,** *6*, 907-918.
256.    Wentrup, C., *Angew. Chem. Int.* **2019,** *58* (42), 14800-14808.

257. Moore, W. C., *J. Am. Chem. Soc.* **1911,** *33* (7), 1091-1099.

258. Yang, G.; Raptis, R. G., *Inorganica Chim. Acta* **2003,** *352*, 98-104.

259. Yang, G.; Raptis, R. G., *Dalton Trans.* **2002,** (21), 3936-3938.

260. Bandini, A. L.; Banditeli, G.; Bonati, F.; Minghetti, G.; Pinillos, M. T., *Inorganica Chim. Acta* **1985,** *99* (2), 165-168.

261. Raptis, R. G.; Fackler, J. P., *Inorg. Chem.* **1990,** *29* (24), 5003-5006.

262. Vanicek, S.; Beerhues, J.; Bens, T.; Levchenko, V.; Wurst, K.; Bildstein, B.; Tilset, M.; Sarkar, B., *Organometallics* **2019,** *38*, 4383-4386.

263. Arduengo, A. J.; Krafczyk, R.; Schmutzler, R.; Craig, H. A.; Goerlich, J. R.; Marshall, W. J.; Unverzagt, M., *Tetrahedron* **1999,** *55* (51), 14523-14534.

264. Arduengo, A. J., III; Davidson, F.; Dias, H. V. R.; Goerlich, J. R.; Khasnis, D.; Marshall, W. J.; Prakasha, T. K., *J. Am. Chem. Soc.* **1997,** *119*, 12742-12749.

265. Levchenko, V. A.; Nova, A.; Øien-Ødegaard, S.; Balcells, D.; Tilset, M., *Eur. J. Inorg. Chem.* **2020,** *2020* (34), 3249-3258.

# Appendix

Paper I


Paper II


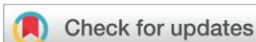Paper III


Paper IV


Supporting information of Paper IV

# Paper I

**Organometallic Chemistry in Aqua Regia: Metal and Ligand Based Oxidation of (NHC)AuCl complexes**

Volodymyr Levchenko, Cristiano Glessi, Sigurd Øien-Ødegaard, and Mats Tilset

# Dalton Transactions

## PAPER

Check for updates

# Organometallic chemistry in *aqua regia*: metal and ligand based oxidations of (NHC)AuCl complexes†‡

Volodymyr Levchenko, [iD] Cristiano Glessi, [iD] Sigurd Øien-Ødegaard [iD] and Mats Tilset [iD] *

The synthesis and characterization of a series of N-heterocyclic carbene (NHC) complexes of Au(III), (NHC)AuCl$_3$, is described. High yields are obtained when the corresponding Au(I) species (NHC)AuCl are oxidized with inexpensive *aqua regia*. The oxidation is in some cases accompanied by substitution and/or anti addition of Cl$_2$ across the backbone C=C bond of unsaturated NHC ligands.

## Introduction

Metallic gold has historically been regarded as one of the most inert of metals, arising from its low reactivity and high resistance to oxidation. The classic dissolution of metallic gold in *aqua regia*,[1] the 1 : 3 mixture of nitric acid and hydrochloric acid, remains important for chemists as the first step in the syntheses of gold complexes from the element. Its capacity to oxidize Au(0) to Au(III) is key to the successful use of aqua in this process (eqn (1)).[2]

$$Au + 4HCl + HNO_3 \rightarrow [AuCl_4]^- + NO + H_3O^+ + H_2O \quad (1)$$
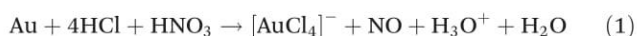
In recent years, gold chemistry has gained a prominent position in the field of catalysis. In homogeneous catalysis, the carbophilic character of Au(I) and Au(III) alike allows the coordination of carbon–carbon π bonds with concomitant bond activation. This facilitates further reactions, including C–C and C-heteroatom bond forming reactions that are employed in the synthesis of complex organic molecules. Au(I) compounds, two-coordinate with linear geometry at Au, have dominated this chemistry. Complexes of the type L–Au–X are frequently used, with a plethora of σ-donating L ligands available, for example phosphines[3] and N-heterocyclic carbenes (NHC's).[4–7] This last class of organogold complexes, frequently in the form (NHC)AuCl, has proven to be an important precursor for the catalytically active (NHC)Au$^+$ species with a weakly

coordinating counteranion. They have found applications in a large range of reactions, in particular involving creating and functionalizing C–C π bonds (alkenes, alkynes, arenes).[4,7–9] Various Au(NHC) complexes have found uses in other applications, such as anticancer drugs[10] and as photosensitizers.[11]

Recently, Au(III) chemistry has gained more attention, and robust synthetic methods to furnish such species are established. Preparative pathways include the decoration of Au(III) salts with appropriate ligands on one side, and oxidation of Au(I) precursors on the other. The oxidation of linear (NHC)Au(I) complexes to square planar (NHC)Au(III) congeners is usually carried out with a halide-containing oxidizing agent such as halogens[12–15] (Cl$_2$, Br$_2$ and I$_2$), CsBr$_3$,[16] N-halosuccinimides,[17] (Me$_2$S)AuCl,[18] and PhICl$_2$.[12,19] The latter as well as gaseous Cl$_2$ are the most commonly used oxidizers for synthesis of (NHC) AuCl$_3$ complexes and usually lead to the formation of the desired products in high yields and purity (Scheme 1). Occasionally, the presence of side products or the difficult handling of these compounds represent a practical challenge, along with safety and environmental issues. Admittedly, *aqua regia* also raises such issues – and eventually the choice of oxidant (however unpleasant) will be made on the basis of a number of factors including selectivity, ease of use, costs, environmental issues, and more. In all circumstances, chemists need a well-equipped toolbox of synthesis methods.

The use of *aqua regia* as a solvent for preparative organometallic chemistry is very limited. It has been previously[20–23]

*Department of Chemistry and Center for Materials Science and Nanotechnology (SMN), Faculty of Mathematics and Natural Sciences, University of Oslo, P.O. Box 1126 Blindern, NO-0318 Oslo, Norway. E-mail: mats.tilset@kjemi.uio.no; Tel: +47-22855502*

†Dedicated to Professor Robin Perutz's on the occasion of his 70th birthday.
‡Electronic supplementary information (ESI) available: Experimental details, NMR spectra and other characterization data. Crystallographic data for **1j**, **2i–k**, **3b**, **4b**. CCDC 1960925–1960930. For ESI and crystallographic data in CIF or other electronic format see DOI: 10.1039/c9dt04472h
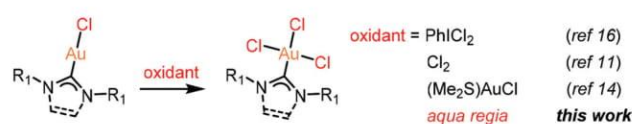


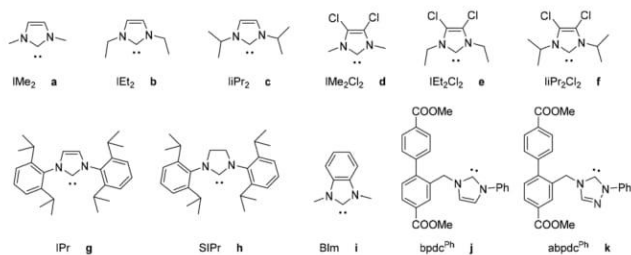**Scheme 1** Synthesis of Au(NHC)Cl$_3$: reported methods and this work.

**Fig. 1** NHC ligands used in this work and their abbreviations.

**Table 1** Reactions of (NHC)AuCl (**1a–k**) to form (NHC)AuCl$_3$ (**2a–c**, **2g–k** and **3a–c**) in aqua regia

| Entry | NHC | (NHC)AuCl | (NHC)AuCl$_3$ | Time, h | Yield, % |
|---|---|---|---|---|---|
| 1 | IMe | **1a** | **2a** | 24 | 7[a] |
| 2 | IEt | **1b** | **2b** | 24 | —[a] |
| 3 | IiPr | **1c** | **2c** | 24 | 82[a] |
| 4 | IMe$_2$Cl$_2$ | **1d** | **3a** | 3 | 77 |
| 5 | IEt$_2$Cl$_2$ | **1e** | **3b** | 3 | 75 |
| 6 | IiPr$_2$Cl$_2$ | **1f** | **3c** | 5 | 84 |
| 7 | IPr | **1g** | **2g** | 5 | 72 |
| 8 | SIPr | **1h** | **2h** | 20 | 45 |
| 9 | BIm | **1i** | **2i** | 7 | 85 |
| 10 | bpdc$^{Ph}$ | **1j** | **2j** | 6 | 63 |
| 11 | abpdc$^{Ph}$ | (**1k**)[b] | **2k** | 3 | 75[b] |

[a] Reaction resulted in a mixture of NHC-backbone-chlorinated products, see text. The numbers given here are % of mixture by NMR, not actual yields. [b] Yield based on two steps from the imidazolium salt, without intermittent isolation of **1k**.
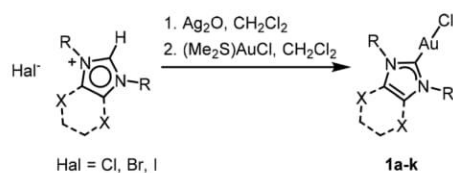
reported that Au(I) complexes with substituted pyrazolato (pz) ligands may be oxidized by *aqua regia* to Au(III) species without loss of the pz ligands, with or without concomitant chlorination of the pz ring. Except for our very recent report[24] that a rather electron poor dicobaltoceniumyltriazolylidene Au(I) complex can be favourably oxidized to Au(III) in *aqua regia* when other oxidants fail, there appears to be no other descriptions of the reactivity of Au complexes with gold–carbon bonds in this reaction medium. In this contribution, we describe the use of *aqua regia* as an oxidation agent for the oxidation of (NHC)AuCl complexes with more conventional NHC ligands to (NHC)AuCl$_3$ analogs. The range of NHC ligands explored is shown in Fig. 1. The reactions, which in most cases are high-yielding and involve simple work-up procedures, represent a surprising and attractive alternative to existing synthetic methods.

## Results and discussion

### Summary of main reactions

The (NHC)AuCl complexes **1a–k** were obtained according to modifications of the published procedures (see ESI‡ for details).[25–28] The appropriate imidazolium salts were used as NHC-ligand precursors and were treated with Ag$_2$O to generate (NHC)Ag(I) species which were transmetalated *in situ* with (Me$_2$S)AuCl to furnish the (NHC)AuCl complexes (Scheme 2). The procedure of Nolan[28] usually works well, but in cases where the NHC precursors are imidazolium bromide or iodide salts, the (NHC)AuBr or (NHC)AuI complexes would be formed. For this reason we favoured the Ag$_2$O method, which leads to the desired (NHC)AuCl complex as the only or major product.

The *aqua regia* (reaction medium as well as oxidant for the reactions) was made by mixing 1 : 3 (v/v) concentrated solutions of nitric (65%) and hydrochloric (37%) acids. The (NHC)

AuCl complexes were suspended in freshly prepared *aqua regia* (8 mL), stirred for a stated period at ambient temperature, filtered, and washed with water. In most cases (except **1a–c**), this procedure yielded the corresponding (NHC)AuCl$_3$ complexes as pure, yellow products in good to high yields. It is noteworthy that the rather harsh reaction conditions do not lead to cleavage of the Au–C(NHC) bonds. The details are given in Table 1. Any further optimizations or modifications for each case are described in ESI‡ for each substrate separately.

In order to aid product identifications, additional reactions with PhICl$_2$ were performed to furnish authentic samples of the respective (NHC)AuCl$_3$ species.[12] Their $^1$H NMR spectra were used to confirm the identity of materials obtained following the *aqua regia* protocol. The $^1$H NMR spectra of previously reported (NHC)AuCl$_3$ species **2d**,[29] **2g**,[12] and **2h**[12] were compared with literature data.

In general, we find that the most diagnostic indication of successful oxidation of (NHC)Au(I) to (NHC)Au(III) is a change of the chemical shift of the C(carbene) signal in the $^{13}$C NMR (CD$_2$Cl$_2$) spectra from the range $\delta$ 168.9–196.4 to 139.0–172.8. The average upfield change was 28.8 ppm.

### The complex oxidations of the simple (NHC)Au(I) complexes 1a–c

The compounds **1a–c** bear simple NHC ligands with an unsubstituted backbone and small aliphatic substituents (Me, Et, iPr) at the N atoms. It appears that oxidation of **1a** and **1b** complexes with the use of the chlorinating agents mentioned in the introduction have not yet been reported, and that the corresponding Au(III) trichloro derivatives remain completely undescribed so far. The oxidation of **1c** with PhICl$_2$ produces the corresponding Au(III) derivative **2c** in high yields (Scheme 3, top). We find that treatment of **1a** and **1b** with a slight excess of PhICl$_2$ also proceeds smoothly by selective oxidation at Au to furnish the respective (NHC)AuCl$_3$ complexes **2a** and **2b** in 65 and 56% unoptimized yields, respectively



**Scheme 2** Synthesis of (NHC)AuCl complexes **1a–k**.
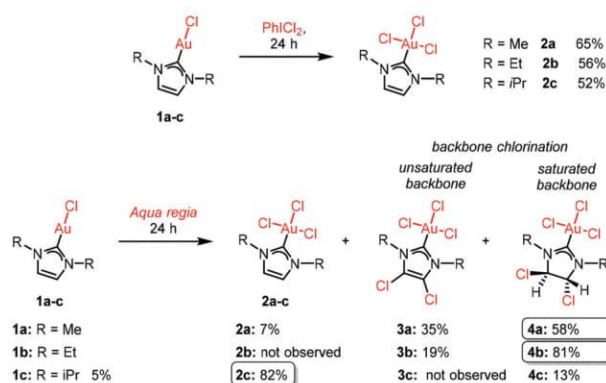
**Scheme 3** Oxidations of **1a**, **1b**, and **1c** with PhICl₂ (top) and *aqua regia* (bottom). Product distributions are given, based on ¹H NMR spectra of the crude reaction mixtures.

(Scheme 3, top). These products were characterized by ¹H NMR and HRMS.

On the other side, the reactions of **1a–c** in *aqua regia* proceeded to give mixtures of up to three (NHC)Au(III) species (Scheme 3, bottom). The products were isolated as mixtures which were not subjected to separation attempts. In all cases, NHC backbone-functionalized species – in which two Cl atoms had substituted the backbone H atoms or added to the backbone C=C bond – had formed at the expense of the simple Au-centered oxidation products **2a–c** although Au(I) to Au(III) oxidation had occurred in all cases. Thus, whereas **1a** furnished a low yield of **2a**, the two backbone-chlorinated species **3a** and **4a** dominated the reaction. Starting from **1b**, none was seen of the simple oxidation product **2b**; the addition product **4b** was the dominant species with substitution product **3b** as side product. For **1c**, the simple Au-centred oxidation product **2c** dominated whereas the addition to the backbone gave the minor product **4c**.

The oxidation products were identified by analysis of 1D and 2D ¹H and ¹³C NMR spectra, high resolution mass spectrometry, and elemental analysis (see ESI‡ for full details). Whereas the species **2a–c** were readily recognized through their =C–H signals (δ *ca.* 7.2) in addition to the matching N–R alkyl signals in the ¹H NMR spectra, **3a–b** exhibited only the N–R signals, whereas **4a–c** each displayed one additional >C(Cl)–H singlet arising from the backbone (δ *ca.* 5.8). Separate signals were seen for the diastereotopic NC*H*₂CH₃ protons in **2b** (*ca.* 1 ppm separated) and NCH*Me*₂ methyls in **2c** (*ca.* 0.1 ppm separated). The *trans* disposition of the two Cl atoms at the NHC backbone cannot be ascertained from the NMR data alone for **4a–c**, but was unambiguously established by a single-crystal X-ray structure determination for **4b** (*vide infra*). A ¹H-NOESY experiment was conducted on the mixture of compounds arising from **1b** and revealed a set of cross-peaks between the two diastereotopic methylene protons and the backbone protons for **4b**, confirming the backbone saturation (see ESI‡ for details). The *trans* geometry at the backbone of **4b** (and, by inference, **4a** and **4c**) strongly suggests that the

addition has involved an electrophilic chlorine reagent, by analogy with the commonly observed *anti* addition seen in addition of Cl₂ to alkenes. The electrophilic chlorine must arise from the chloride ions in the *aqua regia* medium.

The formation of the backbone-substituted products **3a** and **3b** is reminiscent of previous reports of Cl for H substitution reactions in free carbene NHC systems, as reported by the Arduengo[30,31] group. Nolan and coworkers[12] reported on the undesired chlorination of the backbone-bonded methyl groups of the NHC ligand IPr^Me during the chlorination of the corresponding Au(I) complex (IPr^Me)AuCl using Cl₂ as the chlorinating agent. We are unaware of previous cases where such chlorinations occur at the NHC backbone of metal-coordinated NHC complexes. Furthermore, to further investigate the backbone chlorination, the *aqua regia* oxidation procedure was performed on the uncoordinated ligand IEt (of **1b**) in the form of its imidazolium bromide salt. No such reactivity was observed for the salt, although minor quantities of a series of unidentified species were seen: in order to obtain backbone chlorination of the NHC ring, coordination at Au is required. Further mechanistic details are not known; however we note that Au could have an influence on the backbone reactivity either indirectly (Au as a substituent on the ring; the reaction works only on the Au complex) or directly, through a gold-catalysed halogenation.

When the mixture of **3b** and **4b** was dissolved in CH₂Cl₂ followed by slow diffusion of pentane vapours into the solution, the two complexes crystallized nicely in separate crystals which could be hand-picked and subjected to independent structure determinations by X-ray diffraction analysis. ORTEP views of the molecular structures of **3b** and **4b** are shown in Fig. 2. The diffraction analysis of **4b** confirms that the two Cl atoms have been added to the backbone C=C bond in the NHC ligand in **2b** in an *anti* fashion. The Au–C(carbene) bond distances of 2.004(3) (**3b**) and 1.993(3) (**4b**) Å are typical for (NHC)Au(III)
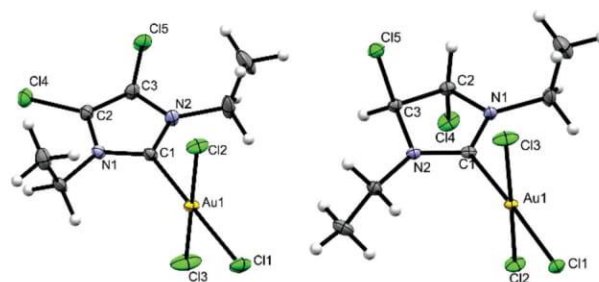


**Fig. 2** ORTEP views of the solid-state molecular structures of **3b** (left) and **4b** (right) with 50% probability elipsoids. Crystals were grown from the isolated mixture of **3b** and **4b** obtained in the reaction of **1b** in *aqua regia* for 24 h. Selected bond distances (Å) and angles (°): **3b**: C1–Au1 2.004(3), Au1–Cl1 2.304(1), Au1–Cl2 2.273(1), Au–Cl3 2.271(1), C2–C3 1.349(6), C2–Cl4 1.692(4), C3–Cl5 1.691(4), C1–Au–Cl1 178.4(1), C1–Au–Cl2 86.9(1), C1–Au–Cl3 90.7(1), Cl4–C2–C3 128.4(3), Cl5–C3–C2 129.3(3). For **4b**: C1–Au1 1.993(3), Au1–Cl1 2.3192(8), Au1–Cl3 2.2744(9), Au1–Cl2 2.2782(9), C2–C3 1.517(4), C3–Cl5 1.805(3), C2–Cl4 1.809(3), C1–Au–Cl1 177.14(9), C1–Au–Cl3 87.57(9), C1–Au–Cl2 87.63(9), Cl5–C3–C2 109.0(2), Cl4–C2–C3 109.4(2).

complexes, which spans the range 1.975–2.024 Å.[12,13,32] The square planar geometry at Au(III) as well as the perpendicular orientation of the NHC ligand with respect coordination plane of Au(III) are as expected. The Cl–C–C angles (128.4° and 129.3°) at the backbone in **3b** deviate slightly from the ideal 120° angle of C(sp[2]). The structure of **4b** has a saturated backbone with Cl–C–C angles of 109.0° and 109.4°.

### The simple oxidation of the backbone-substituted (NHC)Au(I) complexes 1d–f

In order to better understand the nature of the various chlorination reactions of **1a–c**, we performed similar reactions starting with the already chlorinated **1d–f**. In all these cases, no reaction was seen at the backbone and only the products arising from selective oxidation of Au(I) to Au(III), *i.e.* **3a–c**, are obtained (Scheme 4). The *aqua regia* treatment of these compounds was relatively rapid, and extended reaction times led to gradual decomposition. Table 1 lists the optimum reaction times and yields.

### The simple oxidation of the larger (NHC)Au(I) complexes 1g–k

The applicability of the *aqua regia* oxidation protocol was next extended with attempts at synthesizing (NHC)AuCl$_3$ complexes that feature an unsubstituted backbone and bulky aromatic groups on the NHC nitrogens. Specifically, the IPr and SIPr carbenes (starting from **1g** and **1h**) were included, since these are among the most frequently used NHC ligands in Au(I) catalysis.[33] The oxidation of **1g–h** in *aqua regia* led to the smooth formation of the targeted Au(III) compounds **2g–h** in 72 and 45% yields, respectively, without any observable functionalization at the backbone (Table 1 lists the optimum reaction times and yields).

For **1h**, the evolution of the reaction over time was monitored in *aqua regia*. This revealed that the oxidation occurred rapidly during first 3 h, with less than 10% of starting material left at that time. However, the consumption of the rest of the starting material was considerably slower and eventually *ca.* 20 h were needed to effect the complete consumption of **1h** (see ESI‡).

The *aqua regia* reaction protocol was also applied to the benzimidazole-based (NHC)AuCl complex **1i** and again, the reaction proceeded cleanly to furnish the desired Au(III) complex **2i** in 85% yield. This indicates that the scope of the protocol might include a broad range of (NHC)AuCl complexes, as long as reaction times are appropriately adjusted.
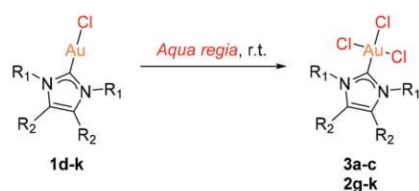
Finally, the developed protocol was applied towards synthesis of (NHC)Au(III) systems with dicarboxylate functionalities that might allow them, after ester deprotection, to be incorporated into UiO-67[34] type metal–organic frameworks (MOFs). Although linkers with pendant imidazolium functionalities for incorporation into MOFs are well known,[35] their functionalization with Au(I) or Au(III) appears to be still unexplored. The imidazolium salt **bpdc-PI** (Scheme 5) was synthesized according to modified literature procedures,[35–37] followed by metalation with Ag$_2$O and transmetalation to (Me$_2$S)AuCl to furnish the (NHC)AuCl complex **1j**. Oxidation in *aqua regia* furnished **2j** in 63% yield based on the imidazolium salt (Scheme 5). Importantly, no backbone functionalization nor degradation of the molecule, including the ester groups, occurred.

The same synthetic protocol was also applied to the preparation of the new triazolium-based NHC system in **2k**, synthesized in a fashion similar to **2j** (full synthesis of **bpdc-PT** is provided in ESI‡). Also in this case high yields were obtained with no backbone side reactivity (Scheme 5).

Crystallographically determined molecular structures of **1j** and **2i–k** are depicted in Fig. 3 and selected bond lengths and angles are provided in Table 2. The X-ray-quality crystals were grown by slow diffusion of pentane vapors into dichloromethane (**2i**), chloroform (**2j**), and acetone (**2k**) solutions. Full crystallographic data are given in the ESI.‡

In Au(I) complex **1j**, the Au–C(carbene) bond distance is 1.986(3) Å, quite typical of (NHC)AuCl complexes (1.958(7)–2.036(2) Å, based on a few reports[38–40]). The Au–Cl distance is 2.3366(8) Å, and the Cl–Au–C(carbene) angle is 178.91(7)°, essentially linear as expected for a d[10] Au(I) complex. In the Au(III) complexes, the Au–C(carbene) bond distances also fall in the range of previously reported ones,[41] with values of 2.008(3) Å in **2i**, 2.003(3) Å in **2j**, and 2.003(4) and 2.009(4) Å for the two independent molecules in **2k**. Furthermore, in the Au(III) species the Au–Cl bond distances *trans* to C(carbene) were in the range 2.310(1) Å (**2k**) to 2.321(1) Å (**2i**), which agrees with typical distances in the range 2.298–2.325 Å seen in similar



**Scheme 4** Selective oxidations of **1d−k** in *aqua regia*.
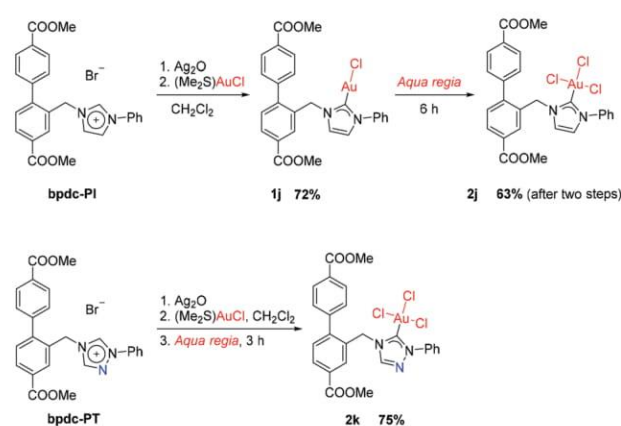


**Scheme 5** Synthesis of **2j** and **2k**, potentially amenable to MOF incorporation.

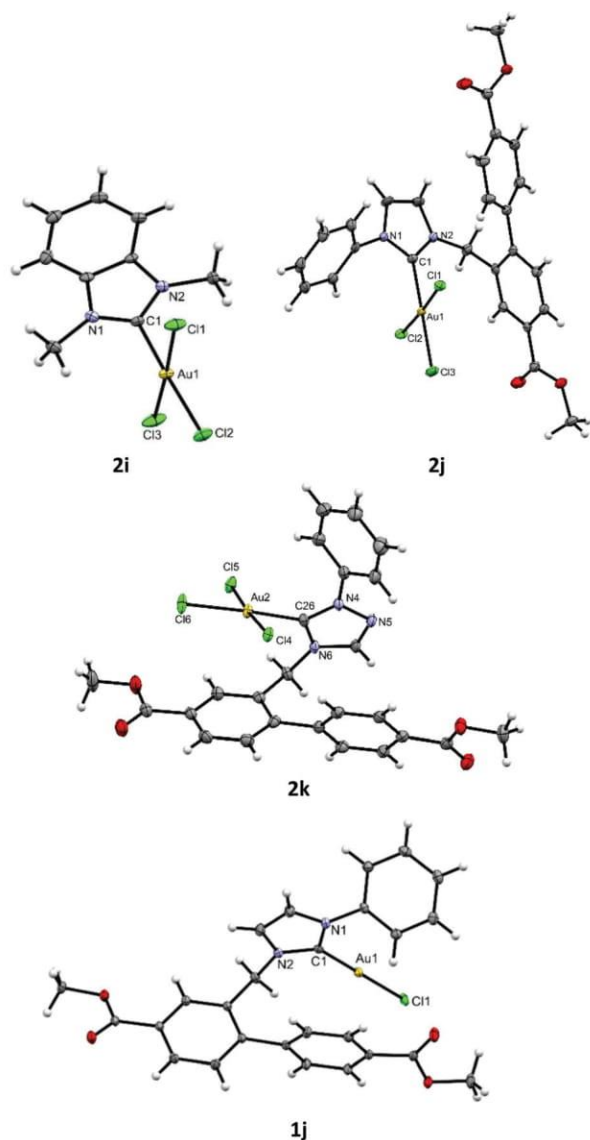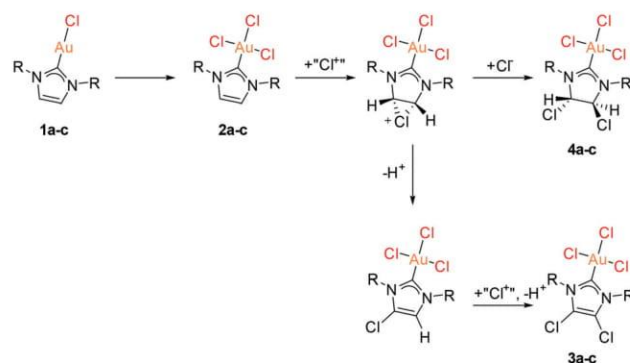**2i**                              **2j**



**2k**



**1j**

**Fig. 3** ORTEP views of the molecular structures of **1j** and **2i−k** with 50% probability elipsoids. Selected bond distances and angles are given in Table 2. Only one of the crystallographically independent molecules in the unit cell for **2k** is shown. Full crystallographic data are provided in ESI.‡



**Scheme 6** Formation of **3a−c** and **4a−c** through backbone activation.

complexes.[12,41] The high *trans* influence of the NHC ligand elongates the Au–Cl bond *trans* to NHC compared to the Au–Cl bonds *cis* to NHC, ranging from 2.276(2) (**2i**) to 2.303(1) Å (**2k**). The C(carbene)–Au–Cl(*trans*) angles are essentially linear in all complexes, from 176.68° to 178.31°.

## Discussion

The fact that none of the reactions in *aqua regia* leads to complexes that are backbone-functionalized, yet not oxidized to Au(ı) to Au(ııı), leads us to hypothesize that the oxidation of Au(ı) to Au(ııı) is the first step of all reactions (Scheme 6). The reactivity of the C=C bond of the NHC ligands in the resulting **2a−c** then is a secondary process which occurs for **2a−c** only. The lack of backbone-functionalization reactivity of **2d−k** under the reaction conditions employed may be a result of contributions from steric effects, and perhaps of poorer solubility of these species (thence, shorter residence times) in *aqua regia*.

It seems likely that the rapid oxidation to Au(ııı) helps protect the Au(ııı)–C(carbene) bond with respect to protolytic cleavage, when compared to the Au(ı)–C(carbene) bond. Once formed, the Au(ııı) species **2a−c** undergoes reactions with an electrophilic source of chlorine, forming a putative chloronium intermediate which ultimately produces the *trans* addition product **4a−c** after nucleophilic attack by chloride, alternatively the substitution products **3a−c** after proton loss and one more round of approach by electrophilic chlorine (Scheme 6). In an independent experiment, complex **2b** was

**Table 2** Selected bond distances (Å) and angles (°) for complexes **1j** and **2i−k**

|                              | **1j**       | **2i**      | **2j**       | **2k**[a]    |          |
|------------------------------|--------------|-------------|--------------|--------------|----------|
| Au–C(carbene)                | 1.986(3)     | 2.008(3)    | 2.003(3)     | 2.009(4)     | 2.003(4) |
| Au–Cl(*trans*)               | 2.3366(8)    | 2.321(1)    | 2.3144(7)    | 2.314(1)     | 2.310(1) |
| Au–Cl(*cis*)                 | n.a.         | 2.281(2)    | 2.2952(7)    | 2.294(1)     | 2.295(1) |
|                              |              | 2.276(2)    | 2.3004(7)    | 2.303(1)     | 2.302(1) |
| C(carbene)–Au–Cl(*trans*)    | 178.91(7)    | 176.68(8)   | 178.31(8)    | 177.1(1)     | 177.4(1) |
| C(carbene)–Au–Cl(*cis*)      | n.a.         | 86.76(8)    | 90.00(8)     | 88.5(1)      | 88.2(1)  |
|                              |              | 90.19(8)    | 87.12(8)     | 89.3(1)      | 89.2(1)  |

[a] Data for two independent molecules in the unit cell.

subjected to *aqua regia* treatment and indeed, a mixture of **3b** and **4b** (24% : 76%) was formed (see ESI, Fig. S22‡). The reaction medium is an obvious possible source of this electrophilic chlorine, although the involvement of gold chloro species should not be discounted. More detailed mechanistic studies are obviously warranted but severely hampered by the poor solubility of reactants in *aqua regia* as well as intractability of *aqua regia* as an NMR solvent in modern NMR spectrometers.

## Concluding remarks

In summary, a new protocol for oxidation of (NHC)AuCl complexes to (NHC)AuCl$_3$ has been described. The reaction workup involves only filtration and washing with water. The described protocol is practical, easy to perform and suitable for various types of NHC ligand systems. Furthermore, the reaction itself involves only the use of aqueous acid solutions, without involvement of organic solvents. Interestingly, sterically unhindered NHC complexes can undergo backbone functionalization, which consists of either chlorine addition or chlorine substitution at the C=C double bond of the unsaturated NHC heterocycle. With improved control of selectivity and yields, this otherwise complicating and undesired side reaction may also be synthetically useful. The reactivity seen in *aqua regia* offers new possibilities and may serve as inspiration for the use of *aqua regia* as a chlorinating agent in preparative organometallic chemistry.

## Experimental

### General procedure for oxidation in *aqua regia*

To the selected (NHC)AuCl complex, 8 mL of freshly made *aqua regia* were added. The suspension was vigorously stirred in a closed vial at room temperature. Afterwards, the suspension was filtered, washed with two portions of water, and dried under a stream of air.

## Conflicts of interest

There are no conflicts to declare.

## Acknowledgements

## Notes and references

1 C. Wentrup, *Angew. Chem., Int. Ed.*, 2019, **58**, 14800.
2 W. C. Moore, *J. Am. Chem. Soc.*, 1911, **33**, 1091.
3 A. H. Christian, Z. L. Niemeyer, M. S. Sigman and F. D. Toste, *ACS Catal.*, 2017, **7**, 3973.
4 N. Marion and S. P. Nolan, *Chem. Soc. Rev.*, 2008, **37**, 1776.
5 S. P. Nolan, *Acc. Chem. Res.*, 2011, **44**, 91.
6 T. Wurm, A. M. Asiri, A. Stephen and K. Hashmi, *NHC-Au(ı) complexes: synthesis, activation, and application*, Wiley-VCH Verlag GmbH & Co. KGaA, 2014.
7 S. A. Shahzad, M. A. Sajid, Z. A. Khan and D. Canseco-Gonzalez, *Synth. Commun.*, 2017, **47**, 735.
8 K. Arumugam, B. Varghese, J. N. Brantley, S. S. M. Konda, V. M. Lynch and C. W. Bielawski, *Eur. J. Org. Chem.*, 2014, 493.
9 J. T. Sarmiento, S. Suárez-Pantiga, A. Olmos, T. Varea and G. Asensio, *ACS Catal.*, 2017, **7**, 7146.
10 M. Porchia, M. Pellei, M. Marinelli, F. Tisato, F. Del Bello and C. Santini, *Eur. J. Med. Chem.*, 2018, **146**, 709.
11 J.-F. Longevial, A. Langlois, A. Buisson, C. H. Devillers, S. Clément, A. van der Lee, P. D. Harvey and S. Richeter, *Organometallics*, 2016, **35**, 663.
12 S. Gaillard, A. M. Z. Slawin, A. T. Bonura, E. D. Stevens and S. P. Nolan, *Organometallics*, 2010, **29**, 394.
13 M. Baron, C. Tubaro, M. Basato, A. Biffis, M. M. Natile and C. Graiff, *Organometallics*, 2011, **30**, 4607.
14 C. Hirtenlehner, C. Krims, J. Hölbling, M. List, M. Zabel, M. Fleck, R. J. F. Berger, W. Schoefberger and U. Monkowius, *Dalton Trans.*, 2011, **40**, 9899.
15 S. Gaillard, X. Bantreil, A. M. Z. Slawin and S. P. Nolan, *Dalton Trans.*, 2009, 6967.
16 M. Kriechbaum, D. Otte, M. List and U. Monkowius, *Dalton Trans.*, 2014, **43**, 8781.
17 M. Baron, M. Dalla Tiezza, A. Carlotto, C. Tubaro, C. Graiff and L. Orian, *J. Organomet. Chem.*, 2018, **866**, 144.
18 T. Samanta, R. N. Munda, G. Roymahapatra, A. Nandy, K. D. Saha, S. S. Al-Deyab and J. Dinda, *J. Organomet. Chem.*, 2015, **791**, 183.
19 S. Orbisaglia, B. Jacques, P. Braunstein, D. Hueber, P. Pale, A. Blanc and P. de Frémont, *Organometallics*, 2013, **32**, 4153.
20 G. Yang and R. G. Raptis, *J. Chem. Soc., Dalton Trans.*, 2002, 3936.
21 A. L. Bandini, G. Banditeli, F. Bonati, G. Minghetti and M. T. Pinillos, *Inorg. Chim. Acta*, 1985, **99**, 165.
22 R. G. Raptis and J. P. Fackler, *Inorg. Chem.*, 1990, **29**, 5003.
23 G. Yang and R. G. Raptis, *Inorg. Chim. Acta*, 2003, **352**, 98.
24 S. Vanicek, J. Beerhues, T. Bens, V. Levchenko, K. Wurst, B. Bildstein, M. Tilset and B. Sarkar, *Organometallics*, 2019, **38**, 4383.
25 S.-T. Liu, C.-I. Lee, C.-F. Fu, C.-H. Chen, Y.-H. Liu, C. J. Elsevier, S.-M. Peng and J.-T. Chen, *Organometallics*, 2009, **28**, 6957.
26 C. Schmidt, B. Karge, R. Misgeld, A. Prokop, R. Franke, M. Brönstrup and I. Ott, *Chem. – Eur. J.*, 2017, **23**, 1869.

27 H. M. J. Wang, C. Y. L. Chen and I. J. B. Lin, *Organometallics*, 1999, **18**, 1216.

28 A. Collado, A. Gomez-Suarez, A. R. Martin, A. M. Z. Slawin and S. P. Nolan, *Chem. Commun.*, 2013, **49**, 5541.

29 E. Schuh, C. Pflüger, A. Citta, A. Folda, M. P. Rigobello, A. Bindoli, A. Casini and F. Mohr, *J. Med. Chem.*, 2012, **55**, 5518.

30 A. J. Arduengo III, F. Davidson, H. V. R. Dias, J. R. Goerlich, D. Khasnis, W. J. Marshall and T. K. Prakasha, *J. Am. Chem. Soc.*, 1997, **119**, 12742.

31 A. J. Arduengo, R. Krafczyk, R. Schmutzler, H. A. Craig, J. R. Goerlich, W. J. Marshall and M. Unverzagt, *Tetrahedron*, 1999, **55**, 14523.

32 J. Gil-Rubio, V. Cámara, D. Bautista and J. Vicente, *Inorg. Chem.*, 2013, **52**, 4071.

33 N. Marion, R. S. Ramón and S. P. Nolan, *J. Am. Chem. Soc.*, 2009, **131**, 448.

34 J. H. Cavka, S. Jakobsen, U. Olsbye, N. Guillou, C. Lamberti, S. Bordiga and K. P. Lillerud, *J. Am. Chem. Soc.*, 2008, **130**, 13850.

35 W. T. Schumacher, M. J. Mathews, S. A. Larson, C. E. Lemmon, K. A. Campbell, B. T. Crabb, B. J. A. Chicoine, L. G. Beauvais and M. C. Perry, *Polyhedron*, 2016, **114**, 422.

36 L.-G. Ding, B.-J. Yao, W.-L. Jiang, J.-T. Li, Q.-J. Fu, Y.-A. Li, Z.-H. Liu, J.-P. Ma and Y.-B. Dong, *Inorg. Chem.*, 2017, **56**, 2337.

37 Y.-H. Hu, J.-C. Wang, S. Yang, Y.-A. Li and Y.-B. Dong, *Inorg. Chem.*, 2017, **56**, 8341.

38 M. Delgado-Rebollo, C. García-Morales, C. Maya, A. Prieto, A. M. Echavarren and P. J. Pérez, *J. Organomet. Chem.*, 2019, **898**, 120856.

39 M. Kaiser, S. P. Leitner, C. Hirtenlehner, M. List, A. Gerisch and U. Monkowius, *Dalton Trans.*, 2013, **42**, 14749.

40 A. Johnson and M. C. Gimeno, *Chem. Commun.*, 2016, **52**, 9664.

41 M. V. Baker, P. J. Barnard, S. J. Berners-Price, S. K. Brayshaw, J. L. Hickey, B. W. Skelton and A. H. White, *J. Organomet. Chem.*, 2005, **690**, 5625.

# Paper II

**Vacuum vs Ambient Pressure Inert Gas Thermogravimetry: A Study of Silver Carboxylates**

Jakub Jurczyk, Cristiano Glessi, Katarzyna Madajska, Luisa Berger, Jeroen Nyrud, Iwona Szymanska, Czeslaw Kapusta, Mats Tilset, and Ivo Utke

# Vacuum versus ambient pressure inert gas thermogravimetry: a study of silver carboxylates

Jakub Jurczyk[1,2] · Cristiano Glessi[3] · Katarzyna Madajska[4] · Luisa Berger[1] · Jeroen Ingolf Ketele Nyrud[3] · Iwona Szymańska[4] · Czesław Kapusta[2] · Mats Tilset[3] · Ivo Utke[1]

## Abstract

A comparative study of vacuum versus ambient pressure inert gas thermogravimetry was performed on silver carboxylates compounds. Some of the complexes from this group have been previously successfully applied as precursors for both chemical vapour deposition and electron beam-induced deposition. Considerable differences were found between the thermogravimetry methods, which we associate with changes in evaporation dynamics. Vacuum thermogravimetry sublimation onsets consistently occurred at lower temperatures than ambient pressure $N_2$-flow thermogravimetry, where the differences reached up to 120 °C. Furthermore, compound sublimation during $N_2$-TGA was suppressed to such an extent that significant thermal decomposition of the compounds into metal and volatile organic fragments was observed while at vacuum the same complexes sublimed as intact molecules. Moreover, thermal stability of silver complexes was investigated using isothermal thermogravimetry. These findings are interesting for the field of thin film synthesis and nanomanufacturing via chemical vapour deposition, atomic layer deposition and focused electron beam induced deposition. In all three methods, delivery of functional precursor over the substrate is crucial. The presented results prove that vacuum thermogravimetry can be used as fast method of pre-screening for novel, especially low-volatility precursors.

**Graphic abstract**
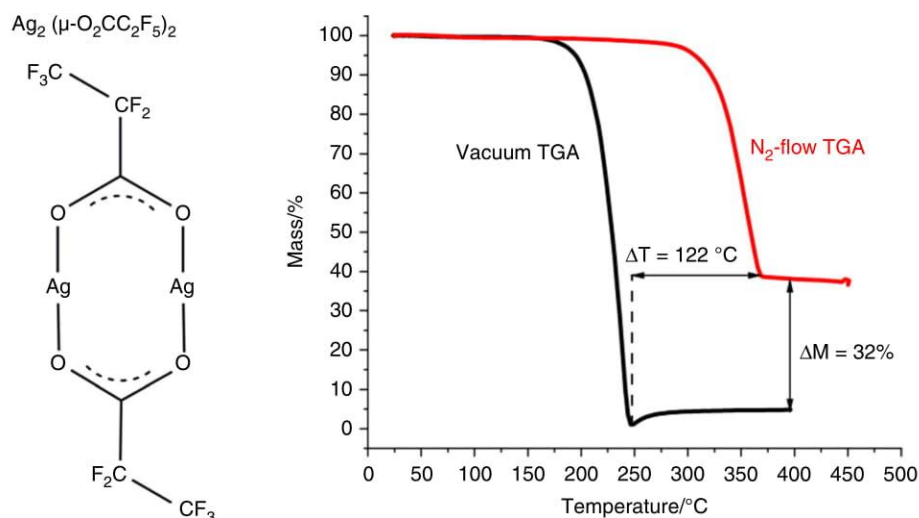
✉ Ivo Utke
    ivo.utke@empa.ch

Extended author information available on the last page of the article

## Introduction

Thermogravimetry (TGA) is an analytical method, which allows to investigate heat-induced mass changes [1]. Depending on the atmosphere, it can be used to study different heat-related phenomena, such as evaporation, drying, sorption of gases [2], thermal decomposition [3, 4] (with formation of volatile species), oxidation [5] and/or oxidative decomposition, as well as certain thermally induced chemical reactions [6, 7]. In some cases, vacuum is used, especially when analysing oxygen-sensitive species [8], e.g. fuels [9]. In-vacuum TGA measurements have also been applied to study early stages of metal oxidation in low-pressure corrosive atmospheres [10].

Depending on the heating strategy, TGA experiments can be divided into two main groups: *dynamic*, where the sample is heated at a constant rate, and *isothermal*, where the temperature is constant. It is also possible to program nonlinear temperature changes, e.g. when the heating rate is controlled by the sample's temperature [1].

TGA is frequently used to examine the thermal stability, decomposition temperature, evaporation process and vapour pressure of potential chemical vapour deposition (CVD) precursors [11–14]. TGA (especially when paired with differential scanning calorimetry) allows to determine both the initiation of evaporation and thermal decomposition temperatures of the measured compound. Additionally, it enables determining if the decomposition occurs in one or multiple steps, which is important from the purity viewpoint of the deposited film, particularly when using metalorganic precursors [12] (so-called MO-CVD).

Besides CVD, metalorganic compounds have found applications as precursors for focused electron beam induced deposition (FEBID), a direct and maskless method of manufacturing structures at the nanometre scale. Gaseous precursor molecules are introduced onto the surface of the substrate through a gas injection system (GIS) inside a scanning electron microscope's (SEM) vacuum chamber. There, the applied focused electron beam locally dissociates the precursor, ideally leaving a pure metal deposit. The detached organic ligands desorb and are pumped out of the chamber [15].

In reality, the purity of the deposit is frequently compromised, mostly due to two unwanted processes, which may occur on the substrate during electron irradiation of adsorbed species, i.e. the co-deposition of ligands and/or incomplete dissociation of precursor molecules. Co-deposition of material from residual hydrocarbon gases is also a process deteriorating deposit purity, but supply of the functional precursor is typically chosen orders of magnitude larger than the residual gases to avoid this. Mentioned processes limit possible applications of produced nanostructures [15–17]. For example, high purity is essential when producing components for plasmonic nanodevices, as usually a metallic character is required [18–20].

To increase the purity, a novel class of a potential FEBID precursor has been proposed: silver carboxylates. Compounds from this family have already been tested as potential CVD precursors [21–23]. Two of them: $[Ag_2(\mu\text{-}O_2CC(Me_2)Et)_2]$ and $[Ag_2(\mu\text{-}O_2CC_2F_5)_2]$ have already been used in FEBID to deposit structures with purity exceeding 70 at%. Despite having been successfully used during deposition, both $[Ag_2(\mu\text{-}O_2CC(Me_2)Et)_2]$ [24] and $[Ag_2(\mu\text{-}O_2CC_2F_5)_2]$ [25, 26] have exhibited low volatility (compared to commercial FEBID compounds) and had to be heated up to 150 °C and 160–180 °C, respectively, to maintain sufficient molecular flux. As the heating occurs within the precursor reservoir, the compound is at risk of thermal decomposition before it reaches the substrate. TGA can be used as a form of pre-screening of potential precursors (same as for CVD) and could allow for determining compound thermal stability and estimating the optimal GIS temperature window prior to deposition. However, looking closer at the TGA results for fluorinated silver carboxylate $[Ag_2(\mu\text{-}O_2CC_2F_5)_2]$, we can see significant discrepancies between the evaporation temperatures given by TGA and the temperatures used in the FEBID process. During FEBID, the compound was sublimed at temperatures approx. 150 °C lower than initial evaporation temperatures derived from TGA [23–25, 27]. Such discrepancies limit the applicability of non-vacuum TGA as a pre-screening method for FEBID.
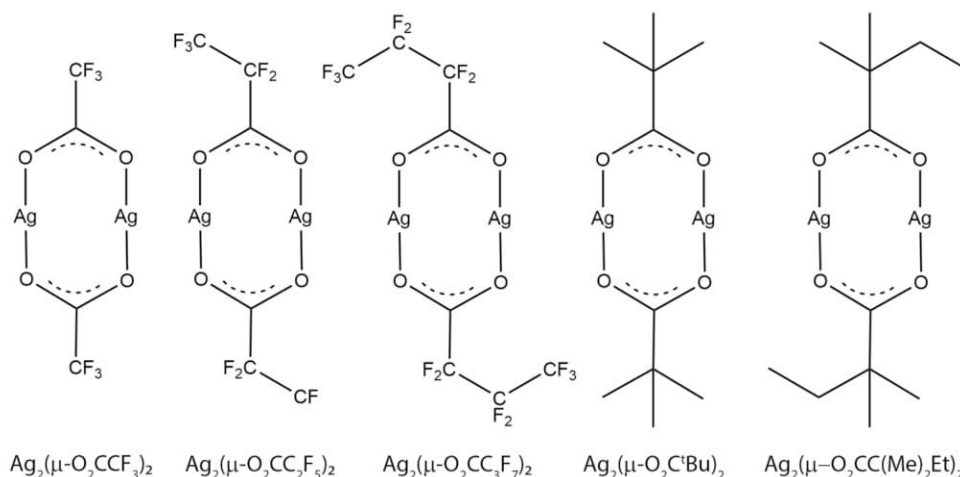
In this work, we propose using in-vacuum thermogravimetry (VTGA) in place of inert gas flow TGA, a method, as aforementioned applied for investigation of fuels, but only rarely used for organometallic compounds [30]. By using low vacuum, mass loss curves were obtained for each investigated compound, where their evaporation temperatures correspond considerably better to the temperatures used during FEBID. Furthermore, the precursors' thermal stability was tested by applying isothermal heating for a few hours, imitating FEBID experimental conditions. The method was tested on several potential silver precursors from the carboxylate family, whose structural formulas are presented in Fig. 1.
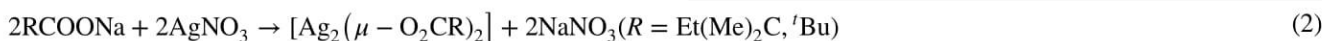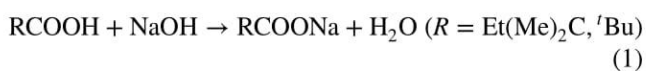
## Experimental

### Precursor synthesis

Silver precursors were synthesised according to previously reported procedures [29, 31]. In the case of non-fluorinated silver carboxylates, an aqueous AgNO₃ solution was added dropwise to the aqueous solution of the sodium salt (obtained by neutralising the acid with a stoichiometric

**Fig. 1** Silver compounds analysed in this work. The dimetric structure was confirmed in gas phase for $[Ag_2(\mu\text{-}O_2C^tBu)_2]$ [28] and was postulated for the other compounds based on gas-phase studies [27, 29]



$Ag_2(\mu\text{-}O_2CCF_3)_2$   $Ag_2(\mu\text{-}O_2CC_2F_5)_2$   $Ag_2(\mu\text{-}O_2CC_3F_7)_2$   $Ag_2(\mu\text{-}O_2C^tBu)_2$   $Ag_2(\mu\text{-}O_2CC(Me)_2Et)_2$

amount of sodium base). A white, amorphous solid was immediately obtained.

$$RCOOH + NaOH \rightarrow RCOONa + H_2O \ (R = Et(Me)_2C, {}^tBu) \tag{1}$$

$$2RCOONa + 2AgNO_3 \rightarrow [Ag_2(\mu - O_2CR)_2] + 2NaNO_3 (R = Et(Me)_2C, {}^tBu) \tag{2}$$

Perfluorinated silver carboxylates were synthesised through the reaction of fluorinated carboxylic acid and silver carbonate in a water–ethanol environment. After solvent evaporation, a white solid formed.

$$Ag_2CO_3 + 2R_FCOOH \rightarrow [Ag_2(\mu - O_2CR_F)_2] + H_2O + CO_2, \tag{3}$$

$$R_F = CF_3, C_2F_5, C_3F_7$$
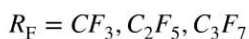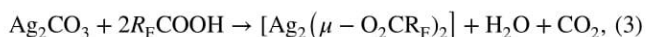
## Thermogravimetry equipment

VTGA experiments were carried out using Netzsch TG209 F1 Libra TGA equipment, connected to Agilent Technologies SH110 dry scroll pump, providing a minimum pressure of $6.6 \times 10^{-2}$ mbar. The precision of the mass readout was 0.0001 mg. The sublimation experiments were performed in $Al_2O_3$ crucibles to avoid crucible/compound sample chemical reactions. The thermal contact between the furnace and crucible is reduced compared to standard TGA, due to the lack of proper atmosphere. Therefore, the temperature was measured and the heating process was controlled using the sample's (crucible's) thermocouple. Proportional, integral, derivative (PID) controller's parameters were optimised to avoid signal oscillations caused by temperature feedback looping. However, the PID parameter settings were not ideal for the end of the main mass loss event and resulted in a small local minimum. This minimum is most probably only

a measurement artefact and has no actual physical meaning. No inert gas flow was applied during process. Each TGA curve was corrected for signal overshooting using an empty crucible measurement curve. The heating rate selected for these tests was 5 K min$^{-1}$. The initial compound sample masses ranged between 9 and 20 mg. Ambient pressure gas flow TGA experiments were performed using Netzsch STA 449 F3 Jupiter, with an applied heating rate of 5 K min$^{-1}$ and a $N_2$ gas flow of 40 mL min$^{-1}$, to avoid reactions between the compound and atmospheric gases. Initial compound sample masses ranged from 15 to 16 mg.

## Results and discussion

VTGA measurements were taken on different silver organometallic complexes: $[Ag_2(\mu\text{-}O_2CC(Me_2)Et)_2]$, $[Ag_2(\mu\text{-}O_2CC_2F_5)_2]$, already successfully applied as FEBID silver precursors, providing high purity deposits [24, 25], and three other fluorinated and non-fluorinated silver carboxylates: $[Ag_2(\mu\text{-}O_2CCF_3)_2]$, $[Ag_2(\mu\text{-}O_2CC_3F_7)_2]$, $[Ag_2(\mu\text{-}O_2{}^tBu)_2]$. The collected results are presented in Fig. 2. We can observe that both non-fluorinated carboxylates decompose partially, leaving non-volatile species within the crucible at $45.0 \pm 2\%$ and $49 \pm 1\%$ of the initial masses of $[Ag_2(\mu\text{-}O_2CC(Me_2)Et)_2]$ and $[Ag_2(\mu\text{-}O_2C^tBu)_2]$, respectively. The measurement error was deduced from the slight mass increase after the local minimum (and main mass loss event) and amounted to 1.0% for $[Ag_2(\mu\text{-}O_2CC(Me_2)Et)_2]$ and 2.0% for $[Ag_2(\mu\text{-}O_2C^tBu)_2]$. The mass reading error of the TGA equipment is negligible as it allows recording of mass changes with precision down to 0.0001 mg, which
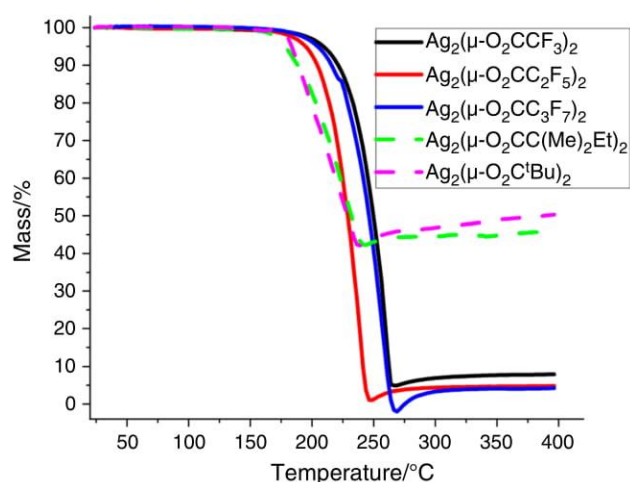
**Fig. 2** Results of VTGA measurements of various silver carboxylates

is five orders of magnitude lower than masses of measured compounds (9–20 mg). The Ag contents in the pristine compounds are 48.4 mass% for $[Ag_2(\mu\text{-}O_2CC(Me_2)Et)_2]$ and 51.7 mass% for $[Ag_2(\mu\text{-}O_2C^tBu)_2]$. The differences to the measured mass residuals are $3.4 \pm 2$ mass% and $1.7 \pm 1$ mass%, respectively, and points to sublimation of a small amount of intact precursor molecules during the temperature ramp. If sublimation occurred in a small temperature window before or simultaneously with thermal decomposition would be the subject of follow-up isothermal TGA measurements. A further observation is that both non-fluorinated silver complexes exhibited initial mass losses at lower temperatures than fluorinated silver carboxylates.

In contrast, all fluorinated compounds left much less residue in the crucibles: approx. 8.0% for $[Ag_2(\mu\text{-}O_2CCF_3)_2]$, 5.0% for $[Ag_2(\mu\text{-}O_2CC_2F_5)_2]$ and 4.0% for $[Ag_2(\mu\text{-}O_2CC_3F_7)_2]$ with estimated errors smaller than $\pm 1\%$ (estimated the same way as above for non-fluorinated silver complexes). These values are considerably lower than the Ag molar mass contents of each complex (48.9%, 39.9% and 33.6%, respectively), proving that silver carriers are present within the gas phase. Silver containing vapour species were also observed previously, using variable temperature infrared spectrometry on the vapours of $[Ag_2(\mu\text{-}O_2CC_2F_5)_2]$ and $[Ag_2(\mu\text{-}O_2CC_3F_7)_2]$ [27]. The results indicate that not only $[Ag_2(\mu\text{-}O_2CC_2F_5)_2]$, but also other fluorinated carboxylates could be potentially used as precursors for the deposition of silver via FEBID. When comparing the mass loss curves of all three fluorinated carboxylates, it can be seen that $[Ag_2(\mu\text{-}O_2CC_2F_5)_2]$ exhibits the lowest sublimation temperature, so higher GIS temperatures will be needed for $[Ag_2(\mu\text{-}O_2CCF_3)_2]$ and $[Ag_2(\mu\text{-}O_2CC_3F_7)_2]$ to achieve comparable molecule fluxes as for $[Ag_2(\mu\text{-}O_2CC_2F_5)_2]$. This VTGA information

is very important in designing the experimental FEBID procedure.

### In-vacuum versus ambient pressure $N_2$ flow TGA for selected silver carboxylates

To investigate the influence of low vacuum on the TGA results, $[Ag_2(\mu\text{-}O_2CC_2F_5)_2]$, $[Ag_2(\mu\text{-}O_2CCF_3)_2]$ and $[Ag_2(\mu\text{-}O_2CC(Me_2)Et)_2]$ were examined using both VTGA and ambient pressure $N_2$-flow TGA. The results are shown in Fig. 3a–c. As outlined in the previous section the error of the mass per cent values reported below are smaller $\pm 1$ mass%.

Firstly, when comparing these methods for $[Ag_2(\mu\text{-}O_2CC_2F_5)_2]$, it is visible that at lower pressure, sublimation begins at lower temperatures. During VTGA, the compound was fully sublimated from 250 °C onwards, whereas under ambient pressure $N_2$ flow TGA, the mass loss stopped at approx. 370 °C. Secondly, under vacuum only 5.0% of the initial mass remained in the crucible. For ambient pressure $N_2$ flow TGA, the amount of remnants reached approx. 37.0% of initial mass. Silver accounts for 39.8% of the molar mass of this complex.

This compound has been used as FEBID precursor in other studies and is known to produce high purity deposits of Ag 76.0 at%. In reported cases, the gas injection system reached temperatures up to 180 °C [25, 26]. It can be seen that the results from FEBID support those from VTGA. Attaining high purity silver deposits is only possible when silver-containing species are present within the gas phase.

Similar results were obtained for another fluorinated silver carboxylate, $[Ag_2(\mu\text{-}O_2CCF_3)_2]$ (Fig. 3b). At low vacuum, this precursor starts sublimating at lower temperatures than at atmospheric pressure and leaves significantly less residues in the crucible (8.0% in vacuum vs. 54.0% atmospheric pressure, $N_2$ flow).

A different behaviour was observed for non-fluorinated $[Ag_2(\mu\text{-}O_2CC(Me_2)Et)_2]$ (Fig. 3c). Under both vacuum and ambient pressure $N_2$ flow conditions, the compound left approx. 45.0% and 49.0%, respectively, of its initial mass in the crucible. The expected leftover mass for silver from thermal decomposition was 48.4% (the mass percentage of Ag in compound's molar mass), which is in line with the observed leftover mass for the ambient pressure experiment. However, the remaining mass obtained from VTGA was lower, indicating that thermal decomposition and evaporation occur concurrently.

Next, compounds $[Ag_2(\mu\text{-}O_2CC_2F_5)_2]$ and $[Ag_2(\mu\text{-}O_2CCF_3)_2]$ were kept for 8 h at 180 °C (highest GIS temperature used for deposition of the first one) to determine their stability during long time isothermal heating (imitating FEBID conditions). The results are presented in Fig. 3d. On the one hand, $[Ag_2(\mu\text{-}O_2CC_2F_5)_2]$ fully sublimed within the first 100 min of the experiment, leaving only 2.0% of

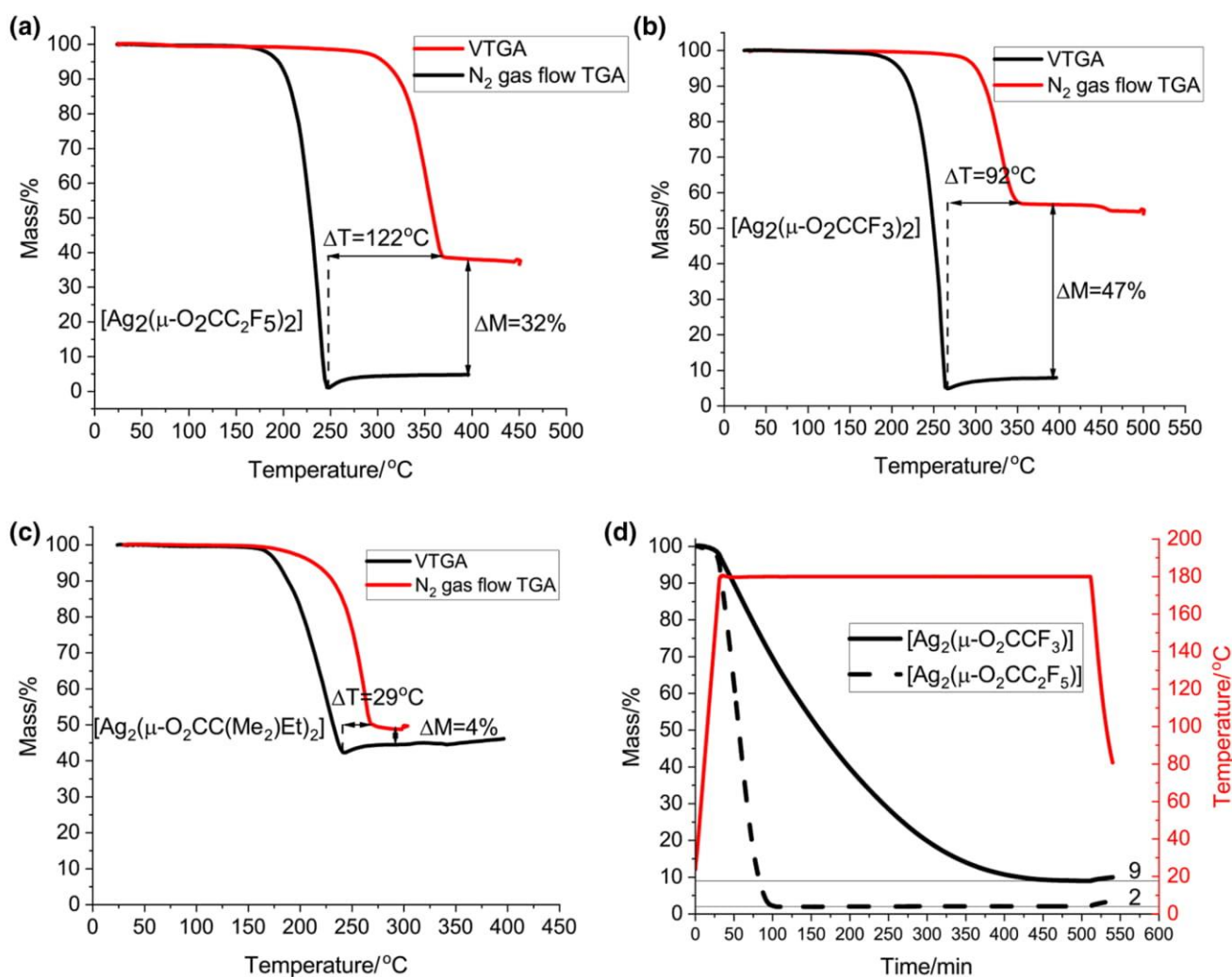**Fig. 3** Results of both in-vacuum (black) and gas flow (red) TGA for $[Ag_2(\mu\text{-}O_2CC_2F_5)_2]$ (**a**), $[Ag_2(\mu\text{-}O_2CCF_3)_2]$ (**b**), $[Ag_2(\mu\text{-}O_2CC(Me_2)Et)_2]$ (**c**) and comparison of isothermal TGA curves for two fluorinated compounds (**d**)

its initial mass in the crucible. We can attribute this value of remnants to possible impurities (e.g. silver coming from photodecomposition), which may be present in the compound or to the slight thermal decomposition of the precursor. On the other hand, $[Ag_2(\mu\text{-}O_2CCF_3)_2]$ sublimed at a much lower rate, stabilising at around 9.0% of mass loss after 450 min. Similarly to $[Ag_2(\mu\text{-}O_2CC_2F_5)_2]$, the mass residues can be attributed to possible impurities; however, they are significantly higher than in the previous case, and therefore, we cannot exclude the possibility of thermal decomposition occurring alongside sublimation. Nevertheless, both compounds have proven to be rather stable during long time heating at low vacuum, which is an important aspect for FEBID experiments. As the initial masses of the compounds were different, we can only compare the relative mass losses versus time. However, it can be observed that the rate of sublimation for $[Ag_2(\mu\text{-}O_2CC_2F_5)_2]$ is faster and that

this compound will give higher molecular fluxes due to GIS heating, which is important from the viewpoint of deposition growth rate during FEBID.

To simplify comparing ambient pressure $N_2$ flow and VTGA measurements, the results are summarised in Table 1, for mass losses of 10.0% and end of mass loss. One can clearly see that non-fluorinated compound decomposition and sublimation occurs at lower temperatures, both in-vacuum and at ambient pressure. For both TGA methods, decomposition plays a significant role, as relatively high percentages of residues were obtained in the crucible after the mass loss process ended. Nevertheless, for all measured carboxylates, the mass loss starts at lower temperatures during VTGA. For fluorinated compounds, the temperatures at which mass loss reached 10.0% were approx. 90–120 °C lower than during gas flow experiments. For $[Ag_2(\mu\text{-}O_2CC(Me_2)Et)_2]$, the difference was around 40 °C.

**Table 1** Temperatures measured during TGA for 10% of mass loss and at the end of mass loss for all examined silver compounds in vacuum and with $N_2$ gas flow

| Compound | Mass loss | | | |
| --- | --- | --- | --- | --- |
| | 10% | | End of mass loss | |
| | VTGA | $N_2$-TGA | VTGA | $N_2$-TGA |
| Temperatures/°C VTGA versus $N_2$-TGA | | | | |
| $Ag_2(\mu\text{-}O_2CC(Me_2)Et)_2$ | 189 | 230 | 241 (45.0%)* | 270 (49.0%)* |
| $Ag_2(\mu\text{-}O_2CCF_3)_2$ | 221 | 311 | 263 (8.0%)* | 355 (54.0%)* |
| $Ag_2(\mu\text{-}O_2CC_2F_5)_2$ | 203 | 321 | 249 (5.0%)* | 371 (37.0%)* |

*In the brackets are given the values of the mass residues in the crucible after the mass loss stopped

Furthermore, for all measured complexes, mass loss stops at lower temperatures under vacuum conditions than at ambient pressure $N_2$-flow.

## Discussion

The difference in initial sublimation temperature between in-vacuum and $N_2$-gas flow TGA can be explained by different pressure levels during both experiments. VTGA was performed with a background pressure level of $10^{-1}$–$10^{-2}$ mbar, which is 4–5 orders of magnitude lower than 1 bar of atmospheric pressure used for $N_2$-flow TGA. The sublimation process in the system containing the compound in solid and gas phase is driven by the chemical potentials of both phases. The chemical potential generally rises with pressure and temperature with different rates for gases and solid materials. As the chemical potential of a gas generally increases more than the chemical potential of a solid [32], more energy is needed to sublimate the precursor, i.e. for ambient pressure ($N_2$ flow TGA) we need to increase the temperature to sublimate the same amount of the substance as for VTGA. This explains why the same level of mass loss during ambient pressure $N_2$ flow TGA was observed at lower temperatures using VTGA. Of note is that the vapour pressure of a measured gas increases slightly with increasing pressure of inert gas. However, this effect is small. For example, for water at 25 °C the vapour pressure would increase by 0.074% when adding 1 atm. of inert gas [32]. Furthermore, the $N_2$-flow and VTGA experiments are not performed in closed systems and not at thermal equilibrium (temperature continuously changes). Considering this, even though vapour pressure is frequently used as a measure of volatility of a compound, this concept does not correctly apply here. Evaporation at low temperatures is industrially used as vacuum distillation in the oil refinery industry [33] or in at laboratory scale for purification of organometallic compounds during synthesis

[34, 35]. However, for precursors used in chemical vapour deposition, atomic layer deposition, and FEBID vacuum TGA curves are generally not at hand although they would be of great help to design the deposition process with respect to precursor reservoir temperatures, carrier gas pressures, substrate temperature and reproducibility of the deposition rate.

The difference in the amount of mass left in the crucible for fluorinated complexes can be explained by the at least partial thermal decomposition of these compounds during TGA measurements, especially at ambient pressure with $N_2$ flow. For all compounds, silver is the heaviest element. Considering the fluorinated complexes measured with both methods, silver mass corresponds to around 39.8% of the molar mass of $[Ag_2(\mu\text{-}O_2CC_2F_5)_2]$ and 48.9% of the molar mass of $[Ag_2(\mu\text{-}O_2CCF_3)_2]$. The mass left in the crucible during ambient pressure $N_2$ flow TGA was on the level of 37.0% for the first and 54.0% of the latter compound. This indicates that the precursor partially thermally decomposes, also in vacuum experiments, leaving silver-containing species in the crucible. The presence of metallic silver, along with some organic impurities, (result of thermal decomposition), has also been reported in previously published ambient pressure $N_2$ flow thermal analysis of $[Ag_2(\mu\text{-}O_2CC_2F_5)_2]$ [27]. In the case of VTGA, where the mass remnants are much lower (5.0% for $[Ag_2(\mu\text{-}O_2CC_2F_5)_2]$ and 8.0% $[Ag_2(\mu\text{-}O_2CCF_3)_2]$) there is probably only very limited thermal decomposition and mostly intact molecules of the precursors are present in the gas phase.

$[Ag_2(\mu\text{-}O_2CC(Me_2)Et)_2]$ thermally decomposed during both VTGA and $N_2$-flow measurements. The mass percentage of silver in the precursor molecule $[Ag_2(\mu\text{-}O_2CC(Me_2)Et)_2]$ amounts to 48.4%. The ambient pressure $N_2$ gas flow TGA showed 49.0% of mass remaining after the measurement, which hints that mostly silver, as the heaviest element, stayed in the crucible. Literature sources also indicate thermal decomposition of the precursor to metallic silver at temperatures between 195 and 250 °C [23]. The remaining mass present after VTGA was slightly lower, reaching 45.0% of initial mass, which indicates the sublimation of at least some part of silver-containing species. The exact amount is hard to estimate, as we do not know the exact pathway of thermal decomposition occurring in the crucible. Interestingly, this compound has been used as a silver FEBID precursor and has been reported to give high purity deposits, i.e. approx. 74.0 at% of Ag [24]. This means that at high vacuum there must be silver containing species within gas phase. As volatile silver-containing ions were detected using the electron ionisation mass spectrometry (EI MS) technique in high vacuum [29], we can assume that lowering background pressure would facilitate sublimation over decomposition.

Summarising, we can state that thermal decomposition and sublimation are two competing processes that occur during heating of the silver carboxylates. By using low vacuum,

we decrease the work necessary for the molecule to overcome the ambient pressure and join the gas phase, making sublimation the more energetically preferable process. That is the reason why for VTGA intact molecules can sublimate at temperatures lower than the thermal decomposition threshold, leaving less mass in the crucible. Quantification of sublimation and decomposition rates will be subject of follow-up studies.

Stable low-temperature sublimation would explain the feasibility of FEBID with silver carboxylates as FEBID is usually performed in high vacuum. With background pressures 2–3 orders of magnitude lower than used in VTGA, the sublimation could start at even lower temperatures, allowing for more silver-containing species to sublimate and reach the substrate surface. There, it can be locally decomposed to high silver content material by the focused electron beam. As was previously mentioned, intact precursor molecules of $[Ag_2(\mu\text{-}O_2CC(Me_2)Et)_2]$ were detected within gas phase in high vacuum with EI MS [29], with similar results for $[Ag_2(\mu\text{-}O_2CCF_3)_2]$ [36].

## Conclusions

VTGA was applied to measure mass loss during heating of known and potential CVD and FEBID silver carboxylate precursors. In all presented cases, under low vacuum the compounds sublimed at lower temperatures, leaving less remnants in the crucible than during $N_2$-gas flow measurements. By lowering the ambient pressure during TGA, it was possible to create thermodynamic conditions facilitating the sublimation of more molecules at temperatures below the thermal decomposition threshold. The sublimation temperatures determined using VTGA stand in better agreement with the temperature ranges used during FEBID than those obtained by means of ambient pressure $N_2$-gas flow TGA.

Based on compound thermal stability analysis, it was determined that the fluorinated carboxylates are more promising as silver FEBID precursors. However, as shown for $[Ag_2(\mu\text{-}O_2CC(Me_2)Et)_2]$, it may still be possible to deposit silver when using non-perfluorinated precursors. In this sense, the VTGA technique proved to be an attractive method for confirming the suitability of precursors for FEBID. The temperature window for the sublimation of low volatility precursors was determined using the ramping temperature mode. The isothermal mode was used to check the thermal stability and sublimation rate at a given temperature for two compounds $[Ag_2(\mu\text{-}O_2CCF_3)_2]$ and $[Ag_2(\mu\text{-}O_2CC_2F_5)_2]$.

We found evidence that the lower temperature onset for sublimation (mass change) favours the entire sublimation of certain carboxylates during the TGA programmed temperature rise before the temperature of thermal decomposition is reached. Further details of the temperature-dependent competition of sublimation and decomposition processes could be obtained by extended isothermal TGA investigations and FTIR or mass spectrometric studies performed in situ during temperature ramp TGA. We hope to initiate these kind of measurements in the field of thermal investigations with our present manuscript.

## Compliance with ethical standards

## References

1. Bottom R. Thermogravimetric analysis. In: Gabbott P, editor. Principles and applications of thermal analysis. London: Blackwell; 2008. p. 87–118.
2. Guo Y, Zhang H, Liu Y. Desorption characteristics and kinetic parameters determination of molecular sieve by thermogravimetric analysis/differential thermogravimetric analysis technique. Adsorpt Sci Technol. 2018;36(7–8):1389–404.
3. Conesa JA, Marcilla A, Font R, Caballero JA. Thermogravimetric studies on the thermal decomposition of polyethylene. J Anal Appl Pyrolysis. 1996;36(1):1–15.

4. Gai C, Zhang Y, Chen W-T, Zhang P, Dong Y. Thermogravimetric and kinetic analysis of thermal decomposition characteristics of low-lipid microalgae. Bioresour Technol. 2013;150:139–48.

5. Coker EN, The oxidation of aluminum at high temperature studied by thermogravimetric analysis and differential scanning calorimetry. Sandia National Laboratories (US); 2013. (SAND2013–8424).

6. Zaki MI, Hasan MA, Pasupulety L, Kumari K. Thermochemistry of manganese oxides in reactive gas atmospheres: probing catalytic $MnO_x$ compositions in the atmosphere of $CO + O_2$. Thermochim Acta. 1998;311(1):97–103.

7. Rao CJ, Ningshen S, Mallika C, Mudali UK. Molten salt corrosion behavior of structural materials in LiCl-KCl-UCl3 by thermogravimetric study. J Nucl Mater. 2018;501:189–99.

8. Ashby EC, Claudy P, Bousquet J, Etienne J. High vacuum DTA-TGA instrumentation for air-sensitive compounds. J Chem Educ. 1975;52(9):618.

9. Zhou G, Roby S, Wei T, Yee N. Fuel heat of vaporization values measured with vacuum thermogravimetric analysis method. Energy Fuels. 2014;28(5):3138–42.

10. Auinger M, Vogel A, Vogel D, Rohwerder M. Early stages of oxidation observed by in situ thermogravimetry in low pressure atmospheres. Corros Sci. 2014;86:183–8.

11. Du L, Chu W, Miao H, Xu C, Ding Y. Synthesis, characterization, thermal properties of silicon(iv) compounds containing guanidinato ligands and their potential as CVD precursors. RSC Adv. 2015;5(88):71637–43.

12. Kunte GV, Shivashankar SA, Umarji AM. Thermogravimetric evaluation of the suitability of precursors for MOCVD. Meas Sci Technol. 2018;19(2):025704.

13. Jakob A, Schmidt H, Djiele P, Shen Y, Lang H. Phosphane/phosphite silver(I) carboxylates as CVD precursors. Microchim Acta. 2006;156(1):77–81.

14. Siddiqi MA, Atakan B. Combined experiments to measure low sublimation pressures and diffusion coefficients of organometallic compounds. Thermochim Acta. 2007;452(2):128–34.

15. Huth M, Porrati F, Dobrovolskiy OV. Focused electron beam induced deposition meets materials science. Microelectronic Eng. 2018;185–186:9–28.

16. Botman A, Mulders JJL, Hagen CW. Creating pure nanostructures from electron-beam-induced deposition using purification techniques: a technology perspective. Nanotechnology. 2009;20(37):372001.

17. Huth M, Porrati F, Schwalb C, Winhold M, Sachser R, Dukic M, Adams J, Fantner G. Focused electron beam induced deposition: a perspective. Beilstein J Nanotech. 2012;3:597–619.

18. Ozbay E. Plasmonics: merging photonics and electronics at nanoscale dimensions. Science. 2006;311(5758):189.

19. Höflich K, Yang RB, Berger A, Leuchs G, Christiansen S. The direct writing of plasmonic gold nanostructures by electron-beam-induced deposition. Adv Mater. 2011;23(22–23):2657–61.

20. Winkler R, Schmidt F-P, Haselmann U, Fowlkes JD, Lewis BB, Kothleitner G, Rack PD, Plank H. Direct-write 3D Nanoprinting Of Plasmonic Structures. ACS Appl Mater Interfaces. 2017;9(9):8233–40.

21. Szłyk E, Piszczek P, Grodzicki A, Chaberski M, Goliński A, Szatkowski J, Błaszczyk T. CVD of AgI complexes with tertiary phosphines and perfluorinated carboxylates—a new class of silver precursors. Chem Vap Depos. 2001;7(3):111–6.

22. Panneerselvam A, Malik MA, O'Brien P, Helliwell M. The aerosol-assisted CVD of silver films from single-source precursors. Chem Vap Depos. 2009;15(1–3):57–63.

23. Szczęsny R, Szłyk E. Thermal decomposition of some silver(I) carboxylates under nitrogen atmosphere. J ThermAnal Calorim. 2013;111(2):1325–30.

24. Höflich K, Jurczyk J, Zhang Y, Puydinger dos Santos MV, Götz M, Guerra-Nuñez C, Best JP, Kapusta C, Utke I. Direct electron beam writing of silver-based nanostructures. ACS Appl Mater Interfaces. 2017;9(28):24071–24077.

25. Berger L, Madajska K, Szymanska IB K. Höflich, Polyakov MN, Jurczyk J, Guerra-Nuñez C, Utke I. Gas-assisted silver deposition with a focused electron beam. Beilstein J Nanotech. 2018;9:224–232.

26. Höflich K, Jurczyk JM, Madajska K, Götz M, Berger L, Guerra-Nuñez C, Haverkamp C, Szymanska I, Utke I. Towards the third dimension in direct electron beam writing of silver. Beilstein J Nanotech. 2018;9:842–9.

27. Szłyk E, Piszczek P, Chaberski M, Goliński A. Studies of thermal decomposition process of Ag(I) perfluorinated carboxylates with temperature variable IR and MS. Polyhedron. 2001;20(22):2853–61.

28. Kuzmina N, Paramonov S, Ivanov R, Kezko V, Polamo K, Troyanov S. Silver pivalate as a new volatile precursor for thin film deposition. J Phys IV France. 1999;09(PR8):923–8.

29. Szymańska I, Piszczek P, Szczęsny R, Szłyk E. Thermal and MS studies of silver(I) 2,2-dimethylbutyrate complexes with tertiary phosphines and their application for CVD of silver films. Polyhedron. 2007;26(12):2440–8.

30. Park K-H, Marshall WJ. Remarkably volatile copper(II) complexes of N,N'-unsymmetrically substituted 1,3-diketimines as precursors for Cu metal deposition via CVD or ALD. J Am Chem Soc. 2005;127(26):9330–1.

31. Szłyk E, Łakomska I, Grodzicki A. Thermal and spectroscopic studies of the Ag(I) salts with fluorinated carboxylic and sulfonic acid residues. Thermochim Acta. 1993;223:207–12.

32. Kaufman M. Principles of thermodynamics. Boca Raton: CRC Press; 2002.

33. Stauffer E, Dolan JA, Newman R. Flammable and combustible liquids. In: Stauffer E, Dolan JA, Newman R, editors. Fire debris analysis. Burlington: Academic Press; 2008. p. 199–233.

34. Zharkova GI, Sysoev SV, Turgambaeva AE, Igumenov IK. Thermal behavior of a series of monomeric Ni(II) complexes with β-iminoketones. Thermochim Acta. 2013;560:7–11.

35. Lim BS, Rahtu A, Park J-S, Gordon RG. Synthesis and characterization of volatile, thermally stable, reactive transition metal amidinates. Inorg Chem. 2003;42(24):7951–8.

36. Adams SK, Edwards DA, Richards R. Silver(I) carboxylates. I. Mass spectra and low frequency infrared spectra. Inorg Chim Acta 1975;12(1):163–166.

## Authors and Affiliations

Jakub Jurczyk[1,2] · Cristiano Glessi[3] · Katarzyna Madajska[4] · Luisa Berger[1] · Jeroen Ingolf Ketele Nyrud[3] · Iwona Szymańska[4] · Czesław Kapusta[2] · Mats Tilset[3] · Ivo Utke[1]

[1] Laboratory for Mechanics of Materials and Nanostructures, Empa—Swiss Federal Laboratories for Materials Science and Technology, Feuerwerkerstrasse 39, 3602 Thun, Switzerland

[2] Faculty of Physics and Applied Computer Science, AGH University of Science and Technology Krakow, Al. Mickiewicza 30, 30-059 Kraków, Poland

[3] Department of Chemistry, University of Oslo, Sem Sælands vei 26, 0371 Oslo, Norway

[4] Faculty of Chemistry, Nicolaus Copernicus University, Gagarina 7, 87-100 Toruń, Poland

# Paper III

**Gold(I) N-heterocyclic carbene precursors for focused electron beam-induced deposition**

Cristiano Glessi, Aya Mahgoub, Cornelis W. Hagen, and Mats Tilset

# Gold(I) N-heterocyclic carbene precursors for focused electron beam-induced deposition

Cristiano Glessi[*1], Aya Mahgoub[2], Cornelis W. Hagen[2] and Mats Tilset[*1]

## Abstract

Seven gold(I) N-heterocyclic carbene (NHC) complexes were synthesized, characterized, and identified as suitable precursors for focused electron beam-induced deposition (FEBID). Several variations on the core Au(NHC)X moiety were introduced, that is, variations of the NHC ring (imidazole or triazole), of the alkyl N-substituents (Me, Et, or iPr), and of the ancillary ligand X (Cl, Br, I, or CF$_3$). The seven complexes were tested as FEBID precursors in an on-substrate custom setup. The effect of the substitutions on deposit composition and growth rate indicates that the most suitable organic ligand for the gold precursor is triazole-based, with the best deposit composition of 15 atom % gold, while the most suitable anionic ligand is the trifluoromethyl group, leading to a growth rate of $1 \times 10^{-2}$ nm$^3$/e$^-$.

## Introduction

Focused electron beam-induced deposition (FEBID) is a nanofabrication technique that allows for the growth of three-dimensional free-standing nanostructures [1-4]. This mask-less nanofabrication technique uses gaseous molecules as precursors. The gas molecules are introduced in the specimen chamber of a scanning electron microscope (SEM), adsorb onto a substrate, and dissociate upon electron irradiation, leaving a solid deposit on the substrate and some volatile fragments. The technique has been employed in applications such as the fabrication of nanoconnectors [5], extreme ultra-violet lithography (EUVL) mask repair [6], AFM probe tips [7-9], nanodevices for plasmonics [10], gas sensors [11,12], optoelectronics [13], and magnetic [14,15] and biomedical applications [16]. FEBID provides a flexible direct-write technique to fabricate complex 3D struc-

tures, which are hard to realize using resist-based planar lithography processes. However, when using organometallic precursors, usually, undesired dissociation fragments also end up in the deposit. A major challenge is therefore to achieve control over the composition of the deposited material through a proper design of the precursor molecule [17,18].

Gold deposition has been one of the earliest interests in FEBID [19], as gold 3D-nanostructures can find a wide range of applications from plasmonics [10] to optoelectronics [13]. Gold FEBID precursors (Figure 1) have had a similar history as other metal precursors, as the first tested compounds were taken from the existing library of gold precursors for chemical vapour deposition (CVD). The first compounds tested were gold dimethyl acetylacetonate, Au(acac)Me$_2$, and its trifluorinated and hexafluorinated derivatives, Au(tfac)Me$_2$ and Au(hfac)Me$_2$ [19]. While for the former two compounds the gold content in the deposits varied over a large range (3–28 atom % [10,20-22] and 3–39 atom % [21,23-25]), the latter complex yielded only traces of gold (2–3 atom % [19]). Within the series of gold acetonate complexes, the highest gold content has been achieved with Au(tfac)Me$_2$ when water was co-injected as an oxidizing

agent during the deposition (91 atom % gold) [26]. To circumvent carbon contamination, a series of inorganic gold(I) complexes has been explored, such as Au(PF$_3$)Cl [27-30] and Au(CO)Cl [31], which gave high-purity deposits. Unfortunately, the high instability of these precursor molecules has severely hindered their use as FEBID precursors.

For the compounds [AuMe$_2$Cl]$_2$ and Au(PMe$_3$)Me [32], it was demonstrated that the presence of alkyl ligands in gold FEBID precursors has a highly positive effect on the stability of the compounds [33,34] and can lead to a satisfactory purity of the obtained nanostructures (19–25 and 29–41 atom % Au, respectively) [32]. The most recent organometallic gold complexes that were tested are Au(CNMe)CF$_3$ and Au(CN(*t*-Bu))CF$_3$. These complexes are stabilized by the presence of a good σ-donor ligand (isocyanide) and their volatility is enhanced by the presence of a trifluoromethyl ligand. Deposits from these precursors contained 22 and 14 atom % of gold, respectively [34].

Although many different ligand architectures of gold organometallic complexes were tested as FEBID gold precursors, the
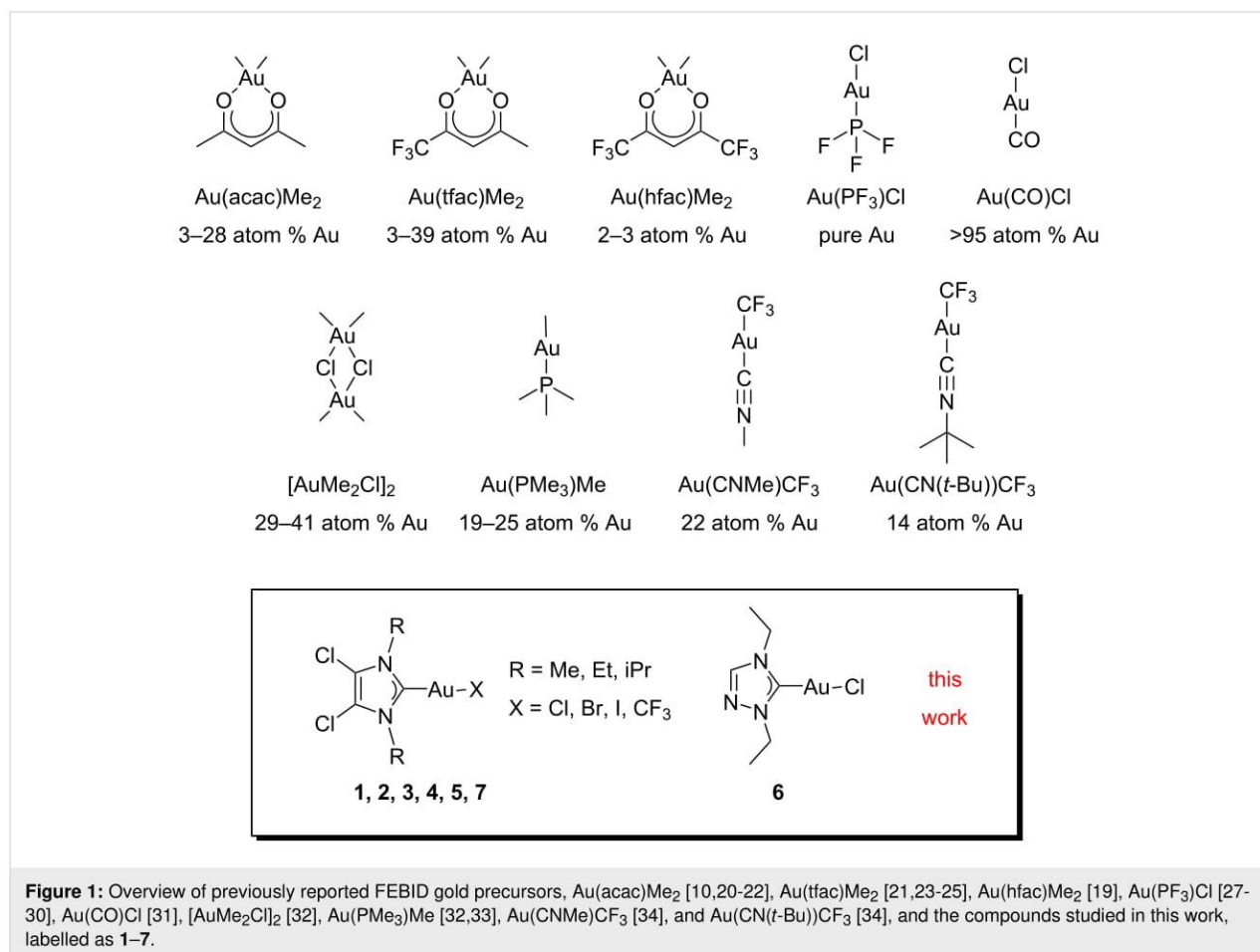


**Figure 1:** Overview of previously reported FEBID gold precursors, Au(acac)Me$_2$ [10,20-22], Au(tfac)Me$_2$ [21,23-25], Au(hfac)Me$_2$ [19], Au(PF$_3$)Cl [27-30], Au(CO)Cl [31], [AuMe$_2$Cl]$_2$ [32], Au(PMe$_3$)Me [32,33], Au(CNMe)CF$_3$ [34], and Au(CN(*t*-Bu))CF$_3$ [34], and the compounds studied in this work, labelled as **1–7**.

effect of different substitutions in the core structure of the molecule on the composition and growth rate of deposits is still largely unexplored. Such studies may reveal groups or ligands in precursors that perform better in FEBID and can perhaps lead to a generalized precursor design.

The objective of this work is to expand the already existing library of gold(I) FEBID precursors and to study the effect of various substitutions at the core structure of a series of gold(I) N-heterocyclic carbene (NHC) complexes on the growth rate and composition of deposits. The precursors that were synthesized had the general formula Au(NHC)X, and the effect of the variation of both the NHC ligand and the ancillary ligand X (X = Cl, Br, I, CF$_3$) (Figure 1) was studied. Because the sublimation temperatures of these precursors exceeded the maximum operating temperature of standard gas injection systems (GIS) in the SEM, an unconventional method was chosen to introduce the precursors from a custom-built reservoir mounted directly on top of a heated substrate on which also the deposits were directly grown. The growth of the deposited pillars was studied as a function of the deposition time, and some larger cube-shaped deposits were made to determine the composition of the deposited material using energy-dispersive X-ray (EDX) spectrometry.

## Experimental
### Synthesis and characterization
All chemicals and solvents needed were commercially available and were used as received. Au(SMe$_2$)Cl was prepared according to a procedure reported in [35]. 1,4-Diethyl-1,2,4-triazolium iodide was prepared according to the procedure reported in [36]. In order to more easily refer to the complexes, we denote the compounds as (Y,R)AuX, where Y is the backbone substitution of the NHC ligand, R is the N-substituent, and X is the negatively charged ancillary ligand. The precursors (Cl,Me)AuCl (**1**), (Cl,Et)AuCl (**2**) and (Cl,iPr)AuCl (**3**) were prepared according to [37]. All reactions were performed under ambient conditions unless specified otherwise. NMR spectra were recorded on Bruker Advance DPX200, DPX300, AVII400, AVIII400 and AVII600 instruments at ambient temperature. $^1$H and $^{13}$C NMR spectra were referenced relative to the residual solvent system (CD$_2$Cl$_2$). $^{19}$F NMR spectra were referenced to hexafluorobenzene (−164.9 ppm). Mass spectra were obtained on a Micromass QTOF II spectrometer and a Bruker Daltronics maXis II spectrometer. Melting point determinations were performed on a Stuart SMP10 melting point apparatus, using flame-sealed capillaries at a pressure of ca. 0.2 mbar in order to mimic a vacuum environment.

[(Cl,Et)AuBr] (**4**): A solution of **2** (100.6 mg, 0.24 mmol, 1 equiv) and LiBr (211.6 mg, 2.4 mmol, 10 equiv) in dried ace-

tone (10 mL) was stirred in the dark under Ar for 20 h. Solvent was removed by rotary evapouration and the resulting white solid was partially dissolved in dichloromethane (DCM) and purified through column chromatography (DCM, silica). The product was obtained as an off-white powder (100.3 mg, 89%). $^1$H NMR (400 MHz, CD$_2$Cl$_2$) δ 4.29 (q, *J* = 7.3 Hz, 4H, -C*H$_2$*-), 1.44 (t, *J* = 7.3 Hz, 6H, -C*H$_3$*); $^{13}$C NMR (101 MHz, CD$_2$Cl$_2$) δ 174.1 (NHC-*C*), 116.9 (=*C*-Cl), 46.3 (-*C*H$_2$-), 16.0 (-*C*H$_3$); MS (ESI$^+$, MeOH): *m/z* 490.896 ([M($^{35}$Cl$^{35}$Cl$^{79}$Br) + Na]$^+$, 62.3%), 492.894 ([M($^{37}$Cl$^{35}$Cl$^{79}$Br) + Na]$^+$, [M($^{35}$Cl$^{35}$Cl$^{81}$Br) + Na]$^+$, 100%), 494.891 ([M($^{37}$Cl$^{37}$Cl$^{79}$Br) + Na]$^+$, [M($^{37}$Cl$^{35}$Cl$^{81}$Br) + Na]$^+$, 46.6%); HRMS (MeOH): *m/z* meas. 490.8963, calcd. 490.8962 for [C$_7$H$_{10}$Au$^{79}$Br$^{35}$Cl$_2$N$_2$Na]$^+$ (Δ = −0.1 ppm); mp 204–205 °C; elemental analysis: calcd. for C$_7$H$_{10}$AuBrCl$_2$N$_2$: C, 17.89; H, 2.14; N, 5.96; found: C, 17.76; H, 2.13; N, 5.82%.

[(Cl,Et)AuI] (**5**): A suspension of **2** (100.3 mg, 0.24 mmol, 1 equiv) and NaI (358.2 mg, 2.4 mmol, 10 equiv) in dried acetone (10 mL) was stirred in the dark under Ar for 20 h. Solvent was removed by rotary evapouration and the resulting white solid was partially dissolved in dichloromethane (DCM), filtered, and purified through column chromatography (DCM, silica). The obtained orange powder was precipitated from layering of DCM and pentane. The product was obtained as a white powder (89.2 mg, 72%). $^1$H NMR (600 MHz, CD$_2$Cl$_2$) δ 4.30 (q, *J* = 7.3 Hz, 4H, C*H$_2$*-), 1.45 (t, *J* = 7.2 Hz, 6H, -C*H$_3$*); $^{13}$C NMR (151 MHz, CD$_2$Cl$_2$) δ 181.0 (NHC-*C*), 117.0 (=*C*-Cl), 46.0 (-*C*H$_2$-), 16.0 (-*C*H$_3$); MS (ESI$^+$, MeOH): *m/z* 538.882 ([M($^{35}$Cl$^{35}$Cl) + Na]$^+$, 100%), 540.880 ([M($^{37}$Cl$^{35}$Cl) + Na]$^+$ 64.5%), 581.010 ([(NHC)$_2$Au]$^+$, 74.1%), 583.007 ([(NHC)$_2$Au]$^+$, 95.9%), 585.005 ([(NHC)$_2$Au]$^+$, 46.3%); HRMS (MeOH): *m/z* meas. 538.8824, calcd. 538.8824 for [C$_7$H$_{10}$Au$^{35}$Cl$_2$IN$_2$Na]$^+$ (Δ = −0.1 ppm); mp 178–179 °C; elemental analysis: calcd. for C$_7$H$_{10}$AuC$_2$IIN$_2$: C, 16.26; H, 1.95; N, 5.42; found: C, 16.07; H, 1.91; N, 5.28%.

[(N,Et)AuCl] (**6**): 1,4-Diethyl-1,2,4-triazolium iodide (400.6 mg, 1.58 mmol, 1 equiv) was solubilized in 60 mL of DCM. Ag$_2$O (185 mg, 0.80 mmol, 0.5 equiv) was added and the resulting suspension was left stirring in the dark for 15 h. To the resulting white suspension solid Au(SMe$_2$)Cl (467.3 mg, 1.58 mmol, 1 equiv) was added and immediately a yellow coloration of the suspension was observed. After 4 h of stirring in the dark the yellow suspension was filtered and concentrated to dryness. The solid was purified by column chromatography (silica, DCM) and an orange product was obtained. Upon recrystallization from layered DCM and pentane, white crystals were obtained (565 mg, 84%). $^1$H NMR (400 MHz, CD$_2$Cl$_2$) δ 8.05 (s, 1H, =C*H*-), 4.41 (q, *J* = 7.3 Hz, 2H, -C*H$_2$*-, N side), 4.24 (q, *J* = 7.4 Hz, 2H, -C*H$_2$*-, CH side), 1.53 (t, *J* = 7.4 Hz, 3H, -C*H$_3$*, CH side), 1.51 (t, *J* = 7.3 Hz, 3H, -C*H$_3$*, N side);

$^{13}$C NMR (101 MHz, CD$_2$Cl$_2$) δ 173.2 (NHC-*C*), 142.2 (=*C*H-), 49.2 (-*C*H$_2$-, N side), 44.9 (-*C*H$_2$-, CH side), 16.6 (-*C*H$_3$, CH side), 15.7 (-*C*H$_3$, N side); MS (ESI$^-$, MeOH): *m/z* 356.023 ([M($^{35}$Cl)-H]$^-$, 100%), 358.020 ([M($^{37}$Cl)-H]$^-$ 31.9%), 392.000 ([M($^{35}$Cl)+Cl]$^-$ 40.3%); HRMS (MeOH): *m/z* meas. 356.0233, calcd. 356.0234 for [C$_6$H$_{10}$Au$^{35}$ClN$_3$]$^-$ (Δ = 0.3 ppm); mp 131–132 °C; elemental analysis: calcd. for C$_6$H$_{11}$AuClN$_3$: C, 20.15; H, 3.10; N, 11.75; found: C, 20.09; H, 3.13; N, 11.78%.

**[(Cl,Et)AuCF$_3$] (7):** AgF (104.0 mg, 0.82 mmol, 2 equiv) was added in a Schlenk flask. Upon addition of dry acetonitrile (10 mL) a grey suspension was obtained under vigorous stirring. Me$_3$SiCF$_3$ (0.3 mL, 2.1 mmol, 5 equiv) was added and a white/grey suspension was immediately formed. After a few minutes, the white suspension turned grey. The reaction mixture was stirred in the dark for 1 h. Solid **2** (176 mg, 0.41 mmol, 1 equiv) was added and the mixture turned into a light grey suspension. After 1 day the reaction mixture was concentrated to dryness and the obtained solid was partially dissolved in DCM, filtered, and concentrated. The dark product was purified by column chromatography (DCM, silica) and the product was obtained as a white powder (122.1 mg, 66%). $^1$H NMR (400 MHz, CD$_2$Cl$_2$) δ 4.28 (q, *J* = 7.3 Hz, 4H, -C*H$_2$*-), 1.45 (t, *J* = 7.3 Hz, 6H, -C*H$_3$*); $^{13}$C NMR (101 MHz, CD$_2$Cl$_2$) δ 184.5 (q, *J* = 14.9 Hz, NHC-*C*), 162.8 (q, *J* = 344.2 Hz, -*C*F$_3$), 117.4 (=*C*-Cl), 46.1 (-*C*H$_2$-), 16.5 (-*C*H$_3$); $^{19}$F NMR (188 MHz, CD$_2$Cl$_2$) δ −30.61 (s, 3F, -C*F$_3$*); MS (ESI$^+$, MeOH): *m/z* 480.973 ([M($^{35}$Cl$^{35}$Cl) + Na]$^+$ 100%), 482.970 ([M($^{37}$Cl$^{35}$Cl) + Na]$^+$ 63.4%); HRMS (MeOH): *m/z* meas. 480.9730, calcd. 480.9731 for [C$_8$H$_{10}$Au$^{35}$Cl$_2$F$_3$N$_2$Na]$^+$ (Δ = 0.2 ppm); mp 146–149 °C; elemental analysis: calcd. for C$_8$H$_{10}$AuCl$_2$F$_3$N$_2$: C, 20.93; H, 2.20; N, 6.10; found: C, 20.99; H, 2.17; N, 6.05%.

## Determination of the sublimation temperature

Sublimation temperatures for compounds **1**–**7** were obtained by cold finger sublimation. The cold finger sublimation setup was immersed in an oil bath and heated by a heating plate. The temperature was controlled and registered by an immersion thermometer immersed in the oil bath at the same height as the bulk material and connected to the heating plate. The pressure measured for each experiment was $1 \times 10^{-3}$ mbar on a VACUU.VIEW or DCP 3000 Vacuubrand manometer mounted on the Schlenk line used. The cold finger was cooled down with continuous water flow. 20 ± 1.5 mg of bulk material were charged in the sublimation apparatus, which was then evacuated and conditioned with Ar or N$_2$ before being evacuated again. The dynamic heating of the sample was carried out at a heating rate of 1 K per 10 min. The sublimation temperature was determined as the point at which the formation of a white film was observed on the initially transparent cold finger. The

material was left subliming at this temperature in order to accumulate a small quantity of sublimate, sufficient for further analysis. The sublimed material was then collected and analyzed by $^1$H NMR spectroscopy. The identity of the sublimed material was assessed by comparison with the $^1$H NMR spectrum of the bulk material (see Supporting Information File 1).

## Deposition setup

All deposition experiments were performed in a Thermo Fisher Scientific Nova Nanolab 600 dual-beam SEM. The base chamber pressure was about $1 \times 10^{-6}$ mbar. Silicon substrates were used for all experiments. The silicon substrates were cleaned by ultrasonication in acetone for 15 min, followed by ultrasonication in isopropanol for 15 min and blow drying with N$_2$, and were kept in a dust free environment. For each precursor a different substrate was used to avoid cross contamination. The substrate was mounted on a custom-built heater [38] shown in Figure 2 and crystals of the precursor were placed directly on the substrate. The low volatility of the compounds required heating above the maximum allowable temperature of a standard GIS to effectively sublime the material. An aluminium plate covered the substrate, leaving a central circular area free for deposition. The precursor material was contained in a recessed hole in the bottom of the plate, connected by a small channel to the deposition area. For each precursor to be tested a new plate was taken to avoid cross contamination.

Precursors were tested for deposition upon e-beam irradiation. When deposition was successful, two types of deposits were created. Firstly, large deposits for composition analysis were written by repeatedly (2000 passes) exposing a 250 × 250 nm$^2$ area, using point exposures with a dwell time of 500 μs and a pitch of 10 nm between the exposure points. Secondly, to characterize the growth, square arrays of 3 × 3 pillars, each pillar grown at a different dwell time, were fabricated. In each array, the pillar separation was 1 μm. Two types of arrays were deposited, one with short dwell times of 0.1, 0.2, 0.5, 1, 2, 5, 10, 20, and 50 s (referred to as type 1), and one with longer dwell times for slow-growth precursors of 1, 5, 10, 20, 40, 60, 80, 100, and 120 s (referred to as type 2).

The Nova Nanolab has a 12-bit DAC to control the beam position. Therefore, the addressable grid runs from 0 to 4095 pixels in the *X* direction and from 280 to 3816 pixels in the *Y* direction. The horizontal field width (4.1 μm) is equivalent to 4096 pixels, that is, one pixel corresponds to 1 nm.

Dimensions of deposits were measured from SEM images, and, in case of tilt images, corrected for the tilt angle. For the determination of the deposited volume, pillars were approximated either as a cone or a cylinder with a cone on top, depending on
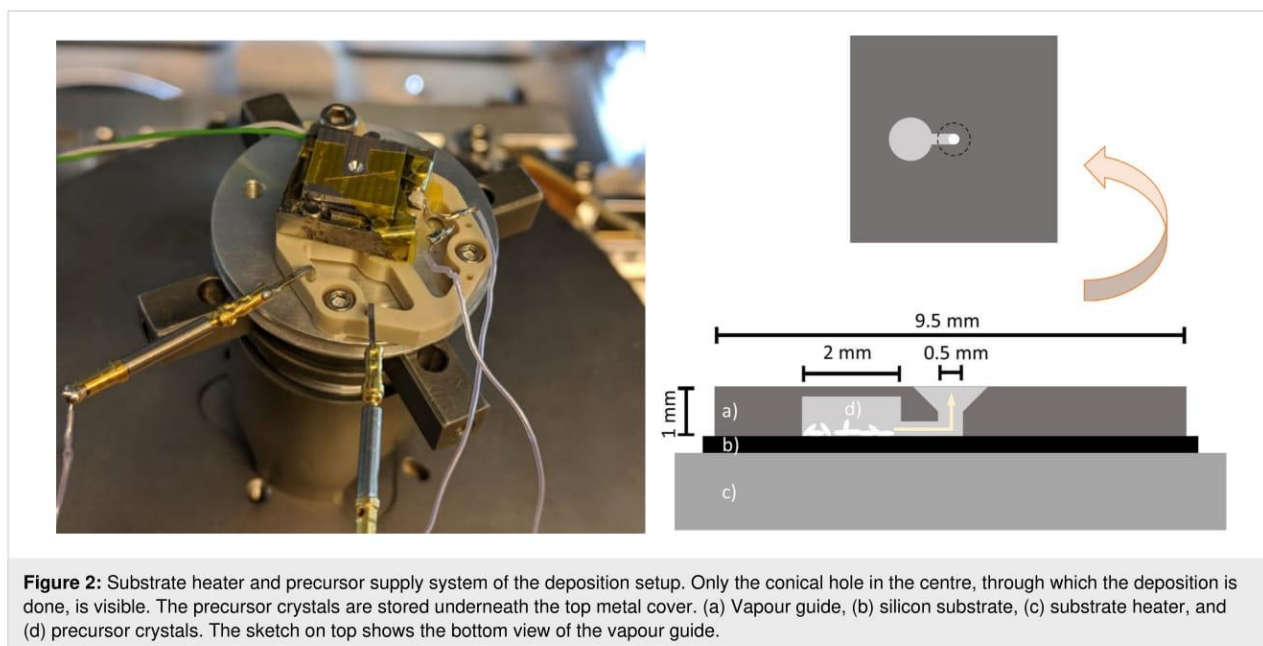
**Figure 2:** Substrate heater and precursor supply system of the deposition setup. Only the conical hole in the centre, through which the deposition is done, is visible. The precursor crystals are stored underneath the top metal cover. (a) Vapour guide, (b) silicon substrate, (c) substrate heater, and (d) precursor crystals. The sketch on top shows the bottom view of the vapour guide.

their shape. The error was calculated based on an error of ±10 nm in measuring the height and diameters of the pillars, except for a few pillars where the height error was ±100 nm. These few pillars were much longer and were thus measured at a lower magnification than the other pillars. Beam energy and current used for all deposits were 5 keV and 40 pA, respectively.

## Composition determination

EDX measurements were performed in the same Nova Nanolab 600 dual-beam SEM using an Oxford Instruments X-MAX 80 EDX detector. Beam energy and current used during the measurements were 5 keV and 600 pA, respectively. The working distance was kept around 5 mm to have the optimum EDX signal. All spectra were analysed using the Oxford Instruments AZtec software.

## Results and Discussion
### Precursor design

The properties of a FEBID precursor molecule are crucial for the deposition process. The precursor molecule should be volatile in a suitable range of pressures and temperatures. Under these conditions, it needs to be easily deliverable in the gas phase, adsorb on a substrate, be sensitive to the electron beam, and decompose in a clean manner to the desired products. Furthermore, it should be inexpensive and easy to prepare, nontoxic, and easy to store and handle [17]. The choice of such molecules requires a compromise to be made between volatility, stability, and reactivity induced by electron irradiation of the molecule. This must then be translated into a structure that can lead to the deposition of the desired material [33]. Most FEBID

precursors are organometallic complexes designed with the aim to obtain pure metal deposits. Normally, the metal content is quite limited, and the deposits are often heavily contaminated with carbon. Therefore, it makes sense to use as little carbon as possible in the design of the molecule [17]. Furthermore, it has been observed that large ligands, such as the methylcyclopentadienyl group in $MeCpPtMe_3$ and acetylacetonate in $Au(acac)Me_2$, do not decompose favourably under electron irradiation. However, this trend is not extended to the recently reported silver carboxylates [39,40]. In gold(I) complexes, only two ligands are present in the coordination sphere, a neutral ligand L and an anionic ligand X. Both ligands influence the complex stability, with an increased stability after the introduction of Au–C bonds [33]. The X ligand has shown to control the volatility of the complex by means of steric hindrance; as the size of X increases, the intramolecular interactions between the precursor molecules, specifically the aurophilic interactions, decrease substantially, rendering the precursor more volatile. This is valid only if the compounds maintain a constant lattice [33,34,41].

Gold(I) NHC complexes are known for their versatility in different applications such as catalysis [42], biomedicine [43], and photochemistry [44]. While chemically very different species are classified as NHCs, they all share a common moiety, a carbene carbon stabilized by two $\alpha$-nitrogen atoms. NHCs are neutral two-electron donors, analogous to the more extensively studied CO and $PR_3$ derivatives. The coordinative capability of the NHCs depends in fact primarily on the $sp^2$-hybridized lone pair of the carbene carbon atom, which has a strong $\sigma$-donor capability [45]. Moreover, the presence of back donation of $\pi$

electrons into the empty p$_z$ orbital of the carbene carbon atom further strengthens the C–Au bond [45]. Such features hint at a strong organometallic bond that precludes ligand dissociation under the temperature and pressure conditions involved in FEBID experiments.

Gold(I) NHC complexes owe their widely ranged adaptability to the great variability of the NHC ligand itself [46]. The NHC ligand can, in principle, be tailored to the desired application. For FEBID the main aim is to diminish the number of carbons in the molecular formula as much as possible in order to minimize the tendency to form contaminated deposits. Furthermore, we aim at the introduction of various heteroatoms such as halogens and nitrogen, in an effort to increase the volatility of the compound. These criteria were fulfilled in the NHC gold(I) complexes **1–7** (Figure 3). Compounds **1–5** and **7** are imidazole-based NHC complexes with short aliphatic substituents on the nitrogen atoms (N-substituents) and two chlorine atoms on the backbone of the aromatic structure. While compounds **1–3** have a chloride as the other ancillary ligand, this has been modified in compounds **4**, **5**, and **7** with the introduction of a bromide, iodide, or trifluoromethyl group, respectively. The effect of the halogen substitution on the performance of FEBID precursors has, to the best of our knowledge, not been investigated yet for gold compounds. The difference between the bromide and chloride ligands has been investigated [47] for platinum precursors. It was shown that under the tested conditions, the chloro compound performed better than the bromo compound in terms of composition and growth rate [47].

Compound **6** is a triazole-based NHC gold(I) complex that presents a further reduced number of carbon atoms compared to the imidazole-based compounds with the replacement of one of the backbone carbon atoms by a nitrogen atom.

Based on the design of these precursors, the expectation is that electron irradiation will decompose the ligands under the formation of nitrogen- and chlorine-containing organic fragments, hopefully leading to more volatile by-products, compared to precursors with purely carbon-based ligands. Furthermore, the synthesis aimed for a series of thermally robust compounds that can be straightforwardly handled and tested.

## Synthesis

The chemical precursors to the selected NHC ligands are salts of their respective imidazolium or triazolium cations. The imidazolium salts were obtained starting from the unsubstituted 4,5-chloroimidazole through two sequential alkylation reactions using the selected alkyl iodides [48]. For the triazolium salt the two alkylation reactions were carried out together in a one-pot synthesis [36]. The resulting salts were then reacted



**Figure 3:** The selected Au(NHC)X complexes studied and their molecular formulae.
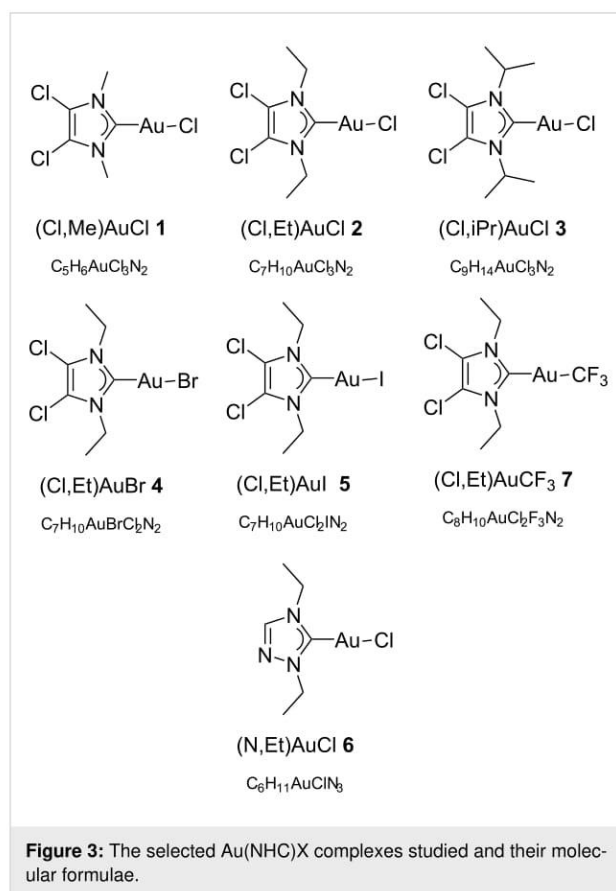
with silver oxide to generate the respective Ag(I) NHC complexes. Upon the addition of 1 equiv of gold precursor Au(SMe$_2$)Cl in situ, a transmetalation reaction took place that yielded the desired Au(NHC)Cl complexes **1**, **2**, **3**, and **6** (Scheme 1a,b) [37]. Compounds **4** and **5** were synthesized through a halide metathesis reaction when a solution of **2** in acetone was stirred with a large excess of a bromide [49] or iodide [50] salt (Scheme 1c). Compound **7** was obtained by reaction of **2** with a mixture of AgF and Me$_3$SiCF$_3$ [51]. This reaction created in situ a AgCF$_3$ species that, through a transmetalation reaction, yielded compound **7** (Scheme 1c).

All these compounds are, under ambient conditions, inert colourless crystals or white powders that are stable to air and moisture and safe to handle.

## Precursor volatility and thermal stability

Table 1 shows the sublimation temperature, obtained from the cold finger setup, for each precursor. No decomposition was observed in the collected sublimed materials by comparison of their $^1$H NMR spectra with those of the bulk material, and no change of the bulk material was observed during the sublimation experiments by visual observation. The correlation between halogen ligand and volatility was recently discussed for a

**Scheme 1:** Synthesis routes for **1–7**.
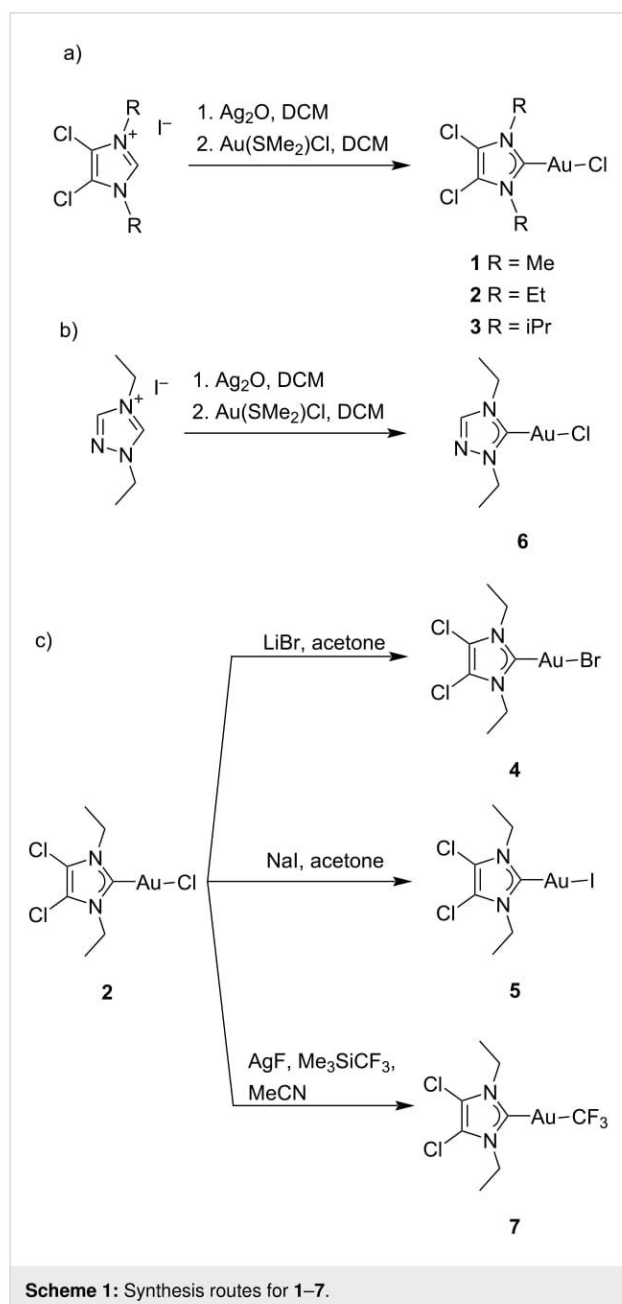
series of isocyanide gold(I) complexes [41]. Halogens with larger radii have been observed to lead to the formation of more volatile complexes, presumably due to the increased intermolecular distances in the packing of the crystals, mainly through weakening of aurophilic interactions [41]. The same trend was observed during cold finger sublimation experiments on the synthesized compounds. However, the magnitude of the sublimation temperature variation was found to be only modest for the halogen series Cl, Br, and I. This can be related to the presence of the NHC moiety, which is predominant in the packing of the molecules, thus reducing the weight of aurophilic interaction in the overall packing energy [52]. The variation of sublimation temperature is more important when a trifluoromethyl group is introduced on the gold atom inducing a decrease of more than 20 °C, in line with observations on isocyanide gold(I) complexes [34]. With the increase of the steric bulk of the N-substituents, the sublimation temperature is decreased. Going from Me to Et substituents causes a decrease in sublimation temperature of 22 °C, while the decrease from Et to iPr is minor (3 °C). Furthermore, the triazole-based gold complex was shown to be more volatile than its imidazole-based counterpart (Table 1).

The melting temperatures of the compounds are found not to be correlated directly with the sublimation temperatures. The sublimation temperature is a lower boundary of the FEBID operating range, to achieve a useful vapour pressure. The upper boundary is the upper pressure limit of the SEM. All deposition experiments were performed in this operating range. A temperature of 100 °C was chosen to explore all precursors, except for the least volatile compound **1** for which a temperature of 120 °C (20 °C more than its sublimation temperature) was necessary to provide a sufficient precursor flow. It is noted that all deposits reported in this work are grown on heated substrates and the resulting growth rates are valid only at the corresponding temperature. A beneficial side effect of heating the substrates to at least 100 °C is that adsorbed water is removed from the substrates, diminishing its influence on the FEBID process.

**Table 1:** Sublimation temperatures, melting points, and the chosen temperature for deposition of the studied precursors.

| Compound | Sublimation temperature[a] (°C) | Melting point[b] (°C) | Deposition temperature (°C) |
|---|---|---|---|
| (Cl,Me)AuCl (**1**) | 100 | 266–269[c] | 120 |
| (Cl,Et)AuCl (**2**) | 78 | 185–186 | 100 |
| (Cl,iPr)AuCl (**3**) | 75 | 202–203 | 100 |
| (Cl,Et)AuBr (**4**) | 77 | 204–205 | 100 |
| (Cl,Et)AuI (**5**) | 73 | 178–179 | 100 |
| (N,Et)AuCl (**6**) | 60 | 131–132 | 100 |
| (Cl,Et)AuCF$_3$ (**7**) | 53 | 146–149 | 100 |

[a]Obtained by cold finger sublimation at $10^{-3}$ mbar. [b]Obtained by melting point apparatus. [c]Decomposition observed starting at 220 °C.

## Testing apparatus

A more flexible setup than a traditional GIS was required for the exploration and testing of a large series of precursors. Commercially available GIS have a limited temperature range. For example, the maximum allowable temperature of the Thermo Fisher Scientific GIS, used with $W(CO)_6$ or $MeCpPtMe_3$, is limited by the software to 65 °C. As the precursors tested here are inert under normal conditions and stable to air and moisture, they lend themselves for exploration in an open system, and they pose no known health hazard to the user. They were first tested by positioning free precursor crystals on a heated substrate, and observing their disappearance upon heating. Furthermore, electron beam-induced deposition was observed in close vicinity of the crystals. A small and easy to handle setup mounted on a substrate surface was then developed, resembling a GIS, comprising a reservoir, an injection channel, and a deposition area (Figure 2). The cylindrical precursor reservoir of 2.5 $mm^3$ (2 mm diameter, 0.8 mm height) and a 1 mm long and 0.5 mm wide channel, which separates the reservoir from the circular deposition area (0.5 mm diameter), were milled from the bottom of an aluminium plate ($9.5 \times 9.5 \times 1$ $mm^3$). The plate lies directly on the $10 \times 10$ $mm^2$ silicon substrate, covering some precursor crystals positioned on the substrate, and is kept in place with vacuum-compatible Kapton tape. Only small quantities are needed to test a precursor, and a wide range of temperatures can be achieved (tested up to 160 °C).

## Deposition and composition results

All compounds were tested for electron beam-induced deposition, after which deposits were made large enough for compositional analysis using EDX. Slightly larger deposits were grown from the (N,Et)AuCl precursor, in order to reduce the silicon signal from the substrate and to obtain EDX measurements with a silicon content comparable to that of the other studied materials (<10 atom %). Figure 4 shows typical deposits, defined as $250 \times 250$ $nm^2$ squares, from all seven tested precursors. The deposits clearly differ in size and shape. The deposits have grown considerably in the lateral direction, almost doubling in size. Clear differences are seen in the vertical dimension ranging from about 0.5 µm (Figure 4a,f) to 3 µm (Figure 4g). While a minor halo is observed for all precursors, only for (N,Et)AuCl (**6**) a significant granular halo is obtained (see Supporting Information File 1, Figure S19), for reasons yet unknown.

The average composition of seven or eight EDX spectra from at least three deposits as those shown in Figure 4 is listed for each precursor in Table 2. The values reported are the mean ± standard error. All deposits have a consistent atomic fraction (atom %) of gold, indicating the successful delivery of the intact parent molecule to the beam incidence area.

For the series (Cl,Et)AuX with X = Cl, Br, I, and $CF_3$ (**2**, **4**, **5**, and **7**), a Au content of 7.3–8.8 atom % was obtained. Although the differences in Au content are only modest, the compounds X = Cl and X = $CF_3$ (**2** and **7**) were observed to contain the highest percentage of gold. Going from Cl over Br to I, the Au content steadily decreased. The decrease in metal content from Cl to Br compounds has been observed for deposits from Pt compounds as well [47]. The relatively high chlorine content of compounds **1**–**3**, compared to that of compounds **4**–**7**, indicates that the backbone and the gold-bonded Cl are co-deposited. Br, I, and F are also present in negligible quantities, demonstrating their suitability as elements to be used in
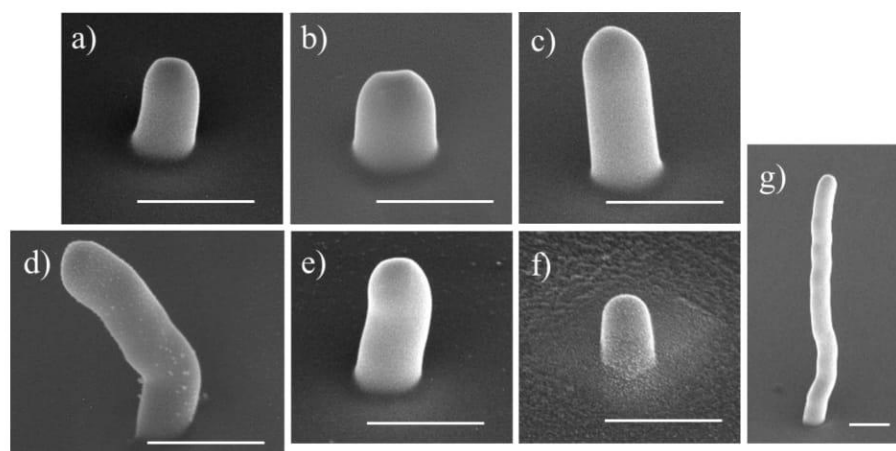


**Figure 4:** SEM images, tilted by 50°, of $250 \times 250$ $nm^2$ square deposits made using a beam energy and current of 5 keV and 40 pA, respectively. (a) **1** (Cl,Me)AuCl, (b) **2** (Cl,Et)AuCl, (c) **3** (Cl,iPr)AuCl, (d) **4** (Cl,Et)AuBr, (e) **5** (Cl,Et)AuI, (f) **6** (N,Et)AuCl, and (g) **7** (Cl,Et)AuCF$_3$. The deposition was performed using the reservoir-on-substrate setup, heated to 100 °C for all compounds except for **1**, which was heated to 120 °C. The scale bars are 1 µm.

**Table 2:** Elemental composition of deposits obtained by EDX with all values given in atom %. In addition, the ratio between carbon content and gold content in the deposits and the corresponding parent molecules are given.

|  | (Cl,Me)AuCl **1** | (Cl,Et)AuCl **2** | (Cl,iPr)AuCl **3** | (Cl,Et)AuBr **4** | (Cl,Et)AuI **5** | (N,Et)AuCl **6** | (Cl,Et)AuCF$_3$ **7** |
|---|---|---|---|---|---|---|---|
| C | 61.2 ± 0.58 | 66.7 ± 1.23 | 68.7 ± 0.96 | 67.0 ± 0.76 | 69.0 ± 0.53 | 60.7 ± 0.61 | 68.0 ± 0.41 |
| N | 14.9 ± 0.38 | 10.9 ± 0.37 | 10.0 ± 0.11 | 11.7 ± 0.30 | 11.9 ± 0.27 | 11.3 ± 0.35 | 12.3 ± 0.32 |
| Au | 10.3 ± 0.32 | 8.8 ± 0.40 | 7.3 ± 0.15 | 8.0 ± 0.26 | 7.3 ± 0.12 | 14.6 ± 0.41 | 8.8 ± 0.19 |
| Si | 7.4 ± 0.53 | 6.8 ± 0.67 | 6.9 ± 0.77 | 6.8 ± 0.39 | 7.3 ± 0.50 | 7.8 ± 0.42 | 7.2 ± 0.48 |
| O | 2.9 ± 0.10 | 3.7 ± 0.24 | 4.8 ± 0.25 | 3.3 ± 0.12 | 3.3 ± 0.04 | 4.0 ± 0.16 | 1.7 ± 0.07 |
| Cl | 3.3 ± 0.11 | 3.1 ± 0.07 | 2.4 ± 0.08 | 0.8 ± 0.04 | 1.3 ± 0.04 | 1.6 ± 0.08 | 1.9 ± 0.23 |
| Br | 0 | 0 | 0 | 2.5 ± 0.10 | 0 | 0 | 0 |
| F | 0 | 0 | 0 | 0 | 0 | 0 | 0.2 ± 0.07 |
| C/Au observed | 5.9 | 7.6 | 9.4 | 8.4 | 9.5 | 4.2 | 7.7 |
| C/Au parent[a] | 5 | 7 | 9 | 7 | 7 | 6 | 8 |

[a]C/Au ratio in the parent molecule.

FEBID precursors. Iodine is detected in EDX analysis only at 8 keV incident energy, and is therefore not shown in Table 2 (see Supporting Information File 1).

For the series (Cl,R)AuCl with R = Me, Et, and iPr (**1–3**) a wider range of gold content was found. This variation can be directly correlated to the number of carbon atoms in the precursor molecule. Going from R = Me over Et to iPr, the Au percentage decreases from 10.3 over 8.8 to 7.3 atom %, respectively, following the trend of the Au/C ratio of the starting material. For all compounds, the C/Au ratio observed in the deposits is comparable to, if not slightly larger than, the ratio in the parent molecules. While gold composition is highly influenced by the variation of the R substituents, the carbon atomic fraction does not proportionally increase with the increase of carbon atoms in the precursor. Br, Cl, I, and F are partially or mostly removed upon irradiation, while N is mostly co-deposited. A similar behaviour was observed for isocyanide-based gold(I) precursors, where N is also partially co-deposited [34]. Recently, it was further demonstrated that nitrogen can be embedded in pre-existent carbon material upon the use of N-containing precursors under electron irradiation [53]. EDX analyses of the deposits show the presence of silicon and oxygen, which are not present in the precursor molecules. Their presence is likely to come from the silicon substrate with its native oxide surface layer.

The triazole-based compound **6** is the best-performing precursor, yielding the highest Au content of 14.6 atom %. In this case, the C/Au ratio in the deposit is considerably lower than in the parent molecule (Table 2 and Table 3). This could be indicative of the effective fragmentation of the triazole-based ligand. Also in this case, Cl is mostly removed, while N is partially removed, leaving carbon and gold as the mainly deposited atoms.

**Table 3:** Ratios between the atomic percentages of elements present in the precursor molecule of **6**, the deposit from **6** and a putative fragment **6a** (see Figure 5).

|  | C/Au ratio | N/Au ratio | Cl/Au ratio |
|---|---|---|---|
| parent molecule of **6** | 6 | 3 | 1 |
| deposit from **6** | 4.2 | 0.8 | 0.1 |
| fragment **6a** | 4 | 1 | 0 |

Based on the N/Au, C/Au, and Cl/Au ratios for compound **6** (Table 3), it is evident that the chloride ligand is removed and that the triazole-ring is fragmented. However, the fragmentation of the NHC ligand is not simple and unambiguous, as various fragmentations can take place either by the removal of the N-substituents or by the effective fragmentation of the NHC ring. Since no fragmentation of the ring occurs for the imidazole-based compounds, the presence of a N–N bond appears to be a requirement. Thus, we postulate that the most plausible fragmentation is the removal of a N=N–Et fragment (**6b**) with the co-deposition of the metal centre and the strongly bonded carbene moiety **6a**, for which the molecular structure is comparable to the imidazole-based precursors (Figure 5). However, we cannot rule out the possibility of different fragmentations occurring at the same time.

## Growth Rate
To evaluate the deposition rate of these novel precursors, square arrays of 3 × 3 pillars were deposited, with each pillar grown with a different deposition time as explained in the Experimental section. Arrays with short deposition times (type 1) were deposited from (Cl,Et)AuCF$_3$, due to its high deposition rate. For all other precursors, arrays with long deposition times
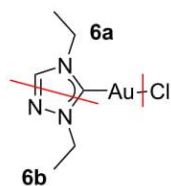
**Figure 5:** Possible fragmentations of (N,Et)AuCl (**6**), with the loss of Cl and a volatile fragment **6b,** and the deposition of **6a.**

(type 2) were fabricated. Figure 6 shows SEM tilt images (at 5 keV and 40 pA) of a typical array of deposited pillars for each precursor. For each deposited pillar its total deposition time is

converted to the total number of incident electrons, or electron dose, used to deposit that pillar.

Figure 6 shows that the shapes of the pillar deposits from different precursors are different. Therefore, the volume was chosen to fairly compare the growth rate of the different precursors. The height and diameter of the pillars were measured and used to calculate the volume. Figure 7 shows the calculated deposit volumes as a function of the electron dose. Clearly different deposition rates are found ranging from $3 \times 10^{-5}$ to $1 \times 10^{-2}$ nm$^3$/e$^-$, assuming linear growth. For the well-known Pt precursor MeCpPtMe$_3$, the deposition rate was recently reported as $2 \times 10^{-2}$ nm$^3$/e$^-$, although deposited under very dif-
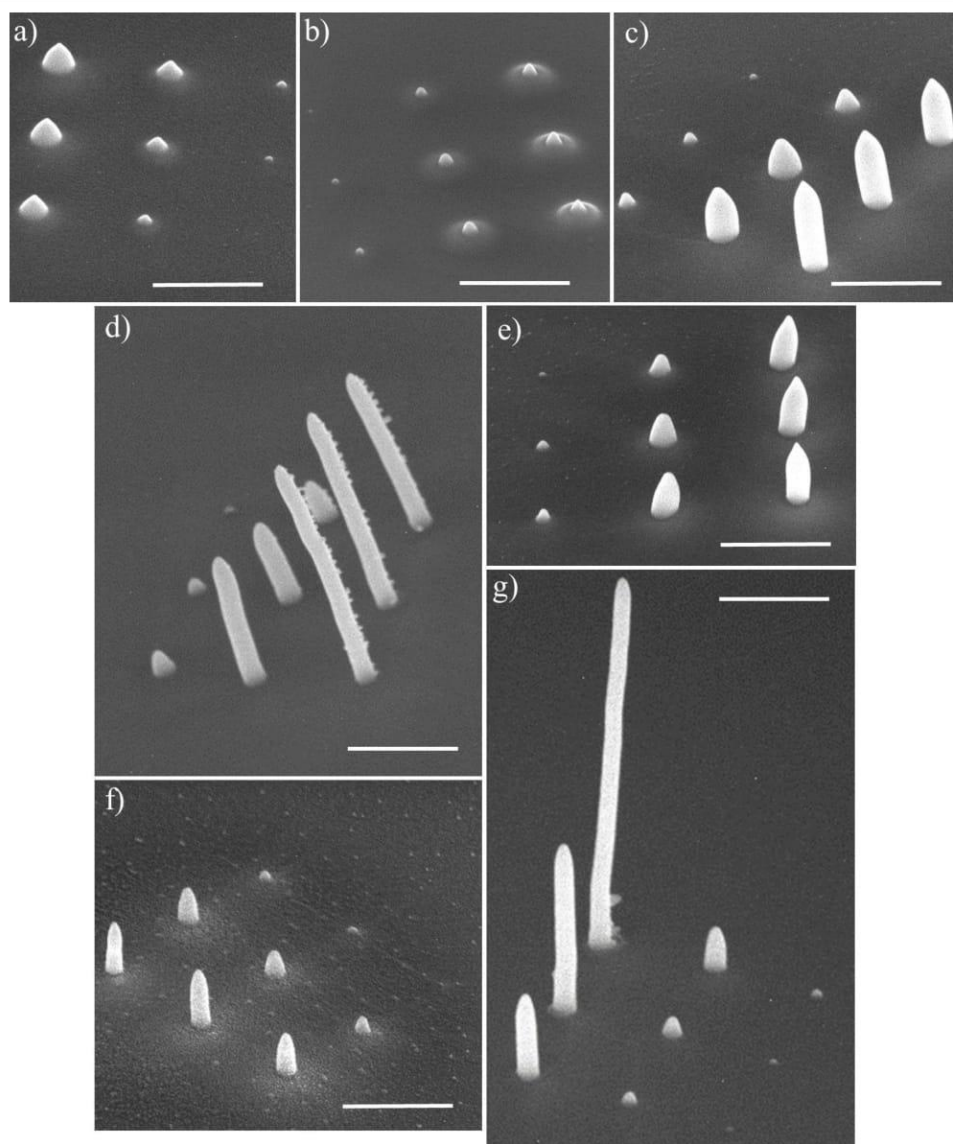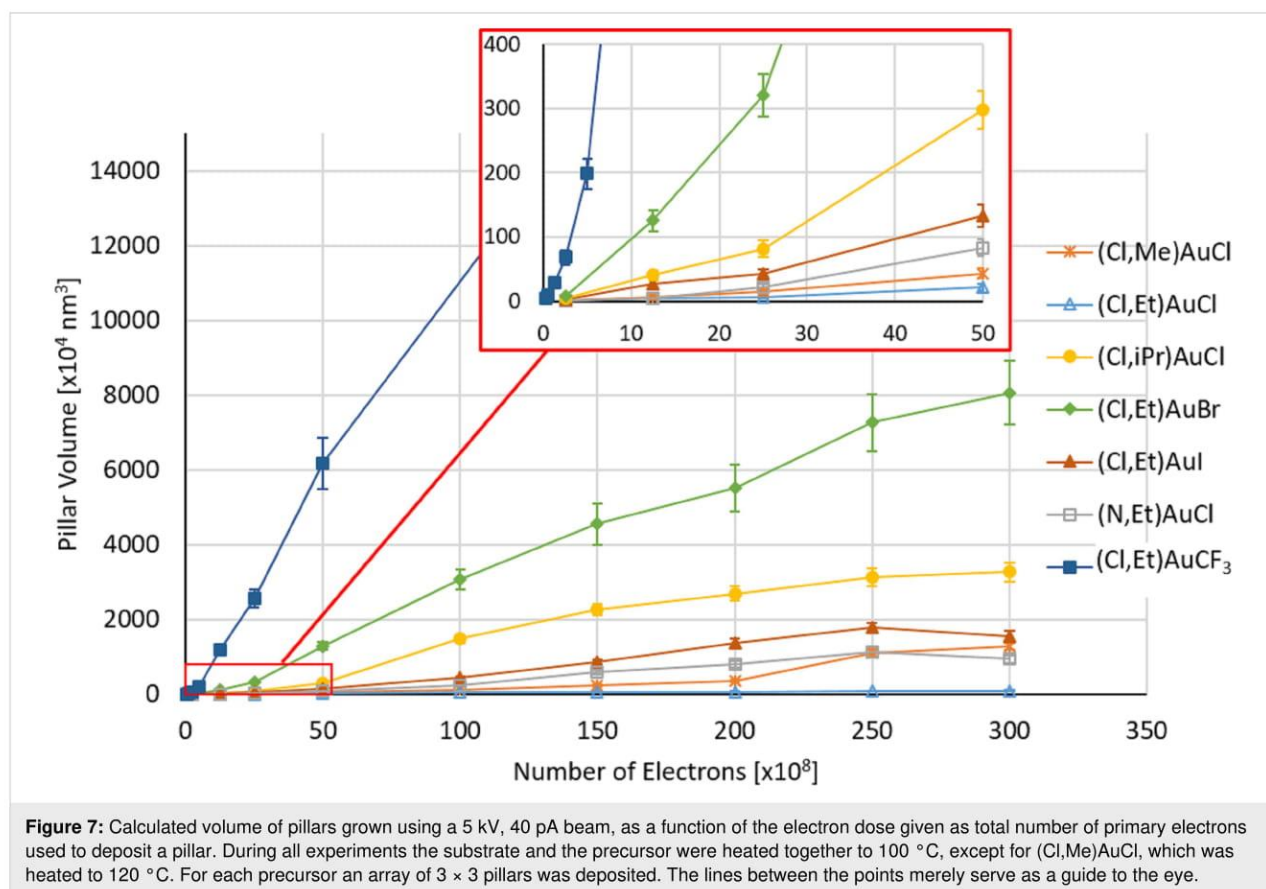


**Figure 6:** Typical SEM images, tilted by 50°, of pillar arrays deposited from all precursors. (a) **1** (Cl,Me)AuCl, (b) **2** (Cl,Et)AuCl, (c) **3** (Cl,iPr)AuCl, (d) **4** (Cl,Et)AuBr, (e) **5** (Cl,Et)AuI, (f) **6** (N,Et)AuCl, and (g) **7** (Cl,Et)AuCF$_3$. The deposition was performed using the reservoir-on-substrate setup heated to 100 °C for all compounds except for **1**, which was heated to 120 °C. The scale bars are 1 µm.

**Figure 7:** Calculated volume of pillars grown using a 5 kV, 40 pA beam, as a function of the electron dose given as total number of primary electrons used to deposit a pillar. During all experiments the substrate and the precursor were heated together to 100 °C, except for (Cl,Me)AuCl, which was heated to 120 °C. For each precursor an array of 3 × 3 pillars was deposited. The lines between the points merely serve as a guide to the eye.

ferent conditions [47]. Except for the compound (Cl,Et)AuCF$_3$, the growth rates of the presently studied gold precursors are considerably lower, which may be due to the elevated substrate temperature at which the deposition was performed. Arranging the precursors according to their growth rate, in increasing order, the following sequence is obtained: (Cl,Et)AuCl < (Cl,Me)AuCl < (N,Et)AuCl < (Cl,Et)AuI < (Cl,iPr)AuCl < (Cl,Et)AuBr < (Cl,Et)AuCF$_3$. No clear correlation between sublimation temperature and growth rate is observed. However, it should be noted that the most volatile compound (Cl,Et)AuCF$_3$ (**7**) led to the highest growth rate. Height and diameter of pillars grown from all precursors **1**–**7**, used to calculate the volume, are plotted in Figure S20 in Supporting Information File 1. Deposits from all precursors show a rather linear increase in height with electron dose (Figure S20a, Supporting Information File 1), whereas the deposit diameter increases at first but saturates at higher doses (Figure S20b, Supporting Information File 1). The saturation values differ between precursors, probably reflecting the difference in composition, which influences the electron scattering in the pillars.

## Conclusion

Seven gold NHC complexes of the form (Y,R)AuX were synthesized and thermally characterized. The sublimation tempera-

ture $T_s$ of the compounds was observed to decrease with the increase of the steric bulk of the N-substituent in the series R = Me, Et, and iPr, that is, $T_{s,Me} > T_{s,Et} > T_{s,iPr}$, and with the variation of the halide ligand X in the series X = Cl , Br, I, and CF$_3$, that is, $T_{s,Cl} \approx T_{s,Br} > T_{s,I} > T_{s,CF3}$. Minor structural variations were observed to cause a sublimation temperature difference of 47 °C between the least volatile compound (Cl,Me)AuCl (**1**) and the most volatile compound (Cl,Et)AuCF$_3$ (**7**). Furthermore, the introduction of a triazole-based ring in (N,Et)AuCl (**6**) leads to a more volatile complex than the imidazole-based counterpart (Cl,Et)AuCl (**2**). The compounds were tested as FEBID precursors on a heated substrate equipped with an on-substrate precursor reservoir. We analyzed the influence of the variation of the NHC ring, of the N-substituents and of the halogen or pseudo halogen ligand X both on composition and deposition rate. The variation of the R group expectedly led to better composition results for the smaller alkyl substituents (R = Me), accompanied by a decrease in volatility. Minor composition differences were registered for the variation of the X group, with X = Cl and CF$_3$ leading to the best results. Of the tested precursors, the most promising is the triazole-based complex **6**, which leads to an un-optimized gold composition of 14.6 atom %. Modest atomic percentages of gold have been achieved, in line with previously reported gold(I) precursors,

but still below the best-performing unstable gold(I) precursors and Au(tfac)Me$_2$. However, there is much room for improvement regarding the deposition conditions, which could lead to better composition of the deposits. The growth rate measurements of the compounds, at the temperature of deposition, have shown that under constant conditions the variation of the X group from a halogen to a trifluoromethyl group is highly beneficial. (Cl,Et)AuCF$_3$ (**7**) shows the highest growth rate while retaining the same gold composition as the halogen-based complexes. This comparison offers an interesting perspective to further explore trifluoromethylated FEBID precursors, rather than the halide counterparts.

## Supporting Information

Supporting Information contains contains NMR characterization of **4**–**7**, $^1$H NMR spectra of sublimation experiments of **1**–**7**, and a graphical representation of vertical growth and diameter of the pillars in Figure 6.

### Supporting Information File 1
Additional experimental data.
[https://www.beilstein-journals.org/bjnano/content/supplementary/2190-4286-12-21-S1.pdf]

## ORCID® iDs
Cristiano Glessi - https://orcid.org/0000-0001-7671-7591
Aya Mahgoub - https://orcid.org/0000-0002-8088-4699

## References

1. Silvis-Cividjian, N.; Hagen, C. W. *Adv. Imaging Electron Phys.* **2006,** *143,* 1–235. doi:10.1016/s1076-5670(06)43001-9
2. Utke, I.; Hoffmann, P.; Melngailis, J. *J. Vac. Sci. Technol., B: Microelectron. Nanometer Struct.–Process., Meas., Phenom.* **2008,** *26,* 1197–1276. doi:10.1116/1.2955728
3. Huth, M.; Porrati, F.; Schwalb, C.; Winhold, M.; Sachser, R.; Dukic, M.; Adams, J.; Fantner, G. *Beilstein J. Nanotechnol.* **2012,** *3,* 597–619. doi:10.3762/bjnano.3.70
4. van Dorp, W. F.; Hagen, C. W. *J. Appl. Phys.* **2008,** *104,* 081301. doi:10.1063/1.2977587
5. Fernández-Pacheco, A.; Serrano-Ramón, L.; Michalik, J. M.; Ibarra, M. R.; De Teresa, J. M.; O'Brien, L.; Petit, D.; Lee, J.; Cowburn, R. P. *Sci. Rep.* **2013,** *3,* 1492. doi:10.1038/srep01492
6. Noh, J. H.; Stanford, M. G.; Lewis, B. B.; Fowlkes, J. D.; Plank, H.; Rack, P. D. *Appl. Phys. A: Mater. Sci. Process.* **2014,** *117,* 1705–1713. doi:10.1007/s00339-014-8745-0
7. Brown, J.; Kocher, P.; Ramanujan, C. S.; Sharp, D. N.; Torimitsu, K.; Ryan, J. F. *Ultramicroscopy* **2013,** *133,* 62–66. doi:10.1016/j.ultramic.2013.05.005
8. Rodriguez, B. J.; Jesse, S.; Seal, K.; Baddorf, A. P.; Kalinin, S. V.; Rack, P. D. *Appl. Phys. Lett.* **2007,** *91,* 093130. doi:10.1063/1.2778762
9. Utke, I.; Hoffmann, P.; Berger, R.; Scandella, L. *Appl. Phys. Lett.* **2002,** *80,* 4792–4794. doi:10.1063/1.1489097
10. Höflich, K.; Yang, R. B.; Berger, A.; Leuchs, G.; Christiansen, S. *Adv. Mater. (Weinheim, Ger.)* **2011,** *23,* 2657–2661. doi:10.1002/adma.201004114
11. Liu, N.; Tang, M. L.; Hentschel, M.; Giessen, H.; Alivisatos, A. P. *Nat. Mater.* **2011,** *10,* 631–636. doi:10.1038/nmat3029
12. Huth, M.; Porrati, F.; Dobrovolskiy, O. V. *Microelectron. Eng.* **2018,** *185–186,* 9–28. doi:10.1016/j.mee.2017.10.012
13. Graells, S.; Aćimović, S.; Volpe, G.; Quidant, R. *Plasmonics* **2010,** *5,* 135–139. doi:10.1007/s11468-010-9128-9
14. De Teresa, J. M.; Fernández-Pacheco, A. *Appl. Phys. A: Mater. Sci. Process.* **2014,** *117,* 1645–1658. doi:10.1007/s00339-014-8617-7
15. Keller, L.; Al Mamoori, M. K. I.; Pieper, J.; Gspan, C.; Stockem, I.; Schröder, C.; Barth, S.; Winkler, R.; Plank, H.; Pohlit, M.; Müller, J.; Huth, M. *Sci. Rep.* **2018,** *8,* 6160. doi:10.1038/s41598-018-24431-x
16. Widyaratih, D. S.; Hagedoorn, P.-L.; Otten, L. G.; Ganjian, M.; Tümer, N.; Apachitei, I.; Hagen, C. W.; Fratila-Apachitei, L. E.; Zadpoor, A. A. *Nanotechnology* **2019,** *30,* 20LT01. doi:10.1088/1361-6528/ab0a3a
17. Carden, W. G.; Lu, H.; Spencer, J. A.; Fairbrother, D. H.; McElwee-White, L. *MRS Commun.* **2018,** *8,* 343–357. doi:10.1557/mrc.2018.77
18. Barth, S.; Huth, M.; Jungwirth, F. *J. Mater. Chem. C* **2020,** *8,* 15884–15919. doi:10.1039/d0tc03689g
19. Folch, A.; Servat, J.; Esteve, J.; Tejada, J.; Seco, M. *J. Vac. Sci. Technol., B: Microelectron. Nanometer Struct.–Process., Meas., Phenom.* **1996,** *14,* 2609–2614. doi:10.1116/1.588994
20. Mulders, J. J. L.; Belova, L. M.; Riazanova, A. *Nanotechnology* **2011,** *22,* 055302. doi:10.1088/0957-4484/22/5/055302
21. Jenke, M. G.; Lerose, D.; Niederberger, C.; Michler, J.; Christiansen, S.; Utke, I. *Nano Lett.* **2011,** *11,* 4213–4217. doi:10.1021/nl2021448
22. Puydinger dos Santos, M. V.; Szkudlarek, A.; Rydosz, A.; Guerra-Nuñez, C.; Béron, F.; Pirota, K. R.; Moshkalev, S.; Diniz, J. A.; Utke, I. *Beilstein J. Nanotechnol.* **2018,** *9,* 91–101. doi:10.3762/bjnano.9.11
23. Koops, H. W. P.; Kretz, J.; Rudolph, M.; Weber, M.; Dahm, G.; Lee, K. L. *Jpn. J. Appl. Phys., Part 1* **1994,** *33,* 7099–7107. doi:10.1143/jjap.33.7099
24. Utke, I.; Jenke, M. G.; Röling, C.; Thiesen, P. H.; Iakovlev, V.; Sirbu, A.; Mereuta, A.; Caliman, A.; Kapon, E. *Nanoscale* **2011,** *3,* 2718–2722. doi:10.1039/c1nr10047e
25. Belić, D.; Shawrav, M. M.; Bertagnolli, E.; Wanzenboeck, H. D. *Beilstein J. Nanotechnol.* **2017,** *8,* 2530–2543. doi:10.3762/bjnano.8.253

26. Shawrav, M. M.; Taus, P.; Wanzenboeck, H. D.; Schinnerl, M.; Stöger-Pollach, M.; Schwarz, S.; Steiger-Thirsfeld, A.; Bertagnolli, E. *Sci. Rep.* **2016,** *6,* 34003. doi:10.1038/srep34003

27. Utke, I.; Hoffmann, P.; Dwir, B.; Leifer, K.; Kapon, E.; Doppelt, P. *J. Vac. Sci. Technol., B: Microelectron. Nanometer Struct.–Process., M eas., Phenom.* **2000,** *18,* 3168–3171. doi:10.1116/1.1319690

28. Brintlinger, T.; Fuhrer, M. S.; Melngailis, J.; Utke, I.; Bret, T.; Perentes, A.; Hoffmann, P.; Abourida, M.; Doppelt, P. *J. Vac. Sci. Technol., B: Microelectron. Nanometer Struct.–Process., M eas., Phenom.* **2005,** *23,* 3174–3177. doi:10.1116/1.2130355

29. Utke, I.; Dwir, B.; Leifer, K.; Cicoira, F.; Doppelt, P.; Hoffmann, P.; Kapon, E. *Microelectron. Eng.* **2000,** *53,* 261–264. doi:10.1016/s0167-9317(00)00311-7

30. Hoffmann, P.; Utke, I.; Cicoira, F.; Dwir, B.; Leifer, K.; Kapon, E.; Doppelt, P. *MRS Online Proc. Libr.* **2000,** *624,* 171. doi:10.1557/proc-624-171

31. Mulders, J. J. L.; Veerhoek, J. M.; Bosch, E. G. T.; Trompenaars, P. H. F. *J. Phys. D: Appl. Phys.* **2012,** *45,* 475301. doi:10.1088/0022-3727/45/47/475301

32. van Dorp, W. F.; Wu, X.; Mulders, J. J. L.; Harder, S.; Rudolf, P.; De Hosson, J. T. M. *Langmuir* **2014,** *30,* 12097–12105. doi:10.1021/la502618t

33. Marashdeh, A.; Tiesma, T.; van Velzen, N. J. C.; Harder, S.; Havenith, R. W. A.; De Hosson, J. T. M.; van Dorp, W. F. *Beilstein J. Nanotechnol.* **2017,** *8,* 2753–2765. doi:10.3762/bjnano.8.274

34. Carden, W. G.; Thorman, R. M.; Unlu, I.; Abboud, K. A.; Fairbrother, D. H.; McElwee-White, L. *ACS Appl. Mater. Interfaces* **2019,** *11,* 11976–11987. doi:10.1021/acsami.8b18368

35. Brandys, M.-C.; Jennings, M. C.; Puddephatt, R. J. *J. Chem. Soc., Dalton Trans.* **2000,** 4601–4606. doi:10.1039/b005251p

36. Elnajjar, F. O.; Binder, J. F.; Kosnik, S. C.; Macdonald, C. L. B. *Z. Anorg. Allg. Chem.* **2016,** *642,* 1251–1258. doi:10.1002/zaac.201600270

37. Levchenko, V.; Glessi, C.; Øien-Ødegaard, S.; Tilset, M. *Dalton Trans.* **2020,** *49,* 3473–3479. doi:10.1039/c9dt04472h

38. Jeevanandam, G.; van der Meijden, V.; Birnie, L. D.; Kruit, P.; Hagen, C. W. *Microelectron. Eng.* **2020,** *224,* 111239. doi:10.1016/j.mee.2020.111239

39. Berger, L.; Madajska, K.; Szymanska, I. B.; Höflich, K.; Polyakov, M. N.; Jurczyk, J.; Guerra-Nuñez, C.; Utke, I. *Beilstein J. Nanotechnol.* **2018,** *9,* 224–232. doi:10.3762/bjnano.9.24

40. Höflich, K.; Jurczyk, J. M.; Madajska, K.; Götz, M.; Berger, L.; Guerra-Nuñez, C.; Haverkamp, C.; Szymanska, I.; Utke, I. *Beilstein J. Nanotechnol.* **2018,** *9,* 842–849. doi:10.3762/bjnano.9.78

41. Carden, W. G.; Pedziwiatr, J.; Abboud, K. A.; McElwee-White, L. *ACS Appl. Mater. Interfaces* **2017,** *9,* 40998–41005. doi:10.1021/acsami.7b12465

42. Marion, N.; Nolan, S. P. *Chem. Soc. Rev.* **2008,** *37,* 1776–1782. doi:10.1039/b711132k

43. Porchia, M.; Pellei, M.; Marinelli, M.; Tisato, F.; Del Bello, F.; Santini, C. *Eur. J. Med. Chem.* **2018,** *146,* 709–746. doi:10.1016/j.ejmech.2018.01.065

44. Longevial, J.-F.; Langlois, A.; Buisson, A.; Devillers, C. H.; Clément, S.; van der Lee, A.; Harvey, P. D.; Richeter, S. *Organometallics* **2016,** *35,* 663–672. doi:10.1021/acs.organomet.5b00966

45. Marchione, D.; Belpassi, L.; Bistoni, G.; Macchioni, A.; Tarantelli, F.; Zuccaccia, D. *Organometallics* **2014,** *33,* 4200–4208. doi:10.1021/om5003667

46. Hopkinson, M. N.; Richter, C.; Schedler, M.; Glorius, F. *Nature* **2014,** *510,* 485–496. doi:10.1038/nature13384

47. Mahgoub, A.; Lu, H.; Thorman, R. M.; Preradovic, K.; Jurca, T.; McElwee-White, L.; Fairbrother, H.; Hagen, C. W. *Beilstein J. Nanotechnol.* **2020,** *11,* 1789–1800. doi:10.3762/bjnano.11.161

48. Solovyev, A.; Ueng, S.-H.; Monot, J.; Fensterbank, L.; Malacria, M.; Lacôte, E.; Curran, D. P. *Org. Lett.* **2010,** *12,* 2998–3001. doi:10.1021/ol101014q

49. de Frémont, P.; Singh, R.; Stevens, E. D.; Petersen, J. L.; Nolan, S. P. *Organometallics* **2007,** *26,* 1376–1385. doi:10.1021/om060887t

50. Baker, M. V.; Barnard, P. J.; Brayshaw, S. K.; Hickey, J. L.; Skelton, B. W.; White, A. H. *Dalton Trans.* **2005,** 37–43. doi:10.1039/b412540a

51. Blaya, M.; Bautista, D.; Gil-Rubio, J.; Vicente, J. *Organometallics* **2014,** *33,* 6358–6368. doi:10.1021/om500669j

52. Pinter, B.; Broeckaert, L.; Turek, J.; Růžička, A.; DeProft, F. *Chem. – Eur. J.* **2014,** *20,* 734–744. doi:10.1002/chem.201302171

53. Rohdenburg, M.; Fröch, J. E.; Martinović, P.; Lobo, C. J.; Swiderek, P. *Micromachines* **2020,** *11,* 769. doi:10.3390/mi11080769